Organisation of primary auditory cortex in the mouse: a topography of inputs and responses

Jonathan JB Webb

A thesis submitted for the degree of
Doctor of Philosophy



Worcester College
University of Oxford
Michaelmas Term 2013

Bruce Phillip Webb, 1926–2000

Abstract

This thesis explores the spatial organisation of response properties and long-range inputs of the mouse auditory cortex. I offer a critical evaluation of two established principles, namely the presence of a tonotopic sound-frequency map and of two distinct primary subfields, and also present evidence in support of a more novel feature: direct connections from other sensory cortices.

Tonotopy remains the single acknowledged organising principle of mammalian primary auditory cortex, but recent studies in the mouse have questioned the reproducibility of tonotopic maps and the scale at which such organisation is recognisable. Here I use high channel-count, extracellular recordings to evaluate tuning and tonotopy across cortical space. Compared to thalamorecipient layers, I find that frequency sensitivity is weaker and less prevalent in superficial and deep layers. The precision and direction of the tonotopic gradient, too, often change with depth. Measuring LFPs rather than multi-unit activity did not significantly alter tonotopy, but presenting a dynamic stimulus rather than pure tones tended to produce higher best frequencies as well as variations in tonotopic organisation. I also report considerable temporal complexity in the frequency sensitivity measured with pure tones.

The two subfields of mouse primary auditory cortex, A1 and AAF, have seldom been explicitly compared. In accordance with some published data suggesting that the two are broadly equivalent, except for a trend toward more rapid processing within AAF, I observe consistently shorter latencies in AAF than A1, across cortical depth. Spike counts are also higher in AAF, but I find no differences in the selectivity or sensitivity of pure tone responses. I also report anatomical data consistent with overlapping inputs from the auditory thalamus.

Recent anatomical and physiological evidence from several species has recast 'unimodal' cortical areas, including A1, as potentially multisensory. Furthering this line of enquiry in the mouse, I use retrograde tracers to describe sparse, predominantly feedback-type cortico-cortical inputs from other early sensory cortices, including S1 and V2, to both A1 and AAF. Moreover, optogenetic stimulation of either medial V2 or non-barrel S1 elicits changes in auditory response properties within A1 and AAF, including some decreases in spike-count and increases in bandwidth, threshold and latency.

Altogether, the physiological and anatomical data herein contribute to the increasing complexity that attends our understanding of the activity and wiring of cortical networks.

Declaration

The work described in this thesis was carried between October 2008 and December 2013 in the Neuronal Oscillations Group and the Auditory Neuroscience Group, both in the Department of Physiology, Anatomy and Genetics at the University of Oxford. All of the research and analysis presented in this thesis is my own original work, performed under the supervision acknowledged on the next page.

Acknowledgements

It strikes me that completing a doctorate is simultaneously one of the most concentrated individual efforts of a lifetime, and one of the most immense accumulations of unrecognised teamwork. Many sacrifices have been made in support of this volume and I owe a great deal to a great many. This is impossible to rectify in a single page, but here is where I try.

Firstly I must thank my supervisors, Dr Louise Upton, Professor Andrew King and Professor Ole Paulsen. Your guidance in matters great and small has always been incisive and your company a pleasure. I am particularly grateful for your support of my year in the wilderness (London) and for your encouragement to return to the DPhil.

For financial support I am indebted to the Clarendon Fund and also to the Rhodes Trust, who funded my MSc and brought me to Oxford in the first place.

A million thanks are due to the members of the Auditory Neuroscience Group for providing an administrative, social and scientific home when my first lab decamped to the Other Place. A further million are due to the members of the Neuronal Oscillations Group, which was my home in all those ways for the first two years; the regrettably small amount of work from that period which appears in this thesis is certainly no reflection on the support you all provided. It has not escaped my attention that these two large, well-run laboratories both benefit from the near constant deployment of identical coffee machines. Each of those machines probably deserves its own acknowledgement here.

For less chemical, more human assistance during the various planning, experimental, analysis and writing phases of this serpentine exercise, I must specifically thank: Vicky Bajo, James Cooke, Mick Craig, Nicol Harper, Michael Kohl, Jan Schnupp and Kerry Walker, as well as the many supremely helpful staff in the Sherrington Building and Veterinary Services. Extra special mentions go to Christian Honey, Neil Rabinowitz and the masterful Ben Willmore, for providing wizardly technical support at the drop of a wizardly hat.

Next, though naming them all would be utterly impractical, I owe my continued mental health to many now lifelong friends, both within and outside science, who sustained me in good and bad times with dinners, lunches, bike rides, musical and theatrical endeavours, sets of tennis, games of cards and bottles of whisky.

Final thanks, above all, to Catherine and to my family, for everything.

List of Abbreviations

A1 / A2	Primary / secondary auditory cortex
AAF	Anterior auditory field
AAV	Adeno-associated virus
ANOVA	Analysis of variance
AU	Arbitrary units
CamKIIa	Ca^{2+}/ calmodulin-dependent protein kinase IIa
ChR2	Channelrhodopsin-2
CI	Confidence interval
CTB	Cholera toxin B
DAPI	4′,6–diamidino–2–phenylindole
DP	Dorsoposterior field
DRC	Dynamic random chord
EEG	Electroencephalogram
EPSP	Excitatory post-synaptic potential
FG	FluoroGold
FRA	Frequency response area
HRP	Horseradish peroxidase
IAF	Insular auditory field
IP	Intraperitoneal
MGB (MGBv)	Medial geniculate body (ventral division)
MUA	Multi-unit activity
PBS	Phosphate buffered saline
PSTH	Peri-stimulus time histogram
S1, S2	Primary, secondary somatosensory cortex
S1BC	Barrel cortex
SD	Standard deviation
SEM	Standard error of the mean
SPL	Sound pressure level
STRF	Spectrotemporal receptive field
V1 / V2	Primary / secondary visual cortex
V2(M) / V2(L)	Medial / lateral V2

Contents

1 Introduction **1**

1.1 Functional architecture of the auditory cortex 2

1.2 A pair of primary fields 5

1.3 Mouse maps: a brief history of increasing complexity 6

1.4 Multisensory activity in early cortical areas 8

1.5 Cortico-cortical connectivity 10

1.6 Classifying cortical projections 12

1.7 Scope of this thesis 14

1.7.1 Specific objectives 15

2 Materials and Methods **16**

2.1 Numbers and strains of mice 16

2.2 *In vivo* recordings 17

2.2.1 Anaesthesia and surgery 18

2.2.2 Data acquisition 19

2.2.3 Stimuli: calibration and delivery 19

2.2.4 Stimuli: noise bursts and pure tones 19

2.2.5 Stimuli: dynamic random chords 20

2.3 Electrophysiological data analysis 20

2.3.1 Signals: multi-unit activity and local field potentials 20

2.3.2 Estimating cortical depth 21

2.3.3 Multi-unit responses to noise bursts 22

2.3.4 Frequency response areas from pure tone responses 23
2.3.5 Spectrotemporal receptive fields from DRC responses 25
2.3.6 Generating cortical maps 26
2.4 Retrograde anatomical tracing 27
2.4.1 Tracer injections 27
2.4.2 Histological preparation of sections 28
2.4.3 Tracing of sections and labelled cells 28
2.5 Anterograde characterisation and optogenetics 29
2.5.1 Virus injections 29
2.5.2 Optogenetic experiments *in vitro* 30
2.5.3 Photostimulation *in vivo* 31
2.5.4 Fluorescence microscopy 32

3 The question of tonotopy **33**
3.1 Introduction 33
3.1.1 Contrasting data from the mouse cortex 35
3.1.2 Aims 36
3.2 Methodological considerations 37
3.2.1 Identifying cortical layers using LFPs 38
3.2.2 Pure tone response analysis: effect of smoothing data 38
3.2.3 Pure tone response analysis: comparison of CF and BF 42
3.2.4 Very high-frequency tuning is rare 44
3.3 Prevalence and strength of frequency tuning across the cortex 46
3.3.1 Is tuning more common in some fields and layers? 47
3.3.2 Is tuning stronger in some fields and layers? 51
3.4 Tonotopy in multi-unit activity 53
3.4.1 Canonical tonotopy is usually but not universally evident in thalamorecipient layers 54
3.4.2 Tonotopy varies in supra- and infragranular layers 57
3.5 Tuning and tonotopy in local field potentials 62

3.5.1 Where present, LFP tuning correlates weakly with multi-unit tuning . 62
3.5.2 LFPs do not significantly improve detection of tonotopy 64
3.6 A possible effect of stimulus complexity 68
3.6.1 Tuning of DRC responses correlates weakly with pure-tone tuning and tends toward higher frequencies 69
3.6.2 Tonotopy is variable in DRC responses 71
3.7 Temporal variation in responses 74
3.7.1 Post-activation suppression produces matched, inhibitory FRAs . . . 74
3.7.2 Late tuning 75
3.7.3 Shifting and expanding frequency responses 78
3.7.4 Choice of response window can dramatically affect calculated tuning 80
3.8 Discussion 82
3.8.1 Overview and implications of results 82
3.8.2 Finding a fit with diverse published data 85
3.8.3 In praise of mess 88

4 Comparing the responses and inputs of A1 and AAF 91
4.1 Introduction 91
4.1.1 How distinct are the physiology and connectivity of A1 and AAF? . . . 92
4.1.2 Aims 95
4.2 Comparing neurophysiology of A1 and AAF: noise responses 95
4.2.1 Latencies are shorter in AAF 98
4.2.2 Noise-driven responses are stronger in AAF than A1, particularly in infragranular layers 99
4.3 Comparing neurophysiology of A1 and AAF: tone responses 100
4.3.1 Strength of frequency tuning is similar across A1 and AAF 100
4.3.2 Bandwidth and threshold are not significantly different between A1 and AAF 101
4.4 Distribution of cells projecting to A1 and AAF 104

4.4.1 A1 and AAF receive overlapping thalamocortical input 105
4.4.2 Contralateral auditory cortical inputs to A1 and AAF may reveal differences in reciprocal connectivity 108
4.5 Discussion 111
4.5.1 Comparison with physiological data from other species 111
4.5.2 Likelihood of a shared thalamic tonotopic axis 113
4.5.3 Implications: more primary than primary? 114

5 Cortical inputs from other senses 116
5.1 Introduction 116
5.1.1 Cross-talk among early cortical areas: anatomy and activity 117
5.1.2 Aims 118
5.2 Retrograde tracing of inputs to primary auditory cortex 118
5.2.1 Three tracer injections into primary areas reveal predominantly scattered, sparse cortico-cortical inputs 119
5.2.2 Projecting cells are distributed across cortical areas 123
5.2.3 The contralateral hemisphere contains a smaller but similarly distributed set of projecting cells 126
5.2.4 The majority of projecting cells are in infragranular layers 128
5.2.5 Choice of candidate projecting areas 131
5.3 Anterograde examination of projections from candidate areas 133
5.3.1 Virus injections into S1 and V2M reveal sparse fibres in A1 and AAF . 134
5.4 Optogenetic activation of candidate areas 137
5.4.1 Expression and activity of ChR2 *in vivo* 139
5.4.2 Bandwidth and threshold measurements 139
5.4.3 S1 stimulation increases tone response thresholds in A1 143
5.4.4 S1 and V2 stimulation increase bandwidth of tone responses, in different layers and subfields 145
5.4.5 S1 and V2 stimulation produce small shifts in magnitude and latency of noise responses 148
5.5 Discussion 154

5.5.1 Overview of results 154
5.5.2 Relating anatomy and activity 154
5.5.3 Why weaker and less specific? 156
5.5.4 Concluding remarks 157

6 General Discussion and Conclusions **158**
6.1 Summary of findings 158
6.2 Auditory maps 160
6.2.1 A property of inputs and outputs? 161
6.2.2 Who cares about sound frequency anyway? 162
6.2.3 Context and timing are crucial 163
6.2.4 Tonotopy is a fragile and untidy guide 164
6.2.5 A1 and AAF: similar but different 166
6.3 Non-auditory inputs 167
6.3.1 Functional relevance of ECC connections 168
6.4 In conclusion 171

Bibliography **172**

List of Figures

1.1 Organisation of mammalian auditory cortex 4
1.2 Hierarchical classification of cortico-cortical connectivity 13

3.1 Electrode layout and depth estimation 39
3.2 Smoothing pure tone data 41
3.3 Calculating CF from smoothed data 43
3.4 CF and BF are correlated and produce similar frequency maps 44
3.5 Overall prevalence of noise responses and tuning 48
3.6 Prevalence of tuning across cortical fields and layers 50
3.7 Strength of tuning across cortical fields and layers 52
3.8 Delineation of subfields based on tonotopy in thalamorecipient layers 54
3.9 Frequency maps from middle layers with varying degrees of organisation . . 56
3.10 Comparing tonotopic maps across cortical depth 59
3.11 Strength and direction of tonotopy across cortical depth 60
3.12 Examples of pure-tone LFP responses 63
3.13 Correlation of LFP tuning with MUA tuning 64
3.14 Comparing tonotopic maps detected by LFPs and MUA 65
3.15 Strength and direction of tonotopy detected by LFPs 67
3.16 Stimulus structure of dynamic random chords (DRCs) 69
3.17 Example receptive fields from DRC responses 70
3.18 Comparing tuning of DRC and pure tone responses 71
3.19 Comparing tonotopic maps produced by DRCs and pure tones 72

3.20 Strength and direction of tonotopy produced by DRCs 73
3.21 A survey of temporal effects on frequency tuning 76
3.22 Two response windows producing divergent sets of BFs 81
3.23 Factors affecting tonotopic fidelity 86

4.1 Variation of frequency tuning and latency across published maps of mouse auditory cortex 93
4.2 Two examples maps of response strength and latency 96
4.3 Variation of response strength and latency with rostrocaudal position 97
4.4 Comparing peak latency in A1 and AAF, across cortical depth 98
4.5 Comparing noise-driven spike-rates in A1 and AAF, across cortical depth . . 99
4.6 Comparing tuning strength in A1 and AAF 102
4.7 Comparing the bandwidth of pure-tone responses in A1 and AAF 103
4.8 Comparing the threshold of pure-tone responses in A1 and AAF 104
4.9 Site of A1 and AAF tracer injections 105
4.10 Comparing thalamocortical inputs to A1 and AAF 107
4.11 Comparing distribution of cells projecting to A1 and AAF from contralateral auditory cortex 110

5.1 Overview of retrogradely labelled cells from mouse 'Marvin' 120
5.2 Overview of retrogradely labelled cells from mouse 'Marcy' 122
5.3 Examples of labelled cells 124
5.4 Scattered, predominantly commingled cells projecting to A1 and AAF from other sensory areas 125
5.5 Distribution of A1/AAF-targeting cells across cortical areas 127
5.6 Distribution of projecting cells in non-auditory areas from both hemispheres 128
5.7 Supra- and infragranular layer breakdown of A1/AAF-targeting cells in non auditory areas 130
5.8 Sparse axons from S1 in primary auditory areas 135
5.9 Sparse axons from V2M in primary auditory areas 136
5.10 Light-driven spiking activity at site of virus injection 140

5.11 Calculating bandwidth and threshold from pure-tone responses 142
5.12 Distribution of response thresholds, with and without S1 and V2 stimulation 144
5.13 Changes in threshold observed with S1 and V2 stimulation 145
5.14 Distribution of tuning bandwidths, with and without S1 and V2 stimulation 146
5.15 Changes in bandwidth observed with S1 and V2 stimulation 147
5.16 Examples of noise-driven spike counts affected by optogenetic activation of V2 149
5.17 Examples of noise-driven spike latencies affected by optogenetic activation of V2 151
5.18 Graphical summary of response and latency changes 153

Chapter 1

Introduction

One of the central concerns in neuroscience, particularly the study of the mammalian cortex, is the spatial variation in response properties and connectivity within a given brain region. Such topography offers important clues as to the function of the myriad, densely intertwined networks which control complex organisms. Particularly in the auditory system, cortical organisation remains a hotly contested subject. For example, there is ongoing discussion concerning the extent to which 'what' and 'where' processing (Bizley and Walker, 2009) and pitch processing (Wang and Walker, 2012) are spatially localised. Even within primary areas, beyond 'tonotopy', the highly conserved, systematic variation of frequency tuning across the cortex, the organisation of other stimulus features is much less certain (see section 1.1 below).

Although the mouse is now well established as a model for research into auditory cortical topography (Stiebler et al., 1997; Rothschild et al., 2010; Christianson et al., 2011; Hackett et al., 2011), certain fundamental, organisational assumptions remain little-studied, even controversial. These include the precision and reproducibility of tonotopic maps

(e.g. compare Bandyopadhyay et al., 2010 and Guo et al., 2012) and the underlying differences between the two primary cortical fields that have been described in this species (Linden et al., 2003; Llano and Sherman, 2008; Horie et al., 2013). In this thesis, I contribute clarifying observations to each of these questions.

With its practical advantages and available genetic tools, the mouse is nonetheless an attractive system for investigating topics at the forefront of cortical physiology, such as the interaction of neuronal populations and networks defined by their genetic identity, their spatial location, their projection profile, or a combination of such parameters (e.g. Letzkus et al., 2011; Little and Carter, 2012; Moore and Wehr, 2013; Chen et al., 2013). One such interaction receiving widespread recent interest is that of direct cross-talk between sensory areas which were originally considered unimodal (Cappe and Barone, 2005; Budinger et al., 2006; Bizley et al., 2007; Campi et al., 2010; Iurilli et al., 2012). The third question addressed below is the degree to which inputs from other sensory areas target neurons, and influence processing, within the mouse auditory cortex.

1.1 Functional architecture of the auditory cortex

Despite the modular nature of the cortex, whereby most areas share a laminar, if not necessarily columnar, structure (Linden and Schreiner, 2003), similarities between the organisation of auditory cortex and other modalities are limited (Read et al., 2002). The defining characteristic of primary auditory areas is a gradient of frequency tuning, inherited from the thalamus and originally the cochlea (Merzenich et al., 1975); this readily bears comparison with retinotopy in the visual system, though even the fidelity of thalamocortical receptive field transmission appears to be lower in the auditory case (Miller et

al., 2001, 2002). Other dimensions of organisation have proved elusive, and despite early indications to the contrary (e.g. Imig and Adrián, 1977) and some evidence of clustered response properties such as binaural category (e.g. Kelly and Sally, 1988; Kelly and Judge, 1994) and tuning bandwidth (Read et al., 2001), no clear equivalent has emerged of ocular dominance or orientation columns.

At the larger scale of defining cortical fields, reports from all mammals studied have described at least one primary or 'core' area, exhibiting typically well-tuned responses with short latencies, and other non-primary or 'belt' areas where responses are more variable (sometimes with the addition of 'parabelt' areas, particularly in primates: Kaas and Hackett, 1998). This includes studies of the auditory cortex of mice (Stiebler et al., 1997), rats (Sally and Kelly, 1988), gerbils (Thomas et al., 1993), prairie voles (Campi et al., 2007), guinea pigs (Redies et al., 1989b), ferrets (Bizley et al., 2005), cats (Downman et al., 1960), monkeys (Merzenich and Brugge, 1973) and humans (Talavage et al., 2000; Zatorre et al., 2002). An overview of auditory cortical maps in the macaque, cat, ferret and mouse is shown in figure 1.1.

The number and characteristics of belt areas vary between species, but most receive projections from the primary auditory cortex (A1) as well as from the dorsal division of the medial geniculate body (MGBd; reviewed by Lee, 2013). Many species also have more than one primary area, as identified by tonotopic maps of frequency tuning and direct inputs from the ventral MGB (MGBv). In particular, rodents (Horikawa et al., 1988; Thomas et al., 1993; Stiebler et al., 1997; Wallace et al., 2000), cats (Merzenich et al., 1975; Knight, 1977) and ferrets (Kowalski et al., 1995) display two tonotopic primary fields, commonly referred to as A1 and AAF (the anterior auditory field).

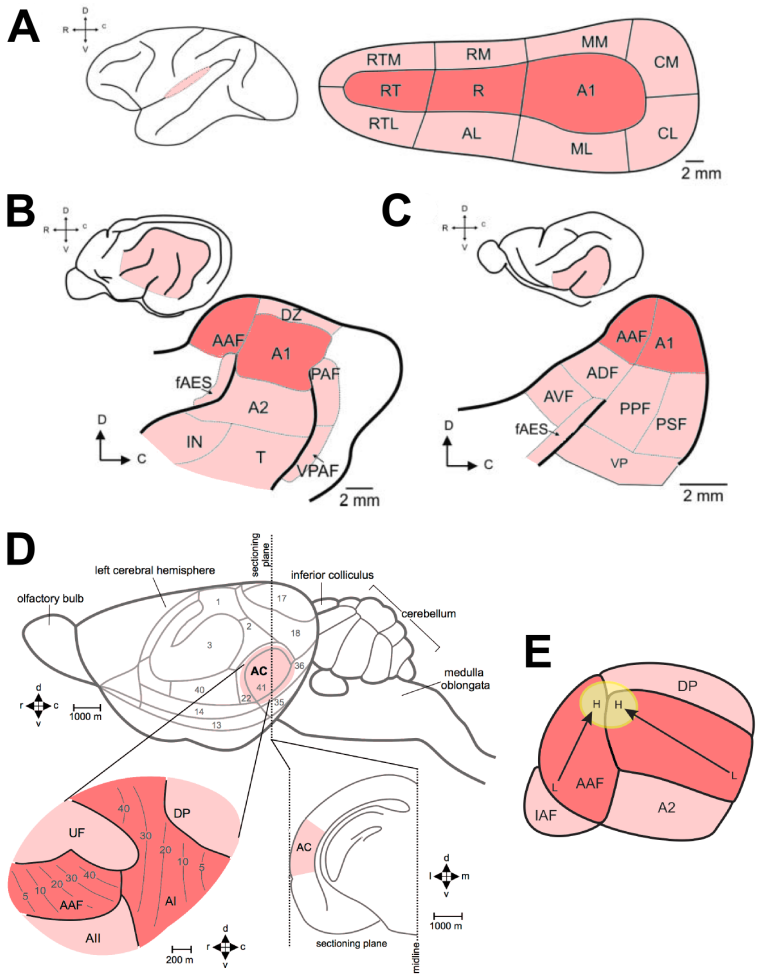


Figure 1.1: **Organisation of mammalian auditory cortex.** Illustrations of the location and gross functional organisation of the auditory cortex, as reported in the macaque (***A***), cat (***B***), ferret (***C***) and mouse (***D***, ***E***). Core fields are highlighted in dark pink. ***D*** includes an illustration of a coronal section containing auditory cortex (bottom right) and the map of mouse subfields originally described by Stiebler (1987b,a), including approximate position of isofrequency bands (frequencies labelled, in kHz). ***E*** is the updated map of mouse auditory cortex proposed by Guo et al. (2012), in which the ultrafrequency (UF) region is absorbed into the high-frequency portion of the tonotopic fields AAF and A1 (H, highlighted in yellow; low–high frequency gradients are indicated by arrows) and an additional insular field (IAF) is added, as described by Sawatari et al. (2011). Note that ***A***–***E*** depict the left cortical hemisphere, with rostral to the left; all figures in chapters 3 and 4 show the right hemisphere, with rostral to the right. Abbreviations: AC = auditory cortex; A1 = primary auditory field; R = rostral field; RT = rostral temporal field; CM = caudomedial belt; CL = caudolateral belt; ML = mediolateral belt; AL = anterolateral belt; MM = mediomedial belt; RM = rostromedial belt; RTM = rostrotemporal medial belt; AAF = anterior auditory field; PAF = posterior auditory field; VPAF = ventral posterior auditory field; A2 = secondary auditory field; fAES = anterior ectosylvian sulcal field; IN = insular; T = temporal; PPF = posterior pseudosylvian field; PSF = posterior suprasylvian field; ADF = anterior dorsal field; AVF = anterior ventral field; VP = ventral posterior field; DP = dorso-posterior field; IAF = insular auditory field. Figures adapted from Bizley and Walker (2010, ***A***–***C***); Geissler and Ehret (2004, ***D***); Guo et al. (2012, ***E***).

1.2 A pair of primary fields

Since a tonotopic gradient was first reported anterior to cat A1 by Merzenich et al. (1975), and Knight (1977) subsequently coined the term AAF, these two primary subfields have predominantly been viewed as the cortical manifestation of two parallel, tonotopic processing streams (e.g. Lee et al., 2004). Both receive direct, tonotopic thalamocortical inputs (Andersen et al., 1980; Budinger et al., 2000; Llano and Sherman, 2008; Lee and Winer, 2008a), and it is likely that the populations of projecting cells occupy overlapping regions within MGBv, even if single cells projecting to both subfields are a rarity (Kishan et al., 2008).

The tonotopic maps of A1 and AAF are well established in thalamorecipient layers, which in the auditory cortex include deep layer 3 as well as layer 4 (e.g. Hashikawa et al., 1995; Anderson et al., 2009). In the mouse, these maps share a high-frequency border, resulting in a 'reversal' of tonotopy on the rostrocaudal axis, which is often used to delineate the boundary between the two subfields (e.g. see figure 3.8). The degree to which this organisation decays outside those middle layers is debated, particularly in mice (compare Guo et al., 2012 with Winkowski and Kanold, 2013).

Precisely how much the two primary areas differ physiologically, and why, remains something of an open question. Some observations appear to generalise across species, most notably shorter response latencies in AAF than A1 (e.g. Kowalski et al., 1995; Eggermont, 1998; Rutkowski et al., 2003; Bizley et al., 2005). This has led to the suggestion that AAF may be specialised for faster temporal processing (see Linden et al., 2003, a study comparing spectrotemporal receptive fields between A1 and AAF in the mouse). Several studies have compared pure-tone response characteristics of the two fields, such

as threshold and bandwidth (Knight, 1977; Thomas et al., 1993; Kowalski et al., 1995; Rutkowski et al., 2003; Imaizumi et al., 2004; Bizley et al., 2005; Polley et al., 2007; Guo et al., 2012). In these cases there is no consensus regarding A1–AAF differences — and even the observation of shorter latencies in AAF has not always been replicated (Knight, 1977; Polley et al., 2007; Profant et al., 2013).

1.3 Mouse maps: a brief history of increasing complexity

The mouse auditory cortex was first mapped in 1987 (Stiebler, 1987a,b), with little further electrophysiology reported until the same first author published a landmark series of mapping experiments ten years later (Stiebler et al., 1997). These early studies described the two tonotopic fields of A1 and AAF, an adjacent ultra-frequency region (UF) which the authors suggested might be specialised for processing mouse vocalisations, and two belt areas (the secondary auditory field A2, and dorsoposterior field DP; see figure 1.1D). In the 1997 publication, Stiebler et al. highlighted differences between the auditory cortex in the left and right hemisphere (left auditory cortex, in the five examples the authors mapped extensively, covered a larger cortical area on average) as well as variations in the size and location of auditory cortical fields between individual mice.

More than another decade later, the first two long-awaited reports of two-photon *in vivo* imaging in mouse auditory cortex were published simultaneously (Rothschild et al., 2010; Bandyopadhyay et al., 2010). Both reported that tonotopy, so central to our understanding of auditory cortical organisation, was barely recognisable among layer 2/3 responses viewed at single-cell resolution. In each set of observations, a frequency gradient was sometimes present at much larger scales, but neighbouring neurons in A1 were

unlikely to be similarly tuned. In superficial layers at least, frequency tuning produces nothing like the fine-scale maps observable in visual cortex using the same technique (Ohki et al., 2006).

This challenge to the pre-eminent status of tonotopy as an organising principle was countered by two subsequent publications, which returned to extracellular recordings in middle cortical layers, as used by Stiebler et al. (1997). Sampling these layers of the mouse cortex more densely than previous electrophysiological work, Hackett et al. (2011) reported precise frequency maps in both A1 and AAF, underpinned by tonotopically organised projections from MGBv. Guo et al. (2012), using the same single-channel recording strategy, specifically measured pure-tone tuning across the extent of mouse auditory cortex and reported finely structured frequency maps; this latter study also argued that such organisation was robust across different anaesthetic states, different cortical layers and even different types of electrophysiological signal (e.g. multi-unit activity *vs.* local field potentials).

By contrast, when Winkowski and Kanold (2013) extended *in vivo* imaging into thalamorecipient layers 3b and 4, they reported substantial laminar variation: the deeper cells showed more homogeneous frequency representation and higher stimulus-correlated spiking activity, compared to those in superficial layers. As the authors suggest, this is consistent with a "laminar transformation" of auditory information, by which frequency organisation becomes less important as signals traverse the cortical layers and more integrative analysis takes place.

Still further complexity was recently added to this picture by the same laboratory, in experiments which demonstrated rapid plasticity of A1 receptive fields in mice, triggered either by frontal cortex stimulation (Winkowski et al., 2013) or by dark exposure (Petrus

et al., 2014). Altogether, the organisation of auditory response properties in the mouse cortex remains an active research question, where some findings are at odds with others, as well as with previously accepted principles. Certainly, straightforward topographic inheritance of frequency tuning from the thalamus, particularly outside the middle layers, cannot be assumed.

1.4 Multisensory activity in early cortical areas

Even in middle layers of the cortex, only a tiny fraction of synapses are thalamocortical (in the order of 5%; reviewed by Douglas and Martin, 2007). When Binzegger et al. (2004) endeavoured to quantify the synaptic network of primary visual cortex (V1) in the cat, they coined the phrase 'cortical dark matter' to describe the surprisingly large proportion of synapses that could not be accounted for by thalamic afferents or established types of local connection. Although the vast majority of cells labelled by cortical injections of retrograde tracers tend to reside within the same area as the injection site (Vezoli et al., 2004), long-range, inter-areal inputs from distributed cortical sources are likely to be a major contributor to this 'dark', certainly under-explored, body of connectivity (Douglas and Martin, 2007). In the past decade, the suggestion that some of these inputs support cross-talk between sensory modalities has attracted considerable attention (e.g. Schroeder and Foxe, 2005; Cappe and Barone, 2005; Ghazanfar and Schroeder, 2006; Bizley and King, 2009; Budinger and Scheich, 2009).

That research has been driven partly by physiological evidence that early sensory areas, such as V1 and A1, exhibit responses with multisensory characteristics. These do not necessarily take the form of spiking responses to stimulation of a different sensory sys-

tem, although some such reports do exist: Bizley et al. (2007), for example, described a small proportion of single units in ferret A1 and AAF which responded to visual stimulation alone, while Kobayasi et al. (2013) recently made a similar observation for a very small number of gerbil A1 units.

Evidence is more common for sub-threshold interactions, whereby multi-modal stimulation increases, decreases, synchronises, or alters the selectivity of neuronal responses compared to the unimodal condition. For example, after two different groups (Schroeder et al., 2001; Fu et al., 2003) demonstrated somatosensory responses in the caudo-medial region of macaque auditory cortex (adjacent to A1 but non-primary), a much-cited 2007 study (Lakatos et al., 2007) described 'phase-resetting' of ongoing oscillations in A1 itself, by concurrent cutaneous–auditory stimulation. The authors suggested that this synchronisation of ongoing activity by cross-modal inputs could facilitate the auditory response. Visual stimulation, particularly during face and voice processing, has also been shown to modulate local field potentials (LFPs) in macaque A1 (Ghazanfar et al., 2005). A visual contribution to speech processing in human auditory cortex has also been reported, using both magneto-encephalography (MEG, Sams et al., 1991) and functional magnetic resonance imaging (fMRI, Calvert et al., 1997).

In rodents, apart from the recent report of visual integration in gerbil A1 mentioned above (Kobayasi et al., 2013) and an earlier demonstration that auditory responses are surprisingly widespread in the cerebral cortex of the prairie vole, including V1 (Campi et al., 2007), a landmark publication in 2012 (Iuirilli et al.) described sound-evoked, inhibitory field potentials and whole-cell currents in mouse V1. In a brief exploratory experiment, those authors also recorded hyperpolarisation of auditory cortical neurons by whisker stimulation (see their figure 3, p. 819); beyond this report, multisensory activity in the

mouse auditory cortex *in vivo* is yet to be characterised.

1.5 Cortico-cortical connectivity

These previously unexpected cross-modal responses entail the convergence of information from different modalities, and this convergence has several possible anatomical substrates (see reviews by Smiley and Falchier, 2009; Cappe et al., 2009; Budinger and Scheich, 2009). Besides the more orthodox explanation of feedback from higher-order cortical areas, or crossover connections from other sensory thalamic nuclei, recent research suggests a contribution from direct, cortico-cortical connections between early sensory areas. In the interest of brevity, in this thesis I refer to connections of this sort as early, cortico-cortical, cross-modal (ECC) inputs; note that I include secondary fields such as V2 and A2 among 'early' areas, though I am most interested in connections that target primary areas.

The first strand of evidence supporting this type of connectivity is anatomical. Within the auditory system, for example, tract-tracing experiments in macaques have revealed a direct input to core auditory cortex from S2 (Cappe and Barone, 2005) and to caudal auditory cortex from V2 (Falchier et al., 2010). Similar work in the ferret, coupled with electrophysiological recordings, revealed projections from V1 direct to primary areas A1 and AAF, as well as between other early visual and auditory areas (Bizley et al., 2007). Rodents also appear to possess ECC projections into primary auditory cortex, as demonstrated by tracing experiments in the prairie vole, describing connections from both V1 and S1 (Campi et al., 2010), and a thorough catalogue of inputs to gerbil A1 (Budinger et al., 2006), which particularly identified connections from S1 and V2. One study in the mouse (Banks et al.,

2011) has also described a direct connection from V2 to A1.

Secondly, some studies (including some of the above) have begun to explore the neurophysiological activity of ECC connections. Bizley and King (2009) observed that the relative abundance of visual cortical projections to the various subfields of ferret auditory cortex broadly matched the prevalence of visual responses in those areas. Banks et al. (2011) showed that the magnitude of calcium transients, driven in acute slices of mouse A1 by electrical stimulation of the underlying white matter, could be modulated by concurrent stimulation of lateral V2 (these experiments are discussed further in section 5.2.5). Perhaps the most direct implication of ECC projections in sensory processing comes from the *in vivo* mouse experiments of Iurilli et al. (2012), who showed that the noise-driven hyperpolarisations they recorded in V1 could be abolished either by pharmacological silencing of the auditory cortex, or by severing the intervening cortical connections.

There is much potential for further exploration of these relatively novel sensory pathways in the mouse. Alongside the anatomical and physiological evidence, outlined above, suggesting that multisensory activity and ECC connectivity are present in rodents, there is the promise of behavioural experiments in which the contribution of multisensory cues is measurable (see Gleiss and Kayser, 2012, a study in which rats showed improved performance and shorter reaction times when the stimuli presented in a forced-choice task were audio-visual rather than unimodal). Importantly, mice represent a tractable experimental system in which long-range connections can be selectively measured and manipulated, and those observations can be linked to behaviour (e.g. Chen et al., 2013).

A first step will be to describe the anatomy and activity of ECC inputs to the mouse auditory cortex. Although connections from auditory to visual cortices in the mouse have been demonstrated anatomically (Laramée et al., 2011, 2013) and physiologically (Iurilli

et al., 2012, described above), and one study has supplied evidence of projections from V2 to A1 (Banks et al., 2011), no wider exploration of cortical inputs from other senses into mouse auditory cortex has been published, and their physiological effects — if any — on auditory processing remain to be demonstrated.

1.6 Classifying cortical projections

When describing the connections made between one brain region and another, different schemes of classification are available. Murray Sherman and colleagues pioneered the 'driver' *vs.* 'modulator' categorisation of glutamatergic pathways (now revised to 'class I' *vs.* 'class II'; for review, see Sherman and Guillery, 2011), originally to describe thalamocortical synapses (e.g. Sherman and Guillery, 1998) but later applied to cortico-cortical (e.g. Covic and Sherman, 2011) and cortico-thalamo-cortical connectivity (e.g. Theyel et al., 2010). This distinction is based principally on synaptic electrophysiology and morphology: driver inputs typically display thick axons with dense terminal arbours, targeting proximal dendrites and eliciting large EPSPs that undergo paired-pulse depression, while modulators consist of sparse axonal arbours that target distal dendrites and elicit smaller, facilitating EPSPs.

A more long-standing categorisation, which is specific to cortico-cortical networks, is that of feedback *vs.* feedforward connections (e.g. Rockland and Pandya, 1979; Maunsell and Van Essen, 1983), sometimes expanded to include a lateral category (e.g. Van Essen et al., 1990; Felleman and Van Essen, 1991). This system was proposed in order to facilitate a hierarchical classification of areas within the primate neocortex, based largely on anatomical evidence from tract-tracing studies. The scheme, based on the laminar

distribution of projecting cells and their axonal terminals, is illustrated in figure 1.2 (reproduced from Felleman and Van Essen, 1991).

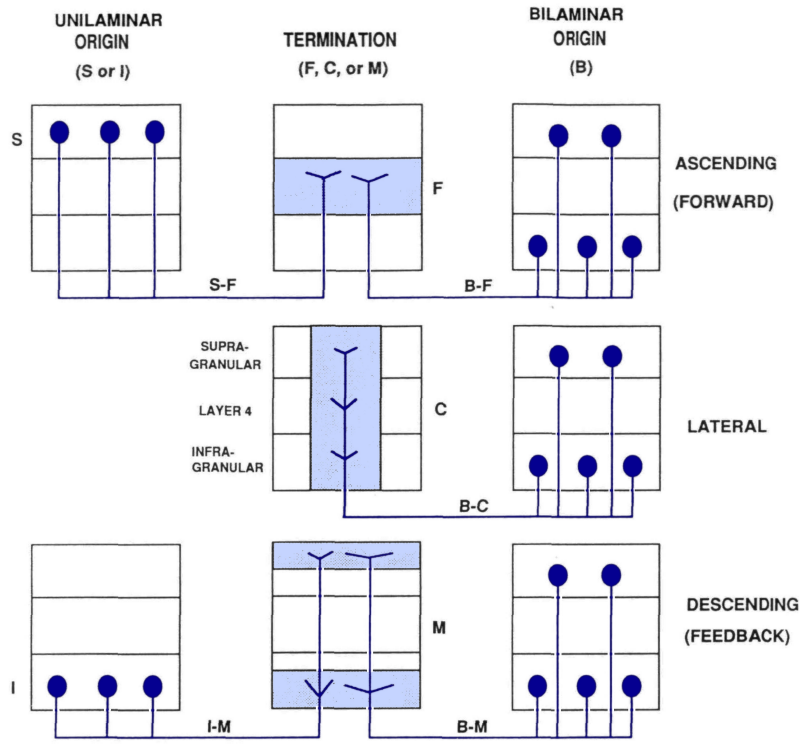


Figure 1.2: **Hierarchical classification of cortico-cortical connectivity.** Diagram summarising the characteristic laminar patterns of origin and termination observed by Van Essen and colleagues (Maunsell and Van Essen, 1983; Van Essen et al., 1990; Felleman and Van Essen, 1991) in the connections between different visual areas in the macaque cortex. This scheme was used to assign each area's position in a hierarchical processing stream and has subsequently been generalised to other cortical pathways. Projections may terminate preferentially in layer 4 (pattern F), avoid layer 4 ('multilaminar' pattern M) or spread across all layers ('columnar' pattern C), as observed using anterograde axon tracing. Cells of origin, identified by retrograde labelling, can show a supragranular (S), infragranular (I) or bilaminar (B) distribution. The authors classified S and F patterns as ascending or feed-forward, I and M patterns as descending or feedback, and C as lateral; all types of connection may be bilaminar (B) in origin. Figure reprinted from Felleman and Van Essen (1991).

Upon the initial investigation of a pattern of connections — for example, when inputs to a particular area are traced using retrograde labelling of cell bodies — the latter classification is the more straightforward distinction to make, since, as illustrated in figure 1.2, the laminar distribution of projecting cells offers an indication of whether the connection

is predominantly feedforward or feedback in structure. Budinger et al. (2006) performed just such experiments to describe the range of connections received by A1 in the Mongolian gerbil, and defined a 'layer index' to quantify that laminar distribution (for more detail, see section 5.2.4).

1.7 Scope of this thesis

In the chapters that follow, I explore two questions relating to the internal topography of the mouse auditory cortex and one relating to its long-range cortical inputs.

As discussed above, the mouse auditory cortex is a useful experimental model but one in which several fundamental characteristics are surprisingly uncertain. The principle of tonotopic organisation is under ongoing discussion (see section 1.3), and the difference between the two primary subfields A1 and AAF is scarcely described (see section 1.2). In particular, little previous work has made use of multi-site recording arrays, configured to sample activity simultaneously from different cortical layers. I contribute data to both of these topics, from extensive multielectrode recordings and some limited anatomical tracing experiments.

Finally, the rapidly expanding field of cortico-cortical, cross-modal connectivity is not yet thoroughly reported in the case of mouse auditory cortex. I seek anatomical evidence for such inputs from both visual and somatosensory areas, and begin to test, for the first time, whether and how non-auditory sensory cortices influence auditory cortical processing, using optogenetic activation *in vivo*.

1.7.1 Specific objectives

This thesis sets out to meet the following aims:

1. Describe the extent and organisation of frequency tuning in the mouse auditory cortex, including whether the degree of tonotopic organisation varies across different cortical layers, or between different types of neurophysiological signal (multi-unit spiking responses *vs.* local field potentials) and auditory stimulus (pure tones *vs.* dynamic random chords).

2. Compare the response properties of, and the inputs received by, the two primary fields A1 and AAF.

3. Identify which other sensory areas, if any, send ECC connections to these fields.

4. Test whether activity in non-auditory sensory areas can influence responses within primary auditory areas.

Chapter 2

Materials and Methods

All animal procedures were performed under license from the UK Home Office in accordance with the Animal (Scientific Procedures) Act 1986, and subject to local ethical review. *In vivo* recordings and *in vitro* preparations were conducted in rooms appropriately designated for rodent experiments.

2.1 Numbers and strains of mice

For the *in vivo* optogenetic experiments reported in section 5.4, I performed virus injections (described in section 2.5.1 below) and *in vivo* recordings (section 2.2) in 9 C57BL/6 mice. I have presented data from the same 9 mice, in the absence of optogenetic stimulation, for the investigation of tonotopy presented in chapter 3 and the electrophysiological comparison of A1 and AAF in sections 4.2 and 4.3.

A further 20 mice received similar virus injections; in these cases I performed less extensive or unsuccessful electrophysiological recordings, or (in 4 cases) perfused the an-

imals directly for histology and fluorescence microscopy (e.g. section 5.3.1).

Additionally, I performed pilot *in vivo* optogenetic experiments on 3 transgenic mice expressing ChR2 under the Thy1 promoter (strain 'Thy1-COP4/EYFP', The Jackson Laboratory, Bar Harbor, ME). These experiments are briefly mentioned in chapter 5 (see section 5.4), as is a set of *in vitro* experiments in acute slices. For the *in vitro* experiments I used a larger number of mice, including 28 with V2M injections and 31 with V2L injections.

For the retrograde tracing described in sections 4.4 and 5.2, I made tracer injections guided by electrophysiology (see section 2.4.1 below) into the auditory cortex of 6 C57BL/6 mice. Earlier, pilot anatomy work included injections of biotinylated dextran amine (BDA) into a further 3 mice; I later abandoned BDA in favour of the specific retrograde tracers Fluoro-Gold (FG) and cholera toxin B (CTB).

2.2 *In vivo* recordings

This section describes the procedures followed for *in vivo* recordings from auditory cortex. Specifically, the protocol below applies to the auditory response data reported in chapters 3–4 and the optogenetic data in section 5.4, which were recorded from C57BL/6 mice between 10 and 12 weeks of age, at least 4 weeks after viral gene delivery (see section 2.5.1). The recordings I used to guide tracer injections for section 5.2 were conducted in the same manner, except for the differences noted in section 2.4.1.

2.2.1 Anaesthesia and surgery

After inducing anaesthesia with an initial, intraperitoneal (IP) injection of ketamine (100 mg kg^{-1}) and medetomidine hydrochloride (0.3 mg kg^{-1}), I placed a cannula for continuous IP delivery of 2.5 mg mL^{-1} ketamine, by an infusion pump (Graseby 3I00, Smiths Medical, Kent). This delivery was usually commenced 1.5–2 hours after induction, at a rate of 0.2–0.4 mL per hour, which equates to 25–50 mg kg^{-1} ketamine, hourly. Approximately every 1.5 hours, a top-up dose of 0.03 mg kg^{-1} medetomidine was injected IP. I adjusted this timing and the infusion delivery rate, based on observation of the animal (e.g. breathing rate and paw-pinch reflex). All anaesthetics were diluted in physiological saline and core temperature was measured and maintained using a DC temperature controller and heating blanket (FHC, Bowdoin, ME). Prior to induction, animals also received a subcutaneous injection of 6 μg atropine sulfate to reduce bronchial secretions and 20 μg dexamethasone to reduce cerebral oedema.

I fixed the head of the mouse in position using the tooth-bar and rubberised ear bars in a stereotaxic frame (Stoelting Europe, Ireland), with the ear bars positioned rostral from the animal's ear canals so as to hold the skull stable while not obstructing hearing. After retracting the muscle over the temporal surface of the skull, I performed a craniotomy some 1.5–2 mm in diameter over auditory cortex. Rather than stereotaxic coordinates, the craniotomy position was based on morphological characteristics of the skull, such as the temporal ridge and the lambda and squamosal sutures (based on information provided by J. Garcia-Lazaro and J. Linden).

2.2.2 Data acquisition

Extracellular neurophysiological signals were recorded with serial penetrations of a 64-channel, 8-shank silicon probe electrode ('A8x8', shank and site spacing 200 μm; NeuroNexus, Ann Arbor, MI), and amplified and digitised at a sample rate of 25 kHz using Z-series hardware by Tucker Davis Technologies (Alachua, FL) including 'Z64' ZIF-Clip headstage, PZ2-64 preamp and RZ2 base station. Signal recording and stimulus presentations were handled by BrainWare software (developed by J. Schnupp in this laboratory) and subsequent analysis performed in MatLab (MathWorks, Natick, MA) as outlined below.

2.2.3 Stimuli: calibration and delivery

I presented sounds in free field conditions, in a sound-attenuated chamber where the surgery was also performed. I used a dynamic ultrasonic speaker and amplifier ('Vifa' and 'UltraSoundGate Player', Avisoft Bioacoustics, Berlin). The speaker was positioned approximately 15 cm from the contralateral ear; prior to experiments, the speaker was calibrated using a Bruël and Kjær (Nærum, Denmark) Type 4138 1/8-inch pressure-field microphone, placed in the same position as the mouse's ear. The frequency response of the speaker was measured and an inverse filter calculated, to flatten the frequency response to within 3 dB in the range 1–80 kHz.

2.2.4 Stimuli: noise bursts and pure tones

Stimuli, generated using an RX6 MultiFunction Processor (TDT, Alachua, FL), included 5 ms bursts of broadband Gaussian noise, and 100 ms pure tones (5 ms rise/fall time,

cosine ramps). Responses to at least 50 noise bursts were recorded, in sweeps of at least 300 ms duration. Pure tones ranged in frequency from 4 to 64 kHz, in 1/6-octave steps, and their intensity varied from 8 to 56 dB SPL, in 8 dB steps. I presented 200 frequency-level combinations in total (25 frequencies, 8 sound levels), which were pseudorandomly interleaved in sweeps of at least 500 ms duration. Each combination was presented at least 3 times alone and 3 times in conjunction with photostimulation of either V2M or S1 (see section 2.5.3 below).

2.2.5 Stimuli: dynamic random chords

Dynamic random chords, or DRCs, were generated largely as described by Rabinowitz et al. (2011). The component tone pulses were drawn from the same 25 frequencies used for pure tone stimulation (i.e. 4 to 64 kHz in 1/6 octave intervals). Chords of 25 ms duration were built from these frequencies, with the level of each frequency drawn from a uniform distribution spanning 25–55 dB SPL. I presented two sequences of chords, each lasting 40 seconds, and repeated each sequence at least 10 times for each recording penetration. A spectrogram illustrating the DRC stimulus paradigm, in comparison with pure tones, is shown in chapter 3 (figure 3.16).

2.3 Electrophysiological data analysis

2.3.1 Signals: multi-unit activity and local field potentials

Peaks which exceeded background noise by a factor of 1.5 to 2 (adjusted during recordings based on visual inspection of the raw signal and spike trains) were recorded as spikes. All

responses from one animal were subjected to spike sorting, with multi-unit clusters cut in BrainWare based on the similarity of spike shapes. (From the absence of obvious refractory periods in their autocorrelation histograms, nearly all clusters were assumed to be multi-unit clusters rather than single units.) This cluster cutting neither increased the number of sites exhibiting stimulus-driven activity, nor made any discernible improvement to the quality of pure-tone responses, viewed as frequency response areas (FRAs). As a result, the entire data set was not spike-sorted, and throughout my thesis I refer to the recorded signals as multi-unit activity (MUA).

To isolate the local field potential (LFP), the raw signal (acquired at 25 kHz) was decimated by a factor of 8, low-pass filtered with a Chebyshev type 1 filter (0.05 dB ripple in passband, 300 Hz cut-off) and finally downsampled to 1 kHz.

2.3.2 Estimating cortical depth

I estimated the cortical depth of recording sites based on LFP responses to noise bursts and previous descriptions of the patterns observed in such responses across different cortical layers, notably the work of Christianson et al. (2011). In particular, a reversal in the polarity of the LFP is seen at approximately the layer 1/2 border, 100-150μm below the pia. This reversal, described in the cortex of various species (including the auditory cortex of cats and rats, respectively: Kral et al., 2000; Szymanski et al., 2009), corresponds to a shift in the distribution of inward and outward current flow across neuronal membranes (current sinks and sources) and can be used to perform current source density analysis (Mitzdorf, 1985).

In the case of my experiments, locating the LFP reversal at a single channel position,

or between two channels, on each electrode shank, together with observing the position of the pia relative to the uppermost electrode channels, allowed me to assign estimated depths to each site (an illustration of this method appears in chapter 3; see figure 3.1). In some cases, this confirmed that the electrode penetration, even though orthogonal to the cortical surface, had distorted the surface such that all shanks were not at the same depth. Consequently the layer assignations sometimes varied between shanks within a single penetration, such as in the cases presented in figures 3.2 and 3.17.

2.3.3 Multi-unit responses to noise bursts

To assess the noise-driven spiking responses recorded at each site, I calculated a peri-stimulus time histogram (PSTH), in 5 ms bins, from the spike times recorded during at least 50 presentations of 5 ms noise bursts. To categorise sites as 'noise responsive' (for example, in the quantification of auditory responses described in section 3.3), I first calculated the mean spontaneous spike-rate, μ_s, for each site, from a 50 ms period prior to stimulus delivery. If any 5 ms bin in the 100 ms following the stimulus exceeded a threshold of $\mu_s + 4\sigma_s$ (where σ_s is the standard deviation of the spontaneous rate μ_s), I categorised the site as responsive to noise. Use of this threshold showed good agreement with visual assessment of responsive and unresponsive histograms. To compare the strength of activity among responsive sites (e.g. figures 4.2, 4.5), I used the spike-rate indicated by the largest peak in each PSTH.

2.3.4 Frequency response areas from pure tone responses

I calculated frequency response areas (FRAs) for each site in a standard manner, quantifying the mean spike counts within a post-stimulus response window, for each frequency–level combination. The response window was chosen for each penetration based on visual inspection, with the aim of including the entire initial response, visible in PSTHs pooled across stimuli (see discussion of response timing in section 3.7). The best frequency (BF) at a given site was determined from the FRA, as the frequency eliciting the strongest response after summing spike counts across all sound levels.

Tuned *vs.* untuned categorisation

To classify a recording site as tuned or untuned to pure tones, I tested whether the responses varied with sound frequency, by grouping its responses to every neighbouring pair of tone frequencies. Halving the number of frequency bins in this manner, and then grouping responses further across the highest 4 sound levels and all stimulus presentations (typically 4 or 5), allowed me to perform a one-way ANOVA on the resulting sets of ~32-40 spike counts. Sites which showed a significant effect of frequency in this test ($p \leq 0.05$) were classified as frequency-sensitive. As discussed in section 3.2.2, for convenience, I refer to these sites as being 'tuned', even if a clear peak, bordered on either side by lower responses, could not be discerned in the firing rate–sound frequency function.

Calculating d' as an indicator of frequency sensitivity

I used the same grouping to quantify the strength of each site's frequency preference (see section 3.3.2). I calculated the discriminability (d') of the grouped responses to each site's

best and worst pair of frequencies. If the means and standard deviations of those best and worst groups are μ_B, μ_W and σ_B, σ_W respectively, d' is calculated as follows:

$$d' = \frac{\mu_B - \mu_W}{\sqrt{\frac{1}{2}(\sigma_B^2 + \sigma_W^2)}}$$

Smoothing and CF calculation

To calculate further parameters of pure-tone responses, including characteristic frequency (CF) for comparison with BF (see section 3.2.3), the raw spike counts comprising each FRA were smoothed, using sliding iterations of a 9-point window to calculate weighted averages (see Sutter and Schreiner, 1991; Bizley et al., 2005). The window entailed factors of 0.5 for vertical and horizontal neighbours and 0.25 for diagonal ones. I evaluated the effect of such smoothing on the degree of frequency tuning observed and the resulting BFs (see figure 3.2 and discussion in section 3.2.2).

While I elected to use raw spike counts and straightforward BF calculations for the bulk of my neurophysiological analysis (particularly the investigation of tonotopy in chapter 3), these smoothed FRAs enabled me to compute additional values such as CF, threshold and bandwidth, by placing a boundary on the tuning curve revealed by each FRA (if any). As the threshold for this boundary, I took the site's mean spontaneous spike-rate + 20% of its peak, stimulus-driven rate, as described by Sutter and Schreiner (1991) and Bizley et al. (2005). Examples illustrating how CF, threshold and bandwidth were derived from this boundary appear in the chapters that follow (specifically, CF in figure 3.3; threshold and bandwidth in figure 5.11).

2.3.5 Spectrotemporal receptive fields from DRC responses

From the spiking activity recorded in response to the two 40 s blocks of DRCs, I calculated a spectrotemporal receptive field (STRF) for each recording site, largely in the manner described by Rabinowitz et al. (2011). The PSTH was binned at 25 ms, to match the temporal resolution of the DRC, and correlated with the stimulus history over the preceding 400 ms. This was used to produce a maximum likelihood estimate of the STRF. I tested the ability of this model receptive field to predict spiking activity over a held-out dataset, comprising 10% of the DRC response that was not used to fit the STRF. The predictive performance of this model was measured as the percentage of signal power explained by the STRF on the held-out dataset (SP_{exp}). This is a corrected version of explained variance, which compensates for the variability in response observed across repeats (see Sahani and Linden, 2003; Rabinowitz et al., 2012).

Since the maximum likelihood estimates of the STRFs contained a large number of parameters (25 frequency bins $\times$ 16 time bins + 1 constant = 401 free parameters), I also compared these results against a model that assumed that the STRF is separable in frequency and time (Linden et al., 2003). This reduced model contained only 42 free parameters (25 for the frequency kernel, 16 for the time kernel, 1 constant). However, the separable STRFs yielded poorer results in the predictive test. I therefore used the full, inseparable STRFs to characterise each site's responses to the DRCs.

As outlined in section 3.6, I set a threshold for a predictive STRF at SP_{exp}>0.1, which offered good agreement with visual classification of coherent STRFs. I then calculated a BF from each predictive STRF, based on the strength of responses in the 100 ms immediately preceding the spike bin.

2.3.6 Generating cortical maps

To draw maps of recording site locations, I took photographs of each penetration, then subsequently aligned and traced them using illustration software (www.inkscape.org). From these illustrations, I extracted x (rostrocaudal) and y (dorsoventral) coordinates for each shank position using a custom Matlab program (Grabit by Jiro Doke, www.mathworks.co.uk). By plotting best frequency (BF) against rostrocaudal position, and fitting a quadratic function to that plot, I then located the tonotopic reversal and placed a vertical (dorsoventral) boundary at that point to delineate A1 from AAF (for example, see figure 3.8). Boundaries between these core fields and the non-core areas in the rostroventral, caudoventral and dorsocaudal portions of auditory cortex (fields IAF, A2 and DP respectively), were positioned by observing shifts away from the tonotopic gradient or changes in other response characteristics, such as the magnitude and latency of responses to broadband noise bursts.

To describe the tonotopy present in each map, I separately correlated BFs from A1 and AAF with their position on a series of axes spanning 360° at 10° intervals. The best-correlated axis, based on its Pearson correlation coefficient, r, was taken as the orientation of the tonotopic gradient. The direction, strength and significance of these correlations could then be compared between different subfields and conditions (for example, see figures 3.9, 3.11).

2.4 Retrograde anatomical tracing

2.4.1 Tracer injections

To make injections of retrograde tracers into primary areas of the auditory cortex, I first made electrophysiological recordings similar to those described above. These experiments were brief (maximum duration 4 hours) and anaesthesia was maintained using periodic injections of the ketamine–medetomidine mixture (see section 2.2.1 above) rather than continuous IP infusion. For these recordings I also used a recording electrode with fewer shanks and more space in between them ('A4x8', shank spacing 400 μm, site spacing 100 μm; NeuroNexus, Ann Arbor, MI) and a lower-resolution grid of frequency–level combinations (4 sound levels separated by 10 dB steps; 21 frequencies spanning 1–64 kHz).

I performed electrophysiology-guided injections into 6 C57BL/6 mice, aged 7–8 weeks. After coarse mapping of the auditory cortex, I made either a single injection of FluoroGold (FG; Fluorochrome, Denver, CO) or two injections of cholera toxin B (CTB) with different fluorescent conjugates (CTB Alexa Fluor 488 or CTB Alexa Fluor 594, Molecular Probes, Eugene, OR). Based on rapid, online analysis of frequency tuning (performed in BrainWare), these injections were placed in the vicinity of well-tuned sites in primary areas. I aimed to inject a volume of 50 nL in each case, using marked intervals on small-bore injection pipettes. In practice, subsequent histology revealed variable injection volumes; of these 6 injections, 1 of the 2 using FG was too large to be confidently located exclusively within A1 and AAF, while 2 of the 4 CTB injection pairs were found to be too small or too close to the boundaries of A1 or AAF. In chapter 5, I present a detailed characterisation of one FG injection and one pair of CTB injections (see section 5.2).

2.4.2 Histological preparation of sections

After a survival period of 7–10 days, each injected mouse was given an overdose of sodium pentobarbital (240 mg kg^{-1}) prior to transcardial perfusion with phosphate buffered saline (PBS) and then 4% paraformaldehyde. The brain was removed and stored in 4% paraformaldehyde for at least 24 hours, then treated overnight in 30% sucrose solution to cryoprotect the tissue. (Paraformaldehyde and sucrose solutions were made up in PBS.) I cut 50 μm coronal sections from the injected brains using a freezing microtome, before washing and storing them in PBS.

Sectioned, FG-injected brains were treated using standard immunohistochemical methods. Briefly, the primary antibody (rabbit anti-FG, Fluorochrome, Denver, CO) was incubated overnight at 4°C (1:1000 in 5% normal goat serum) before further PBS washes, followed by secondary antibody incubation for 2 hours at room temperature (biotinylated goat anti-rabbit, 1:200, Vector Labs, Peterborough) and labelling with horseradish peroxidase (HRP; ABC kit, Vector Labs). Every second section was excluded from this treatment, but treated with DAPI and mounted instead for fluorescent microscopy using Vectashield mounting medium (Vector Labs).

Sectioned, CTB-injected brains were mounted for fluorescence microscopy using Vectashield mounting medium containing DAPI (Vector Labs).

2.4.3 Tracing of sections and labelled cells

To trace mounted sections and mark the position of retrogradely labelled cell bodies, I used Neurolucida software (MBF Bioscience, Williston, VT). I also outlined the injection site itself, including a ‘core’ region of densest labelling and a less dense ‘halo’ surrounding

it. Examining DAPI labelling, either in the same section or (for FG-injected, chromatically stained sections) in adjacent sections, enabled me to categorise labelled cells within the cortex as supragranular or infragranular. I estimated the boundaries of cortical areas (V1, S2, etc) based on the size of the granular layer, which is thicker in primary areas, and comparison of the sections with mouse brain atlases (Paxinos and Franklin, 2007; Rosen et al., 2000). Boundaries of MGB and its subdivisions were similarly estimated based on section morphology, viewed in brightfield and with the DAPI stain, in comparison with brain atlases and other published descriptions (e.g. Anderson and Linden, 2011; Llano and Sherman, 2008).

After mapping retrogradely labelled cells in the cortex and thalamus, I aligned the sections and made 3D reconstructions of each case using Neurolucida Explorer (MBF Bioscience).

2.5 Anterograde characterisation and optogenetics

2.5.1 Virus injections

To enable both (a) visualisation of projections sent by candidate areas (V2M and S1) to the auditory cortex, and (b) optogenetic stimulation of those candidate areas during *in vivo* and *in vitro* experiments, I used viral delivery of genetic constructs encoding Channelrhodopsin-2 (ChR2). The virus used for the experiments reported here was a serotype-2 adeno-associated virus (AAV2) containing the genes for both ChR2 and mCherry under the CaMKIIα promoter, which is known to drive strong transgene expression in excitatory neurons of the forebrain (e.g. Mayford et al., 1996). The virus, AAV-CaMKIIa-

hChR2(E123T/T159C)-mCherry, was packaged by the Vector Core Services at the University of North Carolina (www.genetherapy.unc.edu).

C57BL/6 mice, 6–8 weeks of age, were anaesthetised using 5% isofluorane and transferred to a stereotaxic frame (Stoelting Europe, Ireland), where a surgical plane of anaesthesia was maintained with 1.5–3% isofluorane, adjusted based on the animal's breathing rate. Under aseptic conditions, I made a small craniotomy above the cortical region of interest, based on stereotaxic coordinates measured from lambda and bregma (Paxinos and Franklin, 2007). The injection itself was performed with a Hamilton syringe and 32-gauge needle (Hamilton Bonaduz AG, Switzerland), manoeuvred to approximately 600 μm beneath the pial surface using a digital micromanipulator (Stoelting). I delivered approximately 500 nL of virus at a maximum rate of 100 nL min^{-1}. The needle was then left in place for 1 minute, withdrawn by 200 μm, left for a further 3 minutes and then slowly withdrawn from the brain. I sealed the wound using Vicryl sutures (Ethicon, NJ) and administered topical anaesthetic (lidocaine/prilocaine or EMLA, AstraZeneca, London) as well as IP injection of buprenorphine (0.05 mg kg^{-1}) and meloxicam (1 mg kg^{-1}), to minimise post-operative pain.

2.5.2 Optogenetic experiments *in vitro*

For the *in vitro* experiments outlined briefly in section 5.4, I used a standard acute slice protocol and optical stimulation methods similar to those reported for other work in the same laboratory (e.g. Kohl et al., 2011). I will not describe the procedures here, since those data are not presented in any detail below. This preparation was performed some 59 times, with limited success; for example, from the 28 preparations with ChR2 expression in area V2M, I obtained 49 adequate whole-cell recordings, of which 3 demonstrated light-

driven responses. It was felt that this success rate was too low to justify continuing with these experiments and that a better approach would be to focus on photostimulation of putative inputs to primary auditory cortical areas *in vivo*. The remainder of this section describes the procedures used for these *in vivo* experiments.

2.5.3 Photostimulation *in vivo*

At least 4 weeks after viral gene delivery, mice were anaesthetised and auditory cortical recordings performed as described in section 2.2. In addition, I performed a craniotomy over the injected area (V2M or S1) and delivered light from a blue LED to that area using an optical fibre, positioned on the surface of the cortex using a micromanipulator. The LED produced light of wavelength 463 nm with spectral bandwidth 28.1 nm, at an output power of 100–150 mW mm^{-2} at the fibre tip (LED, driver and fibre from Doric Lenses, Quebec). I tested the activity of ChR2 in each case with a single electrode penetration at the injection site, immediately adjacent to the optical fibre, which recorded spikes driven by pulses of the LED alone. These tests were usually performed with a single-shank electrode in order to minimise damage to the cortex; an example of such a recording made with a 64-channel probe, however, is presented in chapter 5 (see figure 5.10), and demonstrates that light-driven spiking activity was spatially restricted to the area of ChR2 expression.

During auditory cortical recordings, pure tones and noise bursts were presented either alone or, in randomly interleaved trials, in conjunction with an LED pulse over the injected area. In the case of the 5 ms broadband noise bursts, the LED pulse was 25 ms in duration and co-terminated with the noise, and LED-only trials were also included (these never elicited a spiking response in auditory cortex). In the pure tone case, the LED pulse was 50 ms in duration and commenced simultaneously with the 100 ms tone. The onset

and offset of the LED pulse produced a stimulus artefact, which could be eliminated from the recorded spike trains by excluding two corresponding 5 ms windows; I excluded these windows from both LED and control (tone- or noise-only) sweeps. The effect of the artefact on computed LFP traces, however, was more difficult to eliminate and so I have not presented LFP or CSD data from the photostimulation trials.

2.5.4 Fluorescence microscopy

To examine ChR2–mCherry expression in axons from candidate projecting areas, 4 mice injected as described in section 2.5.1 above were used for histological examination rather than *in vivo* experiments. These animals were perfused and their brains prepared as described in section 2.4.2. I then mounted sections in Vectashield mounting medium containing DAPI (Vector Labs, Peterborough) and observed and photographed mCherry fluorescence in neurons and fibres expressing the transgene (for example, see figure 5.8). Similar histology and microscopy were performed following each *in vivo* optogenetic experiment, in order to confirm local expression of ChR2-mCherry in the injected area.

Chapter 3

The question of tonotopy

3.1 Introduction

The manner in which sensory information is organised, as it traverses the hierarchy of mammalian brain structures, originates at the periphery. Some sense organs (nose, tongue) sort information based on chemical characteristics of the stimulus; others (eyes, skin) organise it into spatial dimensions. The extent of this organisation varies between the senses and the different levels in the hierarchy.

Generally speaking, such organisation decays as information proceeds 'higher' in the brain. It interacts with other signals and ongoing processes and gradually sheds the organisational constraints imparted by the peripheral detectors. Neocortex is the acknowledged home of much of this higher-order processing (e.g. Sharpee et al., 2011; Kourtzi and Connor, 2011) and recent evidence from anatomical and neurophysiological studies suggests that associations, including those that span sensory modalities, are formed at surprisingly early cortical stages (see section 1.4). Yet at the level of primary sensory

cortex, recordings in the visual and somatosensory systems still show responses that vary systematically across cortical space according to the dimensions of visual space, or the location of a stimulus on an animal's skin or whiskers, respectively (see reviews by Fox et al., 2000; Diamond et al., 2003; Petersen, 2007; Wandell and Smirnakis, 2009).

In the auditory system, the dimension by which the sensory organ sorts incoming information is sound frequency. This is because the cochlea transduces high-frequency sound at the stiffer, basal portion of the basilar membrane and low-frequency sound at the apical end (see Robles and Ruggero, 2001). The resulting tonotopy confers a gradient of frequency-specificity to fibres in the auditory nerve, which is passed on to neurons in the cochlear nucleus, and then in turn to other nuclei of the brainstem and midbrain. Within these subsequent structures, a spatial gradient of frequency preference can still be observed by measuring neuronal responses to pure tones. As the complexity of computations increases, beginning with binaural integration in the olivary nuclei, the tonotopic map can be distorted (for example by addition of a bias toward particular frequencies; e.g. see Guinan et al., 1972) or duplicated (as it is *en route* to the rodent auditory cortex; e.g. Redies et al., 1989a).

Like the somatotopic and retinotopic maps of the touch and visual systems, at least one and usually two or more tonotopic maps persist in the cortex of all mammalian species studied (e.g. Hind, 1953; Merzenich and Brugge, 1973; Hellweg et al., 1977; Ryan et al., 1982; Kelly et al., 1986; Sally and Kelly, 1988; Cansino et al., 1994; Stiebler et al., 1997). In humans, up to six frequency gradients have been reported, depending on the stimulus paradigm used (Talavage et al., 2004; Humphries et al., 2010). In rodents there appear to be two, and these have been used to delineate two primary auditory areas: the primary auditory cortex (A1) and the anterior auditory field (AAF) (Stiebler et al., 1997; Rutkowski

et al., 2003; Thomas et al., 1993, see also section 1.2 and chapter 4). In recent years, the precision and reproducibility of these cortical tonotopic maps, particularly in the mouse, has become a topic of some debate.

3.1.1 Contrasting data from the mouse cortex

As outlined in section 1.3 above, recent research has rather complicated the picture of mouse auditory cortical organisation outlined by Stiebler et al. in 1997. That study used single-channel electrodes to record multi-unit activity from middle cortical layers (400–500 μm below the pial surface), covering the extent of auditory cortex at intervals of 200–250 μm and defining the two primary fields A1 and AAF. Here, best frequencies (BFs) were arranged in two tonotopic gradients, sharing a high-frequency border, where the gradient reversed, at approximately 40 kHz.

More recent work is somewhat divided. Two studies using similar extracellular recording techniques to Stiebler et al. (1997) have offered evidence of reproducible, robust tonotopic organisation (Hackett et al., 2011; Guo et al., 2012). Guo et al. (2012), in particular, investigated tonotopy across cortical depth and under various conditions. The authors suggested that, despite some degradation in the map outside middle layers and with different neuronal signal types, if irregularly tuned sites (a significant minority of recordings) were eliminated from the analysis, an equivalent organisation of frequency tuning was present in all cases.

Two-photon imaging studies present a less straightforward picture, including the absence of tonotopic organisation at fine scales within layer 2/3 (Rothschild et al., 2010; Bandyopadhyay et al., 2010). Although cells with similar tuning were likely to respond in

synchrony (see analysis of signal and noise correlation by Rothschild et al., 2010), both the original two-photon publications found that any tonotopic trend was remarkably coarse and tuning within local populations was variable. In fact, local clusters of similar neurons were best identified by including (a) stimulus preferences **other** than frequency and (b) subthreshold responses (Bandyopadhyay et al., 2010). A more recent imaging study (Winkowski and Kanold, 2013) also outlined clear differences in the organisation of frequency tuning between superficial and thalamorecipient layers (see section 1.3 above and further discussion in 3.4.2 below).

3.1.2 Aims

In this chapter I aim to distinguish between these contrasting hypotheses about the precision and reliability of frequency organisation in mouse auditory cortex. To do so I have used high channel count multielectrodes to record simultaneously from sites across laminar and orthogonal cortical space. If tonotopy is robust and invariant, then it should be evident in local activity recorded from evenly spaced, relatively sparse electrode arrays, in response to either pure tones or more complex stimuli.

Below I describe the results of these cross-sections of cortical signals, in order to accomplish the following:

- quantify the prevalence and strength of frequency tuning across fields and laminae of mouse auditory cortex;
- evaluate the degree of tonotopy revealed by sparse but extensive sampling of thalamorecipient, supra- and infragranular layers;

- compare the utility of local field potentials (LFPs) with that of multi-unit activity (MUA) for detecting frequency tuning and tonotopy;
- test the effect of stimulus complexity on frequency tuning and tonotopy, by comparing responses to pure tones and dynamic random chords (DRCs); and
- explore the temporal dimension of frequency tuning, by describing how it varies between different temporal components of the response.

3.2 Methodological considerations

Before I consider the extent to which tonotopy is evident under various conditions, I will outline some important aspects of my recording strategy and data analysis. It is particularly worth looking a little closer at how frequency tuning is extracted from raw electrophysiological data (sections 3.2.2, 3.2.3). I will also briefly report the prevalence of pure-tone tuning in mouse auditory cortex, by pairing tone- and noise-driven responses site-by-site across the breadth of my recordings (section 3.3, below).

To commence my investigation of tuning and tonotopy, I registered a traditional frequency response area (FRA) for sites across A1 and AAF in 9 mice, by recording responses to 100 ms pure tones spanning 4–64kHz at 8 levels of attenuation, as well as to 5 ms bursts of broadband noise. I made the recordings by performing up to 12 sequential penetrations with a 64-channel silicon probe, consisting of 8 shanks with the sites and shanks separated by 200 μm (see figure 3.1A; for procedural details see section 2.2).

3.2.1 Identifying cortical layers using LFPs

Mean LFP responses to the noise bursts allowed me to estimate the depth of recording sites, based on the reversal of LFP polarity (see Christianson et al., 2011); an example is shown in figure 3.1B. This method, described in more detail in section 2.3.2, typically assigned one or two sites on each shank to supragranular layers, one or two to granular and three to infragranular layers. In some cases, where the cortical surface was distorted during electrode penetration, different shanks within a single penetration were at slightly different depths, leading to uneven layer assignations (see, for example, the cases illustrated in figures 3.2 and 3.17).

3.2.2 Pure tone response analysis: effect of smoothing data

Recordings from the brain *in vivo* are often highly variable (e.g. Manley and Müller-Preuss, 1978; Vogels et al., 1989) and it can be difficult to distinguish whether that variance is a property of the responses or of the selected experimental techniques. Furthermore the cortex, particularly auditory cortex, produces responses that are less predictable (Abeles and Goldstein, 1970) and more internally correlated (Winkowski and Kanold, 2013; Rothschild et al., 2010, 2013) than those of many subcortical brain regions. It is also widely believed, if not (to my knowledge) experimentally established, that the smaller brain structures and neurons of rodents intensify the signal-to-noise problem in detecting neurophysiological signals, relative to larger mammals. Thus, it is unsurprising that the raw data presented below in the form of unsorted, multi-unit extracellular spiking activity frequently produce, for example, rather mottled FRAs rather than 'clean' tuning curves (see figure 3.2A).

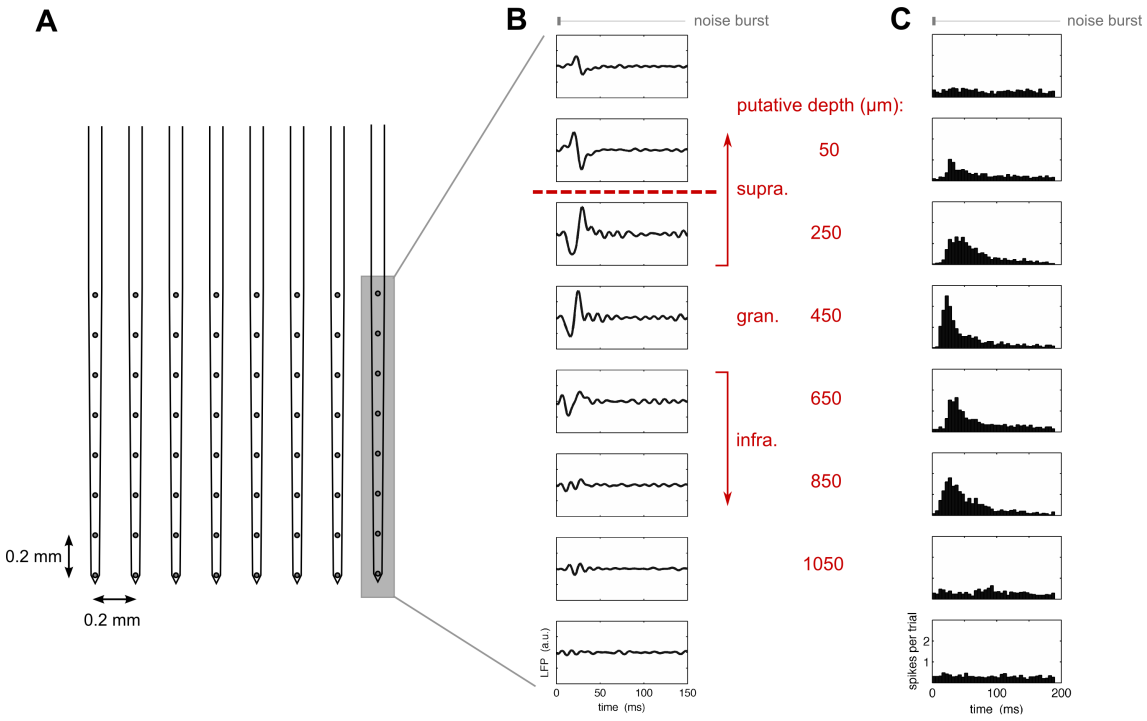


Figure 3.1: **Layout of electrodes and estimation of cortical depth.** ***A***: Illustration of 64-channel (8x8) electrode; note 200 µm site and shank spacing. ***B*** and ***C*** show example responses from a single shank to 50 presentations of a 5 ms noise burst: mean LFP response in ***B*** and multi-unit activity in ***C***, presented as post-stimulus time histograms (5 ms bins). Red markings exemplify how I estimated cortical depth based on the reversal of LFP polarity (highlighted by dashed red line in ***B***). Since the reversal point approximates the layer 1/2 border at 100–150 µm beneath the pia (Christianson et al., 2011; Anderson et al., 2009), depths can be estimated for each recording site. Allowing for errors of ±100 µm in these presumptive depths due to uncertainty about the precise location of the reversal, channels can still be designated supragranular (layers 1–3, < 300 µm, 'supra'), granular (deep layer 3 and layer 4, 300–500 µm, 'gran') or infragranular (layers 5 and 6, > 500 µm, 'infra'). Note that the profile of spiking activity in ***B*** is consistent with the layer assignments (i.e. more spikes at shorter latencies in granular layers) and that the uppermost and deepest sites are likely to be outside the cortex.

Perhaps because of this relative paucity of reliable, stimulus-correlated activity, pure-tone response data from the cortex (usually in the form of FRAs) are often smoothed across neighbouring stimulus combinations using a sliding window. This smoothing can be used for presentation or to facilitate analysis (e.g. identification of secondary response properties, such as bandwidth) or both (Sutter and Schreiner, 1991; Bizley et al., 2005; Guo et al., 2012).

To evaluate some of the costs and benefits of smoothing pure-tone response data, I employed the smoothing method used in an earlier mapping study of ferret auditory cortex from this laboratory (Bizley et al., 2005) and compared the tuning of smoothed and unsmoothed data. Figure 3.2 shows FRAs from an example 64-channel penetration, including an indication of which sites were found to be significantly frequency-sensitive, and their BFs. I evaluated frequency sensitivity by performing a one-way ANOVA on pooled responses to neighbouring frequency pairs at the highest four sound levels (see section 2.3.4); if a site displayed significant variance according to this test (threshold $p < 0.05$), I included it in tuning analyses. I refer to these sites below as 'significantly tuned' though strictly this test categorises whether responses vary with stimulus frequency, rather than whether the site shows a classically tuned receptive field.

This criterion, applied to the raw spike-rates, occasionally labels as 'untuned' sites that do in fact display an area of heightened responses (single asterisks, figure 3.2A); by comparison, smoothing each iteration of the FRA grid before applying this test designates a higher proportion of sites 'tuned', including all those which appear tuned on visual inspection and some which do not (compare figure 3.2B). Visually, smoothing creates more convincing tuning curves in many FRAs, but can also create a possibly misleading appearance of structure.

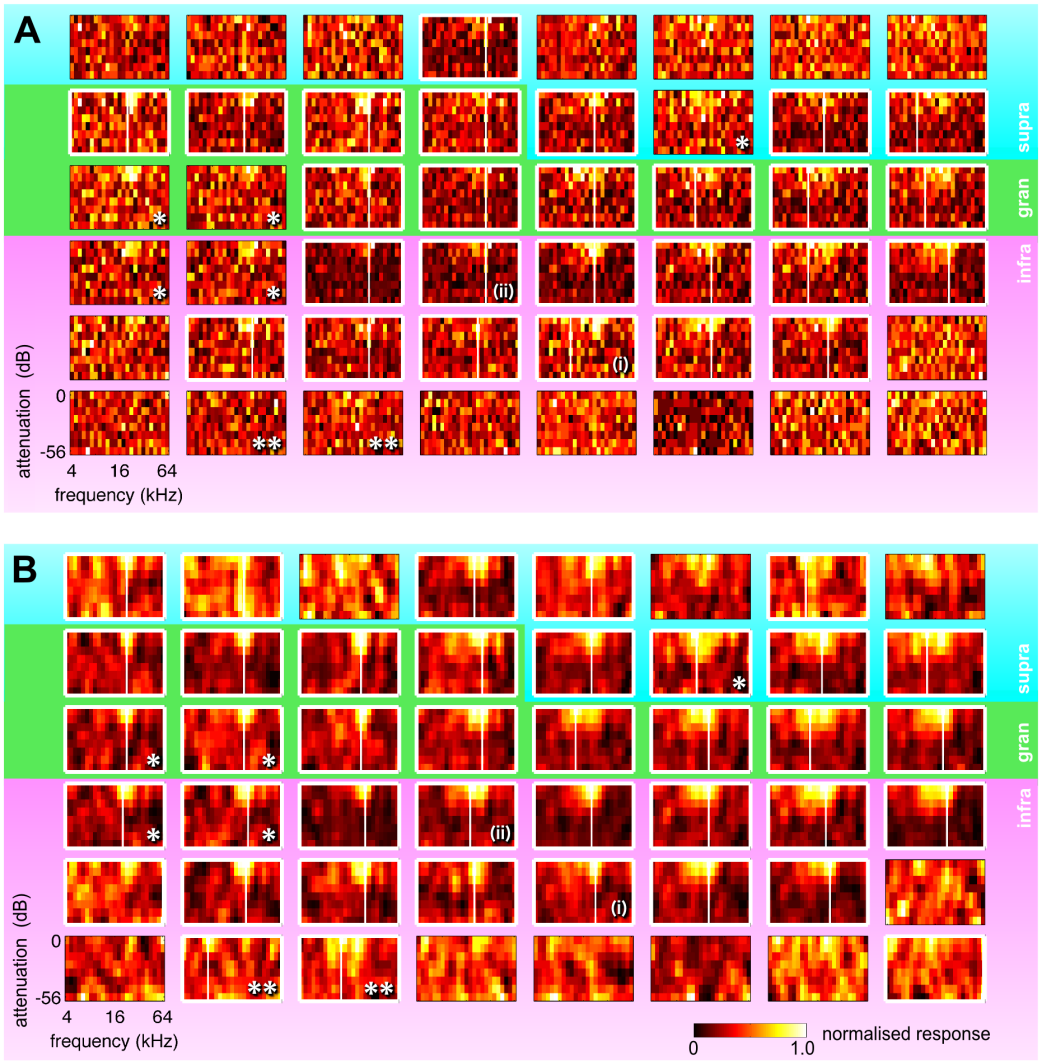


Figure 3.2: **Comparing smoothed and unsmoothed FRAs.** Multi-unit activity from an example 64-channel penetration is illustrated in two forms: ***A***, raw FRAs based purely on spike counts, and ***B*** the same FRAs smoothed using a nine-point sliding window (see section 2.3.4 for details). Channels estimated to be above or below the cortex have been excluded and layer categories have been assigned as indicated by coloured background shading (see figure 3.1; note this is one of the uneven cases mentioned in section 3.2.1). White borders and a vertical line marking best frequency (BF) have been added to those sites which show significant tuning, according to the criterion outlined in the text (for more detail see section 2.3.4). Applying this criterion to unsmoothed data omits some sites which do appear tuned on visual inspection (asterisks); applying it to smoothed data catches these but also leads to the inclusion of potential 'false positives'. Generally, although the smoothed FRAs unsurprisingly appear more coherent, in some cases smoothing imparts possibly false structure to what appears to be noisy raw data (two examples are marked with a double asterisk). Smoothing only rarely causes an obvious shift in a site's calculated BF (vertical line), very occasionally making a better (i) or worse (ii) approximation than the unsmoothed data, based on visual inspection.

Importantly, best frequencies (BFs, defined here as the frequency eliciting the largest response across all sound levels; see discussion in section 3.2.3 below) are similar between the two sets of FRAs (vertical lines, figure 3.2). In order to make a conservative estimate about which sites show frequency sensitivity, I have calculated all subsequent BFs and tuning prevalence based on unsmoothed pure tone responses. The only exceptions are cases where the smoothed data are useful for defining further response characteristics (e.g. characteristic frequency, CF; see figure 3.4). I regard this as an important distinction because, in producing a less 'messy' report of neuronal activity, smoothing may well disguise some of the complexity and variability — indeed, the noisiness — of cortical responses.

3.2.3 Pure tone response analysis: comparison of CF and BF

Several different values can be calculated in order to describe frequency preference in neuronal signals. Best frequency (BF) and characteristic frequency (CF) are the most commonly used. The definition of these terms varies in the literature, but BF most commonly refers to the frequency eliciting the **strongest** response (calculated here across all sound levels; see section 2.3.4), while CF refers to the frequency evoking a significant response **at the lowest sound level** (i.e. at threshold). Here I evaluate both values as measures of frequency tuning in my experimental setup.

In order to calculate the CF of multi-unit activity from a recording site, I determined a boundary for the tone-responsive portion of its FRA. This is typically done by smoothing the data and using a threshold response value to draw the boundary (e.g. mean spontaneous spike-rate plus 20% of peak rate; see Sutter and Schreiner, 1991; Bizley et al., 2005) though other methods have been used (for example, Guo et al. (2012) superimposed an

inverted, smoothed spike-frequency function onto their FRAs). I replicated the procedure of Bizley et al. (2005) to calculate CF alongside BF for every recording site across the auditory cortex of one mouse; two examples are shown in figure 3.3.

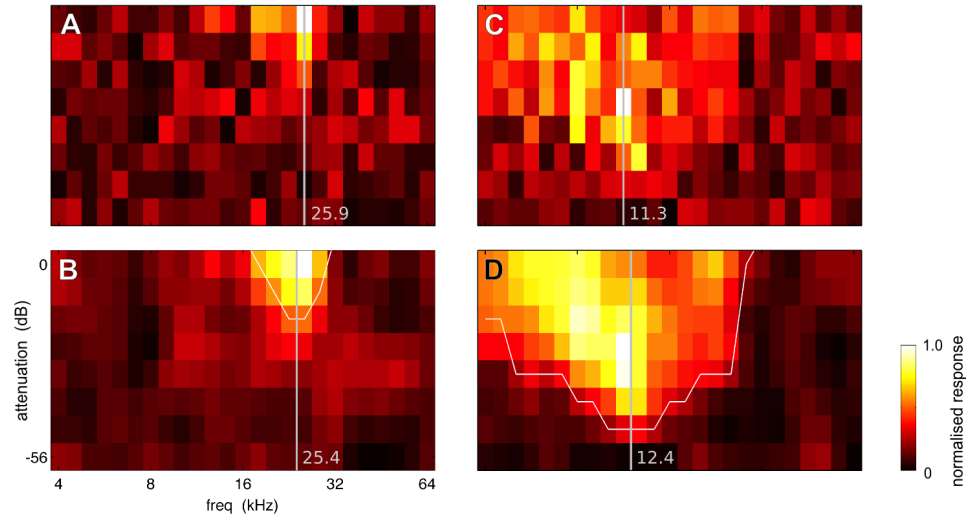


Figure 3.3: **Calculating CF from smoothed data.** FRAs from two example sites are shown using both raw (***A***, ***C***) and smoothed (***B***, ***D***) spike-rate values. Vertical lines in ***A*** and ***C*** indicate BF, defined as the frequency eliciting the strongest response across all sound levels. In ***B*** and ***D***, the boundary of the tone-responsive portion of the FRA is shown in white, calculated using a threshold of the site's mean spontaneous spike-rate + 20% of its peak rate (Sutter and Schreiner, 1991; Bizley et al., 2005); vertical lines here indicate CF, defined as the mean frequency evoking a response at the threshold sound level (i.e. the tip or 'peak' of the tuning curve). Thus, while it may be of limited use in other scenarios (see figure 3.2), smoothing data does enable the calculation of a tuning curve and CF, even in the case of a relatively noisy FRA where a threshold-based calculation using the raw data would be problematic (***C***). In both these examples, BF and CF are similar.

Smoothed FRA data enabled threshold-based calculation of CF in nearly all channels where the raw responses were significantly tuned (221 of 229 recording sites). Focussing on the middle, thalamorecipient layers of the cortex, I created a tuning map using these CFs and found a notably similar, tonotopic organisation to that derived from BFs (figure 3.4A,B). Furthermore, when I compared CF and BF across all tuned recording sites they were positively correlated (figure 3.4C; $r = 0.66$, $p < 10^{-21}$). Since they produce similar results and BF is the more objective, straightforward measure of pure-tone frequency

preference, I have used BF in all other FRA-based analyses in this thesis.

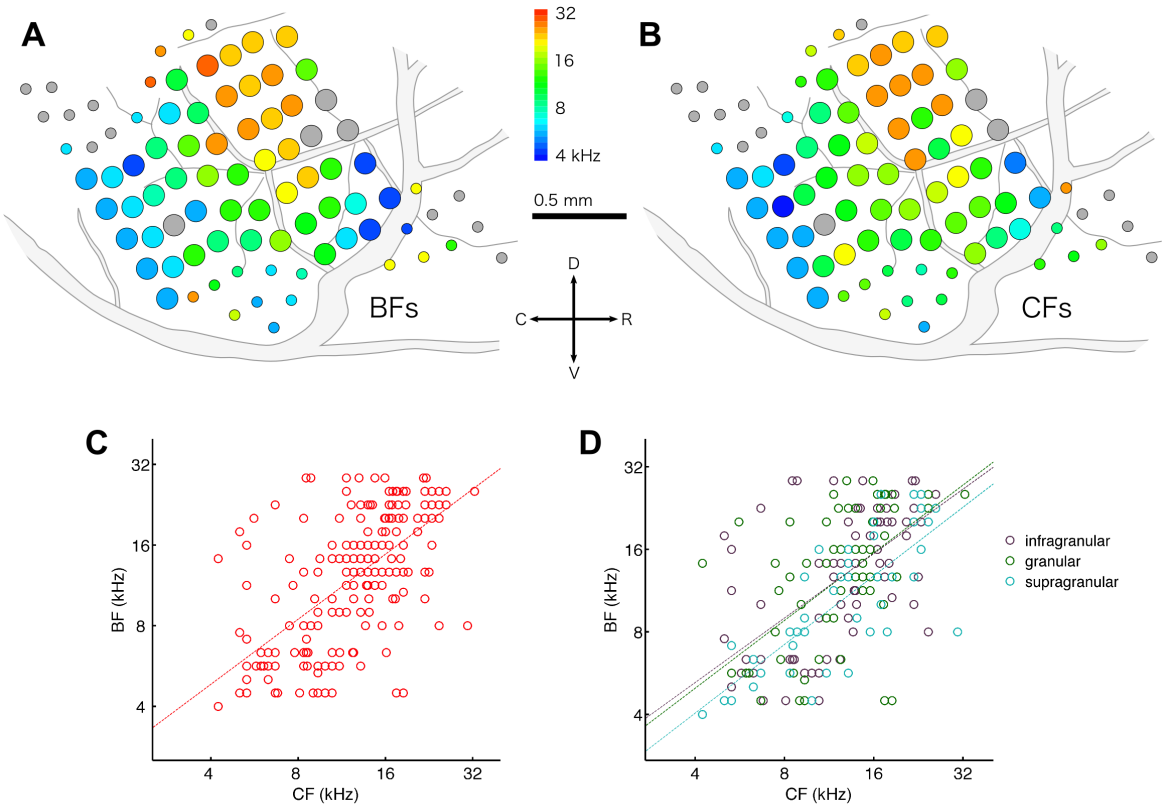


Figure 3.4: **CF and BF are correlated and produce similar frequency maps.** ***A*** and ***B*** show BFs and CFs, respectively, from recording sites in thalamorecipient layers in the auditory cortex of mouse 'Marilyn' (the same case as illustrated in figures 3.8 and 3.9A). As in later figures, small circles represent sites estimated to be outside primary areas; grey circles, sites which were responsive to noise bursts but not significantly tuned. ***C***, scatter plot comparing CF and BF at all significantly tuned sites, spanning cortical layers and subfields (Pearson's correlation coefficient, $r = 0.66$; dotted line shows linear regression fit). ***D***, the same data as in ***C***, colour coded by cortical depth; note the correlation is similar in all three groups ($r = 0.63$ for infragranular sites, 0.64 for granular and 0.77 for supragranular; $p < 10^{-6}$ for all correlations).

3.2.4 Very high-frequency tuning is rare

Interestingly, within my data there are very few recordings with BFs above 32 kHz: 11 of 623 tuned cortical sites, and only 3 of 518 within primary areas (for a histogram of pure-tone tuning, see figure 3.18C). This is despite the fact that I presented pure tones up to 64

kHz and often extended my recordings in a dorso-caudal direction, where ultrafrequency representation is expected (Stiebler et al., 1997; Guo et al., 2012), until tone- and noise-driven responses dwindled (e.g. figure 3.9).

This diverges from the established view of the mouse auditory cortical map (Stiebler et al., 1997) and is surprising given both the ultrafrequency content of mouse vocalisations (Liu et al., 2003) and the sensitivity to ultra-frequencies seen in mouse behavioural studies (Mikaelian and Ruben, 1965; Ehret and Haack, 1982). Nonetheless, this observation is consistent with a number of methodologically similar investigations of the mouse cortex, particularly in the C57BL/6 strain (Hackett et al., 2011; Martin del Campo et al., 2012; Moore and Wehr, 2013). While I have used mice no older than 12 weeks in order to minimise precisely this risk, it is possible that the curtailed frequency representation is a consequence of age-related, high-frequency hearing loss in this strain (Willott et al., 1993). In addition to differences in hearing ability, however (Hunter and Willott, 1987; Zheng et al., 1999), the layout of the auditory cortex itself can vary considerably between individual mice and between strains (Stiebler et al., 1997; Guo et al., 2012; also J. Linden and J. Garcia-Lazaro, personal communication). Since brief startle-response testing prior to each of my experiments revealed no obvious hearing impairment, I favour this explanation for this commonly reported BF distribution in C57BL/6 mice. Similarly, Moore and Wehr (2013) recently used this strain in a cortical tuning study, recorded BFs ranging 4–34 kHz in mice aged up to 4.5 months and reported no evidence of age-related hearing loss.

It is worth noting that under-representation of very high frequencies among cortical BFs does not preclude cortical neurons **processing** sounds with very high frequency content; it is simply an indication of which pure tones drive these neurons to spike most effectively. (In the specific time course of hearing loss in aged C57BL/6 mice, for example,

behavioural thresholds increase at a slower rate than electrophysiological ones; see Henry and Chole, 1980). Even so, the lack of very high BFs in data presented here and elsewhere is a topic for ongoing discussion.

In many of the plots that follow, for the purposes of graphically illustrating the spread of frequency tuning, I have omitted the very small number of sites with BFs higher than 32 kHz; all relevant sites were included in correlations and other statistical measures.

3.3 Prevalence and strength of frequency tuning across the cortex

In comparison with other sensory modalities, neuronal responses in auditory cortex are notoriously sparse and identifying a stimulus paradigm which reliably elicits responses is a challenge (e.g. Abeles and Goldstein, 1970). This means that well-tuned receptive fields, whether or not they are tonotopically arranged, are not a given. In the mouse particularly, responses to pure tones are surprisingly rare and, when present, frequency tuning can be complex or downright messy (J. Garcia-Lazaro, personal communication; Bandyopadhyay et al., 2010; Rothschild et al., 2010). The multisite recordings of mouse auditory cortex reported in this chapter offer an opportunity to quantify frequency tuning across subfields and layers.

I estimated the prevalence of tuning using high channel-number electrodes which sample responses widely across cortical space, as described in section 3.2.1 above. These data have the advantage that 64 multi-unit recordings were performed simultaneously at evenly separated points in space, dramatically reducing any selection bias for highly

driven sites. I measured spike counts in response to 5 ms noise bursts and a grid of frequency-level combinations at 2240 sites (35 penetrations) in 9 mice, of which I later judged 1353 to be within the auditory cortex (others were too shallow or deep, or in neighbouring areas of cortex). I categorised a site as responsive to noise if its mean spike-rate in the period following the stimulus exceeded a threshold of $\mu_s + 4\sigma_s$, where μ_s is the mean spontaneous spike-rate (measured prior to the stimulus in each sweep) and σ_s is its standard deviation (see section 2.3.3). My criterion for designating a site 'tuned' is described above (see sections 3.2.2, 2.3.4).

To make my data more comparable with studies in which individual neurons can be counted (e.g. Winkowski and Kanold, 2013), I restricted my analysis of tuning prevalence to those sites which showed a significant noise response, rather than considering all sites within the cortex. This ensures that all the sites under consideration were at least within recordable proximity of healthy and responsive neurons; such sites were a majority in my pooled data (938 of 1353 sites), although that proportion varied within subfields of auditory cortex, particularly in non-primary fields where I made fewer recordings (see figure 3.5A; for a more detailed comparison of responses in A1 and AAF, see chapter 4). Of those noise-responsive sites, most but not all showed significant pure-tone frequency tuning (623/938), while a comparatively small number of sites (85) showed tuning in the absence of noise responses (see figure 3.5B).

3.3.1 Is tuning more common in some fields and layers?

While on average 62% (±6.1% SEM) of noise-responsive sites recorded from individual mice were tuned, that proportion varied considerably between mice in the various cortical subfields (figure 3.6A; note size of error bars). Thus, no significant differences were

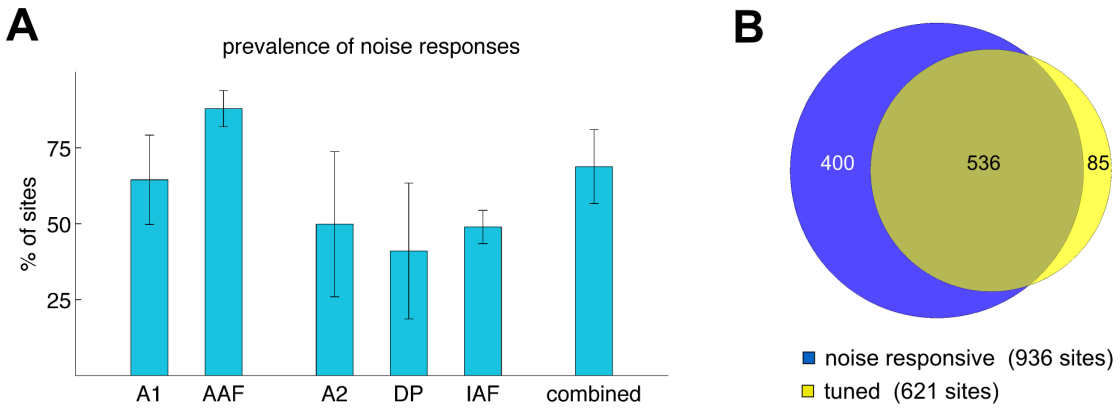


Figure 3.5: **Overall prevalence of noise responses and tuning.** Shown in ***A*** are the mean proportions of noise-responsive sites recorded in 9 mice, within cortical subfields and combined. Error bars, 95% confidence intervals for each mean. Overall and within primary areas (A1 and AAF), a majority of sites responded to noise bursts; proportions varied in non-primary fields where sample sizes were smaller. (Recordings were not made in all subfields in all mice: A1 $n=9$; AAF $n=8$; A2 $n=4$; DP $n=5$; IAF $n=3$). ***B***, Venn diagram illustrating the overlapping populations of noise-responsive and tuned sites. Total number of cortical recording sites = 1353.

observed in the proportion of tuned sites across subfields (one-way ANOVA, $p=0.44$).

To explore the prevalence of tuning across cortical depth, I concentrated on the primary areas of auditory cortex, A1 and AAF, where tonotopy and frequency tuning are expected. Here, the mean proportion of tuned sites was highest in granular layers (71%±7.3 SEM) and lowest in supragranular layers (54% ± 7.4; infragranular 65% ± 5.5) but variations between mice meant that these percentages were not significantly different (one-way ANOVA, $p=0.22$; see figure 3.6B).

Interestingly, however, when I considered the data from each mouse separately there was a strong tendency for the proportion of tuned sites to increase between supragranular and deeper layers (figure 3.6C, D). Indeed, the average **difference** between supragranular and granular layers, assessed with a paired-sample t-test, was significant ($p<0.01$; figure 3.6E).

The variability in the absolute proportion of tuned sites between animals may reflect

differences in anaesthetic state. I endeavoured to minimise such variation by using an infusion pump rather than periodic injections to deliver ketamine constantly during each experiment, but I did vary the rate based on observation of the animal (see section 2.2.1). This means that the dosage varied for each mouse and the depth of anaesthesia may differ slightly between experiments and even between recordings from a single mouse. Since both the choice of drug and depth of anaesthesia are known to affect auditory cortical activity (e.g. Gaese and Ostwald, 2001; Moshitch et al., 2006; Hromádka et al., 2013; Rajan et al., 2013), anaesthetic state almost certainly contributes to the variability seen here (e.g. see spread of y-axis values in figure 3.6C).

The drop I observed in the occurrence of frequency-sensitive activity in superficial layers is consistent with the notion that middle layers receive highly tuned input from the thalamus, but that frequency tuning then becomes less precise as cortical circuits integrate more diverse information in supragranular layers (Winkowski and Kanold, 2013). As in other cortices, infragranular neurons in the auditory cortex send significant corticofugal projections, including back to the thalamus (reviewed by Winer, 2006). Thus, it makes sense for neurons in these deeper layers to possess tuning properties more similar to their thalamorecipient, granular counterparts than their supragranular ones (see further discussion in section 6.2.1).

By comparison with my findings, the two-photon imaging experiments of Winkowski and Kanold (2013) yielded a higher proportion of frequency-sensitive cells in both layer 2/3 and layer 4 (~87% and 88%) — though only 59% and 65% (in layers 2/3 and 4, respectively) showed single-peaked tuning curves. This is somewhat surprising. Since my electrodes are 'blind' and I have made no attempt to sort spikes, my multi-unit recordings will tend to include more spikes from bigger neurons or those spiking more frequently.

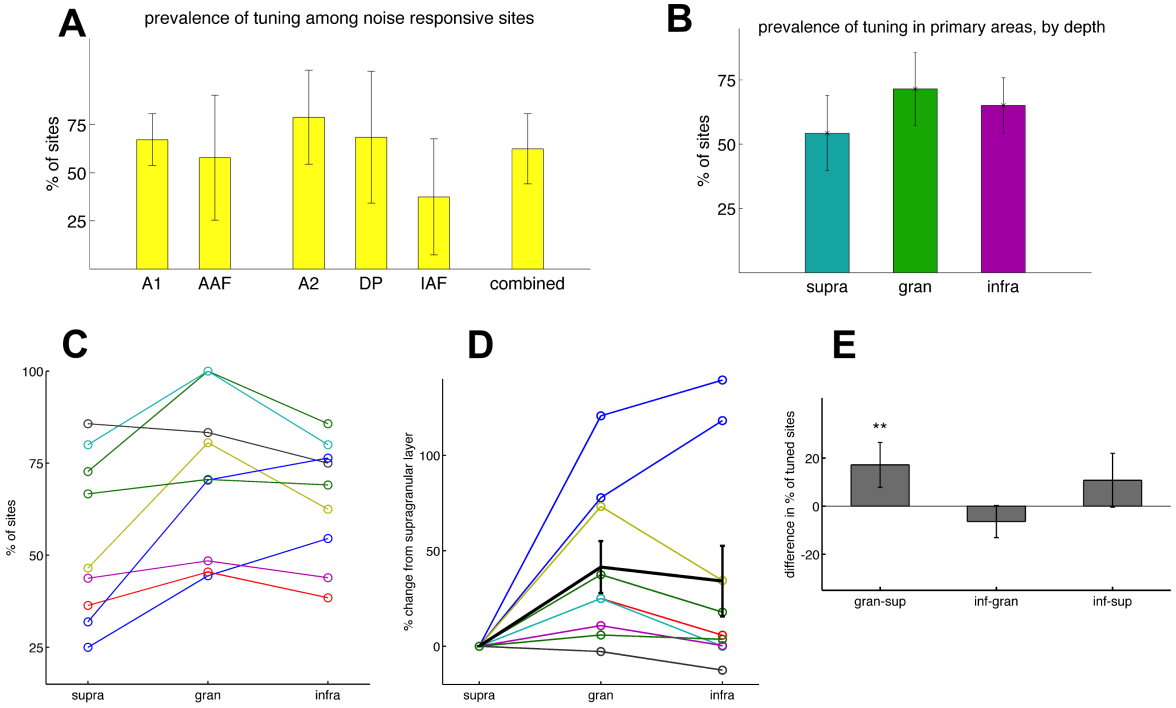


Figure 3.6: **Prevalence of tuning across cortical fields and layers.** ***A***, The mean percentage of noise-responsive sites which also showed significant pure-tone tuning is illustrated for each subfield of auditory cortex. Inter-animal variation produced large error bars (95% confidence intervals for each mean) and no significant differences were detected (ANOVA, $p = 0.44$; n for each is as in figure 3.5). ***B***, Mean percentages of tuned sites within supragranular ('supra'), granular ('gran') and infragranular ('infra') layers of the primary areas (A1 and AAF, pooled). Error bars, 95% confidence limits. Note that granular layers produced the highest percentage of tuned sites and supragranular sites the lowest, although the differences in absolute percentage across 9 mice were not significant (ANOVA, $p = 0.22$). In ***C*** these data are separated mouse-by-mouse (each animal in a different colour) and in ***D*** this is repeated, showing the proportions in granular and infragranular layers **relative to supragranular** (thick black line is the mean, ±SEM). In these presentations, a trend toward more prevalent tuning in granular (and, to a lesser extent, infragranular) layers is evident; ***E*** shows that the **mean difference** in the extent of tuning between granular and supragranular layers is indeed significant (**, paired t-test, $p < 0.01$; error bars, 95% CIs).

Such a bias would likely mean that my proportions of 'responsive sites' over- rather than underestimate the proportion of responsive **neurons** in the cortex. However, despite my exclusion of noise-unresponsive sites, these data are not entirely comparable; my 'supragranular' category includes all sites in the shallowest ~300μm of the cortex rather than focussing on layer 2/3, and there are important differences in our methods for measuring and categorising tuning.

Guo et al. (2012), who also made extracellular multi-unit recordings, briefly consider the prevalence of tuning and note an increase in responsive but poorly tuned recording sites outside of the middle cortical layers (more pronounced in supragranular layers; exact proportions are not given). Of the single-unit recordings they were able to isolate, approximately 50% were well-tuned, as categorised by their own criterion (see Guo et al., 2012, p.9166).

In sum, my data are largely consistent with the few published descriptions of tuning incidence in the mouse cortex. They support a view that pure-tone frequency tuning is common but far from universal, particularly in supragranular layers.

3.3.2 Is tuning stronger in some fields and layers?

I also quantified the degree to which those tuned sites across layers and subfields showed a frequency preference: the 'strength' of their tuning. As a measure of tuning strength, I calculated the discriminability index or d' for each site's spike counts in response to its best and worst pair of neighbouring frequencies (similar to my method for categorising sites as tuned or untuned; see section 2.3.4).

These values were significantly higher in both primary fields and A2, compared to the

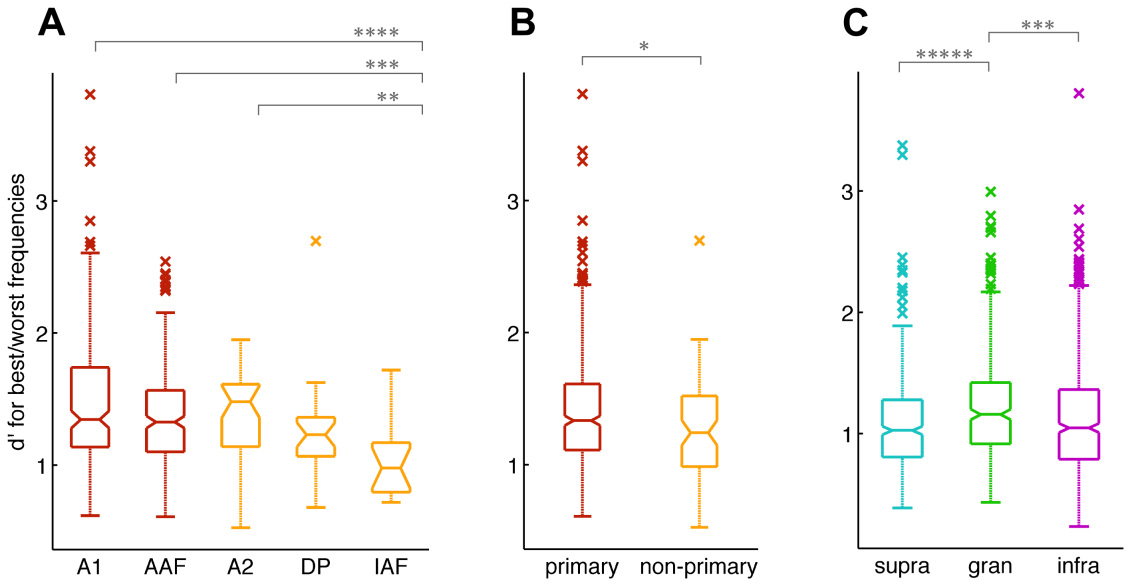


Figure 3.7: **Strength of tuning across cortical fields and layers.** Box-and-whisker plots illustrating the distribution of d' values across (***A***) individual auditory cortical subfields; (***B***) pooled primary and non-primary areas; and (***C***) cortical layers. These are d' values for the discriminability of each site's responses to its best and worst pairs of neighbouring frequencies, thus offering a measure of the strength of each site's preference for its favoured frequencies (see section 2.3.4). Grey brackets and asterisks indicate significant differences between indicated median d' (Kruskal-Wallis test: ***** $p < 10^{-5}$; **** $p < 10^{-4}$; *** $p < 10^{-3}$; ** $p < 0.01$; * $p < 0.05$). Boxes: interquartile range; horizontal line: median; notches: 95% confidence intervals; whiskers: further extent of data up to 1.5× interquartile range; outliers marked with x. A1, $n = 210$; AAF, $n = 250$; A2, $n = 37$; DP, $n = 26$; IAF, $n = 15$; primary, $n = 460$; non-primary, $n = 78$; supra, $n = 116$; gran, $n = 146$; infra, $n = 197$.

non-primary field IAF (see figure 3.7A). Pooling primary and non-primary fields (A1 + AAF *vs.* A2 + DP + IAF; figure 3.7B) revealed significantly higher d' values in primary sites. This finding is consistent with reports comparing frequency sensitivity across auditory cortex in other species (e.g. Bizley et al., 2005) and with the notion that if tonotopy and tuning are important organisational principles in the mouse cortex, they are significantly more so in primary areas.

Comparing tuning strength across cortical layers showed that, perhaps unsurprisingly, the responses in thalamorecipient layers were the most strongly tuned (mean d' 1.22, ±0.036 SEM); d' values in supragranular and infragranular sites were significantly lower than in granular layers but not different from one another (mean d' values 1.09 ± 0.019 and 1.12 ± 0.019, respectively; distributions illustrated in figure 3.7C). In their two-photon data comparing calcium transients across layers 2/3 and 4 in mouse auditory cortex, Winkowski and Kanold (2013) found that individual layer 4 cells' responses to pure tones were larger than those in superficial layers, suggesting higher and more stimulus-driven spike-rates in granular layers. My observations of increased tuning strength in multi-unit activity support this hypothesis.

3.4 Tonotopy in multi-unit activity

Since tuned responses are a prerequisite for frequency maps, the above assessment of tuning strength and prevalence supports the view typified by Hackett et al. (2011) that the most expected cortical manifestation of tonotopy is in the middle layers of anaesthetised cortex, within multi-unit spiking responses to pure tones. Consequently, this is where I looked first.

3.4.1 Canonical tonotopy is usually but not universally evident in thalamorecipient layers

Figure 3.8A shows the the arrangement of BFs in thalamorecipient layers of the auditory cortex in one mouse; this case represents the most extensive map I was able to produce. A rostrocaudal low–high–low tonotopic gradient is apparent. Indeed, as first observed by Stiebler et al. (1997), these gradients also slope upward in a dorsal direction; in a relatively complete map such as figure 3.8A or those reported by Guo et al. (2012), frequency preference seems to be organised almost radially rather than in two distinct linear gradients (see discussion in section 6.2.4; for more detailed consideration of the A1/AAF distinction, see chapter 4).

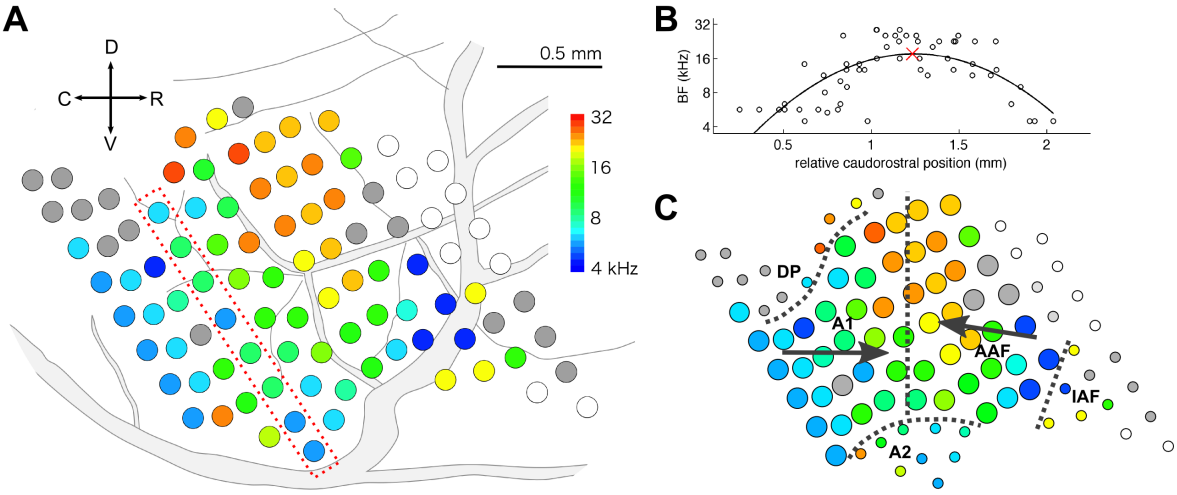


Figure 3.8: **Delineation of subfields based on tonotopy in thalamorecipient layers.** ***A***: Best frequencies derived from multi-unit activity in thalamorecipient layers of mouse auditory cortex. This example (mouse 'Marilyn') is the most extensive map I was able to acquire. Grey circles denote sites that were responsive to 5 ms white noise bursts but were untuned to pure tones; empty circles denote sites that were responsive to neither tones nor noise. Surface vasculature of the cortex is also illustrated. Dotted red rectangle is relevant to figure 3.22, highlighting the electrode penetration analysed there. ***B***: Distribution of BFs along the caudo-rostral axis, fit with a quadratic function; the peak of this function (red x) was used to define the position of the A1–AAF boundary. ***C***: Responsive sites from ***A*** with estimated boundaries of auditory cortex subfields superimposed; x-axis is shared with ***B***. Arrows show direction of tonotopic gradients, determined as described in section 2.3.6 and figure 3.9.

I used this gradient to estimate the boundaries of subfields in auditory cortex, in a manner similar to Hackett et al. (2011, see figure 3.8 B,C). The intersection of A1 and AAF is where the rostrocaudal tonotopic gradient reverses, identified as the peak in a quadratic function fit to the distribution of BFs along that axis (red cross, figure 3.8B). Shifts away from the tonotopic arrangement, as well as changes in other response characteristics (not shown) such as the longer latencies typically seen in A2, can be used to identify the non-core regions at the ventral and dorsocaudal edges of auditory cortex. These regions are labelled in figure 3.8 using a synthesis of terminology from the canonical mapping experiments of Stiebler et al. (1997; DP, dorsoposterior field and A2, secondary auditory field) and a more recent voltage-sensitive dye study which described an insular auditory field (IAF; Sawatari et al., 2011, see also Guo et al., 2012). I have also adopted the revision suggested by Guo et al. (2012) whereby there is no separate 'ultrafrequency' subfield. (The lack of very high frequency tuning in my maps is discussed in section 3.2.4 below.)

Of the 9 mice from which I recorded pure-tone responses, 4 yielded sufficient data for a map of frequency tuning to be drawn (i.e. at least 3 successful multielectrode penetrations; figure 3.9). To identify the direction of each tonotopic gradient and quantify its correlation with neuronal BFs, I separately correlated BFs from A1 and AAF with their position on a series of axes spanning 360° at 10° intervals; the direction with the highest correlation coefficient (r) is indicated by arrows above each map in figure 3.9 and the coefficients are reported in the corresponding graphs. In those mice with only 1 or 2 penetrations, I quantified tonotopy (for comparisons such as figure 3.11) by correlating BF with rostrocaudal position.

In most cases (figure 3.9 A,B,C) the observed tonotopic gradients loosely fit the expected pattern, even if the gradient is only partially represented (e.g. A1 in panel B) or the

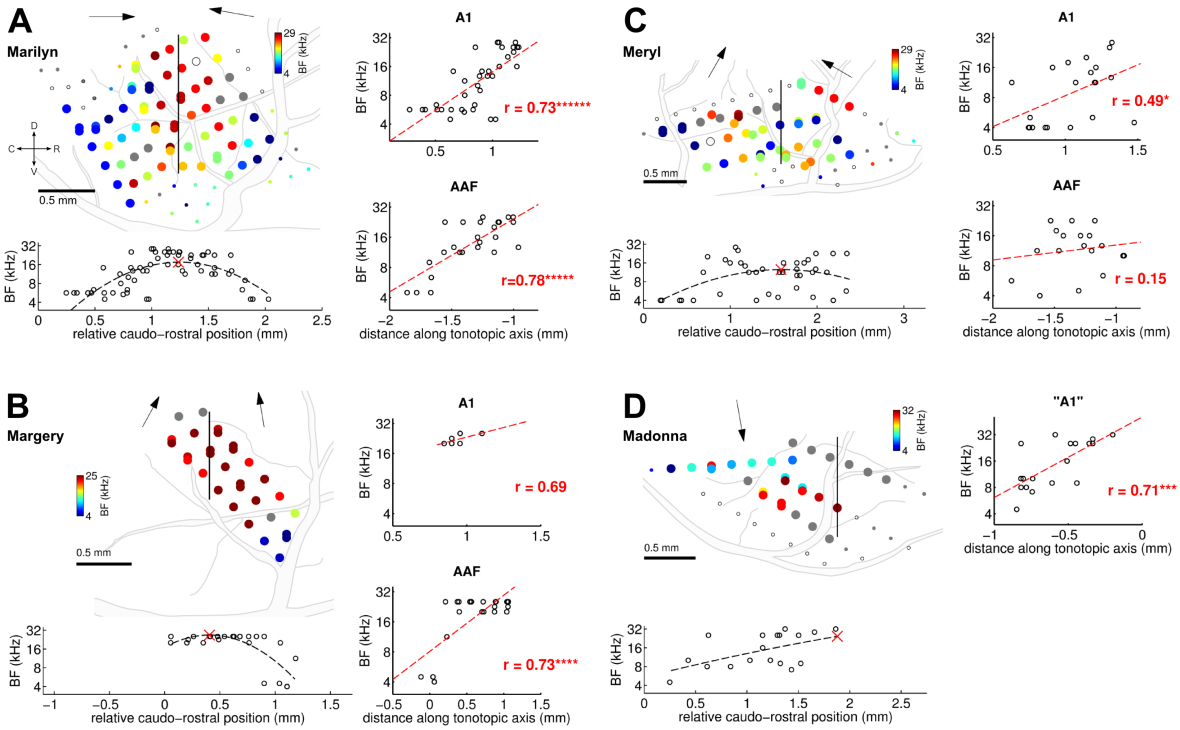


Figure 3.9: **Frequency maps from middle layers with varying degrees of organisation.** Examples of BF distribution in granular layers of auditory cortex, from four different mice. Within the maps, as in figure 3.8A, grey circles indicate sites which were responsive to noise bursts but untuned to pure tones; empty circles indicate sites that were unresponsive to both, and small circles denote sites likely to be outside the primary fields A1 and AAF. The A1–AAF boundary (vertical black line) was placed as shown in figure 3.8B and the corresponding plot is shown underneath each map, on the same x-axis. Arrows above each field indicate the axis (tested at 10° intervals) along which recording positions best correlated with BF. This correlation is illustrated in the plots on the right of each panel, and the correlation coefficient (r) is given in each case (with n asterisks, indicating $p < 10^{-n}$). Note that in most cases (***A***–***C***) the frequency gradients, expected to increase towards the A1–AAF boundary and in the dorsal direction, fit that pattern, although the precise direction varies considerably within this range. In some cases (AAF, ***C***) the correlation is weak, while in ***D*** no reversal was detected, and the single gradient is not oriented as predicted by published maps (see text). Data in ***A*** are repeated from figure 3.8; orientation marker in that panel applies to all maps.

correlation is weak (e.g. AAF in panel C). In mice where a gradient was not detected or the direction was not as expected (e.g. figure 3.9D — single gradient only, oriented dorsal–ventral), my data cannot elucidate whether the canonical pattern is absent altogether or present as a coarse, large-scale trend that has not been detected by these 200 μm-spaced grids of multi-unit activity. The latter is more likely. It implies that my recordings on these occasions 'missed' those sites which **would** have revealed a tonotopic arrangement, but this fits with reports that classical pure-tone frequency tuning in mouse cortex is surprisingly sparse (P. Kanold, personal communication; Bandyopadhyay et al., 2010; Rothschild et al., 2010). Even in layer 4, Winkowski and Kanold (2013) recorded single-peaked tuning curves in only 65% of cells, while Seybold et al. (2012) did not consistently observe a gradient reversal between A1 and AAF and so used response latency as an indicator of different subfields.

If cells' tuning is often complex and organisation is heterogeneous at fine scales, then unbiased sampling from regularly spaced sites will not always retrieve signals that fit a tonotopic pattern; the minority of irregular maps in my data support this view. Nonetheless, in a majority of cases reported here, recordings in thalamorecipient layers did reveal tonotopic organisation of pure tone responses.

3.4.2 Tonotopy varies in supra- and infragranular layers

Frequency tuning could be stronger or weaker and more or less prevalent in different layers, but still organised in cortical space to form a tonotopic gradient. Indeed, the argument for robust tonotopy presented by Guo et al. (2012) suggests that even if supragranular responses are more sparse, tuning is relatively invariant within columns; an earlier, limited set of data from sequential, orthogonal sets of cell-attached recordings made a

similar observation (Shen et al., 1999). To explore how the tonotopic map varies between layers, I have laid out BF maps from middle (granular), supra- and infragranular layers of three different mice (figure 3.10).

In each case, the frequency gradients observed in middle layers show changes in direction, in some cases substantial ones, with the shift into supra- or infragranular layers (compare figure 3.10B with panels A, C). In some cases, the A1–AAF tonotopic reversal itself is shifted (e.g. panel C, left) or no longer revealed by fitting a quadratic function to the data (e.g. panel A, right). Particularly in superficial layers, the changes in tonotopy are accompanied (and probably partly caused) by a decrease in the proportion of sites displaying frequency tuning (note grey circles in figure 3.10A; see section 3.3.1).

Figure 3.11A gives an overview of all the tonotopic gradients observed that could be calculated across 9 mice, in each layer category (excluding cases where recordings from a given layer of A1 or AAF yielded fewer than 5 tuned sites). While the mean correlation coefficient is highest in granular layers, there is much variability of the gradients within mice (along lines) and between mice (compare colours). Paired t-tests reveal no significant changes in r between layers ($p = 0.62$ for supra–gran, 0.81 for gran–infra, 0.85 for supra–infra).

As shown in figure 3.11B, the angles of frequency gradients are also variable. Both A1 and AAF sets show one example where the 3 gradients (from each layer category) are relatively similar (first case A1, third case AAF) but others where the direction or strength of the correlation (length of arrow, if present at all) vary dramatically.

Although I have not observed a consistent drop in the strength of tonotopy in superficial layers, as the heterogeneous tuning reported by Winkowski and Kanold (2013) might suggest, the variability I report across cortical depth is consistent with the notion of lam-

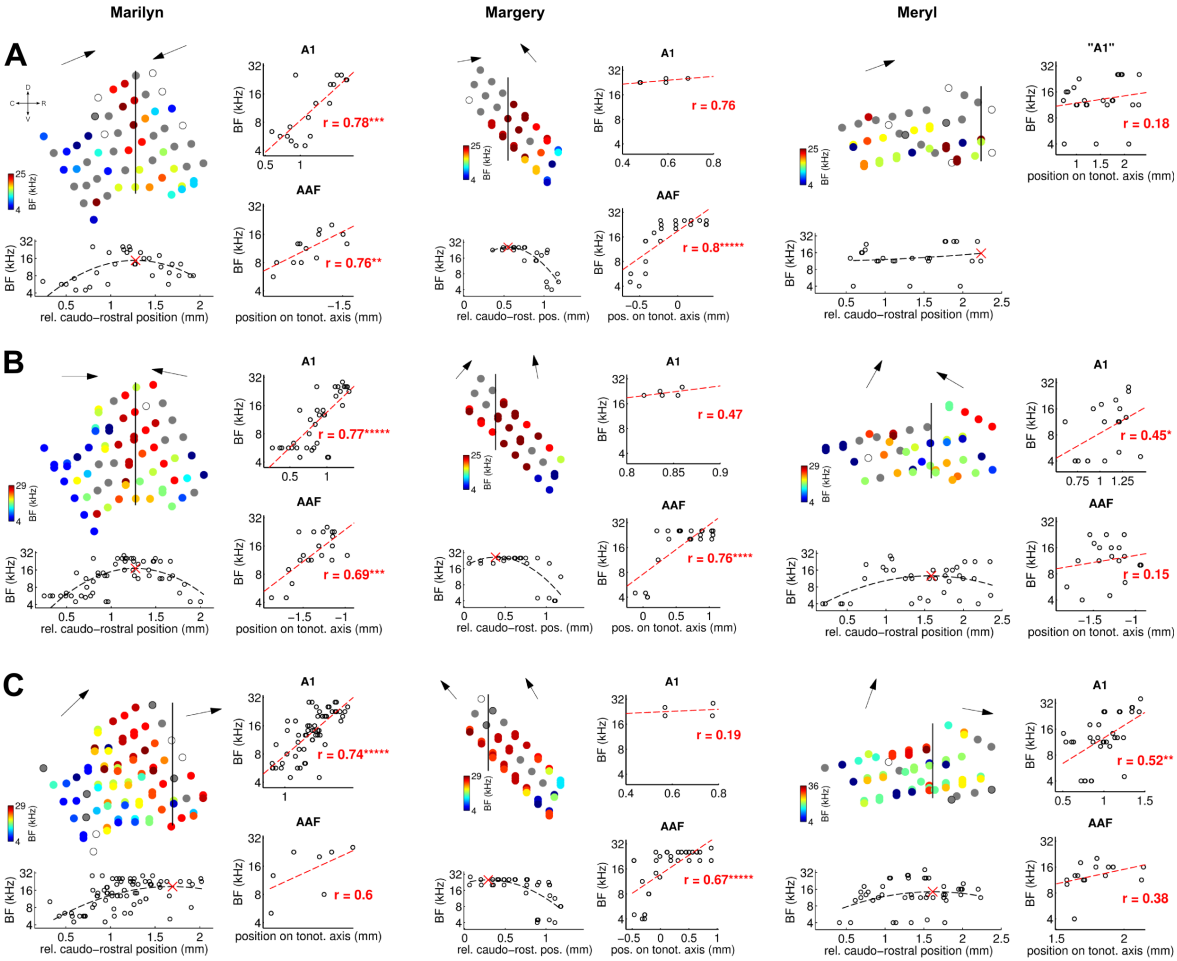


Figure 3.10: **Comparing tonotopic maps across cortical depth.** Topographic distribution of BF in the supragranular (***A***), middle (***B***) and infragranular layers (***C***) of auditory cortex in three different mice (left–right). Note the variety of changes between the layers, in the direction (arrows) and strength (r values in red) of tonotopy, and in the placement of the A1–AAF boundary (vertical black line, determined by the rostrocaudal BF distribution; see figure 3.8). Map and figure conventions are as for figure 3.9, except that sites estimated to be outside the two primary fields are not displayed here, for simplicity. Single asterisk with r value denotes $p < 0.05$; n asterisks denote $p < 10^{-n}$ (up to 5). Data in ***B*** are repeated from figure 3.9 A-C. Cases where a defined subfield contained fewer than 5 tuned recording sites, such as A1 in the middle column, were excluded from the layer-by-layer comparisons illustrated in figure 3.11.

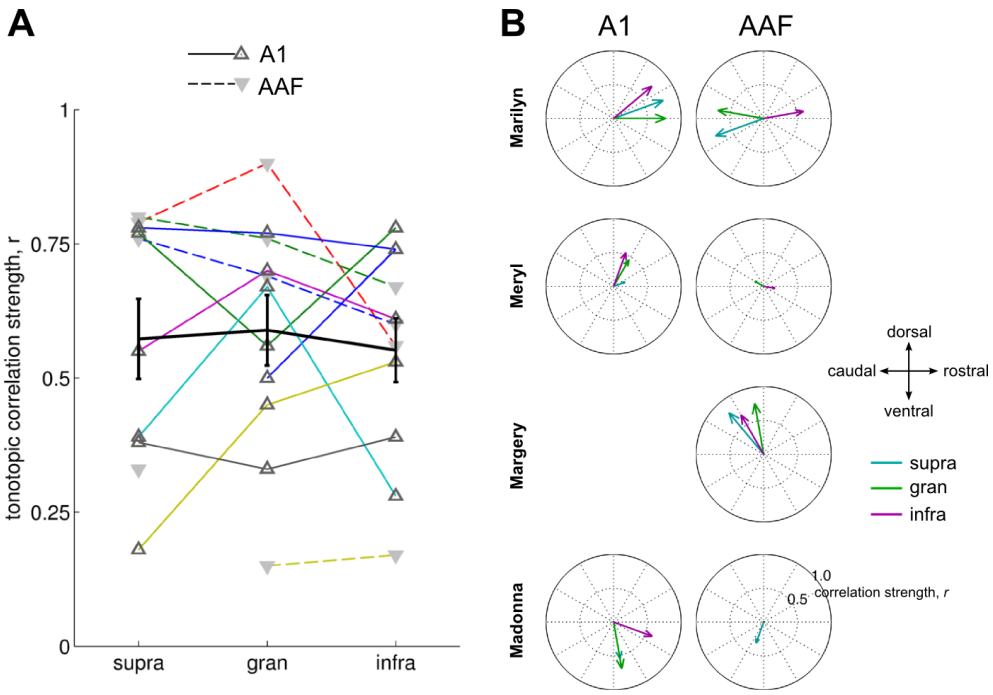


Figure 3.11: **Strength and direction of tonotopy across cortical depth.** ***A***: Correlation coefficients, r, for the variation of BF with location on the tonotopic axis, from the different layers in the two primary subfields (A1 and AAF) of 9 different mice. This includes animals mapped less extensively than those in figures 3.9, 3.10; in such cases BF was correlated with rostrocaudal position. Coloured lines join observations from the same animal, wherever those values could be calculated. Mean value ±SEM is shown in black; none of the mean changes in r between layers were significant (paired t-tests; see text). ***B***: Polar plots indicating the direction of the tonotopic axes, in each layer category (colours) of each subfield (columns) of the four mapped animals (top–bottom); length of the arrows gives the strength of the correlation (r).

inar changes to whatever degree of frequency organisation is present. Interestingly, they see a correlation between the tuning of cells in layer 2/3 and 4 when they consider the **median** BF of paired, vertically separated imaging fields. Since my electrodes sample neuronal activity 'blindly' at fixed intervals across the cortex, the inconsistent maps and the supragranular increase in untuned sites which I have observed are entirely consistent with the suggestion that tonotopy in the mouse cortex, especially in superficial layers, takes the form of a coarse, relatively untidy trend rather than a precise map.

Such laminar variation also fits with recent, presently unpublished observations made in the laboratory of Kevan Martin (Perrella et al., 2013). Their whole-cell reconstructions suggest that layer 4 cells in mouse A1 project to superficial layers in a much more diffuse fashion than, for example, the thalamorecipient cells of an obviously columnar field such as cat V1 (Gilbert and Wiesel, 1989).

When considering their results in detail, my results are also surprisingly consistent with the 'robust' tonotopy reported across the cortical layers by Guo et al. (2012). Outside the middle layers, they only observed an organised frequency map upon exclusion of a significant minority of poorly tuned sites (up to ~40% in superficial layers, reading from their figure 5D on p.9166). Furthermore, the columnar analysis presented by Guo et al. (2012) is limited to a subset of recordings made with a single-shank multielcectrode; if the fine-scale maps they show for middle layers were available at other depths, they might reflect the variability see in my figure 3.10.

3.5 Tuning and tonotopy in local field potentials

If the frequency maps revealed by spike recordings are generally coarse and vary between animals (figure 3.9) and layers of the cortex (figure 3.10), then one strategy for revealing smoother tonotopy might be to measure local field potentials (LFPs). These lower-frequency signal types are thought to integrate neuronal signals from a greater area and to include some contribution from subthreshold activity (Kajikawa and Schroeder, 2011). According to Kaur et al. (2004), in rat A1 this inclusive sampling of synaptic activity results in broader tuning curves than spiking responses.

To explore how the tuning and tonotopy of LFPs compare with the spike data outlined above, I extracted LFPs from each recording using a 300 Hz low-pass filter (for more details see section 2.3.1). I then evaluated the response amplitude of these filtered signals by calculating the standard deviation of each trace, within a 100 ms window commencing 10 ms after stimulus onset. An example of an averaged LFP trace and FRAs derived from these signals are shown in figure 3.12A.

3.5.1 Where present, LFP tuning correlates weakly with multi-unit tuning

LFP-derived FRAs were broadly similar to those assembled using spiking responses (compare figure 3.12 A,B). They also appear at least as noisy as the MUA data and those which do show a clear tuning curve are, similarly, more prevalent in granular layers and layer 5 (figure 3.12A and other data not shown). Fewer sites showed significantly tuned LFPs than tuned MUA, according to the criterion described above (424 versus 518 recording sites out of 1020 in primary areas, from 9 mice; for criterion see section 2.3.4). The pop-

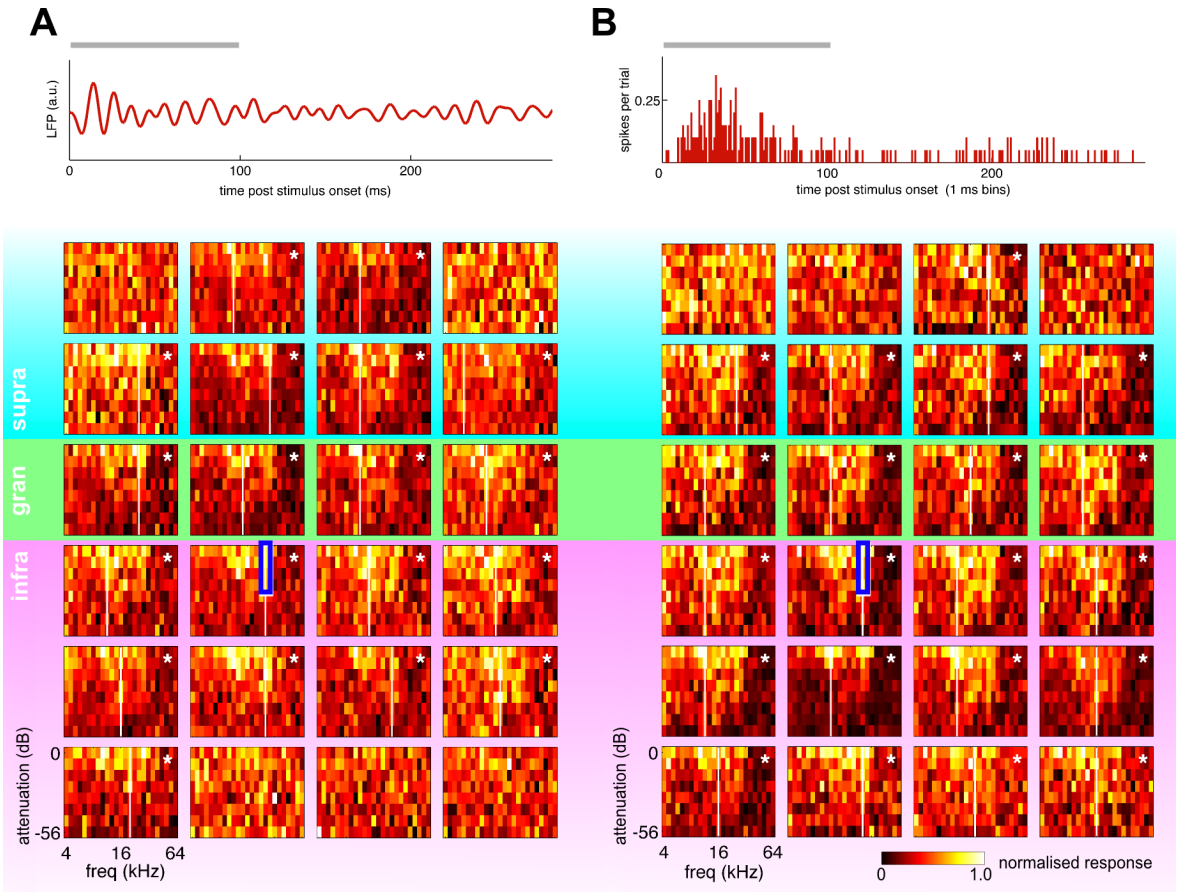


Figure 3.12: **Examples of pure-tone LFP responses.** ***A*** illustrates a sample of LFP responses to pure tones from a cluster of 24 channels in A1, with multi-unit responses from the same sites shown in ***B*** for comparison. Shown at the top are an averaged LFP trace (***A***) and post-stimulus time histogram (***B***) based on 20 sweeps (5 presentations of one site's best frequency, at each of the 4 loudest sound levels: see blue boxes in fourth row of FRAs). Grey bars indicate timing of stimulus. The lower panel shows the FRA for each site and those with significant tuning (see section 2.3.4) are marked with an asterisk. Coloured shading indicates the source layers, as indicated on the far left (depth determined based on position of LFP reversal, as shown in figure 3.1). Note that the LFP-derived FRAs are broadly similar to, and just as noisy as, those produced by multi-unit data.

ulation of sites with tuned LFP responses overlapped but was not the same as the set of sites with tuned spike data (figure 3.13A). Some 318 sites were noise responsive and frequency-tuned in both signal types, and the best frequencies obtained from these sites show a significant, though not particularly strong, positive correlation ($r = 0.52$, $p < 10^{-21}$; see figure 3.13B). Overall, the two sets of differently derived BFs also showed similar distributions (LFP mean BF 14.7 kHz ±8.27 SD; MUA mean BF 15.0 kHz ±8.7; null hypothesis supported by Kruskal-Wallis test with $p = 0.81$).

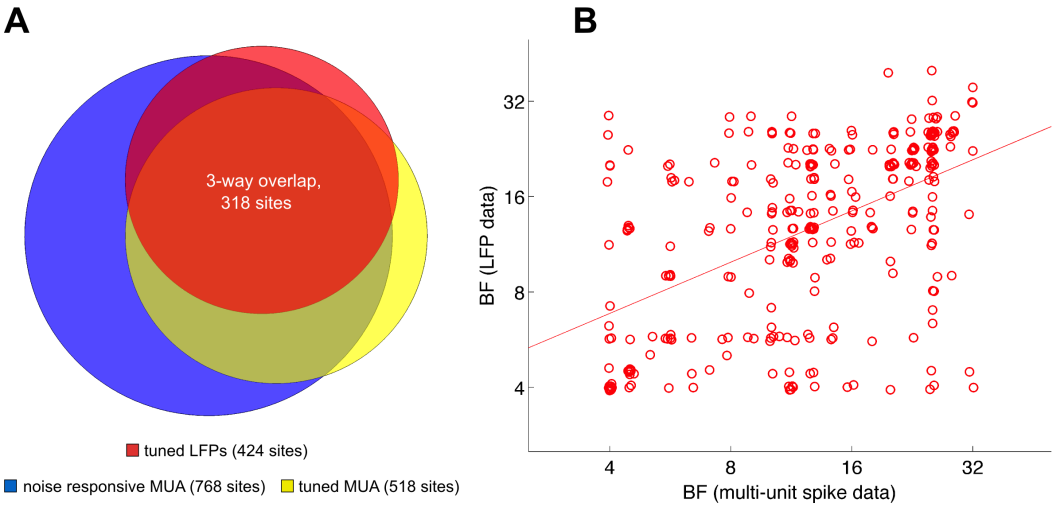


Figure 3.13: **Correlation of LFP tuning with MUA tuning in primary areas.** As shown in ***A***, frequency tuning was observed in LFP responses at 424 sites across primary areas (A1 and AAF) in 9 mice. Most of these sites (382) are also responsive to noise bursts and they overlap with the population of tuned MUA recordings (yellow); 318 sites are in all three groups. The scatter plot in ***B*** demonstrates that best frequencies (BFs) calculated from LFPs and spikes are positively correlated ($r = 0.52$, $p < 10^{-21}$); they are also similarly distributed (Kruskal-Wallis test, $p = 0.81$). Since the BF values come from a discrete set of 25 frequencies (see section 2.2.4), they have been jittered slightly so that all pairs are visible.

3.5.2 LFPs do not significantly improve detection of tonotopy

Since tonotopy in the mouse cortex is absent or degraded on fine scales but usually present at larger scales (Bandyopadhyay et al., 2010; Rothschild et al., 2010; Hackett et al., 2011,

and my figures 3.9, 3.10), I hypothesised that the wider catchment of LFPs as a neurophysiological signal would produce more consistent tonotopic maps. Three examples of the tuning maps produced in this way appear in figure 3.14A, presented for comparison alongside maps derived from MUA in the same animals (same figure, B).

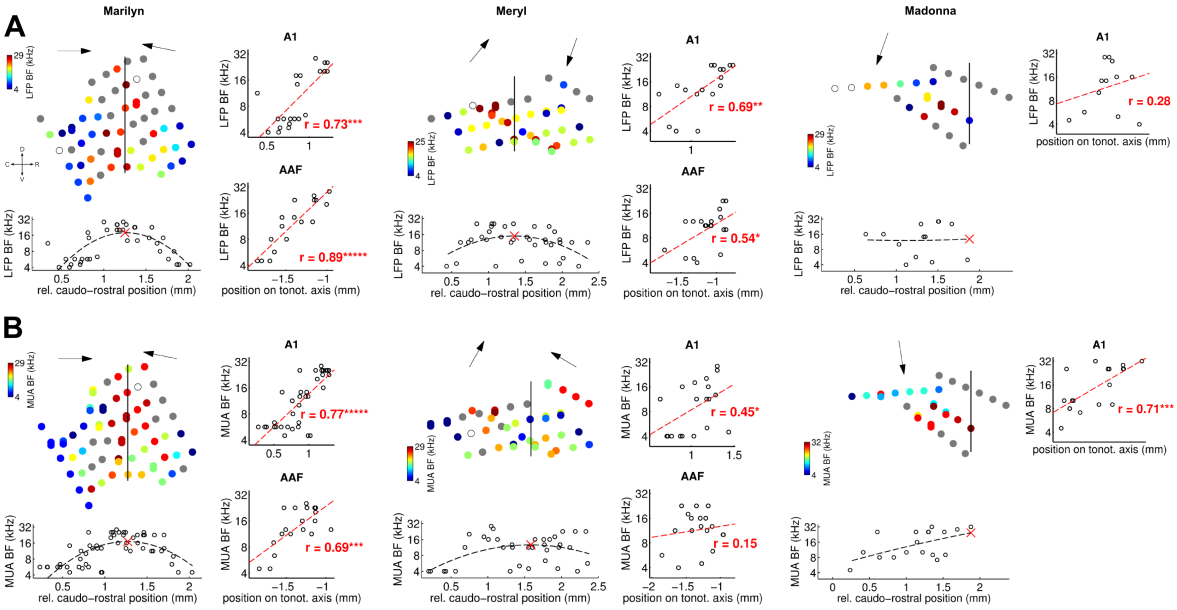


Figure 3.14: **Comparing tonotopic maps detected by LFPs and MUA.** ***A***: Maps of BF across the auditory cortex of three different mice (left–right), derived from LFP responses to pure tones in granular layers. ***B***: Maps from the same animals, derived from spiking responses. Map and plot conventions are as for figures 3.9 and 3.10; data in ***B*** are repeated from figure 3.9 A, C and D, shown here for comparison. Note the similar tonotopic gradients detected in LFP responses, in cases where the MUA also revealed obvious frequency organisation (left panel; A1, middle panel) but changes in both the strength and direction of the correlation in the other cases.

In cases where spike data revealed a clear frequency gradient in granular layers, LFP responses produced similar maps (e.g. figure 3.14, left panel, and A1 in middle panel). In cases where spiking activity was less obviously tonotopic or did not fit the expected pattern, LFPs similarly failed to reveal canonical tonotopic organisation (e.g. right panel, and AAF in middle panel). Comparing the strength and direction of tonotopy across all recorded mice, the LFP- and MUA-derived gradients tend to have similar orientation (fig-

ure 3.15B) and there is a trend towards higher correlations in the LFP data (upward sloping lines in figure 3.15A), but the mean change is not significant (paired t-test, p=0.19).

My hypothesis therefore garners only weak support from these data. Extracting median values across horizontal cortical space may yield BFs more consistent with tonotopy than fine-scale sampling of local neuronal populations (Winkowski and Kanold, 2013), but LFPs, which physically integrate diffuse local activity, produce maps that are not significantly better organised than those from spike data. This has now been shown both in my hands and in those of others (see Guo et al. , 2012; note however that they report maps from both MUA and mid- to high-frequency LFPs that are more precisely organised than much of my data in either case).

Based on the data I have presented so far, tonotopy is a detectable but inconsistent attribute of responses in the coarsely-sampled mouse cortex. Many frequency maps appear patchy and some almost devoid of organisation, despite the same recording sites exhibiting responses to broadband noise. There appear to be many sites where recorded activity is rather indifferent to pure tones, the archetypal stimulus for auditory neurophysiological mapping.

Perhaps tonotopy remains one of the few acknowledged organising principles for auditory cortex because our paradigm for probing the cortex is predisposed to detecting it. This would be consistent with the data above, which were produced within this paradigm but sampled mouse cortex in an extensive and unbiased manner, with decidedly mixed results. To begin exploring how important tonotopy really is to the computational functioning of the cortex, I next look for an effect on these canonical frequency gradients of switching from pure tones to a more complex stimulus.

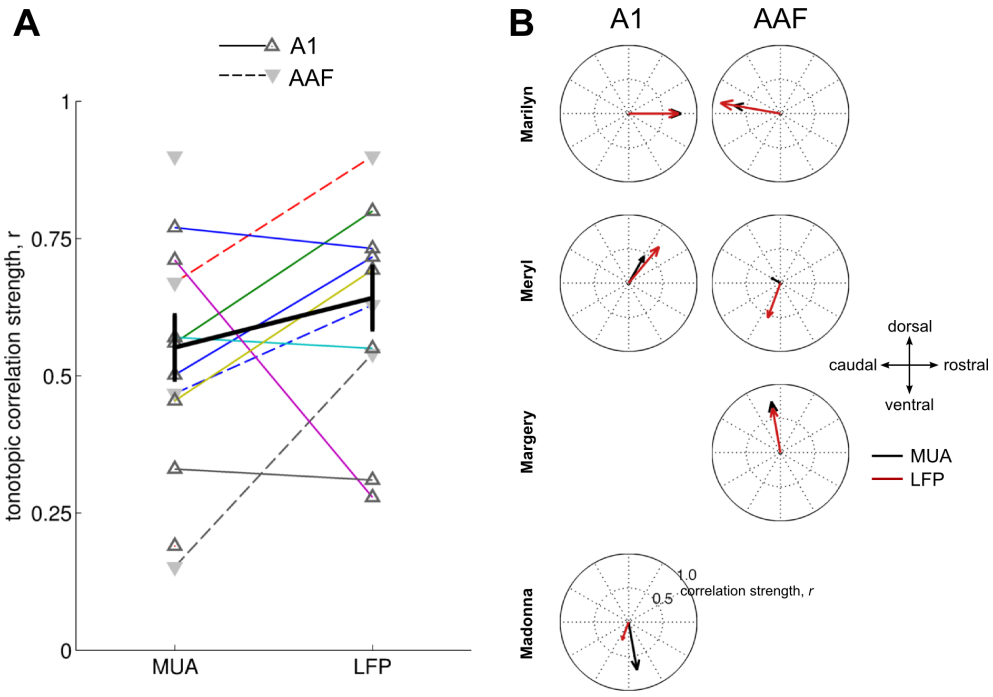


Figure 3.15: **Strength and direction of tonotopy detected by LFPs.** ***A***: Summary of correlation coefficients, r, for the variation of BF with location on the tonotopic axis, derived from either MUA or LFPs in the two primary subfields (A1 and AAF). As in figure 3.11, coloured lines join observations from the same animal and black line indicates mean value ±SEM. The mean change in r derived from MUA (0.55±0.059) and LFPs (0.64±0.057) was not significant (paired t-test; p=0.19). ***B***: Polar plots indicating the direction of the tonotopic axes revealed by each signal type (colours) within each subfield (columns) of the four mapped animals (top–bottom); length of the arrows gives the strength of the correlation (r).

3.6 A possible effect of stimulus complexity

In order to explore whether frequency tuning and tonotopy are more or less evident when the auditory cortex is processing a more complex stimulus, I recorded further multi-unit responses during presentation of dynamic random chords (DRCs). These stimuli are described in more detail in section 2.2.5, but figure 3.16 shows how they compare with simple pure tones. It is important to note that tones are presented simultaneously at a variety of levels, changing (in this case) at 25 ms intervals, so that a neuron's receptive field can be estimated as a spike-triggered average. Because DRCs better approximate the complexity of a natural auditory scene (deCharms et al., 1998), they have proved powerful for illuminating how cortical neurons perform complex tasks such as integrating spatial cues (Schnupp et al., 2001) and adjusting to changes in auditory contrast (Rabinowitz et al., 2011). In the mouse, DRCs have been used to investigate spectrotemporal variation in responses between the subfields A1 and AAF (Linden et al., 2003), but the tuning and frequency maps produced by pure-tone and DRC stimulation have not been compared in detail.

Figure 3.17 displays a sample of the spectrotemporal receptive fields (STRFs) calculated from my recordings, alongside the FRAs calculated for pure-tone responses at the same sites. To determine whether each STRF was a valid estimation of response patterns at the site in question, I excluded 10% of the data from the initial calculation and tested the STRF against it. I quantified the predictive capability of each STRF as the percentage of signal power explained, or SP_{exp}, which is a corrected estimate of the variance in the recorded spike-rate that is accounted for by the model receptive field (for more detail, see section 2.3.5). I set a threshold for a predictive STRF at $SP_{exp} > 0.1$; this categorisation was consistent in nearly all cases with visual assessment of whether or not the STRF showed a

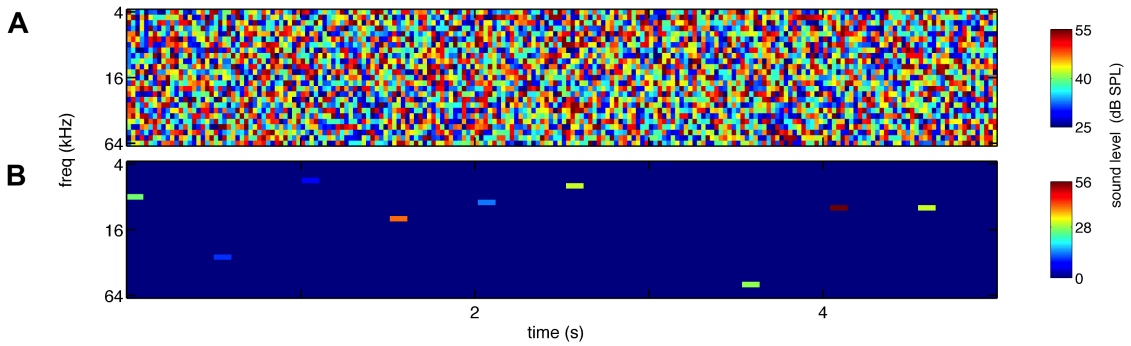


Figure 3.16: **Stimulus structure of dynamic random chords (DRCs).** ***A***: Spectrogram of a 5-second sample from a DRC stimulus. Each 25 ms chord is a superposition of 25 frequencies, spanning 4—64 kHz in 1/6 octave intervals. The level of each frequency is drawn from a uniform distribution spanning 25—55 dB SPL. ***B***: The pure-tone stimulus paradigm, shown on the same time scale for comparison; tone pips were played with 100 ms duration and 0.5 s inter-stimulus interval (ISI), and were drawn from the same set of 25 frequencies as the DRC elements. Their levels were varied from 8—56 dB SPL, in 8 dB steps. (For more detail, see secti ons 2.2.4, 2.2.5).

coherent pattern of excitation and/or inhibition (see figure 3.17A and section 2.3.5). Each site's STRF-derived BF was identified as the frequency driving the strongest response in the 100 ms immediately preceding the spike bin (right-most 4 columns in each STRF, figure 3.17).

3.6.1 Tuning of DRC responses correlates weakly with pure-tone tuning and tends toward higher frequencies

Of the 1020 sites estimated to be within primary fields (A1 and AAF), only 341 yielded a predictive STRF; of these, most (293) were also responsive to broadband noise. There was significant overlap with the 581 recordings that showed pure-tone tuning and some 213 noise-responsive sites also produced both a tuned FRA and a predictive STRF (figure 3.18A). Comparing these sites' BFs in response to DRCs and pure tones revealed a relatively weak, positive correlation (though highly significant: $r = 0.48$, $p < 10^{-13}$; see

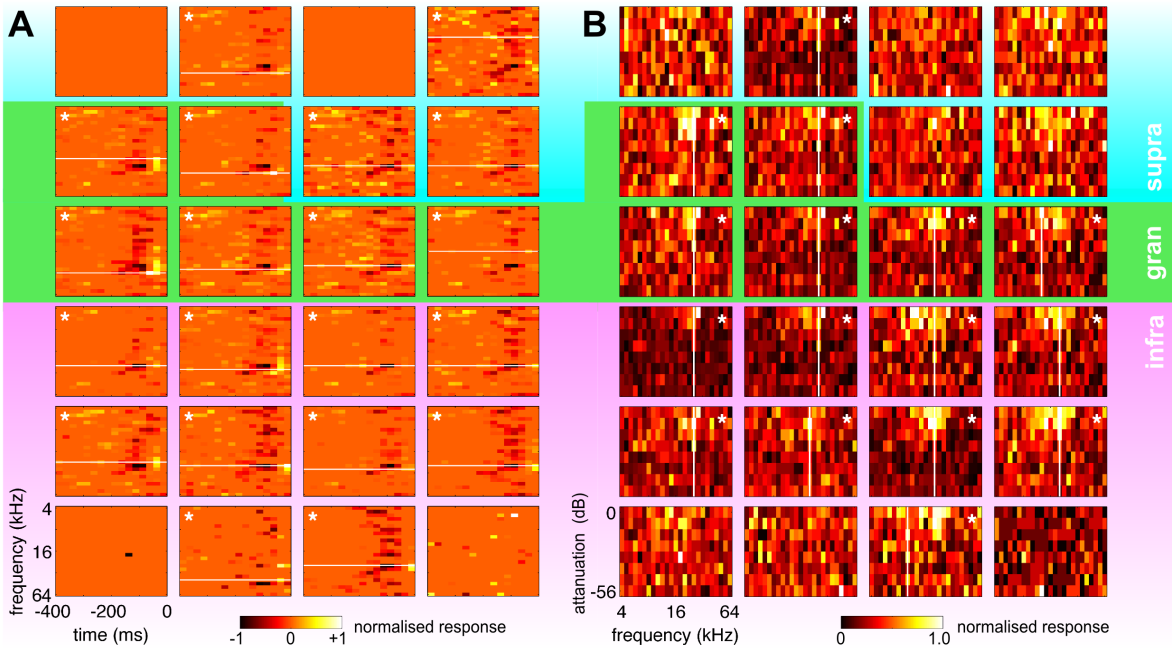


Figure 3.17: **Examples of receptive fields from DRC responses.** ***A*** illustrates a sample of 16 spectrotemporal receptive fields (STRFs) from a cluster of sites within a single A1 penetration; FRAs derived from pure-tone stimulation at the same sites are shown in ***B*** for comparison. Each STRF is a spike-triggered average, with time plotted relative to the spike bin; light and dark areas in each plot indicate excitatory and inhibitory regions of the receptive field, derived from the regression weight, with mid orange indicating a weight of 0. Asterisks in ***A*** denote STRFs satisfying my predictive criterion ($SP_{exp} > 0.1$; see section 2.3.5); most of these show a clear excitatory region within 75 ms of the spike bin, containing the site's BF (white line), preceded by an inhibitory region at a similar frequency. Asterisks in ***B*** denote sites where pure tone responses were significantly tuned (see section 2.3.4; white line marks BF). Note that, with some exceptions, the BFs registered in response to DRCs and pure tones are similar. Granular, supra- and infragranular layers are again indicated by coloured background shading (note this is one of the uneven cases mentioned in section 3.2.1.

figure 3.18B) and two rather different distributions of frequency preference (figure 3.18B, C; Kruskal-Wallis test, $p < 10^{-21}$). BFs within the complex stimulus were higher and more tightly clustered than pure tone BFs (for DRCs, median BF = 22.6 kHz and interquartile range 16—24.5; for pure tones, median BF = 16 kHz and interquartile range 11.3—25.4; for histogram see figure 3.18C).

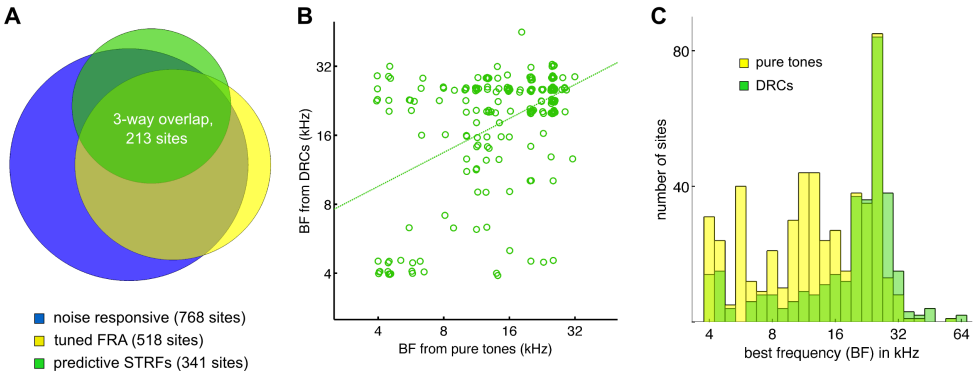


Figure 3.18: **Comparing tuning of DRC and pure tone responses.** ***A*** illustrates the overlapping populations of sites in primary areas which exhibited noise responses (blue), significant tuning in their spiking responses to pure tones (yellow), and responses to DRCs which yielded a predictive STRF (threshold: $SP_{exp} > 0.1$; see section 2.3.5). The scatter plot in ***B*** shows the weak, but significant, positive correlation between BFs arising from pure tone and DRC responses ($r = 0.48$, $p < 10^{-13}$; as in figure 3.13B, values have been jittered so that each pair of BFs is visible). A relative over-representation of higher frequencies is obvious in the DRC-derived tuning and this is also reflected in a histogram of the two populations of BFs (***C***). The difference between the two distributions is highly significant (Kruskal-Wallis test, $p < 10^{-21}$).

3.6.2 Tonotopy is variable in DRC responses

The findings above show that while the stimuli contained the same set of frequencies, tuning across primary cortical recordings from 9 mice was more tightly clustered around a higher median BF when calculated for a dynamic, continuous stimulus. What does this mean for tonotopy?

As shown in figure 3.19 (compare A, B), frequency maps produced from DRC responses reflect the relative over-representation of higher frequencies reported above. The tono-

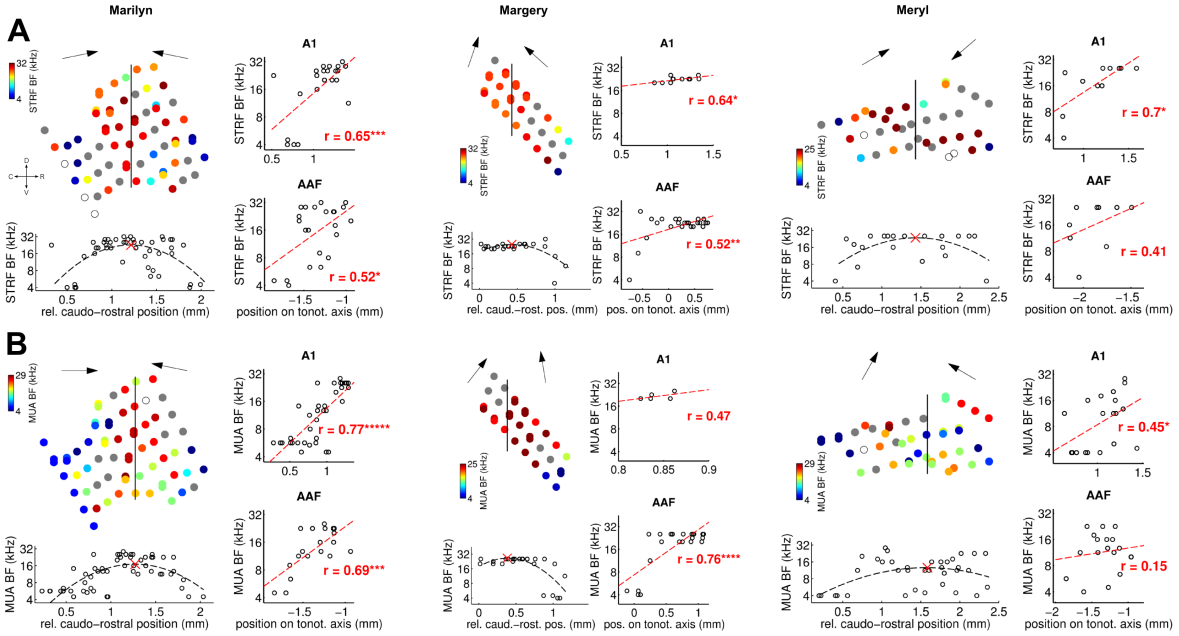


Figure 3.19: **Comparing tonotopic maps produced by DRCs and pure tones.** ***A***: Maps of BF recorded in response to DRCs, from granular layers of three different mice (left–right). ***B***: Maps from the same three animals, derived from pure tone responses (data from figure 3.9 A–C, shown here for comparison; map and plot conventions here are the same as in that figure). Note the tendency toward higher BFs in the DRC responses (quantified in section 3.6.1), as well as some shifts in the direction of tonotopy and some decreases (left panel) and increases (right panel) in the strength of the tonotopic correlation.

topic organisation, however, is not consistently degraded or improved by the switch to DRCs. Changes are evident in nearly every case, in tonotopic strength or direction or both (see also figure 3.20), but there is no obvious trend; the slight mean increase in the tonotopic correlation observed with DRCs (figure 3.20A, black line) is not significant ($p = 0.85$, paired t-test).

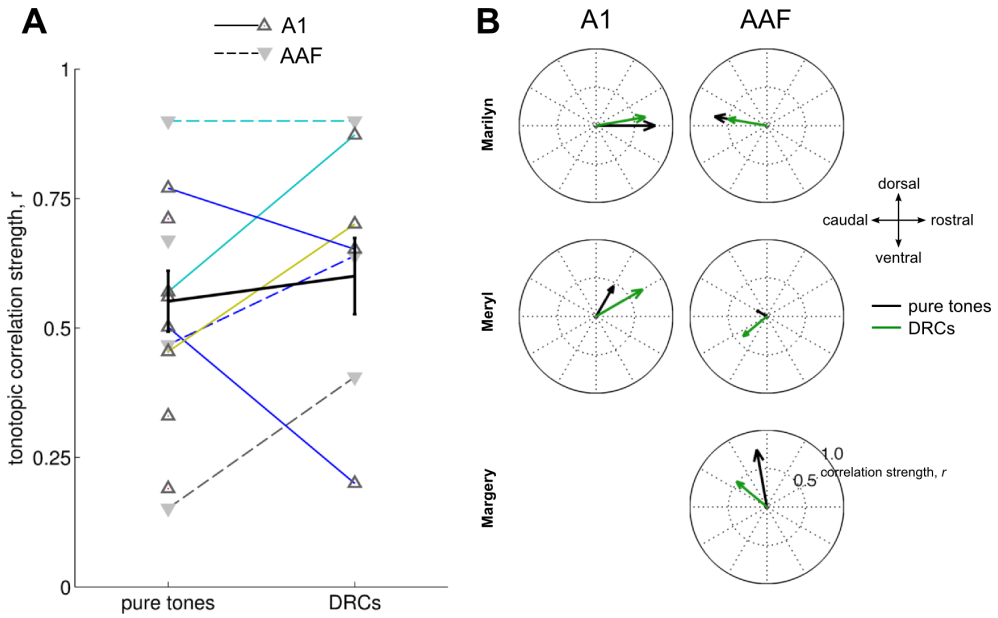


Figure 3.20: **Strength and direction of tonotopy produced by DRCs.** ***A***: Summary of correlation coefficients, r, for the variation of BF with location on the tonotopic axis, derived from either DRC or pure-tone stimulation, in the two primary subfields (A1 and AAF). As in figures 3.11 and 3.15, coloured lines join observations from the same animal and black line indicates mean value ±SEM. There is considerable variability between mice and between conditions, and the mean change in r for DRC stimulation (0.60±0.074 SEM) compared to pure tones (0.55±0.059) was not significant (paired t-test; p=0.85). ***B***: Polar plots indicating the direction of the tonotopic axes revealed by each signal type (colours) within each subfield (columns) of the three mapped animals (top–bottom) for which DRC-based gradients could be calculated; length of the arrows gives the strength of the correlation (r). Pure tone data (left column in ***A***, black arrows in ***B***) are the same as the control (MUA) data presented in figure 3.15 and the granular-layer data presented in figure 3.11.

In summary, using a dynamic stimulus does appear to affect the frequency representation observed in mouse primary auditory cortex, principally by eliciting higher BF values than pure-tone stimulation. It also produces inconsistent changes in tonotopic organisa-

tion.

3.7 Temporal variation in responses

The final dimension I have explored for its effect on frequency tuning is that of time. Work in ferrets has shown that neurons in the auditory cortex can carry significant information about a stimulus up to 500 ms after its offset (Campbell et al., 2010). In my own recordings from the mouse cortex, I have also observed surprisingly late responses with very obvious tuning (for example, figure 3.21B). Even within initial onset responses to pure tones, close examination reveals diverse, time-varying receptive field structures. Figure 3.21 presents a descriptive survey of such effects; I have not quantified the incidence of each, but offer some indication of the minimum number of sites at which each effect was observed out of the 518 tuned sites estimated to be within primary fields.

3.7.1 Post-activation suppression produces matched, inhibitory FRAs

The initial excitatory response in tone-responsive channels is frequently followed by a period of suppressed activity; the time course of this suppression varies (compare first and second columns in figure 3.21A) and pooling responses across all tone presentations for spike histograms can mask the dip below baseline activity. I measured frequency tuning within this post-excitation window and in at least 110 recordings found striking, inverted FRAs, with concentrated areas of absent spikes closely matching the areas of high spike counts in the preceding excitatory FRAs (3.21A). This means that in those trials where there was a strong, selective response to the presented tone, the subsequent period of suppression was pronounced and reliable.

This post-activation inhibitory period is an acknowledged property of auditory cortical responses, often associated with the forward suppression of responses to a subsequent stimulus (e.g. Brosch and Schreiner, 1997; Wehr and Zador, 2005, but note that Scholes et al. (2011) recently demonstrated that forward suppression in guinea pig cortex is tuned more by the probe frequency than neuronal BF). In the mouse it has previously been reported in both primary fields, where suppression is more pronounced in middle and superficial layers (Christianson et al., 2011). I have not explored the laminar distribution of the inhibitory FRAs exemplified in figure 3.21A, but the frequency-specific suppression they reflect is consistent with substantial evidence from whole-cell recordings that excitation and inhibition in auditory cortical neurons are co-tuned (e.g. Wehr and Zador, 2003; Tan et al., 2004; Wu et al., 2008), including in the mouse (Tan and Wehr, 2009). Furthermore, unlike many of the the shifts in excitatory tuning summarised in figure 3.21 B–D, this frequency-matched suppression is mirrored in the pattern of activity recorded in STRFs from the same sites (e.g. bottom panel, 3.21A). Such reverse-correlated measures of neuronal tuning frequently reveal inhibitory echoes, both in my data and elsewhere (e.g. figure 3.17A; Theunissen et al., 2000; Miller et al., 2002; Linden et al., 2003).

3.7.2 Late tuning

Following the period of suppression, many sites exhibit a 'rebound' or 'bounceback' window of activity, during which the spike-rate again exceeds baseline. In at least 49 sites, I observed that this activity was tuned and, interestingly, that tuning differed from what was observed for the initial excitatory response; examples are shown in figure 3.21B. This shifted, long-latency tuning was not consistently higher or lower than that of the primary response and did not appear to be confined to particular layers or cortical subfields (data

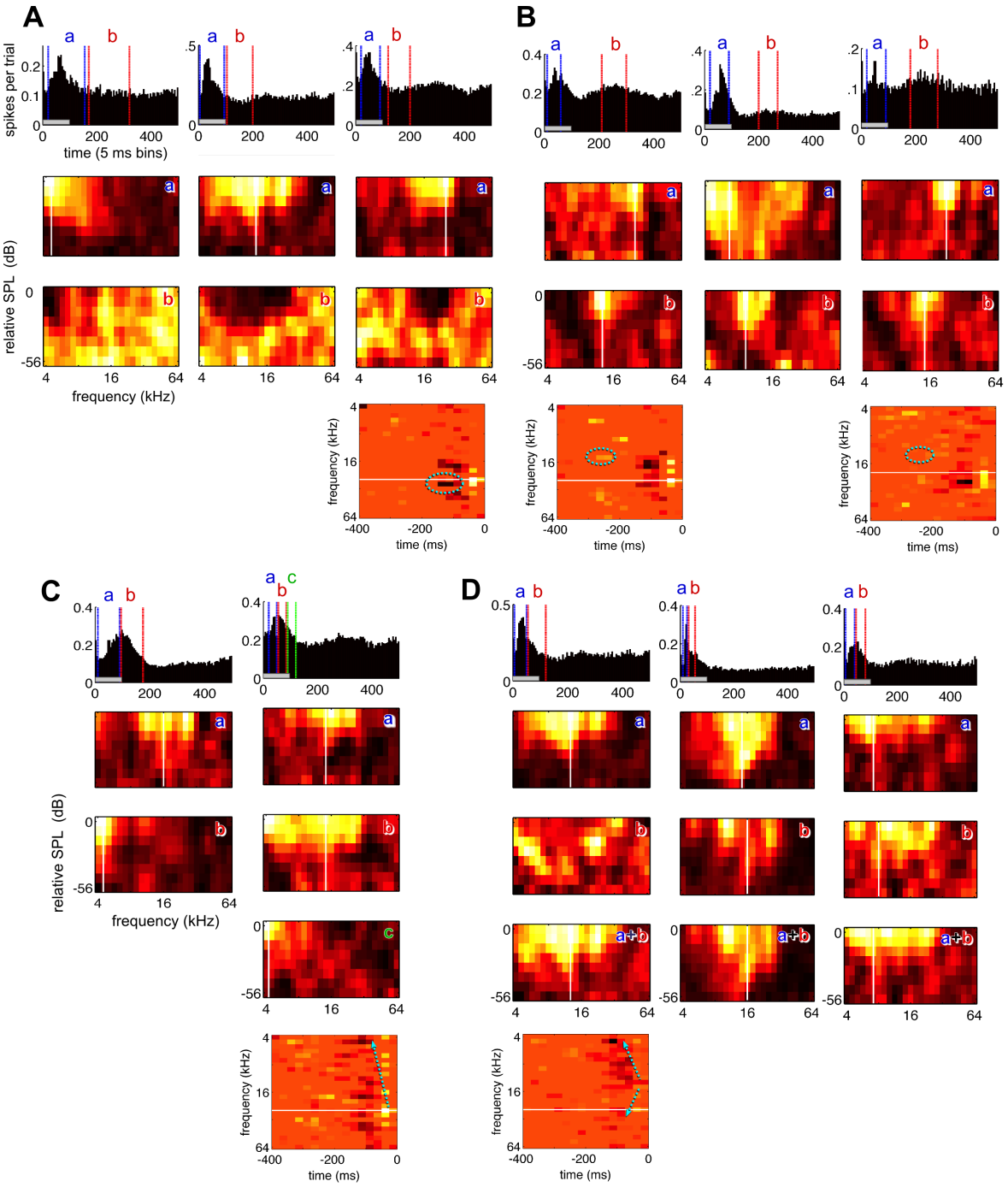


Figure 3.21: **A survey of temporal effects on frequency tuning.** This is a sample of recordings illustrating four different examples of time-varying frequency responses: ***A***, inverted FRAs during the post-activation inhibitory phase; ***B***, late tuned responses; ***C***, shifting tuning during the initial response; and ***D***, expanding tuning during the initial response. In each case, a post-stimulus time histogram (PSTH) for pooled responses to all tone–level combinations is at the top, with coloured lines and labels a–c identifying the time windows used to calculate the FRAs beneath. Grey bar indicates timing of the stimulus. Where the site in question yielded a predictive STRF in response to DRCs, this is presented at the bottom. White line in STRFs and FRAs marks best frequency and FRAs are presented in smoothed form (see section 3.2.2). In most cases, the initial excitatory BF is consistent between corresponding FRAs and STRFs. Dotted markings on each STRF highlight where we might expect to see enhanced or suppressed activity corresponding to the temporal change illustrated above it; this is only occasionally evident. (See text for further discussion.)

not shown). My observations suggest that responses at relatively long latencies, which have only rarely been systematically investigated (see Moshitch et al., 2006; Campbell et al., 2010; Walker et al., 2011; Rajan et al., 2013), should not be discounted when calculating cortical receptive fields.

Activity at the same sites in response to DRCs only rarely produced receptive fields with components that matched this late, shifted frequency tuning. One such example is shown in figure 3.21B (bottom left, dotted circle). In most cases, such as in the right-hand column of the same panel, beyond the initial excitatory response and subsequent suppression there was little coincidence in response tuning between the two data sets. Indeed even the tuning of that initial response, as shown in figure 3.18, was only weakly correlated between FRAs and STRFs. This late tuning, perhaps even more so than that of more immediate responses, appears to be sensitive to the context in which the stimulus is presented.

It is interesting to note that the period of this tuned 'bounceback' response (typically between 200 and 350 ms post-onset) is similar to the frequency at which Christianson et al. (2011) found neurons in primary mouse cortex were best able to follow click trains. That study even showed that train rates of 3–4 Hz could elicit 'augmenting' responses, wherein spikes are driven more strongly by subsequent clicks within a train than by the first click. In discussing their findings, Christianson et al. note that while it is tempting to speculate that this apparently preferred rate of stimulation might reflect specialisation for sound modulation rates that have environmental significance, typical mouse vocalisations show no corresponding pattern (repetition periods are typically 100–180ms; see Liu et al., 2003). The computational significance of this time-, frequency- and context-sensitive pattern of activity remains to be elucidated.

3.7.3 Shifting and expanding frequency responses

Even within the initial excitatory response that precedes the suppression and rebound periods described above, there is often complexity in the temporal structure of pure-tone tuning. I explored these variations by constructing FRAs for smaller time windows within the initial response, and have displayed examples in figure 3.21 (C,D).

Firstly, in recordings from at least 69 sites I noted that tuning shifted in one direction between sub-windows of the initial response. This shift was frequently, but not always, in a downward direction (i.e. towards lower frequencies). On some occasions the different FRAs appeared to represent discrete, non-overlapping responses (eg figure 3.21C, left-hand column) while other examples showed a clear progression from one type of tuning to another, including a period with broad tuning that included the intervening frequencies (same panel, right-hand column).

These patterns are somewhat reminiscent of the shifting **spatial** receptive fields which have been reported in ferret A1 (Mrsic-Flogel et al., 2005). Just as those responses suggest directional motion-sensitivity, the frequency tuning shifts I have observed may have a role in processing stimuli which modulate frequency over time. Others, notably the team of Khaleek Razak, have investigated how mouse auditory cortex responds to frequency-modulated (FM) sweeps, and have indeed revealed both rate and direction sensitivity in primary areas (Trujillo et al., 2011, 2013; Carrasco et al., 2013).

A second type of early temporal complexity is apparent in receptive fields which expand at slightly longer latencies to include a wider range of frequency-level combinations (figure 3.21D). This phenomenon has also been described by Kaur et al. (2004) in rats, Moshitch et al. (2006) in cats and Seybold et al. (2012) in mice. At least 56 of my record-

ings exhibited this type of response. Typically, a focal region of strong excitatory responses within the FRA, present at short latencies, fades away ~20–80 ms later and is replaced by responses at neighbouring frequency-level combinations, such that the windows combine to produce a continuous and fairly broad receptive field (third row of FRAs, figure 3.21).

The Metherate group has explored this pattern of responses in the most detail, proposing that the fast responses in the middle of such an FRA (commonly at the neuron's characteristic frequency) derive primarily from thalamocortical inputs, whereas the slower, expanded responses arise intracortically (Kaur et al., 2004). Intracortical connectivity has been implicated in driving such 'sideband', expanded responses by pharmacological manipulation (Kaur et al., 2004), laminar current source density analysis (Kaur et al., 2005) and chronic reduction in inhibition by conditional gene knockout (Seybold et al., 2012).

Again, as for the slow responses discussed above, there was surprisingly little evidence for these tuning patterns in the same site's responses to a continuous, dynamic stimulus (see annotated STRFs, bottom of figure 3.21 C,D). This may be because the STRFs I have constructed are too coarse in the temporal dimension, such that their 25 ms bins cannot distinguish the changes as clearly as the subdivided FRAs. For example, the STRF shown in figure 3.21C does indicate a broad excitatory response extending to much lower frequencies than the site's BF, but it all falls within a single bin. Alternatively, the shifting and expanding patterns might be a product of the 100 ms tone duration, whereby continued, unchanging stimulation recruits more widespread activity. This would be consistent with the intracortical hypothesis of Kaur et al. (2004, 2005) discussed above.

3.7.4 Choice of response window can dramatically affect calculated tuning

At the notionally straightforward level of recording pure-tone responses to establish a cortical map, the temporal complexity sampled above suggests at the very least that neurophysiologists should consider very carefully their choice of response window. Figure 3.22 illustrates precisely this dilemma with a sample of 48 of my recordings from within a single penetration. Because of the sort of shifts in tuning illustrated in figure 3.21D, two different response windows produce strikingly divergent sets of BFs (compare lower left panels, figure 3.22 A,B). This is despite both windows commencing 10ms after stimulus onset and extending beyond the peak in the recordings' average spike histogram (precise windows were 10–90 ms and 10–170 ms).

It is worth repeating here that when I selected a response window within which to evaluate pure-tone tuning, the decision was made independently for each penetration; I chose a window which maximised the number of informative recording sites (based on the number meeting my criterion for significant tuning) and this was usually an inclusive window ranging from 90–150 ms in length, commencing 10–20 ms after tone onset. Such case-by-case evaluation was desirable because of variation in the overall time course of responses (e.g. compare first two columns of figure 3.21A), either due to regional differences in the cortex or fluctuations in the anaesthetic state of the animal. The process is discussed more fully in section 2.3.4.

These observations all indicate that the complete picture of cortical responses, even to straightforward pure-tone stimuli, is a complex one. Response timing, in particular, is taken for granted at the investigator's peril. Not only does choosing a single window ignore or elide the time-varying responses outlined in figure 3.21 and elsewhere (e.g. Moshitch et al., 2006), which may or may not be desirable for the task at hand: the specific

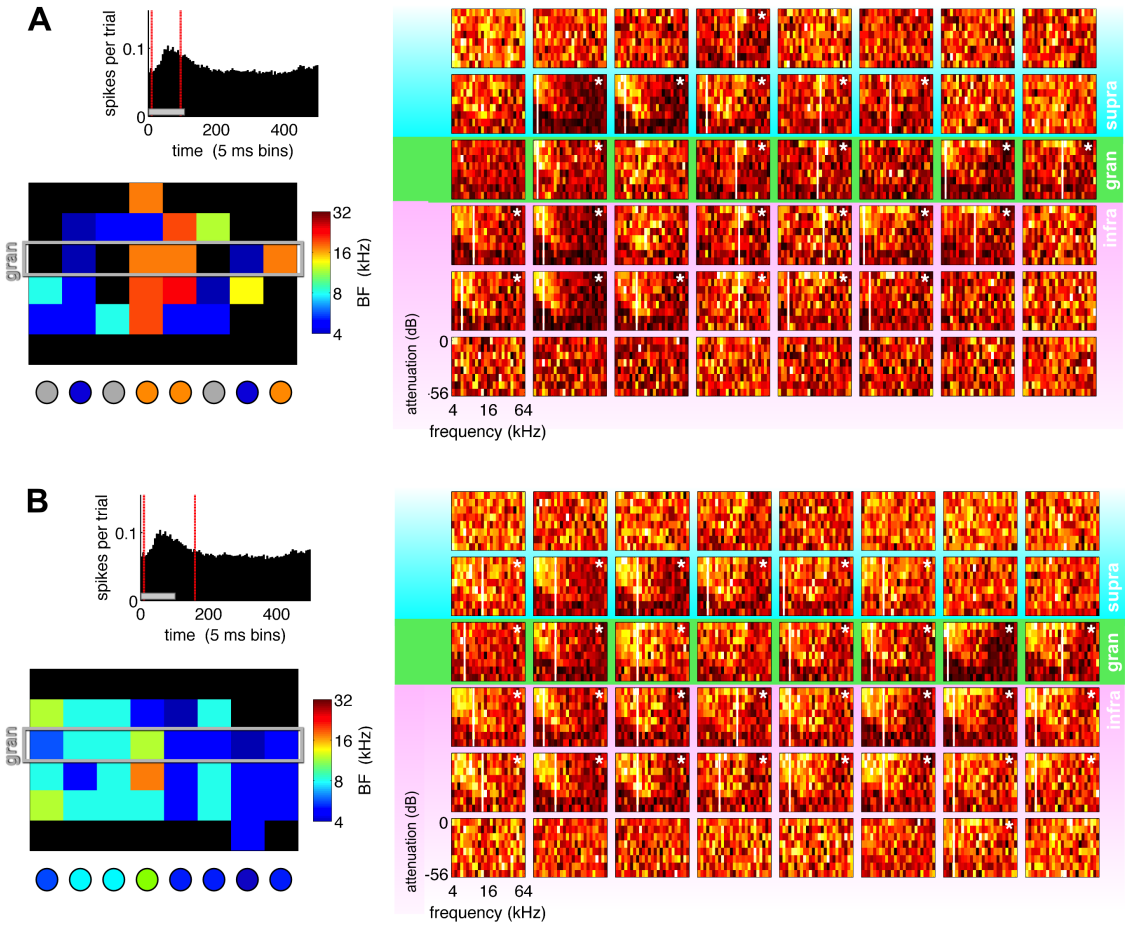


Figure 3.22: **Two response windows producing divergent sets of BFs.** An example of pure-tone responses at 48 sites within a single electrode penetration, analysed using two different response windows: 10–90 ms (***A***) and 10–170 ms (***B***; times post stimulus onset, indicated with red lines on spike histograms). The histograms show the mean response, pooled across all frequency-level combinations at all the recording sites shown; grey bar indicates timing of the stimulus. On the right is the grid of FRAs resulting from spikes within that window at each individual recording site. As in other figures, layer categories are indicated by coloured shading and sites showing significant tuning carry asterisks, with their BFs marked by a vertical white line (for tuning criterion see section 2.3.4). The coloured schematic on the left of each panel summarises these BFs across the grid. On these schematics, a grey outline highlights sites estimated to be within granular layers, and circles underneath illustrate frequencies which would have been placed onto a resulting map of granular-layer frequency tuning. This penetration is the one marked by a dotted red rectangle in figure 3.8A.

choice made can lead to dramatically different results in terms of the computed tuning curves and BFs needed to create a frequency map (as shown in figure 3.22).

Looking at these results another way, varying the timing window at which responses are measured is another perturbation which results in more variable BFs and less coherent tonotopy. Compare, for example, the granular-layer BFs which would be used for frequency mapping based on figure 3.22 A or B (circles, lower left of each panel; to see where this penetration fits into a map, note the dotted rectangle in figure 3.8A). Spike timing thereby joins cortical depth and stimulus complexity as a factor to which, in my hands, tonotopic organisation in the mouse cortex is sensitive.

3.8 Discussion

3.8.1 Overview and implications of results

In the chapter above, I have assessed how frequency tuning and the resultant cortical maps vary under several conditions, in an attempt to help illuminate the contested question of tonotopy in the mouse cortex.

Firstly, I considered the extent to which pure-tone tuning is itself detectable in different parts of the auditory cortex. Overall, of sites which showed a spiking response to noise bursts, a relatively slim majority in each animal were also tuned for sound frequency (mean 62%). I observed a drop in the prevalence of tuning between middle and superficial layers (figure 3.6). This is largely consistent with other published data (see Guo et al., 2012; Winkowski and Kanold, 2013, and discussion in section 3.3.1) and matches my subsequent observation that tuning, when present, also appears to be stronger in middle

layers (see figure 3.7). While it is a separate question from the topographic organisation of frequency preferences, this evidence about the prevalence of tuning helps to explain why tonotopy in mice, both anecdotally and in some published literature, is not always immediately obvious (Bandyopadhyay et al., 2010; Rothschild et al., 2010; Seybold et al., 2012).

Most, but not all mice, in my hands, showed some evidence of the expected, mirrored tonotopic gradients in granular layers of A1 and AAF (see section 3.4.1). Even in cases where such organisation was present, shifting to other layers (particularly supragranular; section 3.4.2) or to a more complex stimulus (DRCs; section 3.6.2) elicited changes in the strength and orientation of those gradients. The use of DRCs instead of pure tones even altered the overall population of BFs relative to that observed for pure tones (section 3.6.1). Additionally, the use of LFPs, which as a more integrative signal type might be expected to produce smoother results than spike counts, yielded similar results in both good and bad examples of tonotopy (section 3.5.2). In section 3.8.2 below, I seek to reconcile these data with varying published accounts of tonotopy in the mouse cortex.

Finally, I explored how pure-tone responses vary with time. In subsets of my results I found shifting and expanding FRAs when subdividing the initial excitatory response, as well as matched, inverted FRAs during post-activation suppression and differently-tuned late or 'rebound' responses (section 3.7). The matched, inverted FRAs are striking, but the question of whether they represent more than a simple population-level refractory period, following strong activation at the relevant frequency-level combinations, remains open. The period of suppression they highlight is also commonly observed as an inhibitory area in STRFs, in my hands as well as others' (e.g. figure 3.17; Christianson et al., 2011). In future, it might be of interest to test whether mapping inhibitory tuning from

this window results in more or less coherent maps than focussing on the initial excitatory response. Since the refractory period of an individual neuron's membrane potential is a matter of a few milliseconds rather than tens or hundreds, this pattern of activity is not internally generated; Wehr and Zador (2005) explore this further and show that the time course of click-driven inhibitory conductances is insufficient to explain the lengthy period of suppression seen in rat A1. Thus, they suggest that this type of suppression is generated intracortically and probably involves synaptic depression as well as GABAergic inhibition. As such it presumably serves an important computational function in the processing of stimuli by cortical networks, most likely some form of forward suppression (Brosch and Schreiner, 1997). The fact that when tone-driven, this post-activation suppression is co-tuned with the excitatory response, is of interest (Scholes et al., 2011).

Since I have not sorted the spikes in the above recordings in order to isolate single units, I cannot be certain that these time-varying responses occur within the spike trains of single neurons; the different receptive field components could arise from different cells in close proximity to the recording site. However, reports of complex time-varying responses in auditory cortex are increasingly common: Moshitch et al. (2006), for example, described dynamic pure-tone receptive fields in single units from cat A1, while Walker et al. (2011) in this laboratory found that individual neurons multiplex information about different stimulus features over varying timescales, and within A1 there was significant information about stimulus periodicity in a window 300—340 ms post-onset. An earlier study from this laboratory (Campbell et al., 2010) found responses as long as 500 ms post-stimulus offset that were informative about spatial cues, while Rajan et al. (2013) recently reported a late component (100–250 ms post-offset) in responses across all depths of A1 in opiate-anaesthetised marmosets. These lines of evidence, and the number of times I

observed dynamic response properties in my recordings, suggest that they are indeed a characteristic of single neurons in the mouse.

Importantly, this time sensitivity of receptive fields means that choosing a more or less inclusive response window can dramatically affect the calculation of FRAs and BFs — and thus, the appearance of tonotopy (section 3.7.4). Altogether, each variation from the classical method of measuring tuning (i.e. an inclusive, ~100 ms post-onset window of multi-unit activity, in granular layers, recorded in response to pure tones) increased the apparent fragility of the tonotopic organisation I observed, which was not universal in the first instance.

3.8.2 Finding a fit with diverse published data

At first sight, then, my evidence supports the salt-and-pepper view of tonotopy outlined by Rothschild et al. (2010) and Bandyopadhyay et al. (2010), as well as the laminar transformation described by Winkowski and Kanold (2013), rather than the robust account of Guo et al. (2012). The latter study is something of an exception; even an earlier paper sharing the same last author (Hackett et al., 2011) put forward the case that evidence for tonotopy is sensitive to a number of factors relating to the recording location and experimental technique (see figure 3.23A). My experimental results conform closely to this view, lending support to several of these suggested factors and adding two more (figure 3.23B).

How, then, can the contrast between my results and those of Guo et al. (2012) in particular be resolved? The maps in their study were produced by sequential, single-channel recordings that were on average closer together than the shanks on my multi-channel probes. This finer sampling might account for some of the obvious differences, and is the

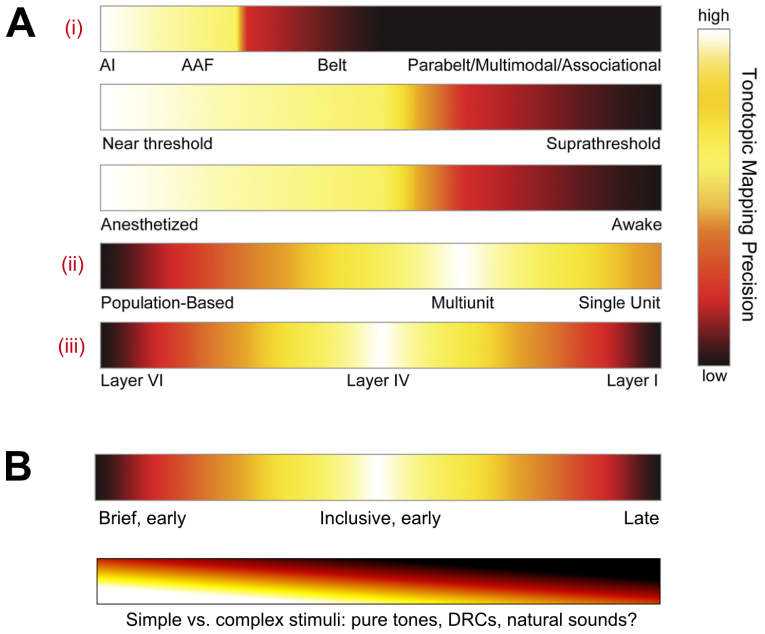


Figure 3.23: **Factors affecting tonotopic fidelity.** ***A***: Schematic taken from Hackett et al. (2011), indicating factors likely to affect the precision of tonotopy observed in neurophysiological recordings from the auditory cortex. From top to bottom, they are: recording site, sound intensity, anaesthetic state, spatial resolution and cortical depth. Roman numerals denote those trends to which data presented in this chapter offer support. (i) While I have not evaluated tonotopy in non-primary areas, nor compared its fidelity between A1 and AAF, I found the strength of tuning to be higher in primary areas (figure 3.7B). (ii) Here, my recordings were very different from the experiments of Hackett et al. (voltage-sensitive dye imaging in acute thalamocortical slices), but my data support the idea that, perhaps surprisingly, more diffuse recording techniques produce maps that are not significantly more coherent than multi-unit spike recordings (figure 3.14). (iii) As expected, the best tonotopic maps were produced from my recordings in thalamorecipient layers (figure 3.10). Indicated in ***B*** are two additional factors suggested by my data: choice of response window, and stimulus complexity. Firstly, I have shown that varying the response window from an inclusive, early period of ~100 ms can have a dramatic impact on the consistency of tuning observed (figure 3.22). Secondly, using a dynamic stimulus significantly altered the tuning I reported (figure 3.18), although the changes it produced in tonotopic maps were inconsistent (figure 3.19); thus, I have used an angled colour gradient in this case, because the precise effect of stimulus complexity on frequency maps will require further research to elucidate. For example, I have not used natural sounds as stimuli in this chapter, but they represent a logical extension of the work described here.

same strategy used in the study by Hackett et al. (2011), who also reported well-ordered tonotopy. Yet if granular layers of **every** mouse cortex contain a robust, smoothly organised map of the sort illustrated by Guo et al. (2012), then relatively disordered maps such as the ones illustrated in my figure 3.9 (C, D) would surely not exist.

Inter-individual variations in the precise location and size of the mouse auditory cortex, if not the degree of tonotopy itself, are acknowledged within the field (Stiebler et al., 1997; Hackett et al., 2011, also J. Linden and J. Garcia-Lazaro, personal communication). Different anaesthetic regimes may also play a role; the Kanold group used isofluorane for their two-photon imaging studies (Bandyopadhyay et al., 2010; Winkowski and Kanold, 2013) while Rothschild et al. (2010) chose a ketamine-medetomidine protocol similar to mine. The fine tonotopy reported by Guo et al. (2012) was recorded under periodic injection of ketamine-xylazine, which seems an unlikely source of the contrast between those results and data obtained under injected ketamine-medetomidine (such as mine, or those of Rothschild et al., 2010).

There is sometimes a tendency in neurophysiology to write off badly tuned or poorly organised recordings as technical failures; Guo et al. (2012) aimed not to bias the placement of their recordings toward more responsive sites, but in the practice of *in vivo* extracellular recordings, this can be difficult to avoid. Furthermore, it was only by excluding sites with irregular tuning, particularly in supragranular layers, that they described a robust, if sometimes sparse, organisation of classically tuned activity across layers, anaesthetic states and signal types (as discussed above in section 3.4.2; note particularly Guo et al., 2012, figure 5). By contrast, I have expressly included successful but ill-fitting recordings and defensibly so: these electrode channels still recorded spiking activity that was significantly driven by noise bursts and by tones – the activity was simply not structured

in a way that fits the canonical model.

Thus, it is perhaps the argument more than the data, upon closer inspection, that differs between the chapter above and the thorough case for tonotopy presented by Guo et al. (2012). I have concentrated on the variability seen between mice, layers and conditions, while they restricted their attention to well-tuned sites and emphasised the persistence of an overall gradient, rather than dwelling on the gaps left behind.

3.8.3 In praise of mess

I would argue that 'messy' examples such as these may reflect a mismatch between the computational function of the probed system and the experimental design used to probe it. The auditory cortex is several synapses and processing stages away from the auditory nerve, where activity can be more easily correlated to stimulus content and for which some of the tools we now use to study the cortex were developed (including FRAs; e.g. Rawdon-Smith and Hawkins, 1939). Despite tantalising, if sometimes ambiguous, evidence from neurophysiological recordings and lesion-type interventions, its functional importance remains surprisingly opaque (King and Schnupp, 2007; Lomber and Malhotra, 2008; Bizley et al., 2009; Bendor et al., 2012). Whatever its specific value is to the mammals relying on it, the auditory cortex is certainly performing more complex tasks than sorting incoming signals into frequency bands. Indeed, as Hackett et al. (2011) demonstrate, even individual pure tones are likely to drive activity in wide and overlapping regions of the cortex. Like other maps, tonotopy is an appealing framework through which to view the organisation of neuronal activity – but perhaps this means we place too much emphasis on it (see also Diamond et al., 1999, 2003, and further discussion in section 6.2).

Extracellular data, particularly from the mouse cortex, can be untidy and thus present a challenge to the investigator seeking order and patterns. For example, looking at the raw receptive fields they produce, whether in response to a dynamic stimulus or pure tones (e.g. figure 3.17), even choosing a single BF often seems inappropriate as a method of summarising a site's frequency response. Within an individual FRA there can be as much evidence supporting one BF as there is for several others. Since studying traditional frequency maps requires just such an extraction, I have endeavoured to overcome this difficulty by using conservative thresholds to select tuned sites and objective, systematic methods to calculate BFs in each case (see sections 2.3.4, 2.3.5). If this results in BFs which sometimes differ from what visual inspection of the FRA or STRF might suggest, I have taken the approach of letting the BFs vary with the data and endeavouring to record plenty of them. The fact that I have indeed recorded convincing tonotopic maps in the granular layers in several cases (see figure 3.9) supports my strategy and implies that the variable tonotopy I observe in other layers and conditions is a faithful representation of cortical response properties.

Results that sit at odds with existing models are important to acknowledge. In general, tonotopy is assumed but not always observed as a property of primary auditory cortices, particularly in the mouse (see my data above; also examples in Rothschild et al. 2010; Bandyopadhyay et al. 2010; and note the difficulty in mapping a tonotopic reversal reported by Seybold et al. 2012). Nonetheless it is a 'textbook' characteristic which underlies many experiments, from those which measure changes in the cortical representation of different frequencies (e.g. Kim and Bao, 2009) to those which aim to selectively and artificially stimulate such representations (e.g. Znamenskiy and Zador, 2013).

The findings above add weight and further dimensions to the model summarised in

figure 3.23 (see also Hackett et al., 2011) whereby, in the auditory cortex, the integrity of observed tonotopy is spatially limited and sensitive to a variety of experimental factors. This suggests to me that tonotopy as an organisational principle is less important to the function of the cortex than it is to those who study it. For experiments in which it is necessary to delineate a tonotopic map, this model – and these data – are useful for facilitating the detection of such a map. More fundamental questions about sensory cortical physiology, meanwhile, may well be answered by strategies which consider activity more broadly, using dynamic stimuli to probe the cortex's computational principles (e.g. Chechik and Nelken, 2012; Rabinowitz et al., 2012), building complex models to account for non-linear response functions (e.g. Ahrens et al., 2008), and distinguishing neurons based on their genetic identity and connectivity as well as their response characteristics (e.g. Adesnik et al., 2012; Chen et al., 2013; Ko et al., 2013).

Chapter 4

Comparing the responses and inputs of A1 and AAF

4.1 Introduction

In the previous chapter I explored the question of tonotopy, one of few known organisational principles of the mammalian auditory cortex. As discussed, despite its central place in our understanding, opinions and evidence vary as to the importance and invariance of tonotopy in the mouse cortex. Another important challenge facing cortical physiologists, closely related to the continuous or modular variation of response properties across the cortex, is that of distinguishing areas and subfields.

The number of subfields described within the auditory cortex varies considerably between species (e.g. Merzenich and Brugge, 1973; Sally and Kelly, 1988; Stiebler et al., 1997; Bizley et al., 2005; Hackett, 2008), but generally they have been separated into primary (or core) areas and non-primary (or belt) areas. In primary fields, neuronal response proper-

ties tend to be simpler and latencies shorter, and frequency tuning organised topographically (see chapter 3).

In the mouse, pioneering studies led by Imme Stiebler (1987a, 1987b, 1997) mapped two primary fields with opposing tonotopic gradients (primary auditory cortex, A1, and the anterior auditory field, AAF), consistent with patterns reported in the cat (Knight, 1977) and gerbil (Thomas et al., 1993), as well as an ultrafrequency field (UF) which did not appear to be tonotopically organised (though anatomical evidence did suggest this area was thalamorecipient and likely 'primary' in nature: Hofstetter and Ehret, 1992). Stiebler et al. (1997) also reported two non-primary fields (secondary auditory, A2, and dorsoposterior, DP). Very few refinements have been made to that view of the cortex in subsequent years. A voltage-sensitive dye study by Sawatari et al. (2011) proposed an additional auditory field, rostral and ventral from the established AAF (insular auditory field, IAF, analogous to a similar field in the rat: Rodgers et al., 2008; Kimura et al., 2010) and recently a detailed investigation into tonotopy (Guo et al., 2012, discussed in chapter 3) suggested that the UF region was in fact also tonotopic and contiguous with A1 and AAF.

4.1.1 How distinct are the physiology and connectivity of A1 and AAF?

The most detailed published maps of response properties in the mouse cortex are those of Guo et al. (2012); they were assembled on the basis of pure-tone responses and display clear tonotopic organisation of best frequencies (BFs) within thalamorecipient layers. Particularly with the inclusion of the UF region within an unbroken tonotopic map, which these authors were the first to describe, the organisation of primary areas (at the level of frequency tuning) appears quite continuous, with no obvious boundary between

A1 and AAF. Visual inspection of these data, without knowledge of the expected field boundaries, might suggest a single, radial tonotopic gradient, emanating from the dorsal high-frequency region (see figure 4.1A). It is only in considering other response parameters that the case for two distinct primary subfields becomes stronger; indeed, Guo et al. (2012) illustrate a trend towards shorter response latency at anterior sites (figure 4.1B) and when they place an A1-AAF boundary at the position of rostrocaudal tonotopic reversal, units within AAF show significantly shorter latencies than those in A1 (see their figure 2H). They also find significantly larger bandwidths in AAF, along with higher 'FRA quality' (a measure of the strength of tone-driven *vs.* non-driven responses).

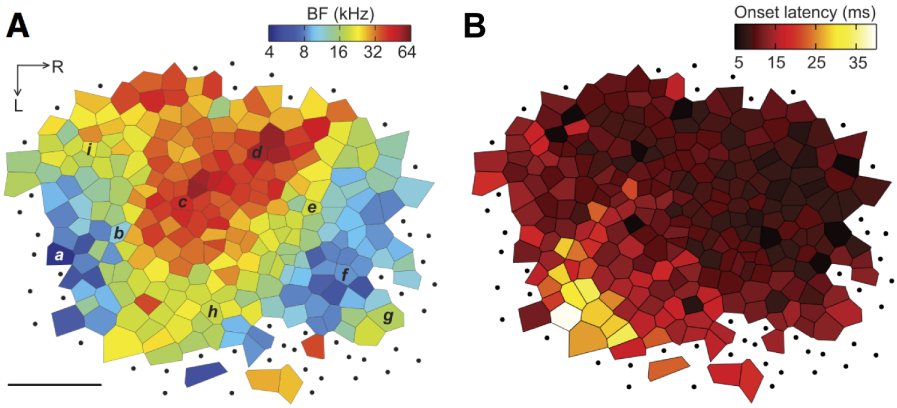


Figure 4.1: **Variation of frequency tuning and latency across published maps of mouse auditory cortex.** ***A***: Figure taken from Guo et al. (2012), describing best frequencies (BFs) across mouse auditory cortex. BF values derive from frequency response areas (FRAs) recorded from middle cortical layers using single-site microelectrodes. Note the lack of an obvious boundary between A1 and AAF and the apparently radial tonotopic gradient. ***B***: Figure from the same paper showing response latency measured at the same sites, including a strong trend towards shorter latencies at more rostral sites. Black dots represent unresponsive sites; R, rostral; L, lateral; scale bar, 0.5 mm.

An earlier report, which used reverse correlation to compare spectrotemporal response properties (Linden et al., 2003), found that mouse AAF, relative to A1, had spectrotemporal receptive fields (STRFs) of shorter duration, shorter peak latency, and slightly broader bandwidth. With the exception of these two examples, very little published work has ex-

plicitly compared the neurophysiology of mouse A1 and AAF. The recordings I have made across the depth and breadth of mouse auditory cortex (reported in terms of their frequency tuning and tonotopic organisation in chapter 3) offer an opportunity to expand this set of observations, particularly by including responses from superficial and deep layers.

Furthermore, recent evidence is rather contradictory as to the degree of connectivity shared by these two subfields. Horie et al. (2013) recently suggested, based on tracer injections guided by flavoprotein autofluorescence imaging, that mouse A1 and AAF receive separate thalamocortical projections from distinct compartments of the ventral MGB. By contrast, Llano and Sherman (2008) reported abundant anterograde (and retrograde) labelling of both A1 and AAF following single tracer injections into MGBv. Even the direction of tonotopy within the MGBv is contested: Hackett et al. (2011) describe a low-to-high frequency gradient in a lateral-medial direction (along with a shallower caudo-rostral gradient), while Horie et al. (2013) report one low-to-high, medial-lateral gradient in the medial portion of MGBv (projecting to AAF) alongside a dorsal-to-ventral gradient in the lateral portion (projecting to A1).

My own retrograde tracing experiments offer some insight on this topic, by virtue of a pair of tracer injections located either side of the presumed A1-AAF boundary (see section 4.4 below). I discuss this contrasting evidence from the mouse literature in relation to other species and my own data in section 4.5.2.

4.1.2 Aims

In this chapter, I compare the neuronal activity of A1 and AAF using multiunit activity recorded in response to pure tones and noise bursts; I also briefly compare the connectivity profile of these two subfields based on paired injections within a single mouse. Specifically, I aim to accomplish the following:

- confirm and quantify the difference in response latency reported by others for middle layers of mouse A1 and AAF, and report whether any such difference is consistent across cortical depth;
- test whether the magnitude of noise responses is different in A1 and AAF;
- look for differences in frequency sensitivity between A1 and AAF, in terms of (a) strength of frequency tuning, (b) threshold and (c) bandwidth of pure-tone responses; and
- compare the distribution of labelled cells in auditory thalamus and cortex following tracer injections into A1 and AAF.

4.2 Comparing neurophysiology of A1 and AAF: noise responses

To evaluate the degree to which response strength and latency vary between A1 and AAF, I compared spiking responses to 5 ms noise bursts from recordings made across the auditory cortex of 9 mice (the data set explored in chapter 3). For each responsive site, I calculated a peak spike-rate and peak latency values from its PSTH (based on the height and

time post-stimulus onset, respectively, of the largest peak in the histogram). Noise-driven sites were defined as described in section 3.3 above (i.e. sites where mean post-stimulus spike-rate exceeds mean spontaneous rate by more than 4 standard deviations; see also section 2.3.3).

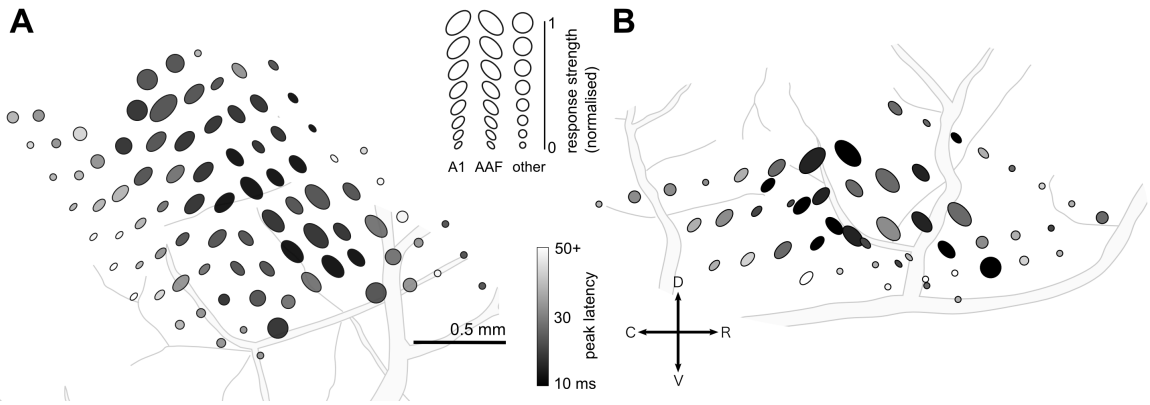


Figure 4.2: **Two example maps of response strength and latency.** These maps of auditory cortex in mice 'Marilyn' (***A***) and 'Meryl' (***B***) show the strength (indicated by size of symbol) and peak latency (indicated by darkness of symbol filling) of spiking responses to 5 ms noise bursts. Each symbol represents the shortest latency value and the largest spiking response recorded on a particular shank and different shapes denote the estimated categorisation of sites within A1, AAF or other (non-primary) areas. Note the tendency towards stronger responses and shorter latencies in anterior sites (explored further in subsequent figures).

As illustrated by the two maps in figure 4.2, visual inspection of the data, arranged across cortical space, confirms a trend toward shorter latencies and stronger responses at more rostral sites. This trend is also apparent in figure 4.3, where all the peak noise-driven spike-rates (A) and latencies (B) from A1 and AAF, pooled across cortical layers in the same two mice, are plotted against their rostrocaudal position. The equivalent data from all 9 mice are pooled in panels C and D. Viewing the distribution of these response properties across the cortex, relative to the boundary between A1 and AAF (defined by tonotopic reversal point; see figure 3.8), there is no obvious divide between the two primary subfields. Nonetheless, there is a consistent trend towards stronger responses (C)

and shorter latencies (D) at more rostral sites, in nearly every animal, even if the correlation between these values and rostrocaudal distance is not always statistically significant in individual cases.

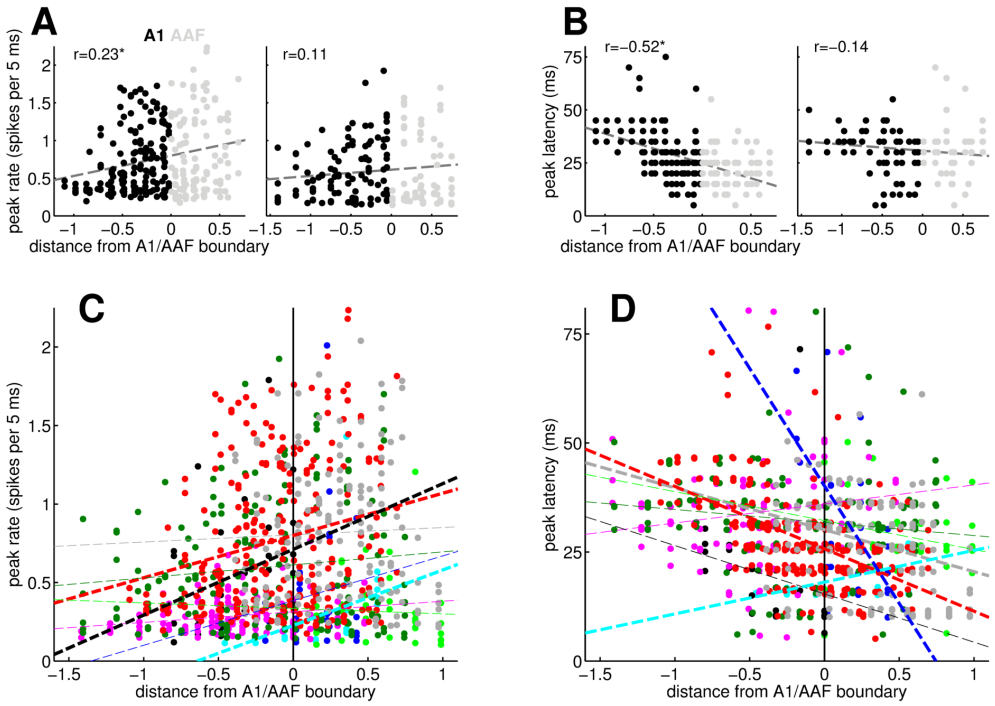


Figure 4.3: **Variation of response strength and latency with rostrocaudal position.** ***A*** and ***B*** show spike-rates and latencies, respectively, from all primary sites in the same two mice as figure 4.2, plotted against the sites' rostrocaudal position (relative to the A1/AAF boundary, which is positioned based on frequency tuning as described in figure 3.8). Linear regression line and correlation coefficient (Pearson's r) are shown in each case; asterisk denotes a significant correlation ($p < 0.05$). A1 and AAF sites are shown in black and grey, respectively, for illustrative purposes. In ***C*** and ***D***, equivalent data from all 9 mice are superimposed in different colours; the regression line is plotted in bold if the correlation is significant ($p < 0.05$) and a vertical black line highlights the position of the A1/AAF boundary. Since peak latency is derived from 5 ms bins, these values have been jittered slightly in ***D*** to improve the visibility of data points. When sites are pooled across all mice, both correlations are weak but highly significant ($r = 0.17$ and $p < 10^{-7}$ for spike-rate, $r = -0.24$ and $p < 10^{-13}$ for latency).

4.2.1 Latencies are shorter in AAF

To quantify the comparison between A1 and AAF, I pooled latencies and spike-rates within each subfield, either across all cortical depths or within layer categories, from all 9 animals. As expected based on published data (Linden et al., 2003; Guo et al., 2012) and the trends observed above, peak latency shows a small but highly significant decrease in AAF compared to A1 (Kruskal-Wallis test, $p < 10^{-5}$; A1 mean 30.4 ms, AAF mean 26.9ms; see figure 4.4 A and first two columns in B). Other studies have not made this comparison at different cortical depths; figure 4.4B demonstrates that AAF response latencies are consistently shorter within supragranular, granular and infragranular layers, though the difference is more significant in the granular comparison.

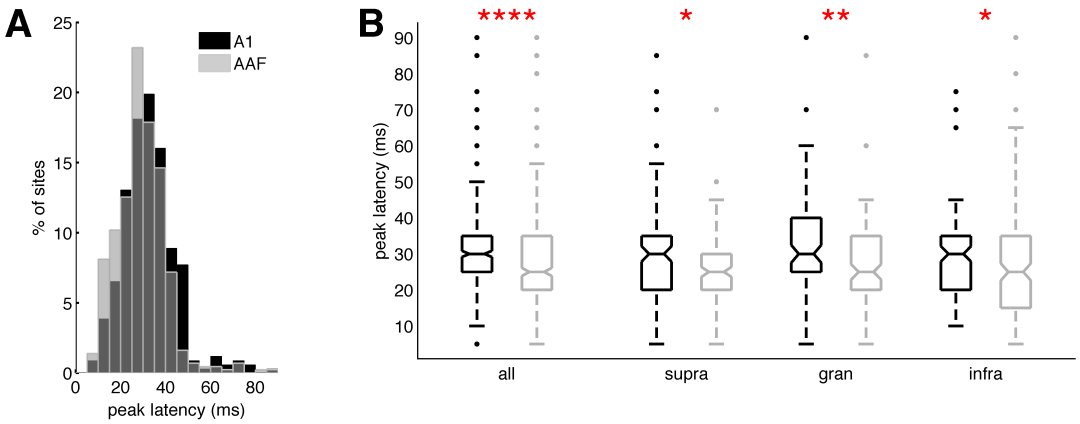


Figure 4.4: **Comparing peak latency in A1 and AAF, across cortical depth.** ***A***: Histogram of peak latency values (derived from the 5 ms bin containing most spikes in each site's noise-driven PSTH) across A1 and AAF, for spiking responses to a 5 ms noise burst. The shift in latency is significant ($p < 10^{-5}$, Kruskal-Wallis test), as indicated by the 'all' comparison in ***B***. Box plots in ***B*** compare latencies between A1 and AAF (black and grey respectively, as for ***A***) across all sites as well as separated by cortical depth (i.e. sites estimated to be within supragranular, granular and infragranular layers; see section 2.3.2). AAF shows significantly shorter latencies in each case. Single asterisk denotes $p < 0.05$; otherwise m asterisks denote $p < 10^{-m}$. A1: $n = 337$ total, 120/92/125 supra/gran/infra. AAF: $n = 431$ total, 132/122/177 supra/gran/infra. Box plot legend: boxes, interquartile range; horizontal line, median; notches, 95% confidence intervals; whiskers, further extent of data up to 1.5× interquartile range, outliers marked with dots.

4.2.2 Noise-driven responses are stronger in AAF than A1, particularly in infragranular layers

In the course of their investigation into tonotopic organisation, Guo et al. (2012) also reported that sites in AAF were more strongly driven by tones than A1 sites. Assuming this finding reflects a trend towards greater, more stimulus-correlated (as well as faster onset) spiking activity in AAF, I expected to find stronger noise responses from AAF sites within my data.

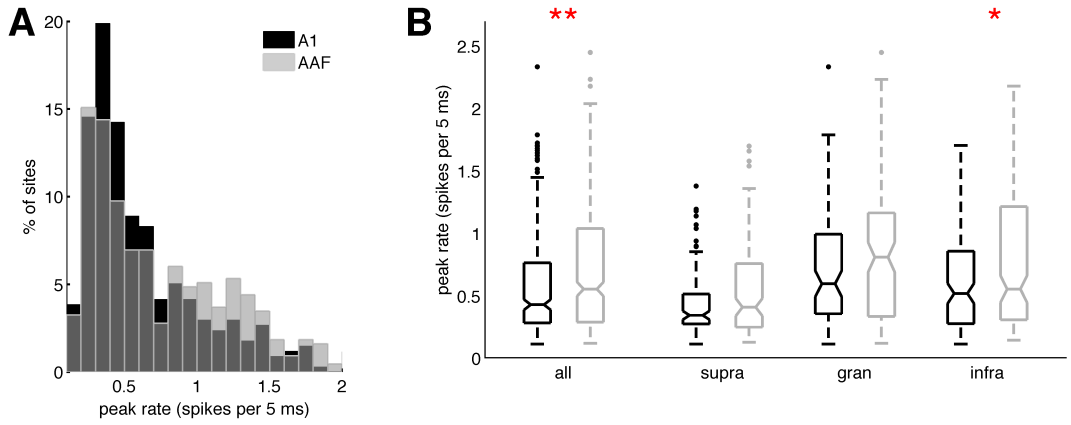


Figure 4.5: **Comparing noise-driven spike-rates in A1 and AAF, across cortical depth.** ***A***: Histogram of peak spike-rates driven by a 5 ms noise burst (calculated from each site's PSTH, based on the number of spikes in the largest 5 ms bin) across A1 and AAF. ***B***: Box plots comparing peak spike-rates from A1 (black) and AAF (grey), either pooled or separated by cortical depth. AAF responses are significantly stronger in the pooled case (double asterisk: $p < 0.01$, Kruskal-Wallis test) and in the set of sites estimated to be within infragranular layers (single asterisk: $p < 0.05$); granular and supragranular layers show the same trend but below a 5% significance threshold. Box plot parameters and n values are as in figure 4.4B.

Figure 4.5 shows that this difference was indeed present; AAF shows significantly higher peak spike-rates in the pooled case (i.e. noise bursts drive higher peak rates, averaged across all sites in AAF, than in A1; $p = 0.01$; see panel A and first box plot comparison in B). Looking at the breakdown across cortical layers, however (figure 4.5B), the median AAF rate is higher in each case, but only infragranular sites show significantly stronger

responses ($p = 0.02$, Kruskal-Wallis test).

The difference in the strength of spiking responses between A1 and AAF overall is quite large, relative to the median spike-rates (medians are 0.43 spikes per 5 ms in A1, and 0.56 in AAF: a 29% increase). Although the difference in thalamorecipient, granular layers alone is not significant, this finding, as well as the latency difference above, is relevant to the question of which field is in fact "more primary" (see section 4.5.3), since simpler response properties and stronger, shorter-latency responses are characteristic features of primary cortical areas receiving direct sensory input from the thalamus.

4.3 Comparing neurophysiology of A1 and AAF: tone responses

Next I investigated whether responses to pure tones in A1 and AAF reveal differences in frequency sensitivity, response threshold and sharpness of tuning. To make these comparisons I have separated the FRA data discussed in chapter 3 into A1 and AAF sites, then again into sites within supragranular, granular or infragranular layers.

4.3.1 Strength of frequency tuning is similar across A1 and AAF

In section 3.3.2 I introduced, as a measure of the strength of a site's frequency preference, a discriminability index (d') calculated from responses to each site's best and worst pair of neighbouring frequencies (i.e. the pairs eliciting the largest and smallest spiking response; see section 3.3.2 and methods in section 2.3.4). There, this measure revealed stronger tuning among sites in granular layers of the cortex, compared with both supra-

and infragranular sites (see figure 3.7). Figure 4.6 now compares the d' values registered from A1 and AAF sites.

In contrast to the latency and strength of noise responses, my recordings from A1 and AAF show no significant differences in this measure of tuning strength, whether pooled or separated by cortical depth ($p > 0.05$, Kruskal-Wallis test; see histogram in figure 4.6A, and box plots in B). This is a relatively simple indication of best/worst frequency discriminability, however. Other parameters, such as FRA bandwidth, are more commonly used to describe the sharpness of frequency tuning; I largely avoided these in chapter 3 because of reservations about smoothing pure-tone response data (see sections 3.2.2, 3.2.3). In order to make a more thorough comparison of frequency tuning between A1 and AAF, an aspect in which others have found significant differences in these subfields' responses (see Linden et al., 2003; Guo et al., 2012; and also work in other species, e.g. Rutkowski et al., 2003; Bizley et al., 2005), below I examine both bandwidth and threshold measurements derived from smoothed FRAs.

4.3.2 Bandwidth and threshold are not significantly different between A1 and AAF

To extract bandwidths and thresholds from smoothed FRA data, I have used a standard method based on previous work in this laboratory (Bizley et al., 2005) and adopted by others (Mao and Pallas, 2012). (A figure illustrating the calculation of bandwidths and thresholds on sample FRAs appears in the next chapter, where I test for changes in tone responses during artificial stimulation of other sensory cortices; see figure 5.11.) Since my stimulus grid used sound levels spaced by 8 dB, the bandwidth measurements I compare

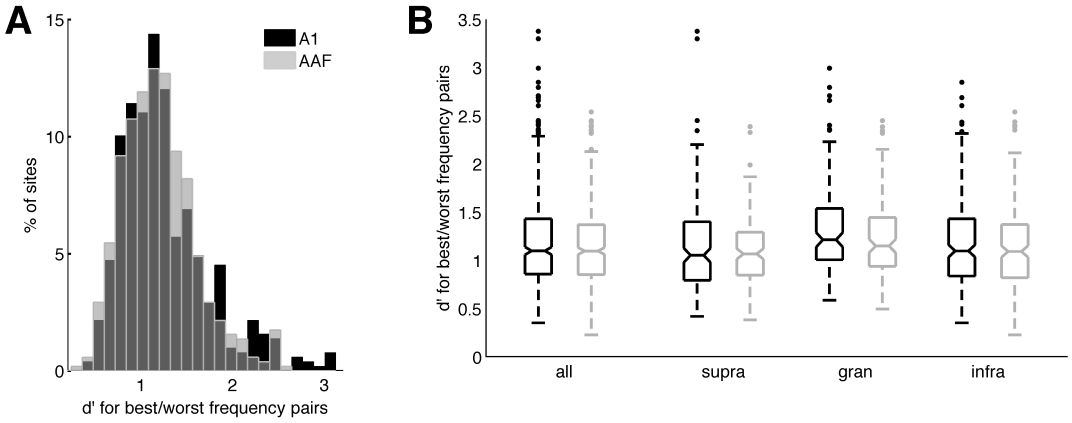


Figure 4.6: **Comparing tuning strength in A1 and AAF using d' for best/worst frequency pairs.** ***A***: Histogram comparing the distribution of d' values (see text and sections 2.3.4, 3.3.2) in sites from A1 and AAF. There is no obvious shift in the distribution and as shown in ***B***, comparison of pooled A1 and AAF sites (black and grey respectively), or indeed within supragranular, granular and infragranular layers, reveals no significant differences (Kruskal-Wallis test, $p > 0.05$ in each A1–AAF comparison). A1: $n = 210$ total, 53/67/90 supra/gran/infra. AAF: $n = 250$ total, 63/80/107 supra/gran/infra. Box plot parameters are as in figure 4.4B.

in the figures below are at 8 and 24 dB (i.e. 1 and 3 sound level steps) above threshold: BW8 and BW24.

As shown in figure 4.7, both sets of bandwidths (BW8, panel A; BW24, panel C) were similar in A1 and AAF. There were no significant differences ($p > 0.05$, Kruskal-Wallis test), whether sites were pooled or separated into layer groups (box plots, panels B, D). The median bandwidth is larger in AAF than A1 (both for BW8 and BW24; see first pair of box plots in figure 4.7 B,D), which, although not statistically significant, is consistent with the brief description by Guo et al. (2012) of slightly broader bandwidths in mouse AAF, relative to A1 (~0.1 octaves at 10 dB above threshold; see their figure 2F and discussion in section 4.5.1 below).

Similarly, I observed no significant differences in the threshold of pure-tone responses between A1 and AAF (figure 4.8). As for the bandwidths above, this was the case whether sites were pooled or separated by cortical depth (see box plot, figure 4.8B).

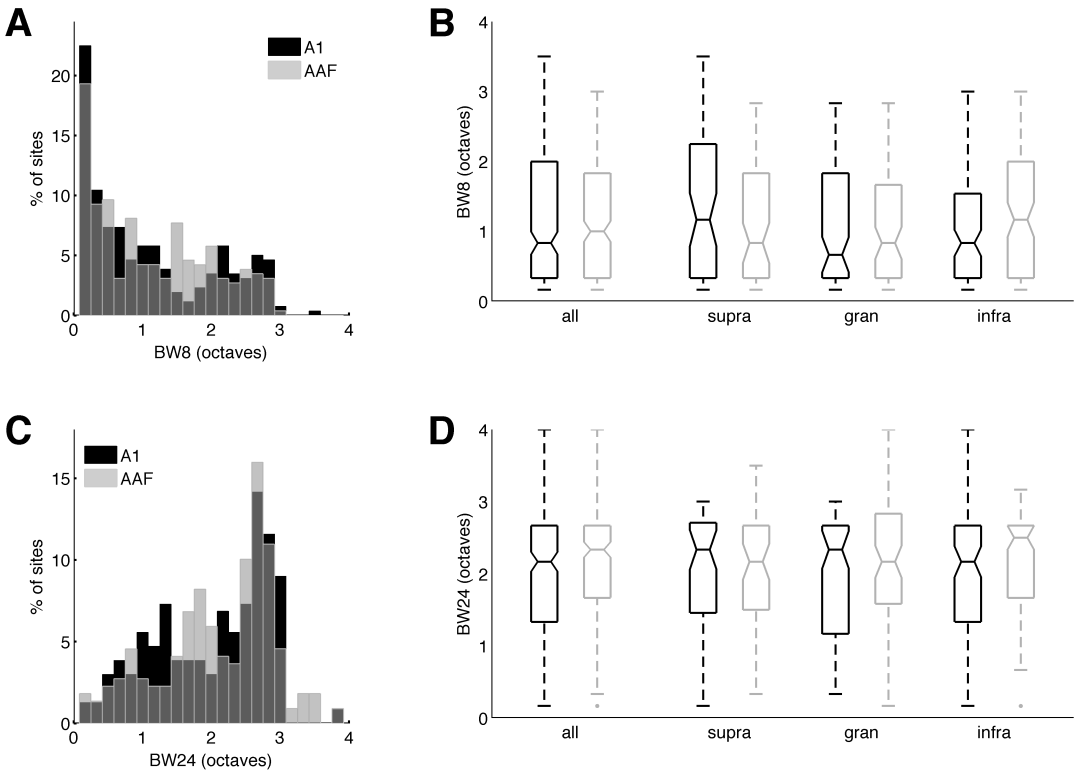


Figure 4.7: **Comparing the bandwidth of pure-tone responses in A1 and AAF.** Histograms and box plots, of the same form as figures 4.4-4.6, comparing bandwidth of pure tone responses at 8 and 24 dB above threshold (BW8, ***A***–***B***; BW24, ***C***–***D***). There are no significant differences between sets of bandwidths recorded from A1 (black) and AAF (grey), whether pooled or separated into groups by estimated cortical depth (supragranular, granular, infragranular). *A1*: $n = 258$ total BW8, 231 total BW24; n =64/89/105 supra/gran/infra BW8, 56/81/94 supra/gran/infra BW24. *AAF*: $n = 258$ total BW8, 224 total BW24; n =66/82/110 supra/gran/infra BW8, 57/75/92 supra/gran/infra BW24. For box plot parameter definitions, see caption figure 4.4B.

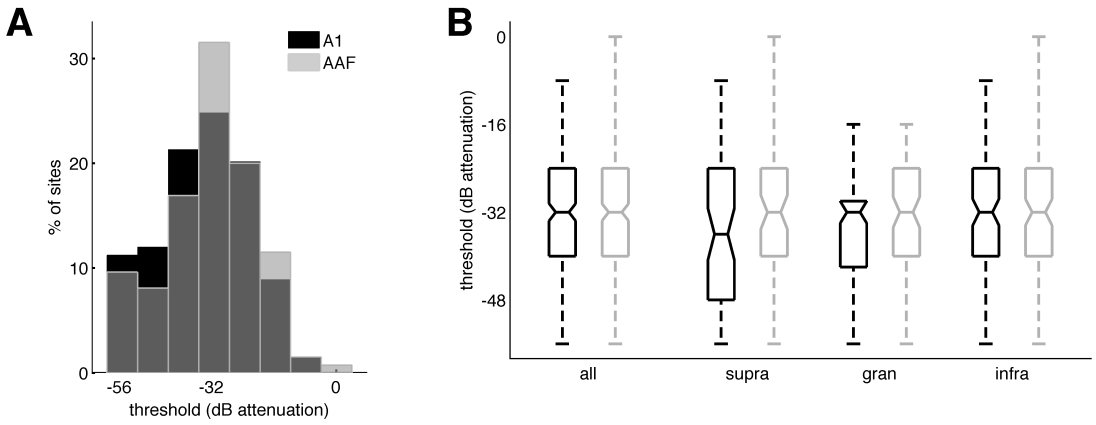


Figure 4.8: **Comparing the threshold of pure-tone responses in A1 and AAF.** Histogram (***A***) and box plot (***B***), of the same form as figures 4.4-4.7, comparing the threshold of pure tone responses in A1 (black) and AAF (grey). There are no significant differences, whether thresholds are pooled or separated into groups by estimated cortical depth of recording site (supragranular, granular, infragranular). A1: $n = 258$ total, 64/89/105 supra/gran/infra. AAF: $n = 260$ total, 67/82/111 supra/gran/infra. Box plot parameters are defined in caption of figure 4.4B.

In my hands, then, pure tone responses are statistically equivalent across A1 and AAF: strength of tuning (d' for best/worst frequency pairs, figure 4.6), response bandwidth (BW8 and BW24, figure 4.7) and threshold (figure 4.8) all fail to reveal significant differences between the two primary subfields. I discuss this in relation to published data from the mouse and other species in section 4.5.1 below.

4.4 Distribution of cells projecting to A1 and AAF

In this section, I briefly explore how the thalamocortical and commissural inputs to A1 and AAF are distributed, by comparing the populations of retrogradely labelled cells following paired tracer injections into these two subfields in a single mouse.

Two injections of cholera toxin B with alternate fluorescent conjugates, CTB-alexa 594 and CTB-alexa 488, were centred in A1 and AAF, respectively (for methods, see section

2.4.1). The coarse map of pure-tone frequency tuning shown in figure 4.9A was recorded prior to the injections and was used to target them to each primary area. FRAs from the recording sites closest to each injection are also shown (figure 4.9 B,C); BF near the A1 injection was 14.9 kHz and near the AAF injection, 9.8 kHz.

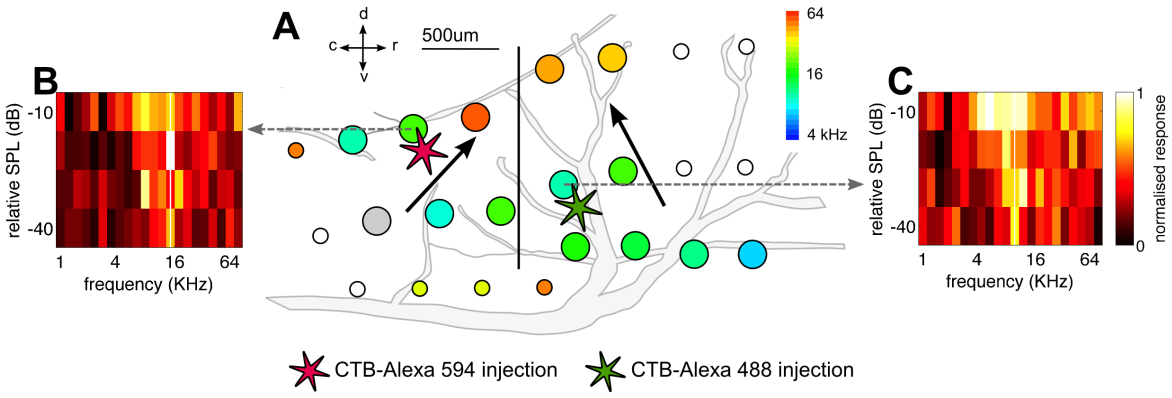


Figure 4.9: **Site of A1 and AAF tracer injections.** ***A***: Map of BFs derived from recordings of multi-unit pure-tone responses in middle layers of auditory cortex in mouse 'Marcy', made using multi-site electrodes prior to injection of neuronal tracers (see section 2.4.1; map conventions are as for chapter 3, e.g. figure 3.8). The A1–AAF boundary and the orientation of tonotopic gradients in A1 and AAF (both calculated as in chapter 3) are marked by a vertical black line and by black arrows on the left and right, respectively. As highlighted by these annotations, the CTB-Alexa 594 injection (red) is most likely in A1 and the CTB-alexa 488 injection (green) in AAF. ***B***, ***C***: FRAs from recording sites close to each injection, as indicated by dashed arrows. BF (the frequency eliciting the strongest response across all sound levels combined; see section 3.2.3) is indicated by a vertical white line on each FRA — 14.9 kHz in ***B*** and 9.8 kHz in ***C***.

4.4.1 A1 and AAF receive overlapping thalamocortical input

As mentioned above, there are varying reports in the recent literature about the orientation of tonotopy in the mouse MGBv (Hackett et al., 2011; Horie et al., 2013), and the question of whether A1 and AAF receive projections from distinct or overlapping thalamic regions (Llano and Sherman, 2008; Horie et al., 2013). Since the two injection sites shown in figure 4.9 were located in A1 and AAF, near sites with slightly different best frequencies,

the distributions of labelled cells they each produced in the MGB are of interest.

As illustrated in figure 4.10, these populations of retrogradely labelled cell bodies both include a concentration of cells towards the medial side of MGBv (see photographs in panels A-C and traced sections in D). This contrasts with the report of Horie et al. (2013), who proposed that AAF receives connections from this (medial) location but that A1 is targeted by a distinct compartment, with its own tonotopic gradient, on the lateral side of MGBv. The distributions in figure 4.10 are more consistent with A1 and AAF both receiving inputs from a single tonotopic axis within MGBv, as suggested by the robust labelling of both A1 and AAF observed by Llano and Sherman (2008) following single MGBv injections.

Furthermore, figure 4.10D and the histogram in panel E both demonstrate that cells labelled by the A1 injection, which had a nearby BF of 14.9 kHz (see figure 4.9), are concentrated more medially than those labelled by the AAF injection, where BF was 9.8 kHz. This is consistent with a tonotopically organised projection from MGBv targeting both A1 and AAF, where the low–high thalamic tonotopic gradient runs lateral-to-medial. Precisely this tonotopic gradient was observed by (Hackett et al., 2011), both in their neurophysiological data and in their evidence for a topographically organised projection to A1; the distinct medial-to-lateral and dorsal-to-ventral gradients reported by Horie et al. (2013), on the other hand, are not supported by my limited data.

The histogram in figure 4.10F shows that, while they overlap almost entirely on the rostrocaudal axis, the population of labelled AAF-projecting cells is more rostral than that labelled by the A1 injection. This may indicate a difference between the thalamocortical connectivity of A1 and AAF, or may reflect the fact that the low–high tonotopic gradient is also slightly oriented from rostral to caudal (since the AAF injection site was tuned to a

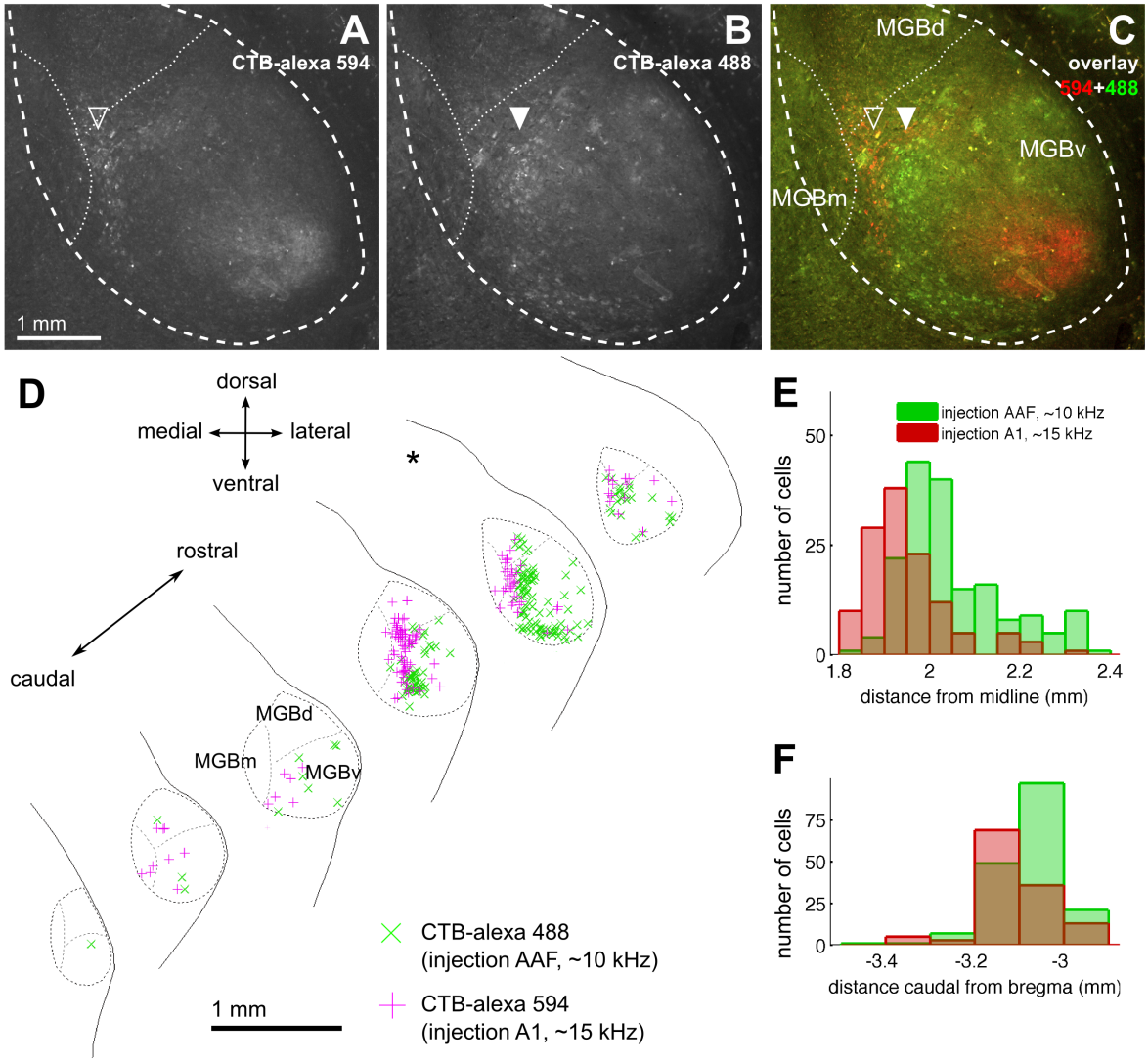


Figure 4.10: **Comparing thalamocortical inputs to A1 and AAF** ***A***–***C***: Photographs of retrogradely labelled cells in the medial geniculate body of the thalamus (MGB, bounded by dashed line; dotted lines indicate estimated boundaries of dorsal, ventral and medial subdivisions, as annotated in ***C***). Note the nearby populations of cells in MGBv labelled with CTB-alexa 594 (hollow arrowhead, ***A***) and CTB-alexa 488 (filled arrowhead, ***B***; see also overlaid images in ***C***). ***D***: Reconstructions of serial MGB sections, traced in Neurolucida, with position of labelled cells indicated. The section photographed in ***A***-***C*** is marked with an asterisk. Total number of labelled cells in MGB was 176 for AAF injection, 126 for A1. ***E***, ***F***: Histograms showing the distribution of MGB cells labelled by each injection, in the lateral and rostrocaudal dimensions, respectively. (See discussion in text.)

lower frequency; see figure 4.9). Again, such a gradient is consistent with the findings of Hackett et al. (2011; see their figure 3).

I observed only very occasional double-labelled cells in the MGB, consistent with the low number of branched projections reported using similar techniques in the cat (Lee et al., 2004; Kishan et al., 2008); these were not fully quantified due to complications presented by relatively rapid photo-bleaching of the fluorescent tracers.

4.4.2 Contralateral auditory cortical inputs to A1 and AAF may reveal differences in reciprocal connectivity

In chapter 5, I investigate cross-modal cortico-cortical inputs to core auditory cortex. As shown in figure 5.4, with the exception of areas adjacent to the auditory cortex, the populations of cells sending this type of long-range projection to A1 and AAF are commingled throughout other cortical areas and display no obvious topographic separation. By far the most abundant cortico-cortical input to A1 and AAF, however, arises in the contralateral auditory cortex (see figure 5.1). This connectivity, and indeed the functional interplay of left and right auditory cortices, is a little-studied subject but one of increasing interest (e.g. Carrasco et al., 2013).

Figure 4.11 compares the distribution of cells labelled by the same pair of injections described above, within ipsilateral and contralateral auditory cortex. Unsurprisingly, both the A1 and AAF injections label abundant cells within ipsilateral auditory cortex (panel A, right-hand sections). On the contralateral side (same panel, left-hand sections), the A1 injection produced more abundant labelling (745 *vs.* 328 cell bodies). This imbalance should not be over-interpreted, however, due to the variability I observed in the in-

jected volume of tracer (see section 2.4.1); indeed, the core and halo, which are somewhat subjective indicators of injection volume (also described in section 2.4.1) and difficult to compare between two different fluorophores, are larger for the A1 injection (estimated halo volume 28 nL for A1, 15 nL for AAF).

Perhaps of greater interest is the fact that a greater majority of A1- than AAF-projecting cells were located in infragranular layers (57% for AAF injection *vs.* 81% for A1 injection; see panel B). This might suggest a difference in the quality of the commissural input received by the two subfields, whereby the projection to A1 shows a more 'feedback'-type projection (see section 1.6).

Furthermore, the pattern of labelled A1-projecting cells on the contralateral side is noticeably more rostral than the ipsilateral distribution (red bars, figure 4.11 C,D); the labelled AAF-projecting cells in both hemispheres are concentrated on the rostral side of the auditory cortex (green bars, same panels). Although I have no physiological data to confirm the location of the contralateral A1–AAF boundary, this difference in coarse rostrocaudal distributions suggests that, while the segregation is far from absolute, A1 receives more commissural input from AAF (red bars, right-hand end of figure 4.11D) than AAF receives from contralateral A1 (green bars, left-hand end of same plot).

In other words, based on these limited data, AAF may send projections that extend more widely across the two contralateral primary auditory fields; in turn, the commissural inputs that AAF **receives** may be less numerous and appear to be less dominated by infragranular cells than those received by A1. Further tracing experiments would be desirable to confirm and expand on this preliminary evidence; it is interesting to note, nonetheless, that both observations are consistent with the suggestion that information flow between A1 and AAF, based on neurophysiological data in the cat, is more abundant

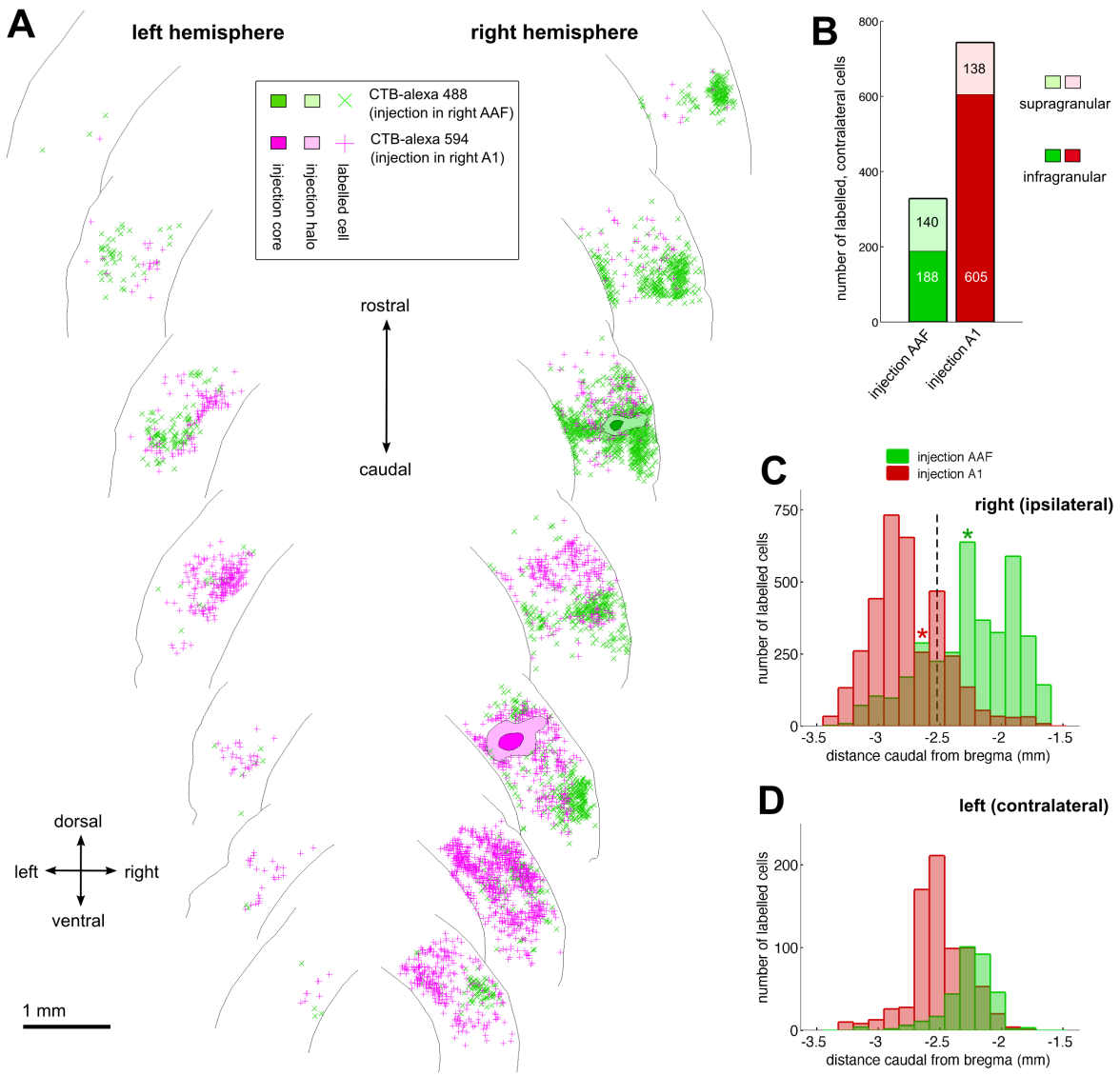


Figure 4.11: **Comparing the distribution of cells projecting to A1 and AAF from contralateral auditory cortex.** ***A***: Overview of labelled cells in serial sections of left and right auditory cortex (a subset of the sections whose right hemisphere is shown in figure 5.2A), following injection of indicated tracers into AAF and A1 (see figure 4.9). ***B***: Comparison of number of cells in contralateral auditory cortex which were labelled by the two injections, including a breakdown of those in supragranular *vs.* infragranular layers. The injection into A1 labelled a larger number of contralateral cells and a greater proportion of them was infragranular. ***C***, ***D***: Histograms comparing the rostrocaudal distribution of labelled cells in each hemisphere. Asterisks in ***C*** indicate rostrocaudal positions of each injection core; dotted line shows approximate position of A1–AAF boundary, based on recorded tuning map (figure 4.9) and location of injection sites within serial sections. Although each is concentrated at the end of the cortex containing the injection site, both the (ipsilateral) distributions in ***C*** encompass most of the rostrocaudal extent of auditory cortex. The distribution of A1-projecting cells labelled in contralateral auditory cortex (***D***), however, is shifted in the rostral direction, relative to the ipsilateral pattern.

in the AAF-to-A1 direction (Carrasco and Lomber, 2009, see also discussion in section 4.5.3 below).

4.5 Discussion

The data presented above suggest that the tuning characteristics of pure-tone responses in A1 and AAF are broadly similar (figures 4.6–4.8), while sites in AAF display both significantly shorter latencies and larger spiking responses to noise bursts than those in A1 (figures 4.2-4.5). In terms of the two subfields' connectivity, the evidence from a pair of tracer injections is consistent with thalamocortical inputs arising from a shared tonotopic axis in the MGB, running lateral-to-medial for low-to-high frequencies (figure 4.10). Meanwhile, connectivity from the contralateral hemisphere appears to favour A1 and may originate more predominantly in AAF.

4.5.1 Comparison with physiological data from other species

Latency

As mentioned above, my findings in support of an A1–AAF latency difference are in line with the few other studies which have made this comparison in the mouse cortex, notably Guo et al. (2012, testing latency of pure-tone responses) and Linden et al. (2003, a STRF-based comparison).

They are also consistent with reports from other species in which A1 and AAF have been directly compared, including rats (Rutkowski et al., 2003), ferrets (Kowalski et al., 1995; Bizley et al., 2005) and cats (Knight, 1977; Eggermont, 1998; Imaizumi et al., 2004).

Not all published findings agree, however; for example neither Polley et al. (2007) nor Profant et al. (2013) found any significant differences in latency between rat A1 and AAF. Thus, the extent to which simple response characteristics, such as latency, are organised across cortical areas remains a topic on which additional contributions are valuable; my data strongly support the predominance of shorter latencies in mouse AAF compared to A1, including within supragranular, granular and infragranular layers (figure 4.4).

Bandwidth and threshold

The similarity of my pure-tone response data across A1 and AAF contrasts with at least one published finding in mice: Guo et al. (2012) briefly mention broader bandwidths in AAF; note Linden et al. (2003) also found that STRFs within AAF exhibited broader frequency tuning than those in A1. Reports from other species, however, have often yielded similar frequency response characteristics in A1 and AAF. This includes early (Knight, 1977) and more recent (Eggermont, 1998) work in the cat, and an extensive study of ferret cortical organisation from this laboratory (Bizley et al., 2005), which found differences in breadth of tuning and response threshold between primary and belt areas, but not between A1 and AAF. Other studies in both those species, however, have indeed described significantly larger bandwidths in AAF (Kowalski et al., 1995; Imaizumi et al., 2004).

Among the other rodents, the rat auditory cortex has received the most attention in relation to these response properties, with diverse results. Rutkowski et al. (2003), for example, reported both broader bandwidths and higher thresholds in AAF, while Polley et al. (2007) measured both those characteristics and observed differences relative to belt areas, but none between A1 and AAF.

Considering these varied reports, the difference between my findings and those of

Guo et al. (2012) is perhaps less surprising. In particular, although the number of recording sites contributing to our observations was similar (all four A1 or AAF data sets, for bandwidth, contain between 200 and 300 sites), our methods of designating an FRA boundary — and thus of calculating bandwidth — differ. Such differences may underlie much of the variation in the literature. Moreover, even if the result did not reach statistical significance, the median BW8 and BW24 in my data are indeed higher in AAF than A1 (see first box plot comparison, figure 4.7 B,D).

4.5.2 Likelihood of a shared thalamic tonotopic axis

In the context of recent publications relating to mouse thalamocortical connectivity (compare Hackett et al., 2011, and Horie et al., 2013), the small set of data presented in figure 4.10 is pertinent. As discussed in section 4.4.1, the paired distributions of projecting cells I observed within MGBv were much more consistent with a single thalamic field serving both A1 and AAF (e.g. see Llano and Sherman, 2008; Hackett et al., 2011) than discrete thalamic compartments with divergent tonotopic axes (Horie et al., 2013).

In other species, particularly the cat, extensive characterisation of the thalamocortical pathway presents a clear picture of parallel, topographically organised thalamocortical projections to A1 and AAF, originating in overlapping regions of the ventral MGB (e.g. Andersen et al., 1980; Lee et al., 2004; Lee and Winer, 2008a) and including a small number of individual neurons with branching axons terminating in both subfields (Lee et al., 2004; Lee and Winer, 2008a; Kishan et al., 2008).

Similar organisation is generally expected, if not specifically investigated, in smaller mammals such as the guinea pig (Redies et al., 1989a), gerbil (Budinger et al., 2000), rat

(Smith et al., 2012) and, indeed, mouse (Anderson and Linden, 2011; Llano and Sherman, 2008). Thus, the recent report of dual compartments by (Horie et al., 2013) is something of an outlier; the principal difference between their methods and mine, and a possible source of the discrepancy in results, was in the electrophysiology used to guide tracer injections (flavoprotein autofluorescence *vs.* extracellular multi-unit recordings).

4.5.3 Implications: more primary than primary?

In sum, the data I have outlined in this chapter present a portrait of mouse A1 and AAF featuring more similarities than differences. As discussed in section 4.1.1 above, the two primary subfields can be difficult to distinguish on the basis of frequency tuning maps, and properties such as response strength and latency also appear to vary fairly continuously, rather than revealing an obvious boundary (see figure 4.3). Even when a boundary is estimated and the fields are considered separately, I have found no significant A1–AAF differences in tuning strength, bandwidth or threshold of pure tone responses. I did, however, observe larger noise-driven spike counts in AAF, particularly in infragranular layers — and a clear difference in peak latency, which is reproducible across cortical depth and consistent with data from other mammals.

The differences suggested by my preliminary comparison of commissural connectivity (section 4.4.2) are also of interest. If A1 receives more contralateral projections, particularly from AAF, this might add weight to the view that AAF is in fact 'true' primary auditory cortex, which is also supported by the shorter latencies it exhibits. Alternatively, Linden et al. (2003) and others have suggested that A1 and AAF are equivalent stations in parallel auditory pathways, with AAF specialised for more rapid temporal processing (see also Schreiner and Urbas, 1988, and discussion in section 6.2.5 below). Thus, while both

A1 and AAF receive concurrent thalamocortical inputs, AAF may perform some faster computations and pass information on to A1 (contralateral and ipsilateral) as well as to non-primary areas. More detailed investigation of A1–AAF connectivity differences may help to distinguish between these hypotheses; anatomical evidence from both the gerbil (Budinger et al., 2000) and the cat (Lee and Winer, 2008b) describes predominantly homotopic commissural projections of A1 and AAF, and while each of those studies reports reciprocal cross-talk between the two primary fields, neither identified a bias towards one field or the other.

Some functional experiments have already explored the reciprocal influence exerted by A1 and AAF on each other's processing of auditory stimuli (Carrasco and Lomber, 2009; Carrasco et al., 2013). By deactivating either A1 or AAF in cats with a cooling loop, the Lomber group has reported that silencing AAF activity decreases response strength, increases thresholds and sharpens tuning in ipsilateral A1 (Carrasco and Lomber, 2009). Intriguingly, cooling A1 had no equivalent effect on AAF responses. This finding supports the notion of AAF as an effectively 'more primary' area; a subsequent study from the same group, however, reported more variable effects of A1 or AAF deactivation on responses in contralateral AAF (Carrasco et al., 2013).

As discussed in the next chapter, with the arrival of optogenetics, neuroscientists can intervene in this type of circuitry with vastly improved precision. The combination of optogenetic manipulation of long-range inputs with high channel-count recordings, particularly spanning both hemispheres, is an attractive possibility for future investigation of the interaction between A1 and AAF.

Chapter 5

Cortical inputs from other senses

5.1 Introduction

As discussed above, primary auditory cortex in the mouse is considered to include two subfields, A1 and AAF. In Chapter 3 I explored the topography of frequency responses in these areas. Their characteristic tonotopic gradients are more apparent in thalamorecipient layers (section 3.4.2; Winkowski and Kanold, 2013) and are inherited from thalamocortical projections to both A1 and AAF (Llano and Sherman, 2008) which are themselves tonotopically organised (Hackett et al., 2011; Horie et al., 2013, see also section 4.4.1 above). In Chapter 4 I compared aspects of the physiology and connectivity of the two subfields. In this chapter I continue to describe the connectivity of mouse primary auditory cortex, looking in particular at the inputs it receives from other early sensory cortices.

5.1.1 Cross-talk among early cortical areas: anatomy and activity

The brain's ability to create unified perceptions of objects and events requires information from different senses to be readily and accurately combined. The cellular manifestation of this convergence is neurons that are responsive to more than one sensory modality (Stein and Stanford, 2008). So-called 'multisensory neurons' are well known in higher-order, associative cortical areas (e.g. Dahl et al., 2009), as well as in subcortical structures, such as the superior colliculus (e.g. Cuppini et al., 2010), which receive branched ascending connections as well as feedback from the cortex.

Fuelled by increasing evidence that primary sensory cortices (including A1, e.g. Ghazanfar et al., 2005; Bizley et al., 2007; Lakatos et al., 2007; Kobayasi et al., 2013) exhibit cross-modal responses, recent years have seen considerable interest in direct, cross-modal connections between early cortical areas originally considered unimodal. As discussed in section 1.5 above, in this thesis I use the abbreviation ECC to describe such early, cortico-cortical, cross-modal connectivity. This burgeoning field has produced anatomical evidence for direct inputs to A1 from S2 in monkeys (Cappe and Barone, 2005), from V1 in ferrets (Bizley et al., 2007), from both S1 and V2 in gerbils (Budinger et al., 2006) and from V1 and S1 in prairie voles (Campi et al., 2010).

In mice, a series of investigations of V1 connectivity has revealed direct connections from primary somatosensory and auditory areas (Charbonneau et al., 2012; Laramée et al., 2011, 2013). Intriguingly, Iurilli et al. (2012) recorded sound-driven, subthreshold inhibitory responses in mouse V1 and further demonstrated that these responses required cortico-cortical connections from the auditory cortex. ECC inputs **to** mouse A1 and AAF, however, have not been thoroughly investigated. One study traced axons from V2 to both supra- and infragranular layers of mouse A1 and also showed that in acute slices, elec-

trical stimulation of lateral V2 modulated electrically driven calcium transients within A1 (Banks et al., 2011). However, the distribution of cells which send such cross-modal inputs to the mouse auditory cortex, in different cortical areas and layers, has not been reported.

5.1.2 Aims

In this chapter, I seek further evidence for the presence of ECC inputs to primary auditory cortex in the mouse and begin to evaluate their functional significance. Specifically, I set out to meet these three objectives:

- catalogue the cortical distribution of cells projecting to primary areas A1 and AAF, particularly those in other early sensory areas, by injection of retrograde tracers;
- identify candidate projecting areas and look for labelled axons in auditory cortex following virus injections into those areas; and
- conduct a preliminary test for an effect of said candidate areas on cells in the auditory cortex, by optogenetic activation during extracellular *in vivo* recordings.

5.2 Retrograde tracing of inputs to primary auditory cortex

In order to locate neurons with long-range, cortico-cortical connections terminating in A1 and/or AAF, I performed injections of retrograde tracers into the auditory cortex of six wildtype C57BL/6 mice. Two were single injections of Fluoro-Gold (FG) and four were paired injections of fluorescinated cholera toxin B (CTB-alexa 488 and CTB-alexa 594). In

each case I performed rapid, coarse mapping of auditory responses using extracellular silicon multielectrodes, to confirm the cortical position of each injection site (e.g. figure 5.1B). The intended injection volume was 50 nL but in practise, subsequent histology showed that the volume delivered was variable from case to case. I performed detailed analysis of one relatively large FG injection (estimated injection core volume from histological reconstruction: 200 nL) and one pair of smaller CTB injections (estimated core volumes 28 and 15 nL; note these values are not estimates of the actual fluid volume injected, and are difficult to compare between fluorophores and between chromatic and fluorescent preparations — see section 2.4.1). Overviews of sections traced in Neurolucida are shown in figures 5.1 and 5.2; examples of labelled cells appear in figure 5.3. For more details on the injection procedure, see section 2.4.1.

5.2.1 Three tracer injections into primary areas reveal predominantly scattered, sparse cortico-cortical inputs

As shown in figure 5.1 A and B, the FG injection in mouse 'Marvin' was centred in superficial layers of primary auditory cortex, most likely including both A1 and AAF. Labelled cells in the ventral portion of the medial geniculate body (MGBv; figure 5.1C) confirmed its location as primary auditory cortex, though I cannot exclude the possibility that the injection included some of A2 because its core was relatively large. Retrograde FG labelling also identified a population of projecting cells across both hemispheres of the cortex, dominated by cells within the auditory cortex but including other sensory areas.

Two key observations can be made from the overview in figure 5.1. Firstly, the most prominent populations of labelled cells outside auditory areas are within fields adjacent

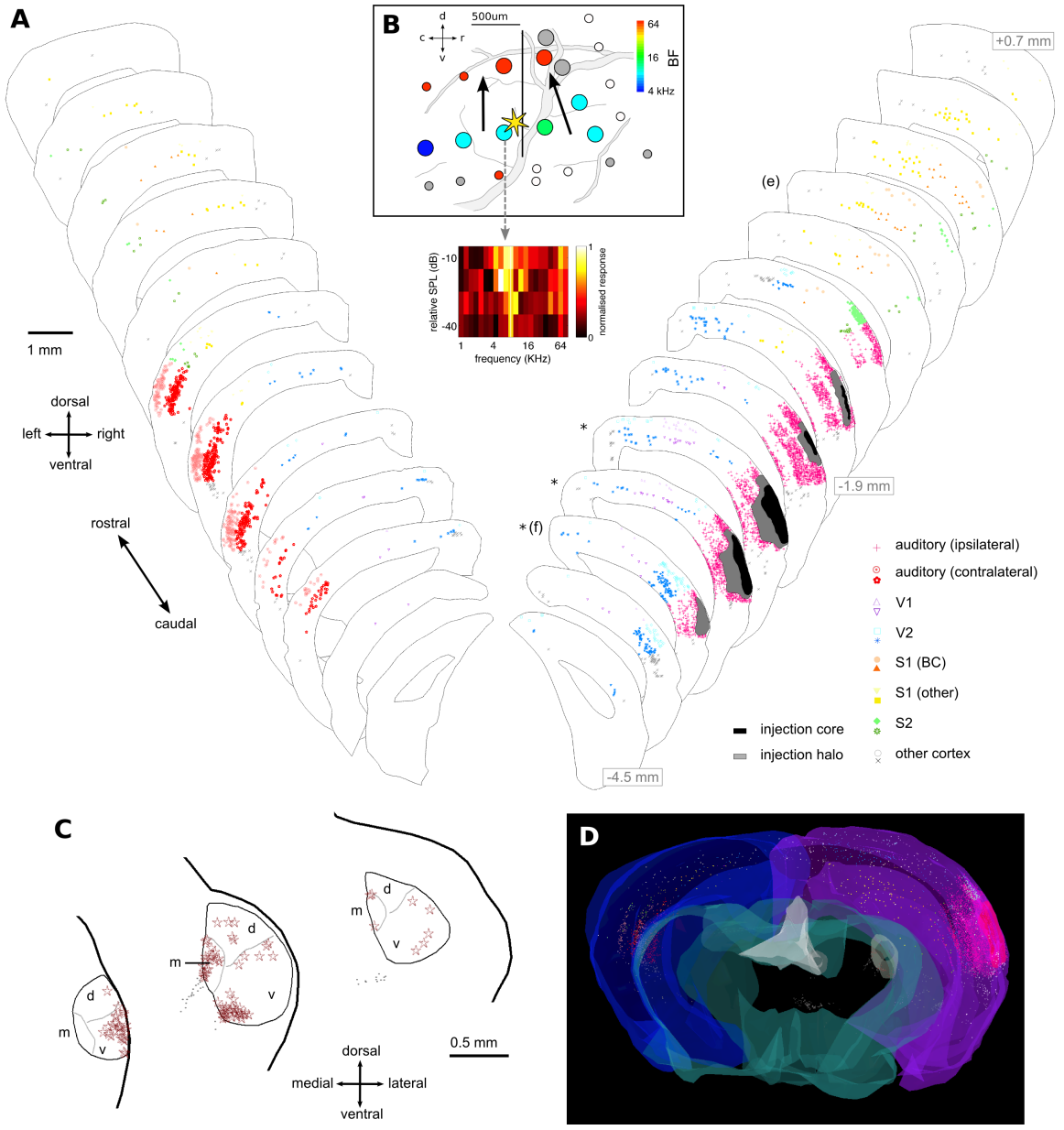


Figure 5.1: **Overview of retrogradely labelled cells from mouse 'Marvin' following single tracer injection into primary auditory cortex.** ***A***: Traced coronal sections of left and right cortex showing the location of FG-labelled cells, colour coded by sensory area. The key indicates the markers used, including different markers for cells in supra- and infra-granular layers (lighter and darker shades, respectively). Grey, boxed numbers indicate estimated rostrocaudal position, relative to bregma. ***B***: Schematic illustration of injection site (gold star) in relation to the coarse map of recorded BFs. (Conventions as in Chapter 3, e.g. figure 3.8.) Note the injection site is near the border of A1 and AAF (vertical line, calculated as in chapter 3; orientation of tonotopic gradients is indicated by black arrows). Below the map is an FRA from the recording site nearest the injection. ***C***: Labelled cells in the auditory thalamus, from three sections indicated by asterisks in ***A***. Dorsal (d), ventral (v) and medial (m) subdivisions of the medial geniculate body (MGB) are indicated. 66 cells are labelled within the MGB (red stars) while some appear nearby in the posterior intralaminar nucleus (grey dots). This is consistent with an injection primarily into the superficial layers of A1/AAF (see injection core in ***A***); more extensive labelling of the ventral MGB would be expected for a deeper injection that included more of layer 4 (see cases in figure 5.2). ***D***: Angled ventral view of a 3D reconstruction assembled from these sections. Cell colours are as in ***A***, the injection site is shown in pink, thalamus in green, and the third ventricle and MGB are outlined in grey. Lowercase letters in ***A*** denote sections photographed in figure 5.3.

to auditory cortex, notably the lateral sector of V2 (V2L) and S2. My estimations of field boundaries are based on comparing both gross morphology and DAPI staining with the mouse atlases of Paxinos and Franklin (2007) and Rosen et al. (2000). While it is sometimes difficult to delineate field boundaries in this way with confidence, I have subsequently observed that both of these areas receive extensive projections from medial V2 (V2M) and S1, respectively (see figures 5.8, 5.9), which suggests they are indeed visual and somatosensory areas rather than continuations of auditory cortex. The concentration of auditory-projecting cells they exhibit may reflect a role in relaying multisensory cross-talk, similar to the A1–V2L–V1 pathway reported by Laramée et al. (2011); alternatively this pattern may result from a more generalised increase in connectivity between neighbouring areas.

Secondly, outside these areas, projecting cells are fairly sparsely scattered across the cortex. The most noticeable collections of cells sending long-range inputs are in V2M and non-barrel S1 (for discussion of my choice of candidate areas to study with virus injections and optogenetics, see section 5.2.5). It is also worth noting that the majority of projecting cells are located in infragranular layers. The distribution of projecting cells between superficial and deep layers is presented in figure 5.7.

Figure 5.2A shows a similar overview, this time of paired tracer injections in mouse 'Marcy'. In this case, only the right hemisphere was surveyed in detail. Thalamic labelling again confirms that both injections are in primary auditory areas (figure 5.2C) and the frequency map produced during the procedure indicates that the injections were either side of the A1–AAF tonotopic reversal (figure 5.2B).

For both of these injections, similar observations can be made as above for mouse 'Marvin'; long-range projecting cells are scattered across cortical areas while the more

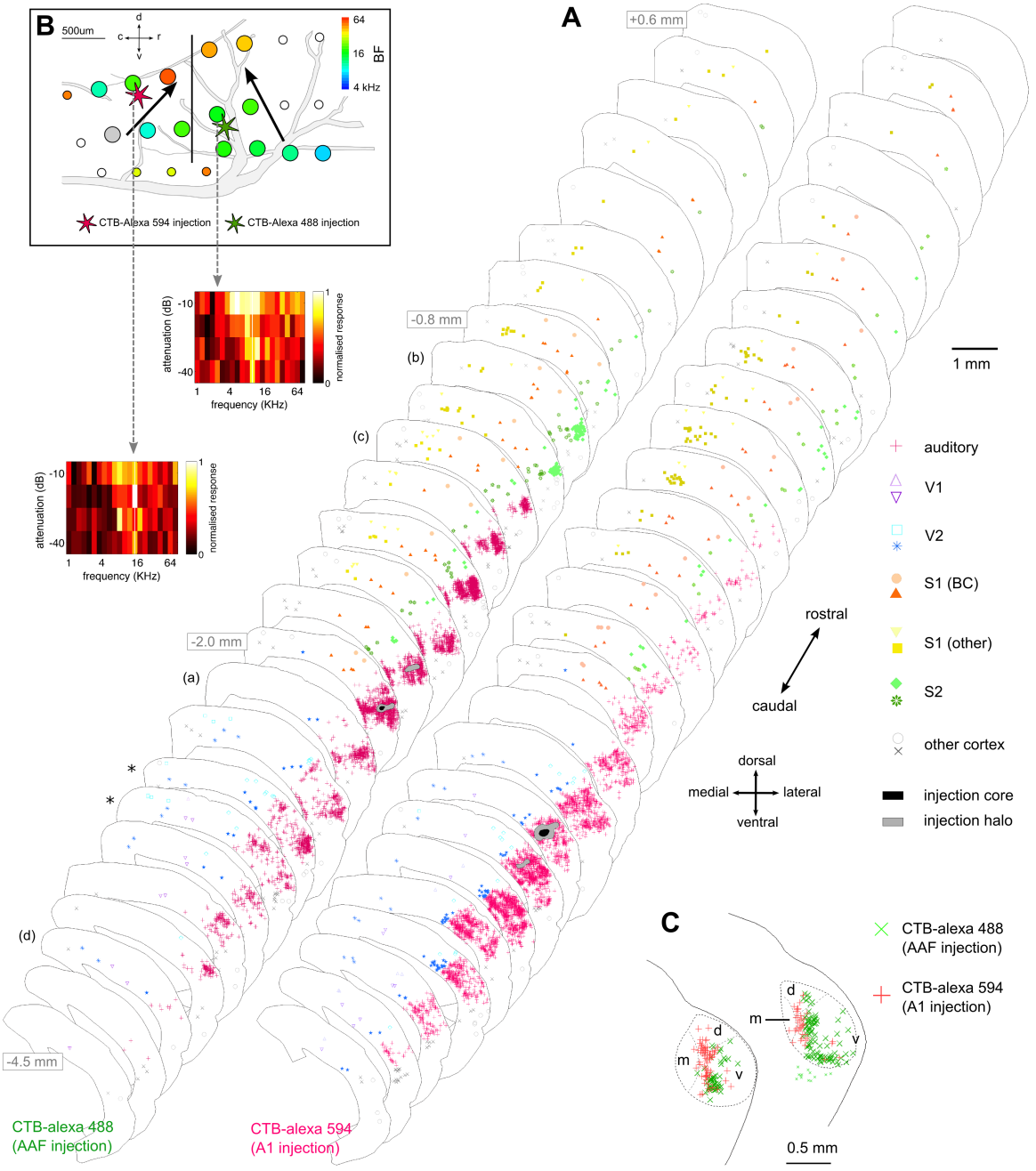


Figure 5.2: **Overview of retrogradely labelled cells from mouse 'Marcy' following dual tracer injections into A1 and AAF.** ***A***: Traced coronal sections of right cortex showing the location of CTB-labelled cells; as in figure 5.1A, markers are colour coded by area and layer. Here, each section is shown twice to distinguish cells labelled by the two injections; grey, boxed numbers on the left indicate estimated rostrocaudal position, relative to bregma. ***B***: Schematic of tuning map and injection sites; note that the estimated boundary between A1 and AAF (vertical line; this and the orientation of tonotopic gradients, indicated by black arrows, were calculated as in chapter 3) situates the CTB-Alexa 594 injection site (red star) within A1, while the CTB-alexa 488 injection site (green) is in AAF. This is the same map shown in figure 4.9, reprinted here for convenience. ***C***: Location of labelled cells within dorsal (d), ventral (v) and medial (m) MGB, from the two sections indicated by asterisks. See section 4.4.1 for discussion of A1/AAF thalamocortical connectivity. Lowercase letters in ***A*** denote sections photographed in figure 5.3.

proximal V2L and S2 contain comparatively high numbers. Interestingly here, V2L is more densely labelled by the injection into A1, and S2 by the AAF injection. This indicates either that the relayed cross-talk hypothesised above is differently mediated for A1 and AAF, or that these connection patterns are indeed a general property of neighbouring cortical areas.

Photographs in figure 5.3 show examples of retrogradely labelled cells from the CTB injections in mouse 'Marcy' and the FG injection in mouse 'Marvin'. The examples in panels c–f come from areas S1 and V2M, which I selected as candidate areas to investigate further (see section 5.2.5). Also included (panels a,b) are photographs showing more dense populations of labelled cells, within auditory cortex and neighbouring S2.

5.2.2 Projecting cells are distributed across cortical areas

Figure 5.4 compares the cortical distributions of A1- and AAF-projecting cells identified by the paired injections in mouse 'Marcy'. Removing auditory cortex from the illustrations, and superimposing both sets of labelled cells within the remaining sensory cortex, reveals cells of both colours scattered across layers and areas. Apart from the aforementioned over-representation of V2L and S2, respectively, these populations of projecting cells appear to be commingled rather than displaying any topographic separation. The question of distinguishing A1 and AAF based on their connectivity and neurophysiology was explored more thoroughly in chapter 4.

This over-representation is also apparent when the cell populations revealed by each injection are compared in pie charts (figure 5.5: note the 84 V2L neurons in A and 183 S2 neurons in B, out of 406 and 531 non-auditory neurons respectively). Outside those

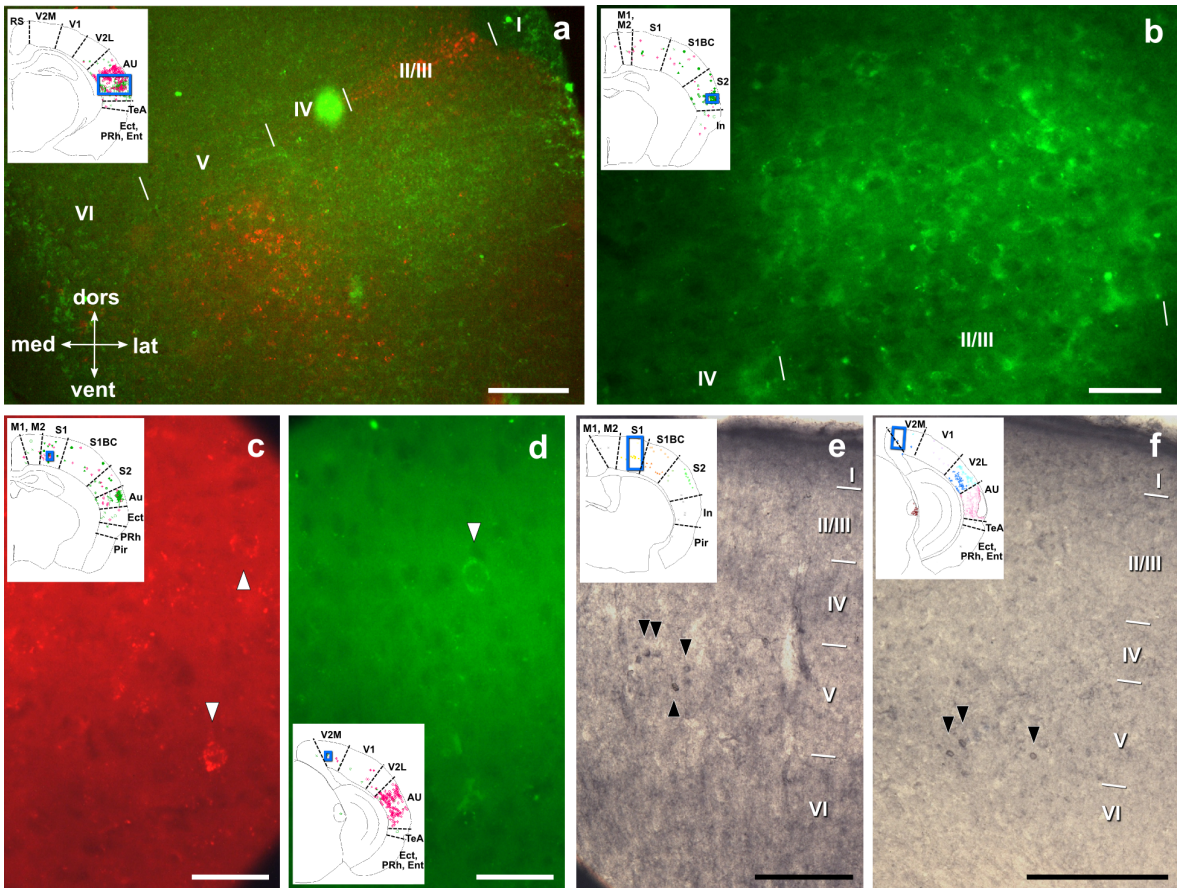


Figure 5.3: **Examples of labelled cells.** **a**: Abundant cells labelled with both CTB-alexa 488 (green) and -alexa 594 (red) in the auditory cortex, in a coronal section between the two injection sites in mouse 'Marcy'. Estimated layer boundaries are indicated, based on DAPI stain (not shown) and inset shows location of the image within the coronal section, marked with cortical areas determined by DAPI stain in conjunction with mouse brain atlases (Paxinos and Franklin, 2007; Rosen et al., 2000). Orientation marker applies to all panels. **b**: Labelled cells from AAF injection (CTB-alexa 488, green) in superficial layers of S2; as discussed in text, labelling of this density was only observed in areas adjacent to auditory cortex. **c,d**: Examples of labelled cells in S1 (non-barrel cortex) and V2M labelled with CTB-alexa 594 and 488, respectively, from the same mouse. **e,f**: Further examples from S1 and V2M in mouse 'Marvin', labelled with anti-Fluoro-Gold antibody. For reference, relevant sections are marked with lowercase letters in overview figures 5.1 and 5.2. Abbreviations for cortical areas: AU, auditory; Ect, ectorhinal; Ent, entorhinal; In, insular; M1/2, primary/secondary motor; Pir, piriform; PRh, perirhinal; RS, retrosplenial; S1/2, primary/secondary somatosensory; S1BC, barrel field; TeA, temporal association; V1, primary visual; V2M/V2L, medial/lateral secondary visual. Scale bars: **a**, 100 µm; **b–d**, 25 µm; **e–f**, 200 µm.

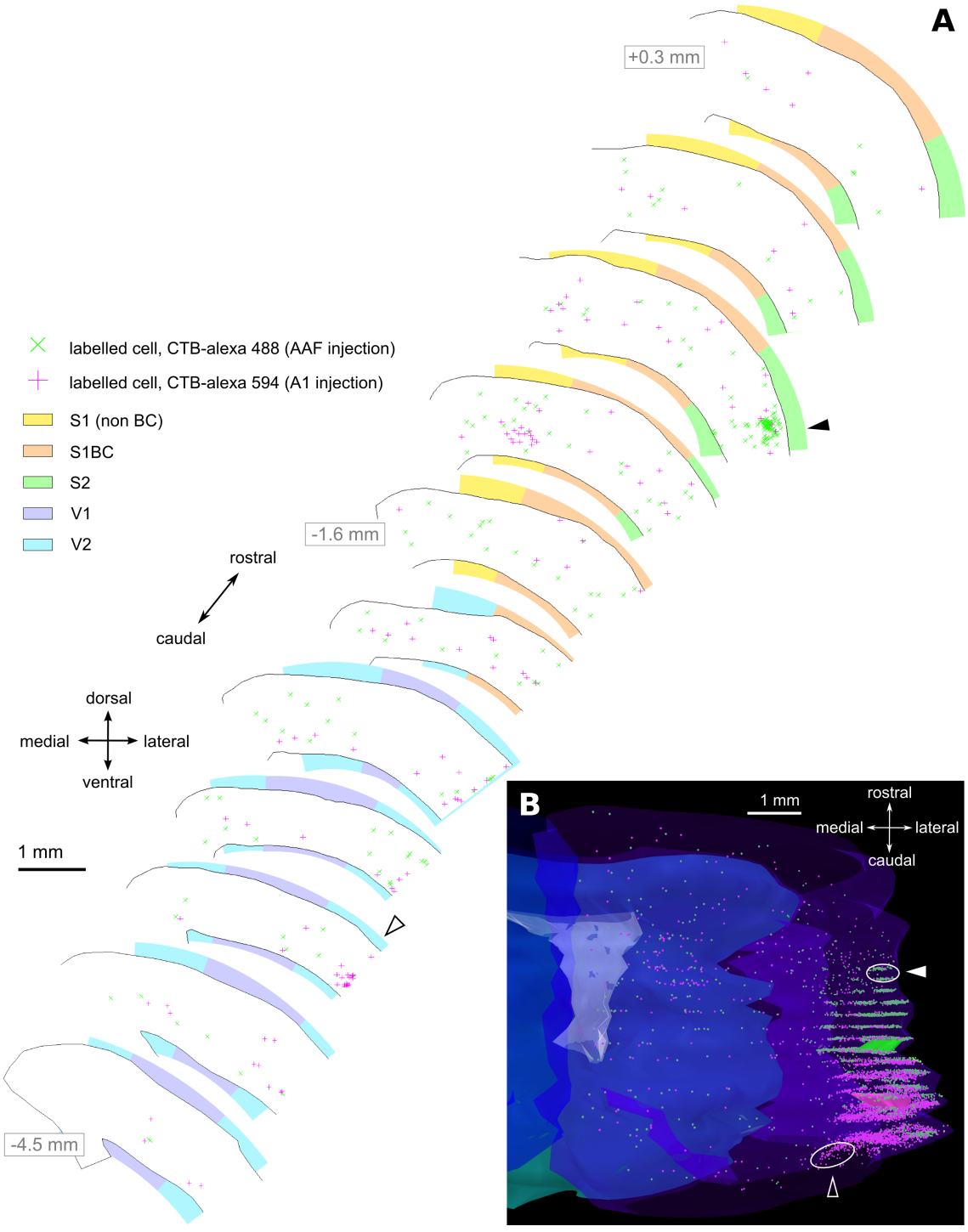


Figure 5.4: **Scattered, predominantly commingled cells projecting to A1 and AAF from other sensory areas.** ***A***: Non-auditory sensory cortical fields from a subset (one-in-two) of the sections shown in figure 5.2. With the exception of concentrations in S2 (filled arrowhead in A and B) and V2L (hollow arrowhead) the cells are sparsely scattered. These areas are adjacent to AAF and A1 respectively, which contain the two injection sites; this can be seen in a dorsal view of the reconstructed right hemisphere of the sectioned brain (***B***). Injection halos in ***B*** are shown in solid green (AAF injection, CTB-alexa 488) and pink (A1 injection, CTB-alexa 594) and grey, boxed numbers in ***A*** again indicate estimated rostrocaudal position, relative to bregma. Across other sensory fields, the projecting cells identified by the two injections show no obvious topographic separation in either the sections or reconstruction.

fields adjacent to auditory cortex, labelling in a spread of other sensory areas was readily apparent in the results of each injection (compare right-hand plots, figure 5.5, A–C) including primary visual and somatosensory cortices. A number of cells were also labelled in temporal association cortex, motor cortex, and perirhinal cortex, in each case; since these areas are not the focus of my investigation these have been grouped together in the figures under 'other cortex'.

Each injection also labelled a large number of cells within auditory cortex, where I did not consider individual subfields because of the difficulty relating published mapping studies (e.g. Stiebler et al., 1997; Guo et al., 2012) to published atlases (Paxinos and Franklin, 2007; Rosen et al., 2000). Moreover, my focus was on other sensory areas. The smaller proportion of auditory cells I report for the FG injection in mouse 'Marvin' (compare left-hand plots, figure 5.5 C *vs.* A,B) is probably due to the difference in labelling methods: I used the native fluorescence of the CTB conjugates in mouse 'Marcy', rather than the HRP-conjugated antibody and chromatic reaction used to label FG in mouse 'Marvin', which obscured densely packed cells near the injection site.

5.2.3 The contralateral hemisphere contains a smaller but similarly distributed set of projecting cells

In mouse 'Marvin' I also surveyed the contralateral (left) cortex, relative to the injection site in right auditory cortex, for retrogradely labelled cell bodies (see section overview in figure 5.1). Here there were noticeably fewer projecting cells, but a spread was still present across primary and secondary, non-auditory sensory areas. The results from contralateral and ipsilateral hemispheres are compared in figure 5.6.

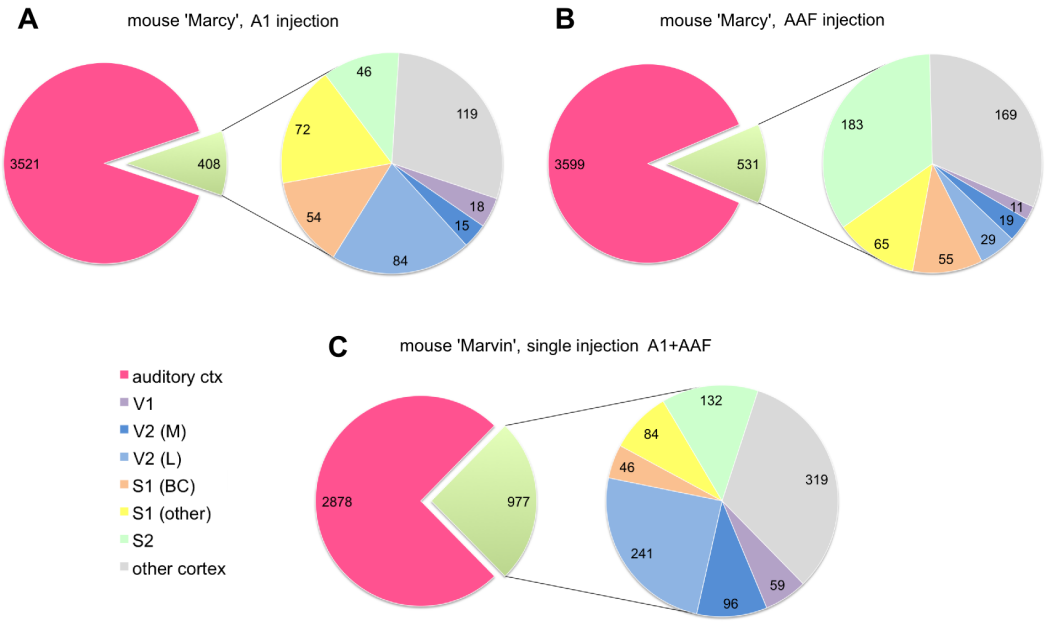


Figure 5.5: **Distribution of A1/AAF-targeting cells across cortical areas.** Breakdowns are shown of the number of retrogradely labelled cells within different cortical areas, from the two CTB injections in mouse 'Marcy' (***A***, ***B***) and the larger FG injection in 'Marvin' (***C***). Primary and secondary somatosensory and visual areas are all represented in each case. Note that apart from the 'other cortex' category, which includes a number of cells in association areas and motor cortex, the cortical field with most labelled cells tends to be adjacent to the injected area (V2L for A1 injection, ***A***; S2 for AAF injection, ***B***; V2L then S2 for the larger injection in ***C***; see section 5.2.5 for discussion). The lower proportion of cells counted within auditory cortex in 'Marvin' is likely due to the different labelling method; in that case, FG was detected with an antibody and subsequent HRP reaction, leading to a larger 'halo' area surrounding the injection site (compare figures 5.1A, 5.2A), where dense labelling arising from the HRP reaction prevented individual cells from being counted.

Only V2L shows an obviously higher proportion of projecting cells in the ipsilateral cortex, compared to the contralateral hemisphere; this may suggest that its relative over-representation in results from mouse 'Marvin' and the A1 injection in 'Marcy' is the result of increased connectivity between neighbouring cortical regions (i.e. V2L and A1 in the same hemisphere). On the other hand, if these shorter-range connections do constitute a specific multisensory input to A1, it is confined to the ipsilateral side and not matched by a commissural V2L projection.

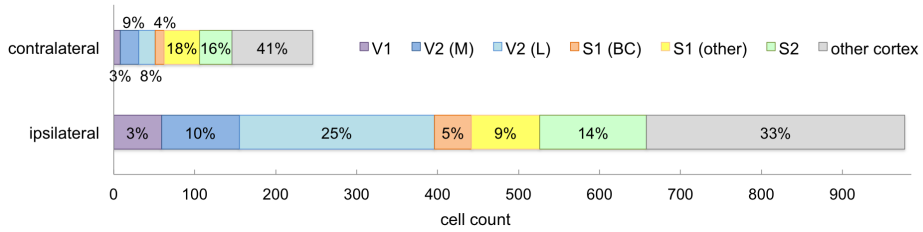


Figure 5.6: **Distribution of projecting cells in non-auditory areas from both hemispheres.** Bar chart comparing the breakdown of labelled cells in non-auditory areas of each hemisphere in mouse 'Marvin'. Among the 977 cells projecting to A1/AAF ipsilaterally and 246 projecting contralaterally, the representation of other sensory areas is broadly similar, with the exception of V2L which is, relatively, over-represented in the ipsilateral hemisphere (as shown in figure 5.5C and discussed in the text).

5.2.4 The majority of projecting cells are in infragranular layers

Returning to focus on the ipsilateral hemisphere, in figure 5.7 A–C I outline the number of projecting cells revealed by each of the three injections, still separated by the cortical area of origin, now further categorised into cells located in supragranular or infragranular layers. Despite some fluctuation, infragranular cells contribute the majority of connections from nearly every area. The obvious exception is S2, which yields a majority of supragranular projecting cells. As discussed above and in section 5.2.5, S2 borders AAF (based on integrating published maps and atlases, e.g. Stiebler et al., 1997; Paxinos and Franklin, 2007) but even following an injection centred within A1, the more caudal subfield, it shows an

even supra- *vs.* infragranular split (24 *vs.* 22 cells, figure 5.7A; see also layer indices in figure 5.7D). This implies that the more superficial distribution of A1/AAF-targeting cells in S2 is not simply a consequence of local connectivity between adjacent cortical fields.

As discussed in section 1.6, long-range connections between cells in different areas of the cortex are often sorted into feedforward (or ascending), feedback (or descending) and lateral inputs (see Felleman and Van Essen, 1991). One of the distinguishing characteristics used for such classification is the laminar termination pattern of the projections concerned. Since my injections traversed cortical layers (in an effort to detect what I expected to be a sparse set of cortico-cortical inputs), these retrograde tracing experiments shed no light on the termination pattern of the connections I am reporting (but see figures 5.8, 5.9 and discussion in section 5.3.1).

Importantly however, the supragranular–infragranular balance in a given connection's originating cells also facilitates its classification according to this scheme. To systematise such analysis, Budinger et al. (2006) defined a 'layer index', L, for a population of projecting cells as a measure of this balance (calculated as $L = (S - I)/(S + I)$, where S and I are the numbers of supragranular and infragranular cells, respectively). This value approaches 1 for feedforward connections (predominantly supragranular in origin), -1 for feedback connections (predominantly infragranular) and 0 for lateral connections, which are more likely to be distributed across layers in both their origin and termination.

Figure 5.7D presents the layer indices calculated for cells in other sensory areas which project to A1 and/or AAF, based on each of the injections analysed. With the exception of the input from S2, as expected, the values are nearly all negative. This suggests that the sparse ECC inputs I have described above, when separated into the projecting cortical fields, predominantly show feedback-type laminar architecture.

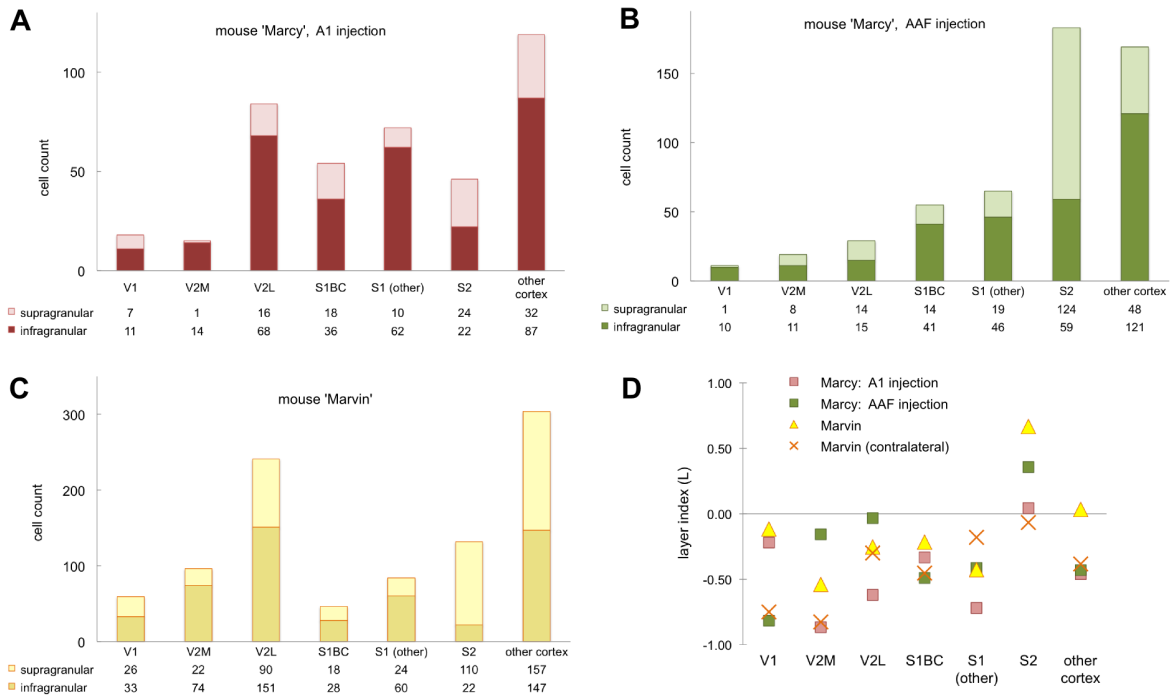


Figure 5.7: **Supra- and infragranular layer breakdown of A1/AAF-targeting cells in non auditory areas.** ***A–C***: Bar charts indicating numbers of labelled cells within ipsilateral cortical areas, further separated by cortical depth (supragranular layers in lighter colours; infragranular, darker), from the A1 and AAF injections in mouse 'Marcy' (***A***, ***B*** respectively) and the larger A1+AAF injection in 'Marvin' (***C***). Note that in nearly every area (with the exception of S2, where supragranular layers are better represented) the majority of projecting cells are infragranular. This is quantified in ***D***, which shows the layer index (L) for each case ($L=(S-I)/(S+I)$ where $S=$ number of supragranular cells and $I=$ number of infragranular cells; see Budinger et al. (2006)). ***D*** also includes the layer indices for cells located in the contralateral cortex of mouse 'Marvin', which were less numerous than ipsilateral cells (see figure 5.6) but are also predominantly infragranular.

5.2.5 Choice of candidate projecting areas

In order to investigate these ECC inputs to A1 and AAF more closely, I selected two candidate areas to target with virus injections, both to examine their projections in the anterograde direction, and to evaluate their influence on auditory processing with optogenetic stimulation. Based on the data summarised above, the cortical areas most highly populated with A1/AAF-targeting neurons are V2L and S2: areas neighbouring the auditory cortex. I had two concerns about targeting these areas in the next phase of my study.

Firstly, I could not entirely rule out the possibility that the comparatively high cell counts in these regions arose from experimental irregularities. Diffusion of the injected bolus of tracer over a wider than intended area, for example, would contribute to such over-representation of neighbouring fields. I have endeavoured to reduce this risk by performing only coarse neurophysiological mapping, so as to minimise damage to the cortex prior to the tracer injection, and by choosing brains for analysis in which the injection core and halo appeared well defined and restricted to auditory areas. Evidence within my collected data suggests that this strategy was successful; for example, if the tracer injection in mouse 'Marvin' had diffused into V2L, I would expect to see much higher numbers of retrogradely labelled cells within V1 (see figure 5.1).

Perhaps more problematic is the fact that my estimation of cortical area boundaries was reliant on comparing DAPI staining and brain morphology with published mouse brain atlases (Paxinos and Franklin, 2007; Rosen et al., 2000). In some cases this is straightforward, for example where there is an obvious change in the width of the granular layer between a secondary and primary field; in other cases it relies on a degree of similarity between the experimental and archetypal mouse brain of which I could not be absolutely confident. Consequently I have been conservative in my estimations of boundaries sur-

rounding the auditory cortex, in order to minimise the possible count of false-positive non-auditory projecting cells. I am confident that the cells assigned to V2L and S2 are indeed within those areas. In support of this assertion, results presented later in this chapter show that these areas correspond to regions of high-density axonal projections originating in V2M and S1, respectively (see figures 5.8, 5.9). Such connectivity suggests that these areas are indeed predominantly somatosensory and visual, and further that they are involved in multisensory cross-talk, perhaps relaying information from those modalities into A1 and AAF. Interestingly, V2L has already been implicated in precisely this type of indirect pathway proceeding in the other direction, from A1 to V1 (Laramée et al., 2011).

Aside from the reliability of the preceding data, my second reason for avoiding neighbouring areas in the remainder of my investigation relates to maintaining specificity in the next set of experiments, which involves viral gene delivery and optogenetic stimulation. Similar concerns about diffusion, in this case of the injected virus, and correspondence between physiological area boundaries and stereotaxic coordinates, led me to choose candidate areas more distant from auditory cortex than V2L and S2.

Based on the number of labelled cells they exhibited in each injection and their position several millimetres from A1 and AAF, I selected V2M and non-barrel S1 for further examination (see figure 5.5 and examples in figure 5.3; I also observed labelled cells in these areas in several of the injected animals not subjected to detailed quantitative analysis). Specifically within non-barrel S1, I targeted the hindlimb and trunk regions (this was done based on stereotaxic coordinates, since mapping somatosensory responses during these experiments was impractical). Subregions such as these were not separated in the analysis above, but based on close comparison with published atlases I estimated this as the best represented S1 location in my retrograde tracer results. It is also the area in

which Budinger et al. (2006) found retrogradely labelled cells following tracer injections into gerbil A1. My choice of V2M was further underpinned by a published account of a direct, descending connection from both medial and lateral V2 to mouse A1 (Banks et al., 2011), which offered evidence from both anterograde anatomical tracing and *in vitro* electrophysiology (though their *in vitro* work concentrated on lateral V2, which I have avoided for the reasons outlined above).

5.3 Anterograde examination of projections from candidate areas

To further evaluate the connection extended by cells in V2M and S1 to primary auditory areas, I delivered a genetic construct encoding Channelrhodopsin2–mCherry to excitatory cells in those areas using an adenovirus (AAV2-CaMKIIa-ChR2-mCherry; see section 2.5.1 for more details). Serotype 2 adeno-associated viruses (AAV2) are known to be taken up efficiently by neurons and thus tend to deliver transgenes to neuronal cell bodies in close proximity to the injection site, rather than spreading over a wider area or being taken up by axon terminals or fibres of passage (Burger et al., 2004; Passini et al., 2004; Shimano et al., 2013). Consequently, this type of gene delivery is useful for labelling cells within a targeted area, including their axonal projections, for subsequent microscopy or photostimulation (e.g. Lima et al., 2009; Kohl et al., 2011). After leaving a period of 4–6 weeks for transgene expression to develop, I either perfused the animals to examine brain sections using fluorescence microscopy (n=4; section 5.3.1) or conducted *in vivo* optogenetic experiments ($n = 9$; 5.4).

5.3.1 Virus injections into S1 and V2M reveal sparse fibres in A1 and AAF

As shown in figure 5.8A, viral delivery successfully generated expression of ChR2–mCherry within S1, particularly in infragranular layers where I targeted the injections. This expression was present throughout the axonal arbours of infected cells, as demonstrated by flourescence in white matter axons near the injection site (figure 5.8A) and the obvious axon cloud in S2 (figure 5.8 B). Within the auditory cortex, by contrast, very few mCherry-positive axons were apparent but I did observe occasional examples of fluorescent fibres, in both supra- and infragranular layers of primary areas (see examples from AAF, figure 5.8 C,D). Because of the low density of labelled projections, together with the fairly rapid photo-bleaching I observed in mCherry fluorescence, I did not attempt to trace or reconstruct these projections; further experiments with dedicated anterograde tracers and a chromatic stain would be the best way to elaborate on these findings. Nonetheless, this evidence is consistent with a direct but sparse, descending input from trunk and hindlimb areas of S1 to primary auditory areas in the mouse.

I obtained similar results from virus injections into V2M. Figure 5.9 shows an example injection, which again produced strong mCherry expression near the injection site (panel A). Similarly to figure 5.8, the dense axon cloud in an expected target area, in this case the other V2 subfield (V2L, figure 5.9 B,D), is presented for comparison with the very sparse projections seen in primary auditory areas (A1 in this case; figure 5.9 C). Both in the case of the more profuse axon clouds in V2L (or S2) and of the isolated examples in auditory cortex, following the axons through focal planes and through adjacent sections showed that they terminated within those areas.

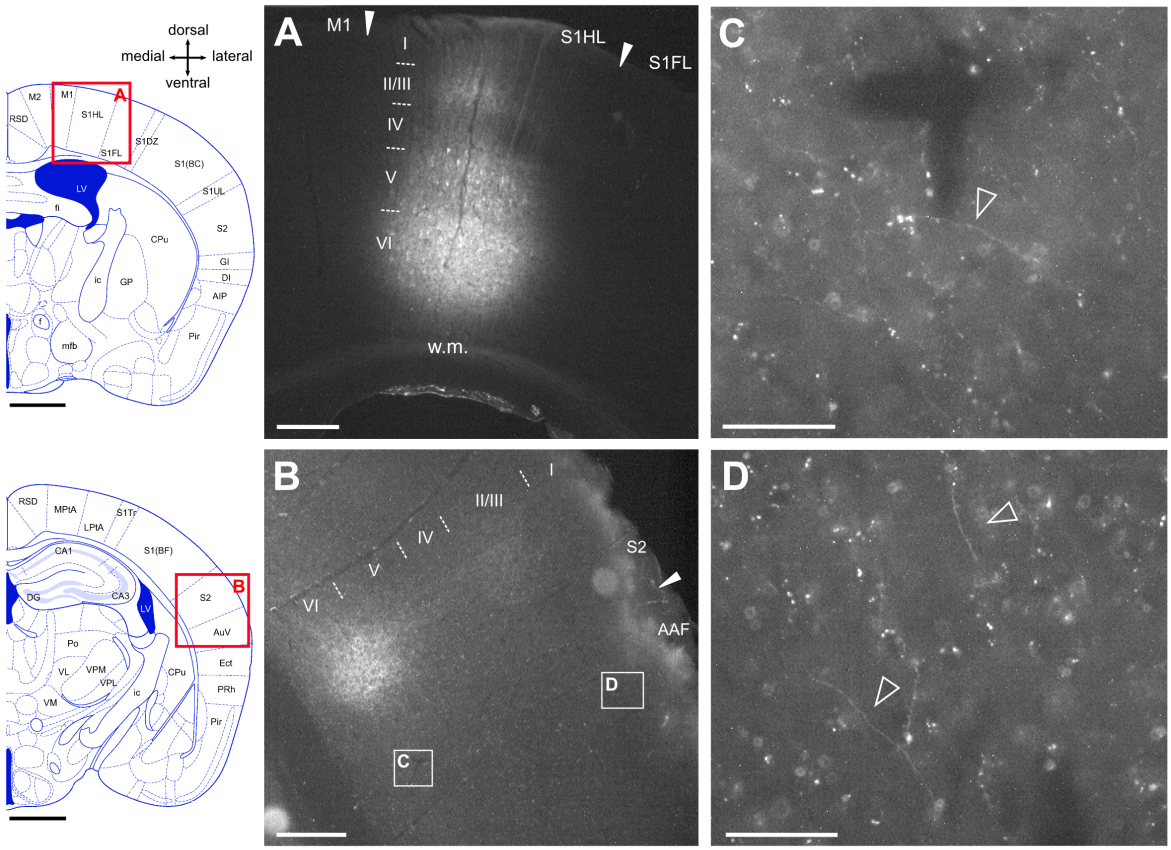


Figure 5.8: **Sparse axons from S1 within AAF.** ***A***: Expression of ChR2–mCherry near the site of a virus injection in S1; expression is most abundant in infragranular layers and is restricted in the lateral plane. Axons expressing the transgene can be seen in the white matter ('w.m.') proceeding both medially and laterally from the injection site. Position of image is marked on a schematic adapted from Paxinos and Franklin's mouse brain atlas (2007), and cortical layers and areas are indicated on the photograph (approximate boundaries marked by dotted lines and filled arrowheads respectively). ***B***: In a section of temporal cortex from the same mouse, S2 shows a distinct cloud of fluorescent axons projecting from transgenic cells in S1. It is most obvious in deep layers but also present in layer 2/3, while no such cloud is apparent in neighbouring auditory cortex. Schematic again shows location of the image; note that the brain atlas uses 'AuV' to describe this ventral part of auditory cortex. My own comparisons of cortical maps and coronal slices, in agreement with others in the field (J. Linden, personal communication), suggest this corresponds to AAF. Although much more sparse than the input to S2, close inspection of A1 and AAF at high magnification does reveal occasional fluorescent axons, including the examples from supra- and infragranular layers of AAF shown in ***C*** and ***D*** (hollow arrowheads). Abbreviations: AIP, agranular insular cortex, posterior region; CA1/CA3 fields of hippocampus; CPu, caudate putamen; DG dentate gyrus; Ect, ectorhinal cortex; f, fornix; fi, fimbria of hippocampus; GI, granular insular cortex; GP, globus pallidus; ic, internal capsule; LV, lateral ventricle; M1/2, primary/secondary motor cortex; mfb, medial forebrain bundle; M/LPtA, medial/lateral parietal association cortex; Pir, piriform cortex; Po, posterior thalamic nucleus; PRh, perirhinal cortex; RSD, retrosplenial dysgranular cortex; S1(BC), barrel cortex; S1DZ, dysgranular zone of S1; S1FL/HL, fore/hindlimb regions of S1; S1Tr, trunk region of S1; S1UL, upper lip region of S1; VL/VM, ventrolateral/ventromedial thalamic nuclei; VPL/VPM ventral posterolateral/posteromedial thalamic nuclei. Scale bars: schematics 1 mm; ***A***,***B*** 200 µm; ***C***,***D*** 25 µm. Orientation marker in upper schematic applies to all panels.

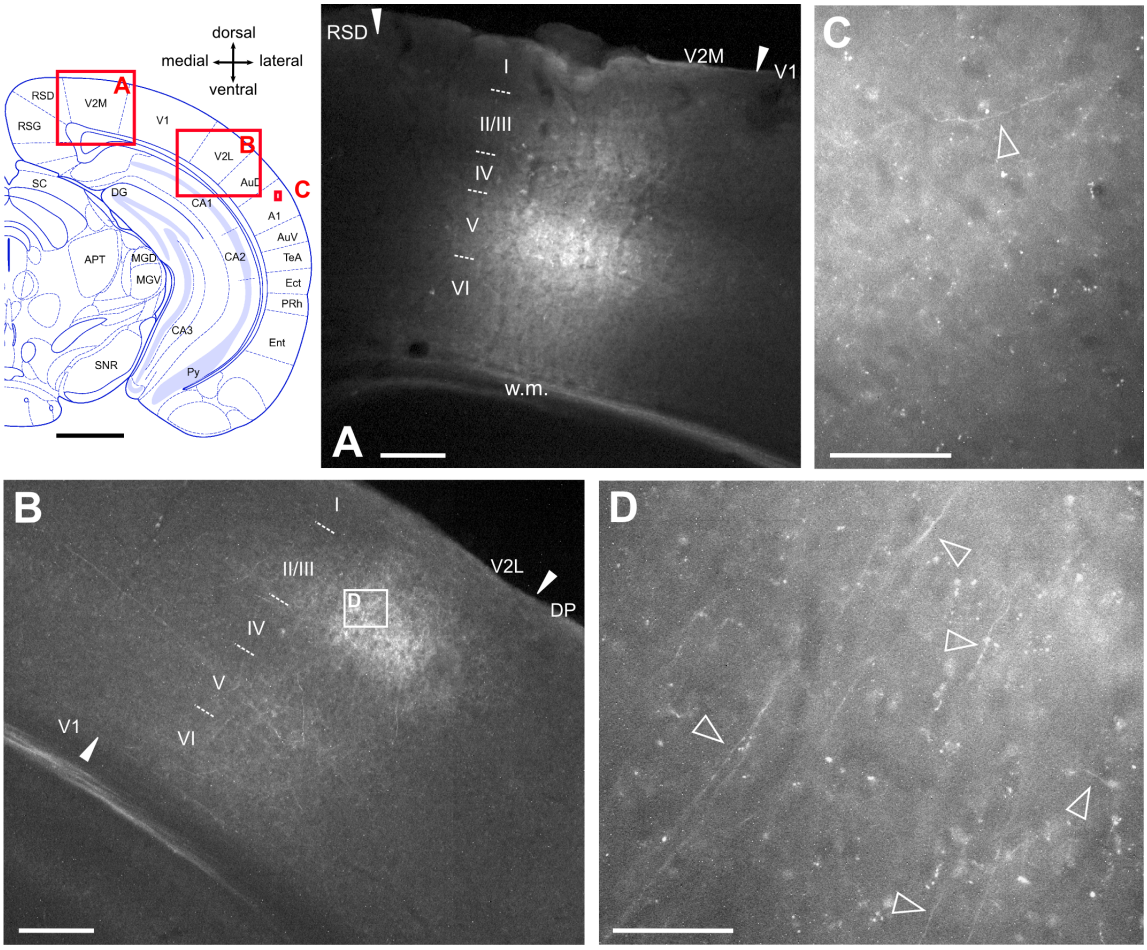


Figure 5.9: **Sparse axons from V2M in primary auditory areas.** ***A***: An example of ChR2-mCherry expression in medial V2 (V2M) following viral gene delivery. As for S1 injection in figure 5.8, expression is most abundant in infragranular layers and is visible in white matter axons (w.m.). ***B***: A cloud of axons expressing the transgene is obvious in the lateral part of V2 (V2L); labelled axons are most apparent in layer 2/3 but are also present in deep layers. A small area from within layer 2/3 is shown at higher magnification in ***D***. By contrast, very sparse axons are present in primary auditory areas, such as the example from A1 shown in ***C***. All images are from the same coronal section and locations are indicated on the schematic, which is based on a corresponding figure from the mouse brain atlas of Paxinos and Franklin (2007). Note that the atlas uses 'AuD' and 'AuV' for the dorsal and ventral regions of auditory cortex, which correspond to auditory subfields DP and A2 at this rostrocaudal position, based on physiological maps (e.g. Stiebler et al., 1997). Abbreviations in schematic are as in figure 5.8, with addition of: APT, anterior pretectal nucleus; Ent, entorhinal cortex; MGD/MGV, medial geniculate body (dorsal/ventral); py, pyramidal tract; RSG, retrosplenial granular cortex; SC, superior colliculus; SNR, substantia nigra (reticular); TeA, temporal association cortex. Scale bars: schematic 1 mm; ***A***,***B*** 200 µm; ***C***,***D*** 25 µm. Orientation marker in schematic applies to all panels.

These findings confirm a direct projection from my two candidate areas to primary fields of the mouse auditory cortex. In both cases I observed sparse, labelled fibres in supragranular and infragranular layers, consistent with a descending or feedback projection from infragranular layers of both S1 and V2M (see discussion in section 1.6 and Felleman and Van Essen, 1991). By comparison with a more dominant connection sent by each of the two areas (to S2 and V2L respectively) these projections were very sparse, but consistent with published anterograde tracing data from V2 in the mouse (Banks et al., 2011) as well as retrograde labelling of both S1 and V2 reported in the Mongolian gerbil (Budinger et al., 2006) and my own retrograde tracing experiments (section 5.2). Inspection of data from an online database of mouse brain connectivity, also produced from AAV injections, similarly reveals sparse, descending projections to A1 from S1 and medial V2 ('projection' dataset in connectivity atlas by Allen Institute for Brain Science, 2012, www.connectivity.brain-map.org/projection).

5.4 Optogenetic activation of candidate areas

Pilot experiments *in vitro* and *in vivo*

With the aim of characterising the synaptic effect of these projections on cells in the auditory cortex, I conducted pilot experiments using acute slices *in vitro*. Published data, particularly from Karel Svoboda's laboratory, has shown that 'channelrhodopsin-2 assisted circuit mapping' or CRACM is useful for identifying the cells targeted by long-range cortical connections (Petreanu et al., 2007) as well as the spatial distribution of such synaptic inputs (Petreanu et al., 2009; Kätzel et al., 2011). In my hands, stimulating ChR2-expressing fibres from V2M during whole-cell recordings in auditory cortex yielded only

small numbers of responsive cells: in slices from 28 mice, I recorded excitatory currents in 3 out of 49 successful recordings (1/19 in supragranular layers, 2/30 in infragranular; data not shown). Since testing cell-by-cell for ECC inputs in this way was relatively inefficient, I proceeded to look for a neurophysiological effect of V2 and S1 on the auditory cortex *in vivo*, using optogenetic stimulation alongside extracellular recordings of auditory responses.

In a further set of pilot experiments not reported here, I stimulated V2M or S1 in transgenic mice expressing ChR2 under the Thy1 promoter, which drives expression in layer 5 throughout the cortex (Arenkiel et al., 2007). I recorded spiking responses in auditory cortex to photostimulation of both V2M and S1, but the widespread expression of ChR2 made it challenging to interpret these results. It is difficult to determine the degree to which the delivered light scatters within the brain and so when expression of ChR2 is widespread, long-range effects may arise from the driven activity of cells within the area targeted by the LED, or of cells nearby that area (within the range of light scatter), or even via antidromic activation of fibres passing through or near it. This severely curtails the specificity that optogenetics has the power to offer.

Consequently I designed experiments in which ChR2 expression was generated specifically within my candidate areas, by virus injection. The injections are described in section 2.5.1 and were also used for anterograde examination of projections from the injected areas, described in section 5.3.1 above.

5.4.1 Expression and activity of ChR2 *in vivo*

Following viral delivery of the ChR2-mCherry gene to either S1 or V2M, I confirmed that photostimulation of the injected area produced strong, local spiking responses. For most such tests I used a single-shank multielectrode, in order to minimise physical damage to the cortex; figure 5.10 however shows an example in which I used an 8-shank, 64-channel probe. Here it is apparent that light-driven spiking activity was spatially restricted to an area that matches the region of ChR2-mCherry expression observed in subsequent examination of fixed brain sections (figure 5.10A).

For simplicity, the figures and text below often refer simply to 'S1-' or 'V2 stimulation'. This refers to optogenetic activation of the trunk and hindlimb areas of S1 or of medial V2 (V2M) respectively; in each case, LED-driven spikes in those candidate areas were confirmed electrophysiologically and local expression of ChR2-mCherry was confirmed with subsequent histology and microscopy.

5.4.2 Bandwidth and threshold measurements

Next I tested whether simple tone and noise responses in primary auditory cortex were affected by such artificial stimulation of V2M or S1. In experiments where a neonatal lesion produced ectopic visual inputs to the ferret auditory thalamus, Mao and Pallas (2012) reported increased thresholds and bandwidths in pure-tone responses of the auditory cortex. My optogenetic tools do not generate aberrant connectivity, but since I am directly driving cells in S1 or V2M with a 25 or 50 ms LED pulse, the activity I produce in these areas and their projections may well involve larger, more sustained bursts of spikes than sensory stimulation. I hypothesised that such artificial activation of other sensory

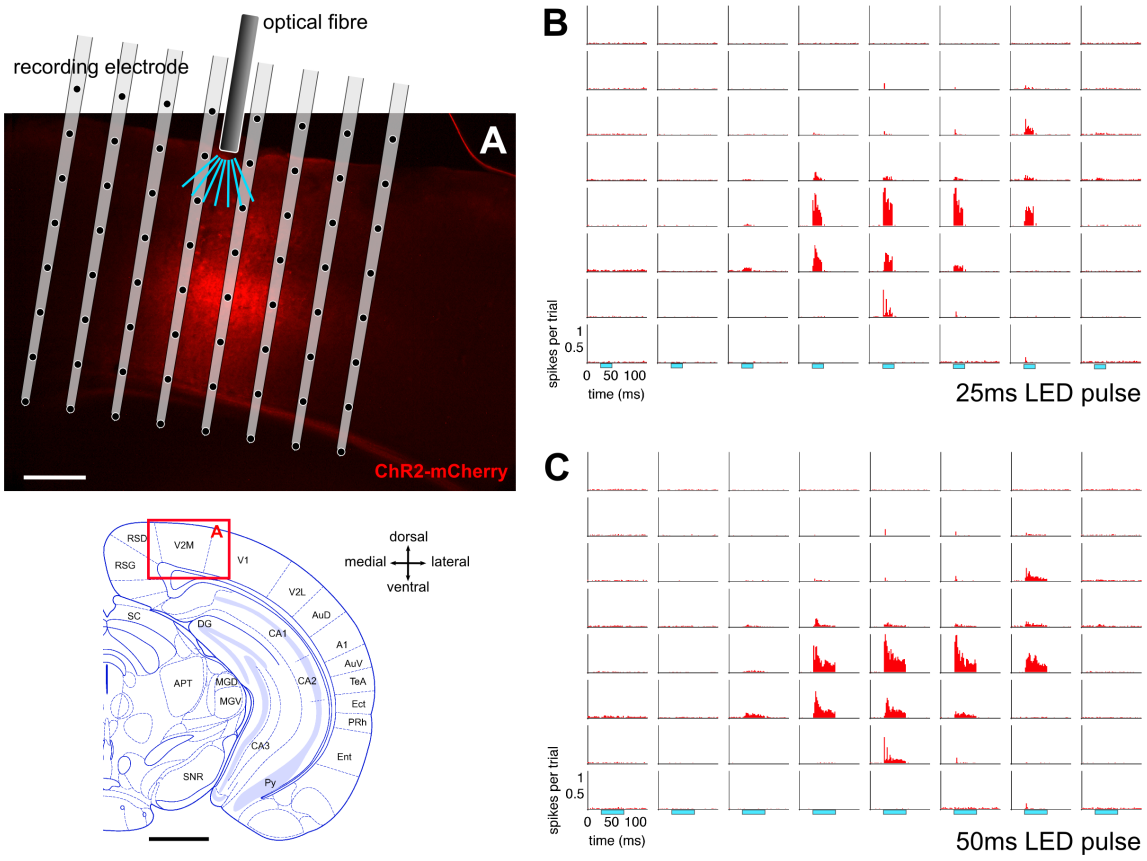


Figure 5.10: **Light-driven spiking activity at site of virus injection.** ***A***: Illustration of light stimulation and positioning of the 64-channel multielectrode used to make the recordings in ***B*** and ***C***. I used a fibreoptic cable to deliver light from a blue LED to the injected area. Photograph shows ChR2-mCherry expression in V2M, the cortical area where these recordings were made, though the section pictured is from a different mouse with an equivalent injection into V2M. Scale bar 200 µm, which was also the site and shank spacing of the recording probe. ***B***, ***C***: Peri-stimulus time histograms (PSTHs; 2 ms bins) from the grid of 64 channels, arranged as indicated in ***A***, during 25 ms or 50 ms LED stimulation respectively. Note that strong spiking responses were generated for the duration of the delivered LED pulse (indicated by blue bars in bottom row) and that these responses were localised to the area showing ChR2-mCherry expression.

cortices might elicit similar changes in threshold and bandwidth to ectopic, surgically induced visual inputs. Such an effect may not reflect the normal, physiological interaction between auditory and visual or somatosensory activity, but would indicate the presence of a network connecting these areas to A1 and AAF that is capable of influencing auditory processing.

To explore changes in pure-tone response properties, I measured responses to a grid of 25 frequencies and 8 sound levels as described in chapter 3, using 64-channel multi-electrodes to record from sites across the auditory cortex of 9 mice. A 100 ms pure tone at each frequency-level combination was presented at least 3 times alone and, in randomly interleaved trials, at least 3 times in conjunction with a 50 ms LED pulse to stimulate either S1 or V2M. Subfields of auditory cortex were determined using the best frequency (BF) maps obtained from middle layers (see figure 3.8) and I focussed my analysis on those within primary areas A1 and AAF.

Figure 5.11 illustrates how I calculated the threshold from a site's frequency response area (FRA) as well as its bandwidth at 8 and 24 dB above threshold, BW8 and BW24. In order to collect these values for as many sites as possible, and to have those values reflect the breadth of each site's tone-driven responses, I used a bandwidth measurement that spanned any instances of multiple tuning peaks, such as in figure 5.11B. This analysis required the use of smoothed FRAs (see method in section 2.3.4 and discussion in section 3.2.2) and was performed on all 518 sites in primary areas whose raw responses showed significant frequency sensitivity (see section 2.3.4 for criterion). Of these, 135 sites came from 5 mice with ChR2 expression in S1, and 383 from 4 mice with expression in V2M.

As discussed in chapter 3, I observed considerable variability in pure-tone responses such as these; furthermore, presenting 400 stimulus combinations limits the number of

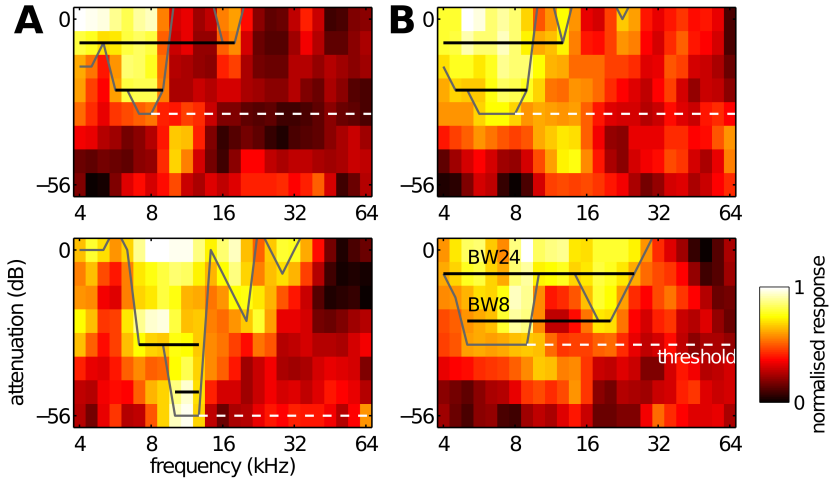


Figure 5.11: **Calculating bandwidth and threshold from pure-tone responses.** ***A***: Frequency response areas (FRAs) from two sites, both located in superficial layers of A1, smoothed using a 3x3 sliding window (see section 2.3.4). ***B***: FRAs from the same sites, recorded in response to co-presentation of a 50 ms LED pulse over S1, commencing at the same time as the 100 ms tone pips. Tone-only and tone+LED trials across the 200 frequency-level combinations were randomly interleaved. Shown in grey on each plot is the boundary of the responsive area, determined using a threshold of the site's mean spontaneous spike-rate + 20% of its peak rate; the minimum sound level encompassed by this boundary is the site's threshold (dashed white line). I took the span of this boundary at 8 and 24 dB (1 and 3 grid steps) above that threshold as 2 measures of each site's bandwidth (BW8 and BW24, solid black lines); this could include multiple peaks if the tuning pattern is complex, such as in the bottom right panel. The case illustrated in the upper panels shows no change in threshold and smaller changes in BW8 and BW24, while in the lower example all three measures are increased by S1 activation.

repeats that is feasible (I presented each stimulus at least 3 times — typically 4 or 5 — with and without photostimulation, but a higher number may have reduced that variability). Consequently, these individual FRA parameters measured with and without the LED pulse were rarely identical. In order to test for significant changes caused by the light activation, I grouped these measurements together, first across all sites in primary areas and then by superficial, middle and deep layers within A1 and AAF. For each group of thresholds or bandwidths, and for S1 and V2M stimulation, I compared the **distribution** of values obtained with and without the LED pulse (using a Kruskal-Wallis test). Then, where possible, I tested the values pairwise to see if each group's **mean difference** in threshold or bandwidth was significant (paired-sample t-test). These results are presented in figures 5.12 – 5.15.

5.4.3 S1 stimulation increases tone response thresholds in A1

As shown in figure 5.12, neither S1 nor V2M stimulation significantly affected the population of threshold values obtained from all primary sites, nor any of the sub-groups divided between supragranular, granular and infragranular layers of A1 and AAF (Kruskal-Wallis test). This was the result using a cut-off for significance of $p = 0.05$ and it is worth noting that p values were smallest in the case of S1 stimulation, both for supragranular sites in A1 (figure 5.12B, top left) and for the pooled data across layers and subfields (figure 5.12A, left).

When I separately evaluated the change in threshold at each site, produced by either S1 or V2M stimulation, the largest effect was again an increase in threshold with S1 stimulation at supragranular sites in A1 (figure 5.13). Indeed, S1 stimulation produced a significant increase in both the group of 25 supragranular A1 sites and the pool of all pri-

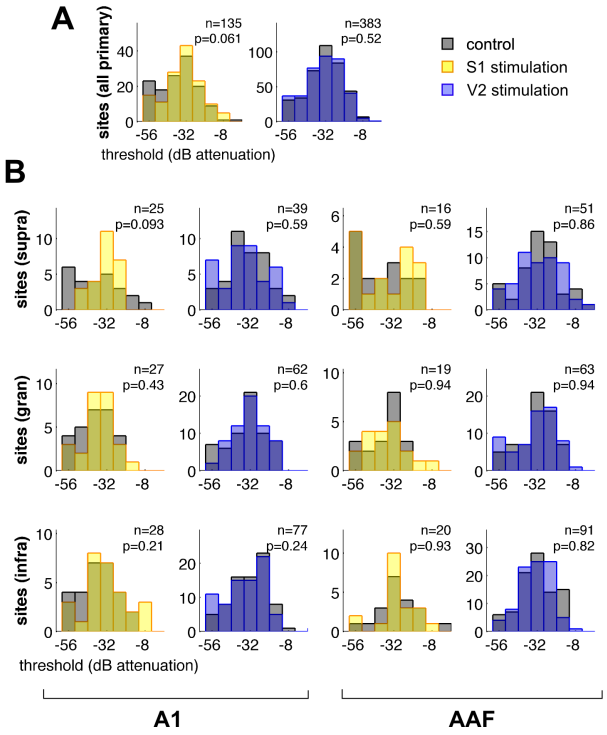


Figure 5.12: **Distribution of response thresholds, with and without S1 and V2 stimulation.** ***A***: Histograms of the pure-tone response thresholds (see figure 5.11) obtained from sites across primary auditory areas A1 and AAF, in mice with ChR2 expression in S1 (left) or V2M (right). Thresholds obtained with concurrent LED stimulation are plotted in colour (see legend) and those from tones alone in grey. ***B***: The same data, plotted in the same way but separated into groups of sites within supragranular, granular and infragranular layers of A1 and AAF. The number of sites contributing to each plot, n, is indicated as well as the probability p that the two plotted sets of thresholds share the same distribution (Kruskal-Wallis test). Using a cut-off of $p = 0.05$, neither S1 nor V2M stimulation significantly altered the thresholds of any of these populations of sites.

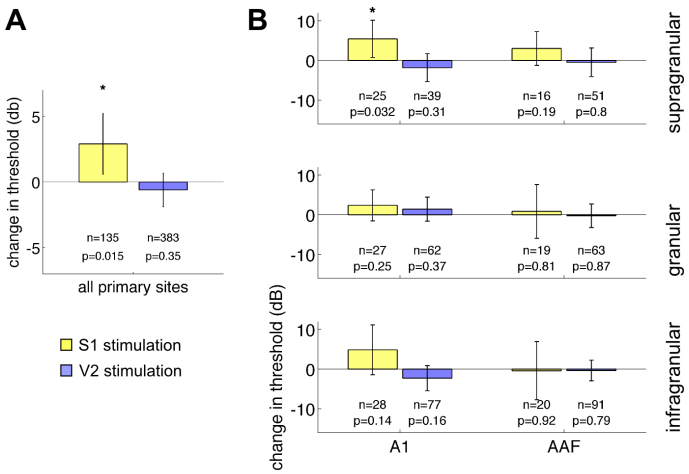


Figure 5.13: **Changes in threshold observed with S1 and V2 stimulation.** The mean difference in pure-tone response threshold observed with S1 and V2 stimulation, in all tuned sites across A1 and AAF (***A***) and separated into supragranular, granular and infragranular sites within those two subfields (***B***). As in figure 5.12, the number of sites n is given for each plot, as well as the probability p that the mean difference is significant (paired-sample t-test). Error bars denote 95% confidence intervals of each mean and asterisks highlight cases where $p < 0.05$.

mary sites (paired-sample T-test, $p = 0.032$ and 0.015 respectively). This mean change, while significant, is relatively small: +5.4 dB (±0.031 SEM) for all primary sites and +2.9 dB (±0.015 SEM) for supragranular sites in A1, which in both cases is less than one 8 dB sound level step in my stimulus grid. Now that I have identified a possible effect of S1 stimulation on A1 response thresholds, further experiments using a higher-resolution stimulus grid and a larger number of stimulus repeats will be the best way to confirm and clarify this observation.

5.4.4 S1 and V2 stimulation increase bandwidth of tone responses, in different layers and subfields

Exploring the bandwidth of each site's tone responses from the same data set, further small changes become apparent. Figure 5.14 shows the distribution of bandwidths mea-

sured at 8 and 24 dB above threshold (BW8, BW24), from sites pooled across A1 and AAF (5.14A, C) or separated into subfields and layers (5.14B, D). None of the sets of bandwidths show significant differences with S1 or V2 stimulation. The number of sites for which bandwidths could be calculated (n on each plot) is sometimes smaller than the number of threshold measurements (compare figure 5.12) because a bandwidth, particularly at 24 dB above threshold, could not be calculated for every FRA (e.g. if responses were only present at high sound levels).

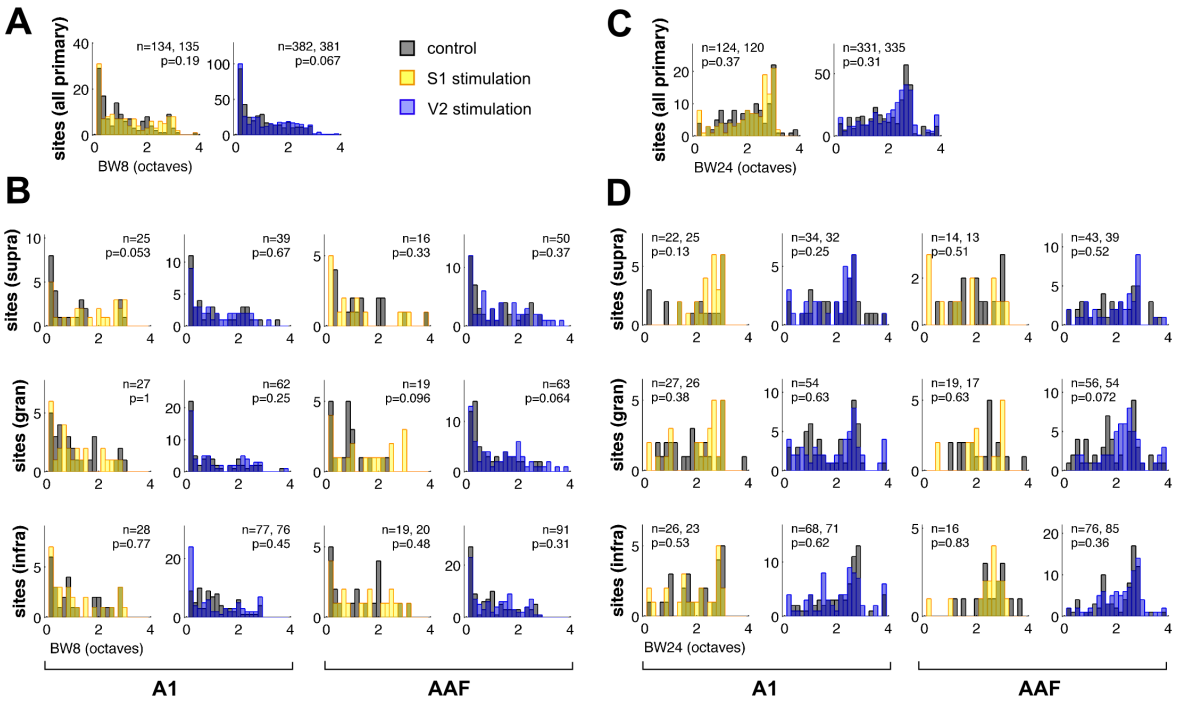


Figure 5.14: **Distribution of tuning bandwidths, with and without S1 and V2 stimulation.** Histograms showing the distribution of bandwidths at 8 dB (BW8, ***A***-***B***) and 24 dB (BW24, ***C***-***D***) above threshold. As in figure 5.12, these measurements are shown for sites pooled across primary sites A1 and AAF (***A***, ***C***) and also separated into layer and subfield groups (***B***, ***D***). The number of sites contributing to each plot, n, is indicated. Since BW8 and/or BW24 could not be calculated for every FRA (e.g. if responses were only present at high sound levels), in some cases different numbers of measurements appear for the control and S1 or V2 stimulation conditions: both numbers are given and the first n is the control sample size. Each panel also gives the probability p that the two plotted sets of bandwidths share the same distribution (Kruskal-Wallis test; no differences at 95% confidence, or $p < 0.05$).

As was the case for the threshold breakdown above, however, pairwise analysis of each

site's FRAs in control and S1- or V2M-stimulated conditions revealed significant bandwidth changes in several cases (figure 5.15). V2M stimulation elicited a significant increase in the mean BW8 and BW24 across pooled primary-area sites (figure 5.15 A and B, left panel; $p < 0.05$, paired-sample t-test); when I separated bandwidths by layer and subfield, it was S1 stimulation for supragranular sites in A1, and V2M stimulation for granular sites in AAF, which yielded significant increases (again in both BW8 and BW24: same figure, right panel).

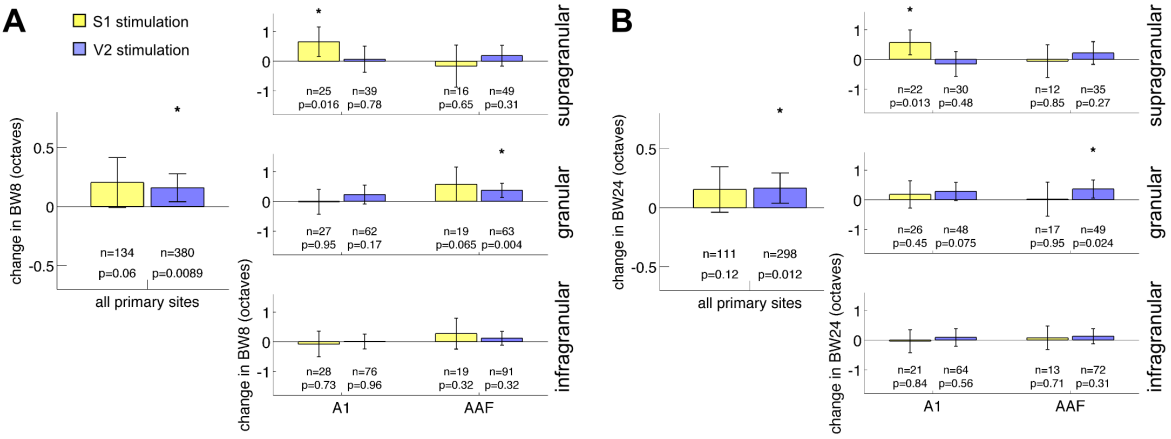


Figure 5.15: **Changes in bandwidth observed with S1 and V2 stimulation.** Similar to the treatment of response thresholds in figure 5.13, these bar graphs show the mean change in BW8 (***A***) and BW24 (***B***) observed with S1 and V2M stimulation (yellow and blue bars, respectively). This includes mean changes for all tuned sites across A1 and AAF (left-hand panels in ***A*** and ***B***) and for sites separated into layer groups within those two subfields (right-hand panels in ***A*** and ***B***). Once again, the number of sites n is given for each plot, as well as the probability p that the mean difference is significant (paired-sample t-test). Error bars denote 95% confidence intervals of each mean and asterisks highlight cases where $p < 0.05$.

Among the significant mean changes in bandwidth, values range from +0.17 octaves (the mean change in BW24 across all primary sites, with V2M stimulation; ±0.065 SEM) to +0.65 octaves (for the supragranular sites within A1, with S1 stimulation; ±0.25 SEM). These amount to a change in the width of a site's tuning curve of some ~1–4 columns within the stimulus grid, which used 25 frequencies at 1/6-octave spacing. In the case

of the effect of S1 stimulation on supragranular sites in A1, this represents quite a large broadening of tuning, particularly considering that the mean BW8 seen in A1 was 1.1 octaves (or ~6 columns in the stimulus grid).

It is also interesting to note that based on these data, S1 and V2M stimulation affect different layers within A1 and AAF. In order to identify these trends and determine their significance, I have grouped single observations from each site into layers and subfields. To investigate which **individual** sites are significantly affected, many repeats of a single stimulus are required. Below I explore the effect of artificial S1 and V2M stimulation on spike counts and latencies at individual sites, during repeated presentation of 5 ms noise bursts.

5.4.5 S1 and V2 stimulation produce small shifts in magnitude and latency of noise responses

During each electrode penetration, as well as presenting the grid of pure tones discussed above, I recorded at least 50 sweeps of responses to 5 ms bursts of broadband noise. These were also in the presence and absence of optogenetic stimulation of S1 or V2M (see section 2.2.4) and were interleaved with presentations of just the LED pulse over S1 or V2M, in silence. These LED-only trials never elicited significant spiking responses in primary auditory areas (data not shown) and at the majority of sites, a 25 ms LED pulse co-terminating with the noise burst also had no significant effect on the noise-driven spike counts or latencies. At a minority of sites, however, two-tailed t-tests of spike counts and first-spike latencies from noise *vs.* noise+LED trials did reveal significant, relatively small shifts (summarised in table 5.1; examples in figures 5.16, 5.17).

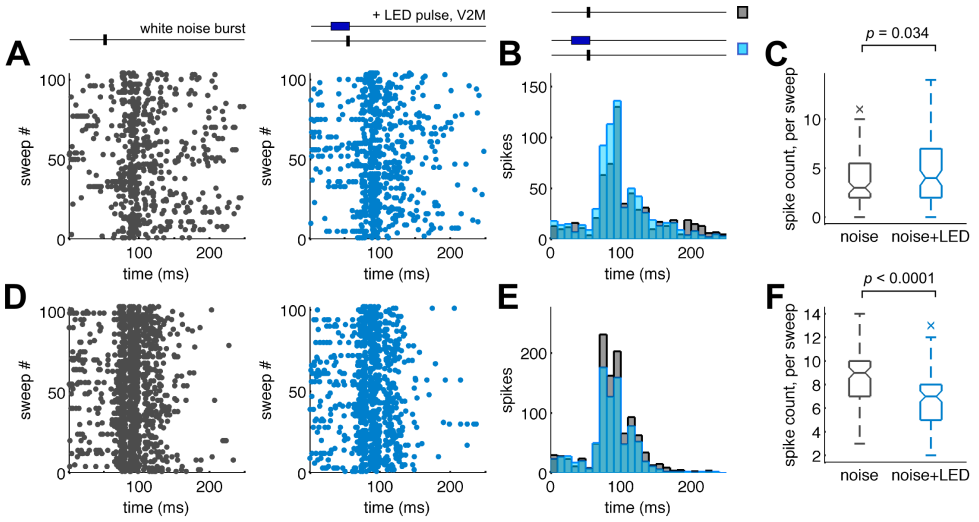


Figure 5.16: **Examples of noise-driven spike counts affected by optogenetic activation of V2.** ***A***,***D***: Trial-by-trial spike rasters from two sites where the response to a 5 ms noise burst was significantly increased or decreased, respectively, by activation of V2. Control sweeps (noise only) are shown on the left in grey; sweeps on the right included a co-terminating 25 ms LED pulse over V2M (see figure 5.10. As can be seen here and in the PSTHs in ***B***, ***E*** (10 ms bins), the effect of activating another sensory area was relatively small. I compared the spike counts from sweeps with and without LED stimulation, within a 75 ms post-stimulus window, using a two-tailed t-test; box-and-whisker plots in ***C*** and ***F*** compare the per-trial spike counts. Typically (as in these cases) the difference was 1–2 spikes per trial or less; decreases in spike count (as in ***D***–***F***) were much more common than increases (see table 5.1). Box plot legend: boxes, interquartile range; horizontal line, median; notches, 95% confidence intervals; whiskers, further extent of data up to 1.5× interquartile range, outliers marked with x. ***A***–***C*** $n = 103$ sweeps; ***D***–***F*** $n = 105$ sweeps.

Figure 5.16 shows recordings from two illustrative sites, one in AAF (A–C) and the other in A1 (D–F), which show increased and decreased spiking responses to noise, respectively, in the presence of V2M stimulation. The change in each case is no more than 2 spikes per trial (mean per-trial spike count was 4.67 in AAF, ±0.17 SEM, and 3.55 ±0.17 in A1) and it is worth noting that among all the affected sites, decreases were more common than increases (see table 5.1).

Similarly, figure 5.17 shows an example of an increase and decrease in mean first-spike latency at two more sites, again one in A1 (A–C) and one in AAF (D–F). The A1 site exhibits increased latency with V2 stimulation (+2.8 ms on mean latency of 18.7 ms) and the AAF site a decrease (–3.5 ms on mean latency 23.0 ms) — however, increased latencies were by far the more common effect (see table 5.1).

Overall, at those sites where I detected an effect, both S1 and V2 stimulation tended to produce smaller spiking responses with longer latencies, though effects in both directions were observed (see breakdown in table 5.1 and overview in figure 5.18 B, D). Interestingly, the effects of V2M were distributed across superficial, middle and deep layers; the numbers of sites affected by S1 stimulation are much smaller, but again there are examples across the three depth categories (see table 5.1). Supragranular sites in A1, however, where the most significant changes in pure-tone responses were seen (see sections 5.4.3, 5.4.4), exhibited no S1-driven changes in this case.

As illustrated in figure 5.18, a greater proportion of sites showed significant changes with V2M stimulation than S1 (compare panels A, C). These diagrams also indicate that these affected sites were not a single sub-population showing changes in both magnitude **and** first-spike latency of their noise responses, either for S1 or V2M stimulation. However, there is some overlap in the case of V2M (some 21 sites showed changes in both la-

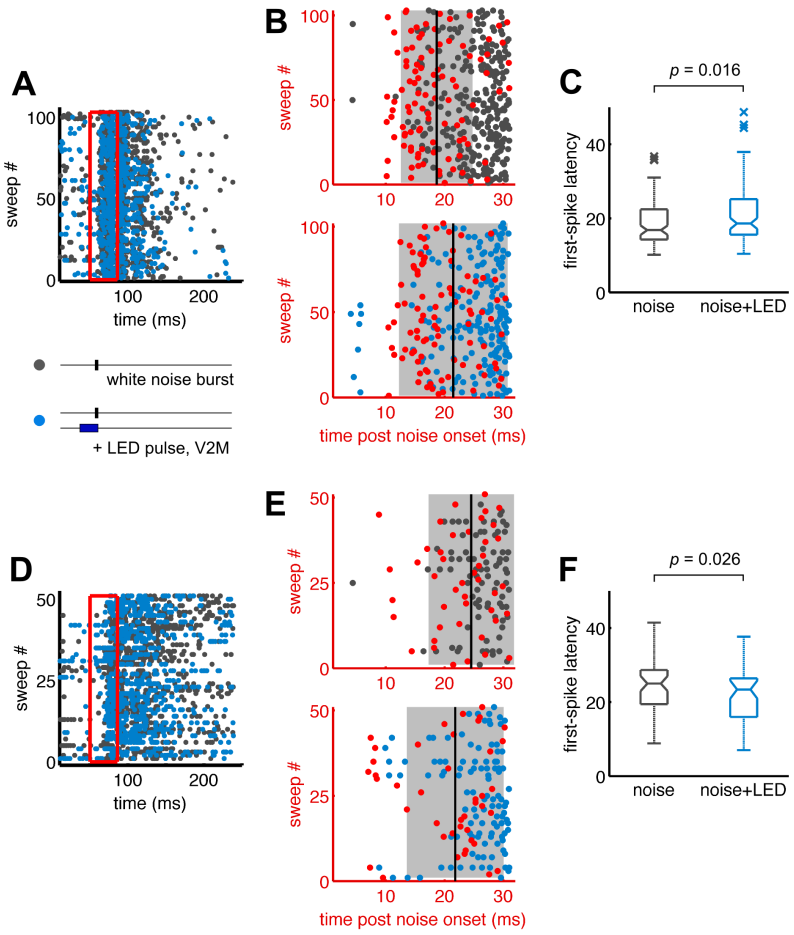


Figure 5.17: **Examples of noise-driven spike latencies affected by optogenetic activation of V2.** As in figure 5.16, responses from two example sites are shown, in this case where first-spike latency of noise responses was increased (***A***–***C***) or decreased (***D***–***F***) by V2 activation. ***A*** and ***D*** show superimposed spike rasters from sweeps with (blue) and without (grey) an LED pulse over V2M. Red boxes highlight the time window expanded in ***B*** and ***E***, which show the first 30 ms post noise onset, with LED off/on trials plotted separately in the upper and lower panels, respectively. First post-onset spike in each sweep is coloured red, with mean latency indicated by black line and standard deviation by grey shading; note that spikes occurring less than 5 ms post-onset were considered outliers and unlikely to be stimulus-related. First-spike latency varies from trial to trial (position of red data points), but in these examples there were nonetheless significant differences between LED on and off conditions, as indicated by box-and-whisker plots in ***C*** and ***F*** (p value for two-tailed t-test). Box plot properties are as in figure 5.16; see table 5.1 for summary of latency changes. ***A***–***C*** $n = 103$ sweeps; ***D***–***F*** $n = 51$ sweeps.

Stimulation	**Recording**	n	n **response up/down [mean change, spikes]**	n **latency up/down [mean change, ms]**
S1	A1	53	0/2 [- /−0.43]	3/1 [+6.3/−7.1]
	A1 (supra)	18	0/0	0/0
	A1 (gran)	13	0/1 [- /−0.55]	0/1 [- /−7.1]
	A1 (infra)	22	0/1 [- /−0.30]	3/0 [+6.3/ -]
	AAF	67	0/3 [- /−0.44]	3/0 [+6.6/ -]
	AAF (supra)	22	0/2 [- /−0.44]	0/0
	AAF (gran)	16	0/1 [- /−0.42]	1/0 [+5.1/ -]
	AAF (infra)	29	0/0	2/0 [+7.4/ -]
V2M	A1	121	5/23 [+1.8/−1.1]	9/3 [+4.7/−8.6]
	A1 (supra)	36	2/5 [+1.3/−1.0]	2/0 [+5.4/ -]
	A1 (gran)	41	2/7 [+2.2/−1.4]	3/3 [+361/−8.6]
	A1 (infra)	44	1/11 [+2.0/−0.89]	4/0 [+5.5/ -]
	AAF	193	7/36 [+1.5/−1.6]	13/4 [+5.6/−3.7]
	AAF (supra)	54	1/10 [+1.0/−1.6]	3/0 [+4.4/ -]
	AAF (gran)	67	3/9 [+1.5/−1.3]	3/2 [+5.8/−3.9]
	AAF (infra)	72	3/17 [+1.7/−1.8]	7/2 [+6.0/−3.6]

Table 5.1: **Summary of sites where spiking responses to noise bursts were affected by S1 and V2M stimulation.** The number of recorded sites in each group is indicated, along with the number showing significantly increased or decreased spiking responses, and the number showing significantly increased or decreased first-spike latency (determined by two-tailed t-test, $p < .05$, on spike counts or first post-stimulus spike times, respectively). The mean increase and/or decrease in spike count or latency is indicated in square brackets. Mean spike count in the control case was 3.55 across A1 (±0.17 SEM) and 4.67 across AAF (±0.17 SEM); mean first-spike latency was 29.9 ms across A1 (±0.57 SEM) and 25.1 ms across AAF (±0.48 SEM).

tency and spike count) and the effects may well be related, since both are consistent with inputs from other sensory cortices (direct or indirect; see discussion below) partially suppressing the noise-driven spiking of auditory cortical neurons, presumably via inhibitory interneurons.

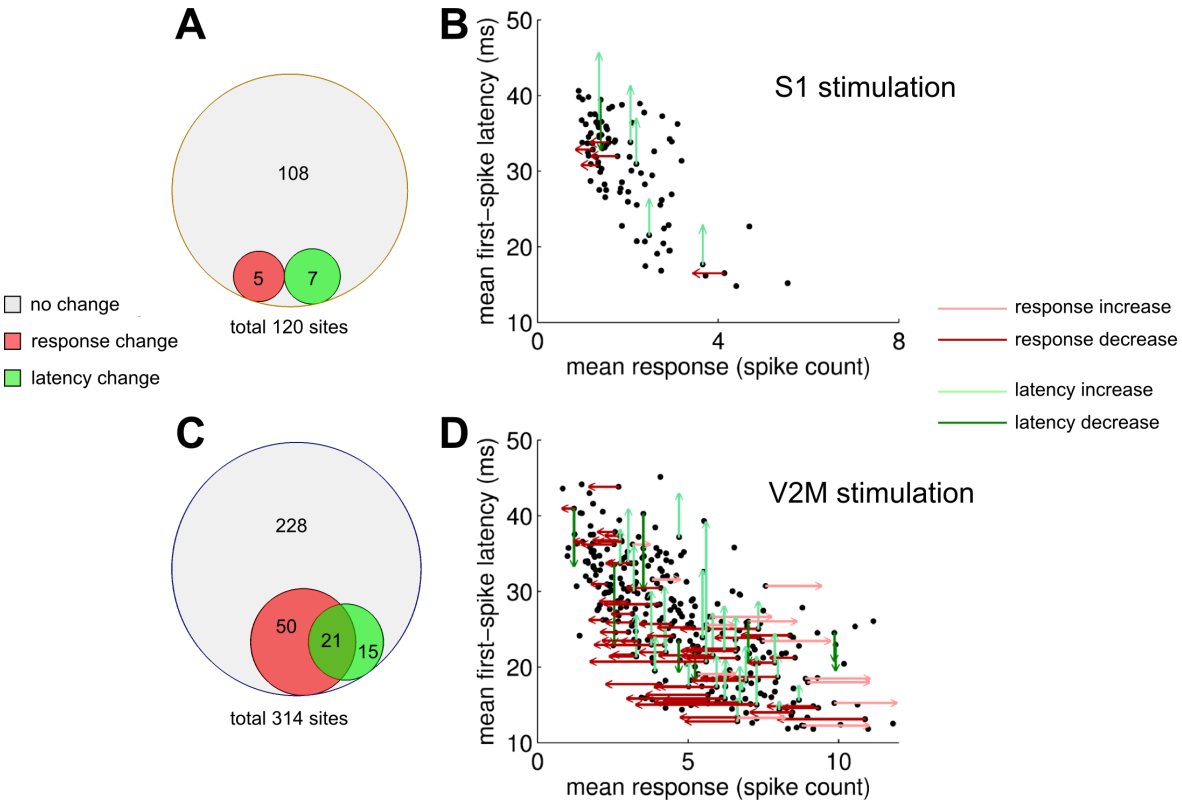


Figure 5.18: **Graphical summary of response and latency changes.** Venn diagrams illustrating the sub-population of sites within primary areas whose noise responses are affected by (***A***) S1 stimulation, or (***C***) V2M stimulation. Large circles represent the pool of analysed sites across primary areas A1 and AAF; red and green circles (as indicated) the groups of sites with altered magnitude and latency of spiking responses, respectively. Plotted in ***B*** and ***D*** are all the mean values of spike count and first-spike latency from primary sites, in cases where S1 (***B***) or V2M (***D***) was stimulated artificially. For sites where a significant change in either measurement was observed, the mean change has been appended to the data point according to the colour scheme shown on the right: thinner lines and darker colours for decreases and paler, thicker lines for increases. Note that most spike count changes are decreases and most latency changes are increases.

5.5 Discussion

5.5.1 Overview of results

The results presented in this chapter support the presence of sparse, direct inputs to mouse primary auditory cortex from other early sensory areas and also demonstrate that artificial activation of those areas can exert an effect on auditory cortical responses.

I have found anatomical evidence for a population of projecting cells spread across primary and secondary, visual and somatosensory areas (figures 5.1–5.5), predominantly in infragranular layers (see figure 5.7). This is consistent with reports in other species, including a thorough catalogue of inputs to gerbil A1 which found a similar distribution of cells in other sensory areas (Budinger et al., 2006). In particular, I identified long-range projections from V2M and S1 as candidates for further investigation (section 5.2.5).

Virus injections into these candidate areas allowed me to confirm the presence of fluorescent axons in supra- and infragranular layers of primary auditory areas, though these were notably sparse in comparison to more dominant projections (see figures 5.8, 5.9). Nonetheless, driving activity in these areas, using optogenetics, elicited small but significant changes in spiking responses to pure tones and noise bursts in primary auditory areas (section 5.4).

5.5.2 Relating anatomy and activity

The experiments I report here cannot distinguish whether the effect of S1 and V2 stimulation on auditory responses is mediated by the direct connections my anatomical data have confirmed. Alternatives include a cortical relay, for example via S2 or V2L, both of

which are adjacent to auditory cortex and send connections to it (see figure 5.1), or a cortico-thalamo-cortical circuit of the sort advocated by Sherman (e.g. 2012, 2007), or a combination of these possibilities.

To implicate cortico-cortical connectivity directly would require an intervention such as severing cortical axons in between the relevant areas. This approach allowed Iurilli et al. (2012) to confirm that sound-driven inhibitory currents in V1 required intact connections from the auditory cortex. Such additional manipulations were not part of my experimental design but probably represent one of the next logical steps.

These effects do indicate, nonetheless, that multisensory effects in mouse auditory cortex, if present, may well be mediated by other early sensory cortices. Certainly, circuitry exists by which these areas are capable of influencing the spiking activity of cells in the auditory cortex. One strategy to confirm their physiological role would be to identify, for example, a visual effect on auditory cortical cells and test whether it is abolished or reduced by silencing inputs from V1 and/or V2, once again using optogenetic methods.

Whether activating or silencing networks, optogenetics is a powerful tool for teasing apart neuronal circuitry in this way. One of its particular strengths is in applying circuit-level manipulations to awake animals, especially during behavioural tasks. An attractive future direction of the work I have outlined above would be to silence cortical areas of interest in behaving rodents, especially if relevant multisensory behavioural paradigms are available, such as the audiovisual detection benefits recently reported by Gleiss and Kayser (2012).

5.5.3 Why weaker and less specific?

The effects observed in my optogenetic experiments show, in the main, a pattern of weakening and broadening auditory responses. Firstly, the only significant effects I detected on grouped, pure-tone responses were increases in bandwidth and threshold (sections 5.4.3, 5.4.4). Secondly, as summarised in figure 5.18, of the changes to noise responses, most shifts in spike count were decreases while most shifts in latency were increases. Although there was only partial overlap between sites showing latency and spike count changes (figure 5.18 A, B), it is unsurprising that these effects are coupled. Even in the scatter plots in the same figure, it is apparent that first-spike latency and spike count are negatively correlated; it seems likely that supra-physiological co-activation of visual or somatosensory cortex shifts auditory responses along this axis towards fewer spikes, commencing later.

Furthermore, a trend toward suppression rather than enhancement of sound-driven spikes by cross-modal inputs is consistent with reports that cross-talk between sensory cortices can be detected as inhibitory synaptic currents (Iurilli et al., 2012). It also fits with the idea that such cross-talk can manifest as synchronisation of ongoing oscillatory activity (Lakatos et al., 2007, 2008).

Physiologically, it may seem counter-intuitive for somatosensory or visual stimuli to suppress simultaneous auditory responses, but my data do not imply that this is always the case. In fact, they do not demonstrate that such sensory interactions take place, since instead of presenting stimuli in these modalities I have driven a sustained burst of spikes in a large population of excitatory cells in S1 or V2M (see figure 5.10). Thus, the effects I have observed in a subset of locations in auditory cortex may reflect the balance of available connectivity between these areas, which would not normally show such coor-

dinated, sustained activity but which makes use of inhibitory interneurons to fine-tune or synchronise sensory processing between modalities.

5.5.4 Concluding remarks

In summary, these data confirm the existence of sparse ECC inputs to mouse A1 and AAF and highlight S1 and V2M as areas of interest in the study of multisensory activity in the mouse auditory cortex. Both my anatomical and optogenetic data represent valuable preliminary explorations, which suggest avenues for further research.

The discussion of ECC projection anatomy could be usefully extended by more detailed anterograde tracing of V2 and S1 axons. Meanwhile, the functional interplay between early sensory cortices may be elucidated in more detail by repeating my optogenetic experiments in conjunction with severing of intervening white-matter axons; future experiments of this type would also benefit from a negative-control, optogenetic activation of a non-projecting area.

A more exciting but more challenging strategy, as mentioned above, requires the identification of multisensory interactions in mouse A1 and/or AAF; these are an expected phenomenon, but not currently well described. Iurilli et al. (2012), in a prelimary figure, reported hyperpolarisations in mouse A1 driven by whisker stimulation, while Kobayasi et al. (2013) recently recorded surprisingly widespread effects of visual stimulation in gerbil A1 (light flashes affected tone responses in 25% of units). Assuming that such multisensory activity can be demonstrated in the mouse auditory cortex, optogenetic silencing of different areas and connections within the cortex will be invaluable in ascertaining its neuroanatomical substrate.

Chapter 6

General Discussion and Conclusions

6.1 Summary of findings

The aims of this thesis, broadly, were fourfold: (1) to evaluate the tonotopic organisation of the primary auditory cortex in the mouse, under various conditions; (2) to compare the responses and connectivity of primary subfields A1 and AAF; (3) to catalogue cortico-cortical inputs to those fields from other early sensory areas; and (4) to test the influence of candidate projecting areas on auditory cortical responses. My key findings are:

1. In most, but not all, cases, I observed mirrored tonotopic gradients in the middle layers of A1 and AAF. However, the proportion of responsive sites displaying significant sensitivity to the frequency of pure tones was only 71% in granular layers, and significantly lower (54%) in supragranular layers. I also showed that of the sites displaying frequency sensitivity, those in granular layers showed stronger preference for their best frequencies than both supragranular and infragranular sites.

2. Compared to middle (granular) layers, I found that the tonotopic organisation seen across supragranular and infragranular sites often varied in both orientation and strength of correlation.

3. Best frequencies derived from LFPs were only weakly correlated with those from multi-unit spike data, but the direction of their tonotopic gradients tended to be similar. Furthermore, the tonotopic correlations in the LFP data were slightly, but not significantly, higher than those I observed from multi-unit activity.

4. Presenting dynamic random chords rather than pure tones produced an altered distribution of BFs, along with some shifts in the direction of tonotopic gradients, and both increases and decreases in the strength of tonotopic correlations.

5. I have shown that different temporal windows within the pure-tone responses from a single multi-unit recording can show a variety of tuning properties, including inverted FRAs during post-activation suppression; altered tuning in late responses (~200-350 ms post stimulus onset); and shifting or expanding tuning in different temporal windows within the initial spiking response. This variability means that the choice of response window can dramatically affect the calculation of a given site's BF.

6. Response latencies, consistent with published data, are significantly shorter in AAF than in A1; furthermore, this difference is present across granular, supra- and infragranular layers. Noise-driven spike counts were also higher in AAF, particularly in deep layers. By contrast, I found that other response characteristics — namely, the strength of pure-tone frequency preferences, tuning bandwidths and response thresholds — were similar between A1 and AAF.

7. My observations within a small anatomical data set, based on a single pair of retrograde tracer injections, suggest that A1 and AAF receive input from populations of projecting cells in the ventral MGB which share a single tonotopic axis.

8. I have described sparse, direct, cortico-cortical inputs from other early sensory areas to both A1 and AAF, notably V2M and S1. The majority of cells contributing these ECC inputs were located in infragranular layers, suggestive of a 'feedback'-type connection pattern.

9. Using optogenetic methods, I have shown that activating either V2M or S1 during concurrent presentation of pure tones and noise bursts can affect auditory responses in A1 and AAF. These effects included increases in threshold and bandwidth of pure-tone responses, while responses to noise bursts showed predominantly decreased spike counts and increased latencies.

Below, I discuss some of the broader implications and limitations of these findings, along with the possibilities they suggest for future research.

6.2 Auditory maps

The systematic variation of response properties across physical dimensions within the brain is appealing to investigators, because it allows us to draw maps and make predictions. Such maps, including the well-known cortical echoes of sensory epithelia (somatotopy, retinotopy and cochleo- or tonototopy), also appear to offer advantages in terms of efficient processing of environmental signals (Diamond et al., 2003). In the auditory cortex, however, the cochlear representation is often inconsistent, particularly in awake

animals (Evans and Whitfield, 1964), and largely absent in non-primary fields (for review, see Schreiner and Winer, 2007). How important, then, is tonotopy to the cortex?

6.2.1 A property of inputs and outputs?

Consider another example of topography within the auditory system: the highly conserved map of sound-source location in the deep layers of the superior colliculus (SC). This map interacts closely with an equivalent representation of visual space in superficial layers (e.g. Jay and Sparks, 1984; King et al., 1998). Visual deprivation has been shown to cause abnormal development of the auditory map in the SC, to varying degrees (Withington-Wray et al., 1990; King and Carlile, 1993) — and yet such deprivation does not impair behavioural sound localisation, in some cases even enhancing it (King and Parsons, 1999). Indeed, some studies have found that performance in sound localisation tasks is impaired by lesions (Nodal et al., 2010) or inactivation (Nodal et al., 2012) of the auditory cortex, where no topographic spatial representations have been detected. If a precise auditory space map is not essential for spatial hearing, then perhaps its presence in the SC is largely for the purpose of interfacing with the corresponding visual and somatosensory maps. Auditory spatial information, computed from non-topographic cues, may be 'translated' into this arrangement in order to facilitate cross-modal computations, such as enhancing spatial tuning (for reviews, see King, 2004, 2009).

Similarly, tonotopic maps might be a developmental consequence of the manner in which information is relayed between different brain regions. The observation that gradients of frequency tuning tend to be less consistent outside thalamorecipient layers (Winkowski and Kanold, 2013; section 3.4.2 above) suggests that tonotopy is inherited by primary areas from their thalamic inputs, but perhaps of limited use in subsequent cortical process-

ing. Nonetheless, responses in both supra- and infragranular layers are tonotopic, to a degree (accounts vary as to the precision and reliability of that organisation: compare, for example, Guo et al., 2012; Winkowski and Kanold, 2013, and figure 3.10 above). Deeper layers of mouse A1 and AAF send 'driver'-type corticofugal projections to the dorsal MGB, which is not tonotopic (Anderson and Linden, 2011), but also 'modulator' projections back to the ventral division (Llano and Sherman, 2008); the need to relay information back into that tonotopic framework might explain the continued evidence of tonotopy in deep layers. The degree of topography maintained in corticofugal projections has not been fully explored in the mouse, but Budinger et al. (2013) showed that gerbil A1 sends both tonotopic and non-tonotopic connections to subcortical structures, and this distinction largely correlates with the tonotopic organisation (or otherwise) of the recipient nuclei. Thus, the variable tonotopy reported above may reflect an organising principle that is more useful for the mapping of extra-cortical connections than for cortical processing itself.

6.2.2 Who cares about sound frequency anyway?

As discussed in section 3.4.1 above, anecdotal and some published evidence suggests that classical V-shaped frequency tuning curves are comparatively scarce in the mouse cortex. Not many studies have assessed the degree to which cortical neurons in mice discriminate pure tones, and the proportion of neurons across cortical space that do so. It is broad surveys such as mine, at the large scale, and thorough mapping of entire, local neuronal populations, at the small scale (Bandyopadhyay et al., 2010; Rothschild et al., 2010, 2013; Winkowski and Kanold, 2013) which are best able to quantify tuning in this way.

My report that some 38% of all noise-responsive sites showed no significant frequency

preference — and a higher proportion in supra- and infragranular layers, alongside a drop in the strength of those preferences — is broadly consistent with the few published data on this question (see section 3.3.1). It also helps to explain why delineating tonotopic gradients can be problematic in the mouse (e.g. Seybold et al., 2012) without very dense sampling of thalamorecipient layers (Hackett et al., 2011; Guo et al., 2012).

6.2.3 Context and timing are crucial

Among those sites which were frequency-sensitive, I found that their tuning — certainly their best frequencies — in response to a more complex stimulus (DRCs) was often different from that recorded for pure tones. This comparison between the tuning properties revealed by different types of stimuli has rarely been made and warrants further exploration.

Linden et al. (2003) also presented both DRCs and pure tones to mice, and recorded STRFs and FRAs from A1 and AAF. They found tuning to be broadly similar, although the larger bandwidths they reported for STRFs within A1 were not replicated in the bandwidth of conventional FRAs from the same sites. Ongoing work in this laboratory suggests that changing the rate at which DRCs are presented (e.g. 25, 50 or 100 ms chords) elicits qualitative differences in the resulting STRFs (J. Cooke and B. Willmore, personal communication). A larger data set comparing pure-tone and DRC tuning, within which temporal parameters such as this are deliberately varied, would help to confirm whether dynamic and tonal stimuli reproducibly elicit different tuning in the mouse auditory cortex. It is worth noting that STRFs in particular can be highly plastic: Fritz et al. (2003), in A1 recordings from behaving ferrets, reported that STRF tuning was modulated by the task being performed. As such, every effort should be made in anaesthetised recordings

to ensure that the animal's physiological state is as constant as possible when comparing responses to different types of stimuli.

Temporal variations in pure-tone tuning within the responses to a single sound presentation, such as I report above, are also not widely reported in the literature (with some exceptions: see Kaur et al., 2004; Moshitch et al., 2006; Seybold et al., 2012; Rajan et al., 2013). Interestingly, among the various time-dependent response properties I observed (see section 3.7 above), I never detected obvious onset–offset (or on–off) responses. In the auditory cortex of awake cats, Qin et al. (2007) reported a variety of tuning properties among responses to tone-offset, which were not always consistent with onset tuning. They argue that such activity usually goes unreported because of the anaesthetics used in the majority of auditory neurophysiology experiments. The fact that I did not see offset responses may indeed result from altered cortical activity under anaesthesia, or a species difference between cats and rodents, or both.

While there is variation in specific results, all these data suggest that response timing and the context and complexity of presented stimuli are important factors in the investigation of how the cortex encodes frequency and potentially other information.

6.2.4 Tonotopy is a fragile and untidy guide

Among the data presented in chapter 3 above, I observed much variability in the tonotopic gradients between different recording locations (cortical subfields and layers) and between experimental conditions. Even when relatively well-organised gradients are present, such as in the left-hand case in figure 3.10, visual inspection of the data might suggest a radial pattern rather than two distinct, mirrored axes. Certainly, brute categorisation of

the rostrocaudal axis as 'tonotopic' and dorsoventral as 'isofrequency' (such as used by Oviedo et al., 2010) is probably too simplistic.

If we consider the connections received by mouse A1 and AAF, particularly the fact that thalamocortical projections are highly topographic (Hackett et al., 2011) and that intracortical connectivity appears, at least in acute slices, to amplify those inputs in a linear fashion (Li et al., 2013), we might expect at least the middle layers to exhibit obvious and straightforward tonotopic maps. As discussed at length above however, recordings *in vivo* rarely reflect such clean organisation — and furthermore, recent research has demonstrated plasticity at thalamocortical synapses, including in the adult brain (Chun et al., 2013; Petrus et al., 2014). The observation that plasticity is widespread, even at the level of inputs to auditory cortex, may help to explain some of the variability that is common in the study of cortical maps.

In summary, I would argue that because of the relative fragility of cortical frequency maps, care should be taken not to overstate their importance. Such over-emphasis may lead physiologists to disregard data which is 'messy' and does not conform to expected patterns. Even smoothing of data may mask real variability in responses. As discussed in section 3.2.2, I have used unsmoothed data wherever possible in this thesis (e.g. throughout chapter 3; on the other hand, bandwidth and threshold calculations, such as in sections 4.3.2 and 5.4.2, made use of smoothed FRAs). This may be overly cautious; as demonstrated by recent work in this laboratory (Honey and Schnupp, in prep), it is possible to determine mathematically an optimal degree of smoothing, which takes into account the amount of trial-to-trial variability in responses to specific stimuli.

The outstanding question of tonotopy's relevance to sensory processing will be best addressed by experiments that unpick the networks involved, such as the dissection of

layer 4 inputs by Li et al. (2013) (a paradigm which the optogenetic toolkit has made increasingly feasible *in vivo*), and which differentiate the activity of sub-populations of neurons within each layer (e.g. Sun et al., 2013; Moore and Wehr, 2013).

6.2.5 A1 and AAF: similar but different

What is the significance of the pair of mirrored primary fields seen in the auditory cortex of mice and several other mammals? In the data I present above (see chapter 4), a number of comparisons revealed no significant differences between A1 and AAF; shorter response latencies in AAF remain the most striking difference between the two.

This observation has been replicated in other species (though not universally; see discussion in section 4.5.1) and in my case, the trend was evident across the depth of the cortex. Whether or not the distinction between A1 and AAF is clear-cut, these data are consistent with the suggestion (Linden et al., 2003) that the rostral portion of primary auditory cortex is specialised for faster temporal processing — for example, the preferred rate of temporal stimulus modulation is faster for neurons in cat AAF than A1 (Schreiner and Urbas, 1988), while Linden et al. (2003) reported that STRFs from mouse AAF were of shorter duration than those from A1.

Although some studies have begun to intervene in auditory processing by A1 and AAF in an effort to distinguish their functional importance (Carrasco and Lomber, 2009; Carrasco et al., 2013), these have not specifically explored temporal processing. Again, the availability of optogenetic strategies for silencing specific areas and inputs may prove fruitful for further defining roles for these subfields, including in awake and behaving animals.

6.3 Non-auditory inputs

In chapter 5, I outlined the spread of early, cortico-cortical, cross-modal (ECC) connections targeting A1 and AAF, including a previously reported input from V2 (Banks et al., 2011) and distributed projections from other sensory areas, notably non-barrel S1 (see sections 5.2.5, 5.3.1). Based on the laminar distribution of retrogradely labelled cells, these projections are largely of the feedback type, within the Van Essen hierarchical classification scheme (Felleman and Van Essen, 1991, and see section 1.6). Whether they are driver or modulator projections (also discussed in section 1.6) remains to be elucidated; modulator-type inputs are perhaps more likely, since the proponents of that classification system (Lee and Sherman, 2010) argue that cortico-cortical connections tend to be modulatory, while driver-type pathways originating in A1 or AAF are relayed by the thalamus (e.g. Lee and Sherman, 2008).

Physiological multisensory responses are yet to be described in the primary auditory cortex of the mouse, although they have been reported in other mammals, including rodents (e.g. rats and gerbils, respectively: Wallace et al., 2004; Kobayasi et al., 2013) and other species (e.g. ferrets: Bizley et al., 2007). As discussed in section 1.5 above, there are several pathways which might underpin such activity, including feedback from higher-order cortices, cross-talk between early sensory cortices, or crossover from non-auditory thalamic nuclei. My optogenetic data, which demonstrate that activation of S1 or V2 can influence responses in both A1 and AAF, suggest that of these possibilities, either cortico-cortical or cortico-thalamo-cortical inputs are strong candidates.

Arguably a more powerful application of optogenetics than artificial stimulation, such as reported here, is in **silencing** specific areas and networks within the awake, behav-

ing brain. Assuming that the 'non-physiological' influences detected by my experiments indeed reflect a role for early cortical cross-talk in multisensory processing within auditory cortex, a promising next step would be to silence S1 or V2 during a behavioural task with measurable cross-modal demands, such as the forced-choice, audiovisual detection paradigm described by Gleiss and Kayser (2012). Using viral gene delivery of, for example, an archaerhodopsin (Chow et al., 2010), to the candidate projecting area followed by LED silencing within the auditory cortex, it would even be possible to specifically silence direct, cortico-cortical inputs from S1 or V2.

6.3.1 Functional relevance of ECC connections

Although their presence has been demonstrated anatomically in a number of species, a specific function for ECC inputs to the primary auditory cortex, or any other sensory area, is yet to be conclusively identified.

Work in ferrets has suggested a possible role for visual-auditory cortical connections in enhancing spatial processing (Bizley and King, 2008). Those authors, in this laboratory, measured the spatial sensitivity of visual, auditory and bisensory units within the various fields of ferret auditory cortex. Interestingly, they found the greatest representation of spatial information within the anterior dorsal field — the area previously shown (Bizley et al., 2007) to receive inputs from a more 'spatial' field within extrastriate visual cortex (area SSY, thought to be the ferret homologue of primate area MT: Philipp et al., 2006). Liang et al. (2013) also recently proposed a spatial processing role for multisensory activity in primary cortical areas, when they used multivariate fMRI analysis to show that, among other comparisons, human A1 responses could be used to distinguish between visual and somatosensory stimuli in different locations.

When Lakatos et al. (2007) described the resetting of neuronal oscillations in primate A1 by somatosensory stimulation, they suggested that the resulting amplification of simultaneous auditory signals might play a role in somatosensory heightening of auditory perception, as described in psychophysical studies (e.g. Schürmann et al., 2004). Subsequently, Fiebelkorn et al. (2011) argued for a similar phase-reset in the human visual cortex, based on the periodicity they detected in the auditory enhancement of a visual detection task, while Mercier et al. (2013) used subdural EEG to directly record an auditory influence on visual cortical oscillations.

Other experiments in non-human primates have reported both enhancement and suppression of responses in core and belt areas, by audio-visual presentation of vocalisations compared to auditory presentation alone (e.g. Ghazanfar et al., 2005; Kayser et al., 2010). While the study of face–voice processing is difficult to adapt to rodent neurophsyiology, relevant non-auditory cues — in this case from the olfactory system — have been shown to influence responses to vocalisations in mouse A1, particularly responses to pup calls in lactating mothers (Cohen et al., 2011).

None of these experiments, however, have been able to determine the connectivity that mediates such cross-modal effects. In their study of face–voice integration in macaques, Ghazanfar et al. (2008) infer a role for direct cross-talk between auditory cortex and the superior temporal sulcus (STS, an association area) based on simultaneous recordings in both areas. Lakatos et al. (2007), meanwhile, note that the predominantly supragranular profile of their somatosensory-driven A1 activity, alongside its short latency, is suggestive of feedforward inputs from non-specific thalamic nuclei (e.g. magnocellular nucleus of the MGB: Molinari et al., 1995). It is worth noting that my own experiments, using direct, artificial S1 stimulation, also produced a mainly supragranular

effect (figures 5.13, 5.15) and although I am similarly unable to confirm the connectivity responsible, either cortico-thalamo-cortical or direct, cortico-cortical projections appear to be the most likely candidates. Technical difficulties (see section 2.5.3) also meant that I was unable to perform current source density analyses, and so cannot determine whether phase resetting was occurring in my experiments; the decreased responses and increased latencies I recorded, however (see table 5.1), are suggestive of inhibitory interactions, which would be consistent with the only other *in vivo* study of ECC connections in the mouse (Iurilli et al., 2012, see also section 5.5.3).

An intriguing recent observation, with a sample size of one, was made by Ro et al. (2013). In a study which described direct connections between normal human A1 and ipsilateral S1 and S2 using diffusion tensor imaging-based tractography, they also reported that the S2–A1 link was more pronounced in a patient with a somatosensory thalamic lesion and consequent auditory-tactile synaesthesia. Others have argued that abnormal cross-modal activity in the cortex, such as that which follows sensory impairment, is likely to arise neither from novel cortical inputs, nor from a strengthening of latent ones, but rather from a reorganisation of subcortical connectivity, such as within the brainstem (Meredith and Allman, 2012). Nonetheless the account of Ro et al. (2013), at the very least, offers a conversational talking point for researchers who study cortical, cross-modal neuroanatomy in rodents but whose friends and family, upon mention of the topic, inevitably and understandably enquire about its functional relevance to synaesthesia.

6.4 In conclusion

I have used high channel-count extracellular recordings and anatomical tracing to provide data that contribute to our understanding of cortical organisation in the mouse. In particular, I have shown that frequency tuning and its organisation into tonotopic maps, while usually evident in thalamorecipient layers, varies with several factors, including cortical depth and the presentation of dynamic *vs.* simple stimuli. In comparing the two primary subfields A1 and AAF, the most significant difference I observed was in response latency, which is shorter in superficial, middle and deep layers of AAF. Based on my anatomical data, these fields also receive overlapping thalamic inputs in the mouse. Finally, cross-modal inputs from other early sensory areas target both A1 and AAF, and activation of either S1 or V2 is able to influence the threshold, bandwidth and latency of auditory cortical responses. Further experiments are required to determine whether cortico-cortical connections mediate these effects and to discern their behavioural relevance.

Bibliography

Abeles M, Goldstein MH (1970) Functional architecture in cat primary auditory cortex: columnar organization and organization according to depth. *J Neurophysiol* 33:172–187.

Adesnik H, Bruns W, Taniguchi H, Huang ZJ, Scanziani M (2012) A neural circuit for spatial summation in visual cortex. *Nature* 490:226–231.

Ahrens MB, Linden JF, Sahani M (2008) Nonlinearities and contextual influences in auditory cortical responses modeled with multilinear spectrotemporal methods. *J Neurosci* 28:1929–1942.

Allen Institute for Brain Science (2012) Allen Mouse Brain Connectivity Atlas: www.connectivity.brain-map.org.

Andersen RA, Knight PL, Merzenich MM (1980) The thalamocortical and corticothalamic conections of AI, AII, and the anteriior auditory field (AFF) in the cat: Evidence for two largely sergregarted systems of connections. *J Comp Neurol* 194:663–701.

Anderson LA, Christianson GB, Linden JF (2009) Mouse auditory cortex differs from visual and somatosensory cortices in the laminar distribution of cytochrome oxidase and acetylcholinesterase. *Brain Res* 1252:130–142.

Anderson LA, Linden JF (2011) Physiological differences between histologically defined subdivisions in the mouse auditory thalamus. *Hear Res* 274:48–60.

Arenkiel BR, Peca J, Davison IG, Feliciano C, Deisseroth K, Augustine GJ, Ehlers MD, Feng G (2007) In vivo light-induced activation of neural circuitry in transgenic mice expressing channelrhodopsin-2. *Neuron* 54:205–218.

Bandyopadhyay S, Shamma SA, Kanold PO (2010) Dichotomy of functional organization in the mouse auditory cortex. *Nat Neurosci* 13:361–368.

Banks MI, Uhlrich DJ, Smith PH, Krause BM, Manning KA (2011) Descending projections from extrastriate visual cortex modulate responses of cells in primary auditory cortex. *Cereb Cortex* 21:2620–2638.

Bendor D, Osmanski MS, Wang X (2012) Dual-pitch processing mechanisms in primate auditory cortex. *J Neurosci* 32:16149–16161.

Binzegger T, Douglas RJ, Martin KAC (2004) A quantitative map of the circuit of cat primary visual cortex. *J Neurosci* 24:8441–8453.

Bizley JK, King AJ (2008) Visual-auditory spatial processing in auditory cortical neurons. *Brain Res* 1242:24–36.

Bizley JK, King AJ (2009) Visual influences on ferret auditory cortex. *Hear Res* 258:55–63.

Bizley JK, Nodal FR, Bajo VM, Nelken I, King AJ (2007) Physiological and anatomical evidence for multisensory interactions in auditory cortex. *Cereb Cortex* 17:2172–2189.

Bizley JK, Nodal FR, Nelken I, King AJ (2005) Functional organization of ferret auditory cortex. *Cereb Cortex* 15:1637–1653.

Bizley JK, Walker KMM (2009) Distributed sensitivity to conspecific vocalizations and implications for the auditory dual stream hypothesis. *J Neurosci* 29:3011–3013.

Bizley JK, Walker KMM (2010) Sensitivity and selectivity of neurons in auditory cortex to the pitch, timbre, and location of sounds. *The Neuroscientist : a review journal bringing neurobiology, neurology and psychiatry* 16:453–469.

Bizley JK, Walker KMM, Silverman BW, King AJ, Schnupp JWH (2009) Interdependent encoding of pitch, timbre, and spatial location in auditory cortex. *J Neurosci* 29:2064–2075.

Brosch M, Schreiner C (1997) Time course of forward masking tuning curves in cat primary auditory cortex. *J Neurophysiol* 77:923–943.

Budinger E, Heil P, Hess A, Scheich H (2006) Multisensory processing via early cortical stages: Connections of the primary auditory cortical field with other sensory systems. *Neuroscience* 143:1065–1083.

Budinger E, Heil P, Scheich H (2000) Functional organization of auditory cortex in the Mongolian gerbil (Meriones unguiculatus). III. Anatomical subdivisions and corticocortical connections. *Eur J Neurosci* 12:2425–2451.

Budinger E, Brosch M, Scheich H, Mylius J (2013) The subcortical auditory structures in the Mongolian gerbil: II. Frequency-related topography of the connections with cortical field AI. *J Comp Neurol* 521:2772–2797.

Budinger E, Heil P, Scheich H (2000) Functional organization of auditory cortex in the Mongolian gerbil (Meriones unguiculatus). IV. Connections with anatomically characterized subcortical structures. *Eur J Neurosci* 12:2452–2474.

Budinger E, Scheich H (2009) Anatomical connections suitable for the direct processing of neuronal information of different modalities via the rodent primary auditory cortex. *Hear Res* 258:16–27.

Burger C, Gorbatyuk OS, Velardo MJ, Peden CS, Williams P, Zolotukhin S, Reier PJ, Mandel RJ, Muzyczka N (2004) Recombinant AAV viral vectors pseudotyped with viral capsids from serotypes 1, 2, and 5 display differential efficiency and cell tropism after delivery to different regions of the central nervous system. *Molecular Therapy* 10:302–317.

Calvert GA, Bullmore ET, Brammer MJ, Campbell R, Williams SC, McGuire PK, Woodruff PW, Iversen SD, David AS (1997) Activation of auditory cortex during silent lipreading. *Science* 276:593–596.

Campbell RAA, Schulz AL, King AJ, Schnupp JWH (2010) Brief sounds evoke prolonged responses in anesthetized ferret auditory cortex. *J Neurophysiol* 103:2783–2793.

Campi KL, Bales KL, Grunewald R, Krubitzer L (2010) Connections of auditory and visual cortex in the prairie vole (Microtus ochrogaster): evidence for multisensory processing in primary sensory areas. *Cereb Cortex* 20:89–108.

Campi KL, Karlen SJ, Bales KL, Krubitzer L (2007) Organization of sensory neocortex in prairie voles (Microtus ochrogaster). *J Comp Neurol* 502:414–426.

Cansino S, Williamson SJ, Karron D (1994) Tonotopic organization of human auditory association cortex. *Brain Res* 663:38–50.

Cappe C, Rouiller EM, Barone P (2009) Multisensory anatomical pathways. *Hear Res* 258:28–36.

Cappe C, Barone P (2005) Heteromodal connections supporting multisensory integration at low levels of cortical processing in the monkey. *Eur J Neurosci* 22:2886–2902.

Carrasco A, Kok MA, Lomber SG (2013) Effects of Core Auditory Cortex Deactivation on Neuronal Response to Simple and Complex Acoustic Signals in the Contralateral Anterior Auditory Field. *Cereb Cortex* .

Carrasco A, Lomber SG (2009) Differential modulatory influences between primary auditory cortex and the anterior auditory field. *J Neurosci* 29:8350–8362.

Carrasco MM, Trujillo M, Razak K (2013) Development of response selectivity in the mouse auditory cortex. *Hear Res* 296:107–120.

Charbonneau V, Laramee ME, Boucher V, Bronchti G, Boire D (2012) Cortical and subcortical projections to primary visual cortex in anophthalmic, enucleated and sighted mice. *J Comp Neurol* 36:2949–2963.

Chechik G, Nelken I (2012) Auditory abstraction from spectro-temporal features to coding auditory entities. *Proceedings of the National Academy of Sciences* 109:18968–18973.

Chen JL, Carta S, Soldado-Magraner J, Schneider BL, Helmchen F (2013) Behaviour-dependent recruitment of long-range projection neurons in somatosensory cortex. *Nature* 499:336–340.

Chow BY, Han X, Dobry AS, Qian X, Chuong AS, Li M, Henninger MA, Belfort GM, Lin Y, Monahan PE, Boyden ES (2010) High-performance genetically targetable optical neural silencing by light-driven proton pumps. *Nature* 463:98–102.

Christianson GB, Sahani M, Linden JF (2011) Depth-dependent temporal response properties in core auditory cortex. *J Neurosci* 31:12837–12848.

Chun S, Bayazitov IT, Blundon JA, Zakharenko SS (2013) Thalamocortical long-term potentiation becomes gated after the early critical period in the auditory cortex. *J Neurosci* 33:7345–7357.

Cohen L, Rothschild G, Mizrahi A (2011) Multisensory Integration of Natural Odors and Sounds in the Auditory Cortex. *Neuron* 72:357–369.

Covic EN, Sherman SM (2011) Synaptic Properties of Connections between the Primary and Secondary Auditory Cortices in Mice. *Cereb Cortex* 21:2425–2441.

Cuppini C, Ursino M, Magosso E, Rowland BA, Stein BE (2010) An emergent model of multisensory integration in superior colliculus neurons. *Front Integr Neurosci* 4:6.

Dahl CD, Logothetis NK, Kayser C (2009) Spatial Organization of Multisensory Responses in Temporal Association Cortex. *J Neurosci* 29:11924–11932.

deCharms RC, Blake DT, Merzenich MM (1998) Optimizing sound features for cortical neurons. *Science* 280:1439–1443.

Diamond ME, Petersen RS, Harris JA (1999) Learning through maps: Functional significance of topographic organization in primary sensory cortex. *J. Neurobiol.* 41:64–68.

Diamond ME, Petersen RS, Harris JA, Panzeri S (2003) Investigations into the organization of information in sensory cortex. *Journal of Physiology-Paris* 97:529–536.

Douglas RJ, Martin KAC (2007) Mapping the matrix: the ways of neocortex. *Neuron* 56:226–238.

Downman CB, Woolsey CN, Lende RA (1960) Auditory areas I, II, and Ep: cochlear representation, afferent paths and interconnections. *Bull Johns Hopkins Hosp* 106:127–142.

Eggermont JJ (1998) Representation of spectral and temporal sound features in three cortical fields of the cat. Similarities outweigh differences. *J Neurophysiol* 80:2743–2764.

Ehret Gn, Haack B (1982) Ultrasound recognition in house mice: Key-Stimulus configuration and recognition mechanism. *J. Comp. Physiol.* 148:245–251.

Evans EF, Whitfield IC (1964) Classification of unit responses in the auditory cortex of the unanaesthetized and unrestrained cat. *J Physiol (Lond)* 171:476–493.

Falchier A, Schroeder CE, Hackett TA, Lakatos P, Nascimento-Silva S, Ulbert I, Karmos G, Smiley JF (2010) Projection from visual areas V2 and prostriata to caudal auditory cortex in the monkey. *Cereb Cortex* 20:1529–1538.

Felleman DJ, Van Essen DC (1991) Distributed hierarchical processing in the primate cerebral cortex. *Cereb Cortex* 1:1–47.

Fiebelkorn IC, Foxe JJ, Butler JS, Mercier MR, Snyder AC, Molholm S (2011) Ready, set, reset: stimulus-locked periodicity in behavioral performance demonstrates the consequences of cross-sensory phase reset. *J Neurosci* 31:9971–9981.

Fox K, Glazewski S, Schulze S (2000) Plasticity and stability of somatosensory maps in thalamus and cortex. *Curr Opin Neurobiol* 10:494–497.

Fritz J, Shamma S, Elhilali M, Klein D (2003) Rapid task-related plasticity of spectrotemporal receptive fields in primary auditory cortex. *Nat Neurosci* 6:1216–1223.

Fu KMG, Johnston TA, Shah AS, Arnold L, Smiley J, Hackett TA, Garraghty PE, Schroeder CE (2003) Auditory cortical neurons respond to somatosensory stimulation. *J Neurosci* 23:7510–7515.

Gaese BH, Ostwald J (2001) Anesthesia changes frequency tuning of neurons in the rat primary auditory cortex. *J Neurophysiol* 86:1062–1066.

Geissler DB, Ehret G (2004) Auditory perception vs. recognition: representation of complex communication sounds in the mouse auditory cortical fields. *Eur J Neurosci* 19:1027–1040.

Ghazanfar AA, Chandrasekaran C, Logothetis NK (2008) Interactions between the Superior Temporal Sulcus and Auditory Cortex Mediate Dynamic Face/Voice Integration in Rhesus Monkeys. *J Neurosci* 28:4457–4469.

Ghazanfar AA, Maier JX, Hoffman KL, Logothetis NK (2005) Multisensory integration of dynamic faces and voices in rhesus monkey auditory cortex. *J Neurosci* 25:5004–5012.

Ghazanfar AA, Schroeder CE (2006) Is neocortex essentially multisensory? *Trends Cogn Sci (Regul Ed)* 10:278–285.

Gilbert CD, Wiesel TN (1989) Columnar specificity of intrinsic horizontal and corticocortical connections in cat visual cortex. *J. Neurosci.* 9:2432–2442.

Gleiss S, Kayser C (2012) Audio-visual detection benefits in the rat. *PLoS ONE* 7:e45677.

Guinan JJ, Norris BE, Guinan SS (1972) Single auditory units in the superior olivary complex: II: locations of unit categories and tonotopic organization. *International Journal of Neuroscience* 4:147–166.

Guo W, Chambers AR, Darrow KN, Hancock KE, Shinn-Cunningham BG, Polley DB (2012) Robustness of cortical topography across fields, laminae, anesthetic states, and neurophysiological signal types. *J Neurosci* 32:9159–9172.

Hackett T, Barkat T, O'Brien B, Hensch TK, Polley DB (2011) Linking topography to tonotopy in the mouse auditory thalamocortical circuit. *J. Neurosci.* 31:2983–2995.

Hackett TA (2008) Anatomical organization of the auditory cortex. *J Am Acad Audiol* 19:774–779.

Hashikawa T, Molinari M, Rausell E, Jones EG (1995) Patchy and laminar terminations of medial geniculate axons in monkey auditory cortex. *J Comp Neurol* 362:195–208.

Hellweg FC, Koch R, Vollrath M (1977) Representation of the cochlea in the neocortex of guinea pigs. *Exp Brain Res* 29:467–474.

Henry KR, Chole RA (1980) Genotypic differences in behavioral, physiological and anatomical expressions of age-related hearing loss in the laboratory mouse. *Audiology* 19:369–383.

Hind JE (1953) An electrophysiological determination of tonotopic organization in auditory cortex of cat. *J Neurophysiol* 16:475–489.

Hofstetter KM, Ehret G (1992) The auditory cortex of the mouse: connections of the ultrasonic field. *J Comp Neurol* 323:370–386.

Horie M, Tsukano H, Hishida R, Takebayashi H, Shibuki K (2013) Dual compartments of the ventral division of the medial geniculate body projecting to the core region of the auditory cortex in C57BL/6 mice. *Neuroscience research* .

Horikawa J, Ito S, Hosokawa Y, Homma T, Murata K (1988) Tonotopic representation in the rat auditory cortex. *Proceedings of the Japan Academy. Ser. B: Physical and Biological Sciences* 64:260–263.

Hromádka T, Zador AM, DeWeese MR (2013) Up states are rare in awake auditory cortex. *J Neurophysiol* 109:1989–1995.

Humphries C, Liebenthal E, Binder JR (2010) Tonotopic organization of human auditory cortex. *NeuroImage* 50:1202–1211.

Hunter KP, Willott JF (1987) Aging and the auditory brainstem response in mice with severe or minimal presbycusis. *Hear Res* 30:207–218.

Imaizumi K, Priebe NJ, Crum PAC, Bedenbaugh PH, Cheung SW, Schreiner CE (2004) Modular functional organization of cat anterior auditory field. *J Neurophysiol* 92:444–457.

Imig TJ, Adrián HO (1977) Binaural columns in the primary field (A1) of cat auditory cortex. *Brain Res* 138:241–257.

Iurilli G, Ghezzi D, Olcese U, Lassi G, Nazzaro C, Tonini R, Tucci V, Benfenati F, Medini P (2012) Sound-Driven Synaptic Inhibition in Primary Visual Cortex. *Neuron* 73:814–828.

Jay MF, Sparks DL (1984) Auditory receptive fields in primate superior colliculus shift with changes in eye position. *Nature* 309:345–347.

Kaas JH, Hackett TA (1998) Subdivisions of AuditoryCortex and Levels of Processing in Primates. *Audiol Neurootol* 3:73–85.

Kajikawa Y, Schroeder CE (2011) How local is the local field potential? *Neuron* 72:847–858.

Kätzel D, Zemelman BV, Buetfering C, Wölfel M, Miesenböck G (2011) The columnar and laminar organization of inhibitory connections to neocortical excitatory cells. *Nat Neurosci* 14:100–107.

Kaur S, Rose HJ, Lazar R, Liang K, Metherate R (2005) Spectral integration in primary auditory cortex: laminar processing of afferent input, in vivo and in vitro. *Neuroscience* 134:1033–1045.

Kaur S, Lazar R, Metherate R (2004) Intracortical pathways determine breadth of subthreshold frequency receptive fields in primary auditory cortex. *J Neurophysiol* 91:2551–2567.

Kayser C, Logothetis NK, Panzeri S (2010) Visual Enhancement of the Information Representation in Auditory Cortex. *Current Biology* 20:19–24.

Kelly JB, Judge PW (1994) Binaural organization of primary auditory cortex in the ferret (Mustela putorius). *J Neurophysiol* 71:904–913.

Kelly JB, Judge PW, Phillips DP (1986) Representation of the cochlea in primary auditory cortex of the ferret (Mustela putorius). *Hear Res* 24:111–115.

Kelly JB, Sally SL (1988) Organization of auditory cortex in the albino rat: binaural response properties. *J Neurophysiol* 59:1756–1769.

Kim H, Bao S (2009) Selective increase in representations of sounds repeated at an ethological rate. *J Neurosci* 29:5163–5169.

Kimura A, Imbe H, Donishi T (2010) Efferent connections of an auditory area in the caudal insular cortex of the rat: anatomical nodes for cortical streams of auditory processing and cross-modal sensory interactions. *Neuroscience* 166:1140–1157.

King AJ, Carlile S (1993) Changes induced in the representation of auditory space in the superior colliculus by rearing ferrets with binocular eyelid suture. *Exp Brain Res* 94:444–455.

King AJ, Schnupp JW, Thompson ID (1998) Signals from the superficial layers of the superior colliculus enable the development of the auditory space map in the deeper layers. *J. Neurosci.* 18:9394–9408.

King AJ (2004) The superior colliculus. *Curr Biol* 14:R335–8.

King AJ (2009) Visual influences on auditory spatial learning. *Philos Trans R Soc Lond, B, Biol Sci* 364:331–339.

King AJ, Parsons CH (1999) Improved auditory spatial acuity in visually deprived ferrets. *European Journal of Neuroscience* 11:3945–3956.

King AJ, Schnupp JWH (2007) The auditory cortex. *Curr Biol* 17:R236–9.

Kishan AU, Lee CC, Winer JA (2008) Branched projections in the auditory thalamocortical and corticocortical systems. *Neuroscience* 154:283–293.

Knight PL (1977) Representation of the cochlea within the anterior auditory field (AAF) of the cat. *J Neurosci Methods* 130:447–467.

Ko H, Cossell L, Baragli C, Antolik J, Clopath C, Hofer SB, Mrsic-Flogel TD (2013) The emergence of functional microcircuits in visual cortex. *Nature* 496:96–100.

Kobayasi KI, Suwa Y, Riquimaroux H (2013) Audiovisual integration in the primary auditory cortex of an awake rodent. *Neurosci Lett* 534:24–29.

Kohl MM, Shipton OA, Deacon RM, Rawlins JNP, Deisseroth K, Paulsen O (2011) Hemisphere-specific optogenetic stimulation reveals left-right asymmetry of hippocampal plasticity. *Nat Neurosci* 14:1413–1415.

Kourtzi Z, Connor CE (2011) Neural representations for object perception: structure, category, and adaptive coding. *Annual review of neuroscience* 34:45–67.

Kowalski N, Versnel H, Shamma SA (1995) Comparison of responses in the anterior and primary auditory fields of the ferret cortex. *J Neurophysiol* 73:1513–1523.

Kral A, Hartmann R, Tillein J, Heid S, Klinke R (2000) Congenital auditory deprivation reduces synaptic activity within the auditory cortex in a layer-specific manner. *Cereb Cortex* 10:714–726.

Lakatos P, Chen CM, O'connell MN, Mills A, Schroeder CE (2007) Neuronal oscillations and multisensory interaction in primary auditory cortex. *Neuron* 53:279–292.

Lakatos P, Karmos G, Mehta AD, Ulbert I, Schroeder CE (2008) Entrainment of neuronal oscillations as a mechanism of attentional selection. *Science* 320:110–113.

Laramée ME, Kurotani T, Rockland KS, Bronchti G, Boire D (2011) Indirect pathway between the primary auditory and visual cortices through layer V pyramidal neurons in V2L in mouse and the effects of bilateral enucleation. *Eur J Neurosci* 34:65–78.

Laramée ME, Rockland KS, Prince S, Bronchti G, Boire D (2013) Principal component and cluster analysis of layer V pyramidal cells in visual and non-visual cortical areas projecting to the primary visual cortex of the mouse. *Cereb Cortex* 23:714–728.

Lee CC (2013) Thalamic and cortical pathways supporting auditory processing. *Brain Lang* 126:22–28.

Lee CC, Imaizumi K, Schreiner CE, Winer JA (2004) Concurrent tonotopic processing streams in auditory cortex. *Cereb Cortex* 14:441–451.

Lee CC, Sherman SM (2008) Synaptic properties of thalamic and intracortical inputs to layer 4 of the first- and higher-order cortical areas in the auditory and somatosensory systems. *J Neurophysiol* 100:317–326.

Lee CC, Sherman SM (2010) Drivers and modulators in the central auditory pathways. *Front Neurosci* 4:79.

Lee CC, Winer JA (2008a) Connections of cat auditory cortex: I. Thalamocortical system. *J Comp Neurol* 507:1879–1900.

Lee CC, Winer JA (2008b) Connections of cat auditory cortex: II. Commissural system. *J Comp Neurol* 507:1901–1919.

Letzkus JJ, Wolff SBE, Meyer EMM, Tovote P, Courtin J, Herry C, Lüthi A (2011) A disinhibitory microcircuit for associative fear learning in the auditory cortex. *Nature* 480:331–335.

Li Ly, Li Yt, Zhou M, Tao HW, Zhang LI (2013) Intracortical multiplication of thalamocortical signals in mouse auditory cortex. *Nat Neurosci* 16:1179–1181.

Liang M, Mouraux A, Hu L, Iannetti GD (2013) Primary sensory cortices contain distinguishable spatial patterns of activity for each sense. *Nat Commun* 4:1979.

Lima SQ, Hromádka T, Znamenskiy P, Zador AM (2009) PINP: a new method of tagging neuronal populations for identification during in vivo electrophysiological recording. *PLoS ONE* 4:e6099.

Linden JF, Liu RC, Sahani M, Schreiner CE, Merzenich MM (2003) Spectrotemporal structure of receptive fields in areas AI and AAF of mouse auditory cortex. *J Neurophysiol* 90:2660–2675.

Linden JF, Schreiner CE (2003) Columnar transformations in auditory cortex? A comparison to visual and somatosensory cortices. *Cereb Cortex* 13:83–89.

Little JP, Carter AG (2012) Subcellular synaptic connectivity of layer 2 pyramidal neurons in the medial prefrontal cortex. *J Neurosci* 32:12808–12819.

Liu RC, Miller KD, Merzenich MM, Schreiner CE (2003) Acoustic variability and distinguishability among mouse ultrasound vocalizations. *J Acoust Soc Am* 114:3412–3422.

Llano DA, Sherman SM (2008) Evidence for nonreciprocal organization of the mouse auditory thalamocortical-corticothalamic projection systems. *J Comp Neurol* 507:1209–1227.

Lomber SG, Malhotra S (2008) Double dissociation of 'what' and 'where' processing in auditory cortex. *Nat Neurosci* 11:609–616.

Manley JA, Müller-Preuss P (1978) Response variability of auditory cortex cells in the squirrel monkey to constant acoustic stimuli. *Exp Brain Res* 32:171–180.

Mao YT, Pallas SL (2012) Compromise of auditory cortical tuning and topography after cross-modal invasion by visual inputs. *J Neurosci* 32:10338–10351.

Martin del Campo HN, Measor KR, Razak KA (2012) Parvalbumin immunoreactivity in the auditory cortex of a mouse model of presbycusis. *Hear Res* 294:31–39.

Maunsell JH, Van Essen DC (1983) The connections of the middle temporal visual area (MT) and their relationship to a cortical hierarchy in the macaque monkey. *J. Neurosci.* 3:2563–2586.

Mayford M, Bach ME, Huang YY, Wang L, Hawkins RD, Kandel ER (1996) Control of memory formation through regulated expression of a CaMKII transgene. *Science* 274:1678–1683.

Mercier MR, Foxe JJ, Fiebelkorn IC, Butler JS, Schwartz TH, Molholm S (2013) Auditory-driven phase reset in visual cortex: human electrocorticography reveals mechanisms of early multisensory integration. *NeuroImage* 79:19–29.

Meredith MA, Allman BL (2012) Early Hearing-Impairment Results in Crossmodal Reorganization of Ferret Core Auditory Cortex. *Neural Plasticity* 2012:1–13.

Merzenich MM, Brugge JF (1973) Representation of the cochlear partition of the superior temporal plane of the macaque monkey. *Brain Res* 50:275–296.

Merzenich MM, Knight PL, Roth GL (1975) Representation of cochlea within primary auditory cortex in the cat. *J Neurophysiol* 38:231–249.

Mikaelian D, Ruben RJ (1965) Development of hearing in the normal CBA-J mouse: Correlation of physiological observations with behavioral responses and with cochlear anatomy. *Acta Otolaryngol.* 59:451–461.

Miller LM, Escabí MA, Read HL, Schreiner C (2001) Functional convergence of response properties in the auditory thalamocortical system. *Neuron* 32:151–160.

Miller LM, Escabí MA, Read HL, Schreiner CE (2002) Spectrotemporal receptive fields in the lemniscal auditory thalamus and cortex. *J Neurophysiol* 87:516–527.

Mitzdorf U (1985) Current source-density method and application in cat cerebral cortex: investigation of evoked potentials and EEG phenomena. *Physiol. Rev.* 65:37–100.

Molinari M, Dell'Anna ME, Rausell E, Leggio MG, Hashikawa T, Jones EG (1995) Auditory thalamocortical pathways defined in monkeys by calcium-binding protein immunoreactivity. *J Comp Neurol* 362:171–194.

Moore AK, Wehr M (2013) Parvalbumin-expressing inhibitory interneurons in auditory cortex are well-tuned for frequency. *J Neurosci* 33:13713–13723.

Moshitch D, Las L, Ulanovsky N, Bar-Yosef O, Nelken I (2006) Responses of neurons in primary auditory cortex (A1) to pure tones in the halothane-anesthetized cat. *J Neurophysiol* 95:3756–3769.

Mrsic-Flogel TD, King AJ, Schnupp JWH (2005) Encoding of virtual acoustic space stimuli by neurons in ferret primary auditory cortex. *J Neurophysiol* 93:3489–3503.

Nodal FR, Bajo VM, King AJ (2012) Plasticity of spatial hearing: behavioural effects of cortical inactivation. *J Physiol (Lond)* 590:3965–3986.

Nodal FR, Kacelnik O, Bajo VM, Bizley JK, Moore DR, King AJ (2010) Lesions of the auditory cortex impair azimuthal sound localization and its recalibration in ferrets. *J Neurophysiol* 103:1209–1225.

Ohki K, Chung S, Kara P, Hübener M, Bonhoeffer T, Reid RC (2006) Highly ordered arrangement of single neurons in orientation pinwheels. *Nature* 442:925–928.

Oviedo HV, Bureau I, Svoboda K, Zador AM (2010) The functional asymmetry of auditory cortex is reflected in the organization of local cortical circuits. *Nat Neurosci* 13:1413–1420.

Passini MA, Watson DJ, Wolfe JH (2004) Gene delivery to the mouse brain with adeno-associated virus. *Methods Mol Biol* 246:225–236.

Paxinos G, Franklin KBJ (2007) *The mouse brain in stereotaxic coordinates* Elsevier, New York, 3rd edition.

Perrella M, da Costa NM, Martin KAC (2013) Mapping the matrix of mouse auditory cortex [poster] In *17th Annual Meeting of the Swiss Society for Neuroscience*, Geneva.

Petersen CCH (2007) The functional organization of the barrel cortex. *Neuron* 56:339–355.

Petreanu L, Huber D, Sobczyk A, Svoboda K (2007) Channelrhodopsin-2-assisted circuit mapping of long-range callosal projections. *Nat Neurosci* 10:663–668.

Petreanu L, Mao T, Sternson SM, Svoboda K (2009) The subcellular organization of neocortical excitatory connections. *Nature* 457:1142–1145.

Petrus E, Isaiah A, Jones AP, Li D, Wang H, Lee HK, Kanold PO (2014) Cross-modal induction of thalamocortical potentiation leads to enhanced information processing in the auditory cortex. *Neuron [in press]* .

Philipp R, Distler C, Hoffmann KP (2006) A motion-sensitive area in ferret extrastriate visual cortex: an analysis in pigmented and albino animals. *Cereb Cortex* 16:779–790.

Polley DB, Read HL, Storace DA, Merzenich MM (2007) Multiparametric auditory receptive field organization across five cortical fields in the albino rat. *J Neurophysiol* 97:3621–3638.

Profant O, Burianová J, Syka J (2013) The response properties of neurons in different fields of the auditory cortex in the rat. *Hear Res* 296:51–59.

Qin L, Chimoto S, Sakai M, Wang J, Sato Y (2007) Comparison between offset and onset responses of primary auditory cortex ON-OFF neurons in awake cats. *J Neurophysiol* 97:3421–3431.

Rabinowitz NC, Willmore BD, Schnupp JWH, King AJ (2011) Contrast gain control in auditory cortex. *Neuron* 70:1178–1191.

Rabinowitz NC, Willmore BD, Schnupp JWH, King AJ (2012) Spectrotemporal contrast kernels for neurons in primary auditory cortex. *J Neurosci* 32:11271–11284.

Rajan R, Dubaj V, Reser DH, Rosa MGP (2013) Auditory cortex of the marmoset monkey - complex responses to tones and vocalizations under opiate anaesthesia in core and belt areas. *Eur J Neurosci* 37:924–941.

Rawdon-Smith AF, Hawkins JE (1939) The Electrical Activity of a Denervated Ear. *Proceedings of the Royal Society of Medicine* 32:496.

Read HL, Winer JA, Schreiner CE (2001) Modular organization of intrinsic connections associated with spectral tuning in cat auditory cortex. *Proc Natl Acad Sci USA* 98:8042–8047.

Read HL, Winer JA, Schreiner CE (2002) Functional architecture of auditory cortex. *Curr Opin Neurobiol* 12:433–440.

Redies H, Brandner S, Creutzfeldt OD (1989a) Anatomy of the auditory thalamocortical system of the guinea pig. *J Comp Neurol* 282:489–511.

Redies H, Sieben U, Creutzfeldt OD (1989b) Functional subdivisions in the auditory cortex of the guinea pig. *J Comp Neurol* 282:473–488.

Ro T, Ellmore TM, Beauchamp MS (2013) A neural link between feeling and hearing. *Cereb Cortex* 23:1724–1730.

Robles L, Ruggero MA (2001) Mechanics of the mammalian cochlea. *Physiol. Rev.* 81:1305–1352.

Rockland KS, Pandya DN (1979) Laminar origins and terminations of cortical connections of the occipital lobe in the rhesus monkey. *Brain Res* 179:3–20.

Rodgers KM, Benison AM, Klein A, Barth DS (2008) Auditory, somatosensory, and multisensory insular cortex in the rat. *Cereb Cortex* 18:2941–2951.

Rosen GD, Williams AG, Capra JA, Connolly MT, Cruz B, Lu L, Airey DC, Kulkarni K, Williams RW (2000) The Mouse Brain Library www.mbl.org.

Rothschild G, Cohen L, Mizrahi A, Nelken I (2013) Elevated correlations in neuronal ensembles of mouse auditory cortex following parturition. *J Neurosci* 33:12851–12861.

Rothschild G, Nelken I, Mizrahi A (2010) Functional organization and population dynamics in the mouse primary auditory cortex. *Nat Neurosci* 13:353–360.

Rutkowski RG, Miasnikov AA, Weinberger NM (2003) Characterisation of multiple physiological fields within the anatomical core of rat auditory cortex. *Hear Res* 181:116–130.

Ryan AF, Woolf NK, Sharp FR (1982) Tonotopic organization in the central auditory pathway of the Mongolian gerbil: a 2-deoxyglucose study. *J Comp Neurol* 207:369–380.

Sahani M, Linden JF (2003) How Linear are Auditory Cortical Responses? In Becker S, Thrun S, Obermayer K, editors, *Advances in Neural Information Processing Systems 15*. MIT Press, Cambridge, MA.

Sally SL, Kelly JB (1988) Organization of auditory cortex in the albino rat: sound frequency. *J Neurophysiol* 59:1627–1638.

Sams M, Aulanko R, Hämäläinen M, Hari R, Lounasmaa OV, Lu ST, Simola J (1991) Seeing speech: visual information from lip movements modifies activity in the human auditory cortex. *Neurosci Lett* 127:141–145.

Sawatari H, Tanaka Y, Takemoto M, Nishimura M, Hasegawa K, Saitoh K, Song WJ (2011) Identification and characterization of an insular auditory field in mice. *Eur J Neurosci* 34:1944–1952.

Schnupp JW, Mrsic-Flogel TD, King AJ (2001) Linear processing of spatial cues in primary auditory cortex. *Nature* 414:200–204.

Scholes C, Palmer AR, Sumner CJ (2011) Forward suppression in the auditory cortex is frequency-specific. *European Journal of Neuroscience* 33:1240–1251.

Schreiner C, Urbas JV (1988) Representation of amplitude modulation in the auditory cortex of the cat. II. Comparison between cortical fields. *Hear Res* 32:49–63.

Schreiner CE, Winer JA (2007) Auditory cortex mapmaking: principles, projections, and plasticity. *Neuron* 56:356–365.

Schroeder CE, Foxe JJ (2005) Multisensory contributions to low-level, 'unisensory' processing. *Curr Opin Neurobiol* 15:454–458.

Schroeder CE, Lindsley RW, Specht C, Marcovici A, Smiley JF, Javitt DC (2001) Somatosensory input to auditory association cortex in the macaque monkey. *J Neurophysiol* 85:1322–1327.

Schürmann M, Caetano G, Jousmäki V, Hari R (2004) Hands help hearing: facilitatory audiotactile interaction at low sound-intensity levels. *J Acoust Soc Am* 115:830–832.

Seybold BA, Stanco A, Cho KKA, Potter GB, Kim C, Sohal VS, Rubenstein JLR, Schreiner CE (2012) Chronic reduction in inhibition reduces receptive field size in mouse auditory cortex. *Proceedings of the National Academy of Sciences* 109:13829–13834.

Sharpee TO, Atencio CA, Schreiner CE (2011) Hierarchical representations in the auditory cortex. *Curr Opin Neurobiol* 21:761–767.

Shen JX, Xu ZM, Yao YD (1999) Evidence for columnar organization in the auditory cortex of the mouse. *Hear Res* 137:174–177.

Sherman SM, Guillery RW (1998) On the actions that one nerve cell can have on another: distinguishing "drivers" from "modulators". *Proc Natl Acad Sci USA* 95:7121–7126.

Sherman SM (2007) The thalamus is more than just a relay. *Curr Opin Neurobiol* 17:417–422.

Sherman SM (2012) Thalamocortical interactions. *Curr Opin Neurobiol* 22:575–579.

Sherman SM, Guillery RW (2011) Distinct functions for direct and transthalamic corticocortical connections. *J Neurophysiol* 106:1068–1077.

Shimano T, Fyk-Kolodziej B, Mirza N, Asako M, Tomoda K, Bledsoe S, Pan ZH, Molitor S, Holt AG (2013) Assessment of the AAV-mediated expression of channelrhodopsin-2 and halorhodopsin in brainstem neurons mediating auditory signaling. *J Neurosci Methods* 1511:138–152.

Smiley JF, Falchier A (2009) Multisensory connections of monkey auditory cerebral cortex. *Hear Res* 258:37–46.

Smith PH, Uhlrich DJ, Manning KA, Banks MI (2012) Thalamocortical projections to rat auditory cortex from the ventral and dorsal divisions of the medial geniculate nucleus. *J Comp Neurol* 520:34–51.

Stein BE, Stanford TR (2008) Multisensory integration: current issues from the perspective of the single neuron. *Nat Rev Neurosci* 9:255–266.

Stiebler I (1987a) A distinct ultrasound-processing area in the auditory cortex of the mouse. *Naturwissenschaften* 74:96–97.

Stiebler I (1987b) *Frequenzrepräsentation und Schallempfindlichkeit im Colliculus inferior und auditorischen Cortex der Hausmaus (Mus musculus)*. Hartung-Gorre, Konstanz.

Stiebler I, Neulist R, Fichtel I, Ehret G (1997) The auditory cortex of the house mouse: left-right differences, tonotopic organization and quantitative analysis of frequency representation. *J Comp Physiol A* 181:559–571.

Sun YJ, Kim YJ, Ibrahim LA, Tao HW, Zhang LI (2013) Synaptic Mechanisms Underlying Functional Dichotomy between Intrinsic-Bursting and Regular-Spiking Neurons in Auditory Cortical Layer 5. *J Neurosci* 33:5326–5339.

Sutter ML, Schreiner C (1991) Physiology and topography of neurons with multipeaked tuning curves in cat primary auditory cortex. *J Neurophysiol* 65:1207–1226.

Szymanski FD, Garcia-Lazaro JA, Schnupp JWH (2009) Current source density profiles of stimulus-specific adaptation in rat auditory cortex. *J Neurophysiol* 102:1483–1490.

Talavage TM, Ledden PJ, Benson RR, Rosen BR, Melcher JR (2000) Frequency-dependent responses exhibited by multiple regions in human auditory cortex. *Hear Res* 150:225–244.

Talavage TM, Sereno MI, Melcher JR, Ledden PJ, Rosen BR, Dale AM (2004) Tonotopic organization in human auditory cortex revealed by progressions of frequency sensitivity. *J Neurophysiol* 91:1282–1296.

Tan AYY, Wehr M (2009) Balanced tone-evoked synaptic excitation and inhibition in mouse auditory cortex. *Neuroscience* 163:1302–1315.

Tan AYY, Zhang LI, Merzenich MM, Schreiner CE (2004) Tone-evoked excitatory and inhibitory synaptic conductances of primary auditory cortex neurons. *J Neurophysiol* 92:630–643.

Theunissen FE, Sen K, Doupe AJ (2000) Spectral-temporal receptive fields of nonlinear auditory neurons obtained using natural sounds. *J Neurosci* 20:2315–2331.

Theyel BB, Llano DA, Sherman SM (2010) The corticothalamocortical circuit drives higher-order cortex in the mouse. *Nat Neurosci* 13:84–88.

Thomas H, Tillein J, Heil P, Scheich H (1993) Functional organization of auditory cortex in the mongolian gerbil (Meriones unguiculatus). I. Electrophysiological mapping of frequency representation and distinction of fields. *Eur J Neurosci* 5:882–897.

Trujillo M, Carrasco MM, Razak K (2013) Response properties underlying selectivity for the rate of frequency modulated sweeps in the auditory cortex of the mouse. *Hear Res* 298:80–92.

Trujillo M, Measor K, Carrasco MM, Razak KA (2011) Selectivity for the rate of frequency-modulated sweeps in the mouse auditory cortex. *J Neurophysiol* 106:2825–2837.

Van Essen DC, Felleman DJ, DeYoe EA, Olavarria J, Knierim J (1990) Modular and Hierarchical Organization of Extrastriate Visual Cortex in the Macaque Monkey. *Cold Spring Harbor Symposia on Quantitative Biology* 55:679–696.

Vezoli J, Falchier A, Jouve B, Knoblauch K, Young M, Kennedy H (2004) Quantitative analysis of connectivity in the visual cortex: extracting function from structure. *The Neuroscientist* 10:476–482.

Vogels R, Spileers W, Orban GA (1989) The response variability of striate cortical neurons in the behaving monkey. *Experimental Brain Research* 77:432–436.

Walker KMM, Bizley JK, King AJ, Schnupp JWH (2011) Multiplexed and robust representations of sound features in auditory cortex. *J Neurosci* 31:14565–14576.

Wallace MN, Rutkowski RG, Palmer AR (2000) Identification and localisation of auditory areas in guinea pig cortex. *Exp Brain Res* 132:445–456.

Wallace MT, Ramachandran R, Stein BE (2004) A revised view of sensory cortical parcellation. *Proc Natl Acad Sci USA* 101:2167–2172.

Wandell BA, Smirnakis SM (2009) Plasticity and stability of visual field maps in adult primary visual cortex. *Nat Rev Neurosci* 10:873–884.

Wang X, Walker KMM (2012) Neural mechanisms for the abstraction and use of pitch information in auditory cortex. *J Neurosci* 32:13339–13342.

Wehr M, Zador AM (2003) Balanced inhibition underlies tuning and sharpens spike timing in auditory cortex. *Nature* 426:442–446.

Wehr M, Zador AM (2005) Synaptic mechanisms of forward suppression in rat auditory cortex. *Neuron* 47:437–445.

Willott JF, Aitkin LM, McFadden SL (1993) Plasticity of auditory cortex associated with sensorineural hearing loss in adult C57BL/6J mice. *J Comp Neurol* 329:402–411.

Winer JA (2006) Decoding the auditory corticofugal systems. *Hear Res* 212:1–8.

Winkowski DE, Bandyopadhyay S, Shamma SA, Kanold PO (2013) Frontal cortex activation causes rapid plasticity of auditory cortical processing. *J Neurosci* 33:18134–18148.

Winkowski DE, Kanold PO (2013) Laminar transformation of frequency organization in auditory cortex. *J Neurosci* 33:1498–1508.

Withington-Wray DJ, Binns KE, Keating MJ (1990) The Maturation of the Superior Collicular Map of Auditory Space in the Guinea Pig is Disrupted by Developmental Visual Deprivation. *Eur J Neurosci* 2:682–692.

Wu GK, Arbuckle R, Liu BH, Tao HW, Zhang LI (2008) Lateral sharpening of cortical frequency tuning by approximately balanced inhibition. *Neuron* 58:132–143.

Zatorre RJ, Bouffard M, Ahad P, Belin P (2002) Where is 'where' in the human auditory cortex? *Nat Neurosci* 5:905–909.

Zheng QY, Johnson KR, Erway LC (1999) Assessment of hearing in 80 inbred strains of mice by ABR threshold analyses. *Hear Res* 130:94–107.

Znamenskiy P, Zador AM (2013) Corticostriatal neurons in auditory cortex drive decisions during auditory discrimination. *Nature* 497:482–485.